https://doi.org/10.15388/vu.thesis.957
https://orcid.org/0009-0002-0243-1421

VILNIAUS UNIVERSITETAS
GAMTOS TYRIMŲ CENTRAS
KLAIPĖDOS UNIVERSITETAS

Laurynas Klimavičius

Kompleksiniai klimato įvykiai rytinėje Baltijos jūros regiono dalyje

DAKTARO DISERTACIJA

Gamtos mokslai,
fizinė geografija (N 006)

VILNIUS 2026

Disertacija rengta 2022–2026 metais Vilniaus universitete.

Mokslinis vadovas – prof. dr. Egidijus Rimkus (Vilniaus universitetas, gamtos mokslai, fizinė geografija, N 006).

Gynimo taryba:
Pirmininkas – prof. dr. Donatas Pupienis (Vilniaus universitetas, gamtos mokslai, fizinė geografija, N 006).
Nariai:
prof. dr. Arūnas Bukantis (Vilniaus universitetas, gamtos mokslai, fizinė geografija, N 006),
dr. Jovita Mėžinė (Klaipėdos universitetas, gamtos mokslai, fizinė geografija, N 006),
prof. dr. Piia Post (Tartu universitetas, gamtos mokslai, fizinė geografija, N 006),
doc. dr. Laura Šukienė (Vilniaus universitetas, gamtos mokslai, fizinė geografija, N 006).

Disertacija ginama viešame Gynimo tarybos posėdyje 2026 m. rugsėjo mėn. 25 d. 14 val. Vilniaus universiteto Chemijos ir geomokslų fakulteto Geomokslų instituto 313 auditorijoje. Adresas: M. K. Čiurlionio g. 21, Vilnius, Lietuva, tel. +37052398292.

https://doi.org/10.15388/vu.thesis.957
https://orcid.org/0009-0002-0243-1421

VILNIUS UNIVERSITY
NATURE RESEARCH CENTRE
KLAIPĖDA UNIVERSITY

Laurynas Klimavičius

Compound Climate Events in the Eastern Part of the Baltic Sea Region

DOCTORAL DISSERTATION

Natural Sciences,
Physical Geography (N 006)

VILNIUS 2026

The dissertation was prepared between 2022 and 2026 at the Vilnius University.

Academic Supervisor – Prof. Dr. Egidijus Rimkus (Vilnius University, Natural Sciences, Physical Geography, N 006).

This doctoral dissertation will be defended in a public meeting of the Dissertation Defence Panel:

Chairman – Prof. Dr. Donatas Pupienis (Vilnius University, Natural Sciences, Physical Geography, N 006).
Members:
Prof. Dr. Arūnas Bukantis (Vilnius University, Natural Sciences, Physical Geography, N 006),
Dr. Jovita Mėžinė (Klaipėda University, Natural Sciences, Physical Geography, N 006),
Prof. Dr. Piia Post (University of Tartu, Natural Sciences, Physical Geography, N 006),
Assoc. Prof. Dr. Laura Šukienė (Vilnius University, Natural Sciences, Physical Geography, N 006).

The dissertation shall be defended at a public meeting of the Dissertation Defence Panel at 2 p. m. on 25th September 2026 in Room 313 of the Faculty of Chemistry and Geosciences, Institute of Geosciences (Vilnius University).
Address: M. K. Čiurlionio str. 21, Room No. 313, Vilnius, Lithuania
Tel. +37052398292.

SANTRUMPOS

Santrumpa	Reikšmė anglų kalba	Reikšmė lietuvių kalba
CCE	Compound Climate Event	Kompleksinis klimato įvykis
CDHE	Compound drought and heatwave event	Kompleksinis sausros ir karščio bangos įvykis
CMIP6	Coupled Model Intercomparison Project Phase 6	Šešta susieto modelių palyginimo projekto fazė
CPWE	Compound Precipitation and Wind Extreme	Kompleksinis kritulių kiekio ir vėjo greičio ekstremumas
ECMWF	European Centre for Medium-Range Weather Forecasts	Europos vidutinės trukmės orų prognozių centras
FS	False Spring	Vėlyva pavasario šalna
GDD	Growing Degree Days	Aktyviųjų temperatūrų suma
IPCC	Intergovernmental Panel on Climate Change	Tarpvyriausybinė klimato kaitos komisija
LSF	Last Spring Frost	Paskutinė pavasario šalna
MAE	Mean Absolute Error	Vidutinė absoliutinė paklaida
P	Daily precipitation	Paros kritulių kiekis
p	Significance level	Reikšmingumo lygmuo
r	Pearson correlation coefficient	Pirsono koreliacijos koeficientas
SGS	Start of the Growing Season	Vegetacijos sezono pradžia
SPI	Standardised Precipitation Index	Standartizuotas kritulių indeksas
SSP	Shared Socioeconomic Pathway	Bendrasis socialinis ir ekonominis kelias
t_{avg}	Daily mean air temperature	Vidutinė paros oro temperatūra
t_{max}	Daily maximum air temperature	Maksimali paros oro temperatūra
t_{min}	Daily minimum air temperature	Minimali paros oro temperatūra
WGF	Wind Gust Factor	Vėjo gūsių faktorius
w_{max}	Maximum wind speed	Maksimalus vėjo greitis

TURINYS

TURINYS 6
PUBLIKACIJŲ SĄRAŠAS 7
AUTORIAUS INDĖLIS PUBLIKACIJOSE 8
TYRIMŲ REZULTATŲ APROBAVIMAS 9
ĮVADAS 11
1. DUOMENYS IR METODIKA 17
1.1. Tyrimo teritorija 17
1.2. Darbe panaudoti duomenys 18
1.3. Kompleksinių klimato įvykių identifikavimas ir vertinimas 21
1.3.1. Kompleksinių sausros ir karščio bangos įvykių nustatymas 21
1.3.2. Vėlyvų pavasario šalnų nustatymas 23
1.3.3. Kompleksinių kritulių kiekio ir vėjo greičio ekstremumų nustatymas 24
1.4. Kompleksinių klimato įvykių susiformavimą lemiančių atmosferos sąlygų vertinimas 25
2. TYRIMŲ REZULTATAI 27
2.1. Kompleksiniai sausros ir karščio bangos įvykiai 27
2.2. Vėlyvos pavasario šalnos 29
2.3. Kompleksiniai kritulių kiekio ir vėjo greičio ekstremumai 32
REZULTATŲ APTARIMAS 35
IŠVADOS 42
SUMMARY 44
LITERATŪROS SĄRAŠAS 61
PADĖKA 75
CURRICULUM VITAE 76
PUBLIKACIJŲ KOPIJOS 77

PUBLIKACIJŲ SĄRAŠAS

Daktaro disertacija yra paremta toliau pateiktomis publikacijomis, paskelbtomis tarptautiniuose mokslo žurnaluose, turinčiuose cituojamumo rodiklį *Clarivate Analytics Web of Science* (*CA WoS*) duomenų bazėje:

I. **Klimavičius, L.**, & Rimkus, E. (2024). Compound drought and heatwave events in the eastern part of the Baltic Sea region. *Oceanologia*, 66(1), 26–36. https://doi.org/10.1016/j.oceano.2023.06.010

II. **Klimavičius, L.**, & Rimkus, E. (2024). False spring events in the eastern part of the Baltic Sea region. *Theoretical and Applied Climatology*, 155(10), 9351–9365. https://doi.org/10.1007/s00704-024-05194-0

III. **Klimavičius, L.**, Rimkus, E., & Stankūnavičius, G. (2025). Compound precipitation and wind extremes in the eastern part of the Baltic Sea region. *Atmosphere*, 16(3), 276. https://doi.org/10.3390/atmos16030276

IV. **Klimavičius, L.**, & Rimkus, E. (2025). Future projections of false spring events in the eastern part of the Baltic Sea region. *Baltica*, 38(2), 160–173. https://doi.org/10.5200/baltica.2025.2.4

AUTORIAUS INDĖLIS PUBLIKACIJOSE

Visose publikacijose Lauryno Klimavičiaus indėlis daugiau nei 70 %. Visais atvejais jis atliko duomenų analizę, rengė publikacijos tekstą, formulavo išvadas. Kitų bendraautorių indėlis yra tik fragmentinis skirtingose publikacijos dalyse.

TYRIMŲ REZULTATŲ APROBAVIMAS

Autorius pristatė pagrindinius daktaro disertacijos rezultatus septyniose tarptautinėse ir septyniose nacionalinėse konferencijose:

1. **Klimavičius, L.** (2023). Kompleksiniai sausros ir karščio bangos įvykiai rytinėje Baltijos jūros regiono dalyje. *VII-osios nacionalinės jaunųjų geografų konferencijos medžiaga*, 21–22. https://www.hkk.gf.vu.lt/wordpress/wp-content/uploads/2024/04/GJ_VII_leidinys.pdf
2. **Klimavičius, L.**, & Rimkus, E. (2023). Compound drought and heatwave events in the eastern part of the Baltic Sea region, *EGU General Assembly 2023*, EGU23-3273. https://doi.org/10.5194/egusphere-egu23-3273
3. **Klimavičius, L**. (2023). False spring events in the eastern part of the Baltic Sea region. *EMS Annual Meeting 2023*, EMS2023-438, https://doi.org/10.5194/ems2023-438
4. **Klimavičius, L**. (2024). Kompleksiniai vėjo greičio ir kritulių kiekio įvykiai rytinėje Baltijos jūros regiono dalyje. *VIII-osios nacionalinės jaunųjų geografų konferencijos medžiaga*, 16–17. https://www.hkk.gf.vu.lt/wordpress/wp-content/uploads/2024/04/GJ_VIII_leidinys-1.pdf
5. **Klimavičius, L.**, & Rimkus, E. (2024). Kompleksiniai klimato įvykiai rytinėje Baltijos jūros regiono dalyje 1950–2022 metais. *I-osios nacionalinės Chemijos ir Geomokslų konferencijos tezės*, 52. https://www.chgf.vu.lt/files/doc/chemija_ir_geomokslai_2024_tezes.pdf
6. **Klimavičius, L.**, & Rimkus, E. (2024). Compound late-spring frost and drought events in the eastern part of the Baltic Sea region. *5th Baltic Earth Conference. Conference Proceedings*, 36–37. https://baltic.earth/imperia/md/assets/baltic_earth/baltic_earth/baltic_earth/5bec_proceedings.pdf
7. **Klimavičius, L.** (2024). Compound precipitation and wind extremes in the eastern part of the Baltic Sea region. *EMS Annual Meeting 2024*, EMS2024-716. https://doi.org/10.5194/ems2024-716
8. **Klimavičius, L.**, Rimkus E., & Stankūnavičius, G. (2025). Kompleksinių kritulių kiekio ir vėjo greičio ekstremumų susidarymas ir pasikartojimas Baltijos šalyse 1950–2022 metais. *II-osios nacionalinės Chemijos ir Geomokslų konferencijos tezės*, 62. https://www.chgf.vu.lt/files/doc/abstraktu_knyga_03-14_05.pdf
9. **Klimavičius, L.** (2025). Vėlyvų pavasario šalnų prognozės rytinėje Baltijos jūros regiono dalyje. *IX-osios nacionalinės jaunųjų geografų*

konferencijos medžiaga, 30–31. https://www.hkk.gf.vu.lt/wordpress/wp-content/uploads/2025/04/GJ_IX_leidinys_2025.pdf

10. **Klimavičius, L.**, & Rimkus, E. (2025). Future amplification of compound drought and heatwave events in the eastern part of the Baltic Sea region. *AGU Annual Meeting 2025*, A51R-0983. https://agu.confex.com/agu/agu25/meetingapp.cgi/Paper/1923528
11. **Klimavičius, L.**, & Rimkus, E. (2026). Kompleksiniai klimato įvykiai rytinėje Baltijos jūros regiono dalyje. *III-osios nacionalinės Chemijos ir Geomokslų konferencijos tezės*, 18. https://www.chgfkonferencija.chgf.vu.lt/images/Abstraktu%20knyga_2026.pdf
12. **Klimavičius, L.** (2026). Kompleksinių sausros ir karščio bangos įvykių prognozės rytinėje Baltijos jūros regiono dalyje. *X-osios nacionalinės jaunųjų geografų konferencijos medžiaga*, 26–27. https://www.hkk.gf.vu.lt/wordpress/wp-content/uploads/2026/05/Geographia-Juventa_X_leidinys.pdf
13. **Klimavičius, L.**, & Rimkus, E. (2026). Future changes in compound precipitation and wind extremes in the Baltic States under CMIP6 projections. *6th Baltic Earth Conference. Conference Proceedings*.
14. **Klimavičius, L.**, & Rimkus, E. (2026). Spatiotemporal variability and future projections of compound climate events in the eastern part of the Baltic Sea region, *EGU General Assembly 2026*, EGU26-17338. https://doi.org/10.5194/egusphere-egu26-17338

ĮVADAS

Nuo XIX a. vidurio iki šių dienų dėl žmogaus sukeltos klimato kaitos globali sausumos bei vandenynų paviršiaus temperatūra augo 0,06 °C per dešimtmetį, o nuo 1975 m. šis pokytis siekė 0,2 °C per dešimtmetį (Lindsey & Dahlman, 2025). Sparčiausiai oro temperatūra Europoje kilo pavasarį, vidutiniškai 0,061 °C per metus (Twardosz ir kt. 2021). Kylanti oro temperatūra lemia vis dažnesnį įvairių ekstremalių orų bei klimato reiškinių (sausrų, ekstremalaus kritulių kiekio, karščio bangų, potvynių, stiprių pavasario šalnų ir kt.) susidarymą skirtinguose regionuose (AghaKouchak ir kt., 2020; Di Capua & Rahmstorf, 2023; Seneviratne ir kt., 2021). Tokie įvykiai daro žalą žmonėms, jų gyvenamajai aplinkai, infrastruktūrai, gamtai ir ekonomikai (Clarke ir kt., 2022; Seneviratne ir kt., 2021). Nuo 2000 iki 2020 m. ekstremalių orų ir klimato reiškinių metu globaliu mastu nukentėjo 773 milijonai žmonių, o padaryta žala įvertinta 1,3 trilijono JAV dolerių (Clarke ir kt., 2022). Vien tik Europos Sąjungoje 1980–2023 m. tokie reiškiniai sukėlė daugiau nei 200 000 mirčių (European Environment..., 2025).

Iki praėjusio dešimtmečio įvairius orų bei klimato ekstremumus buvo priimta tirti atskirai. Tačiau nustatyta, kad didesnė žala padaroma, kai keli, nebūtinai ekstremalūs reiškiniai, vyksta tuo pat metu arba sąveikauja tarpusavyje (Seneviratne ir kt., 2012; Zscheischler ir kt., 2020). Toks bendras kelių procesų derinys, lemiantis stiprų socioekonominį poveikį, yra vadinamas kompleksiniu klimato įvykiu (angl. *Compound Climate Event – CCE*) (Seneviratne ir kt., 2012; Zscheischler ir kt., 2018). Šiuo metu tiriami įvairūs CCE (Zscheischler ir kt., 2020), įprastai jie skirstomi į keturis tipus (1 pav.):

1. Sudėtiniai įvykiai (angl. *multivariate*) – keleto kartu vykstančių procesų rezultatas. Pavyzdys – kompleksiniai sausros ir karščio bangos įvykiai, kai abu reiškiniai susiformuoja toje pačioje teritorijoje tuo pat metu. Būtent sudėtiniai įvykiai analizuojami dažniausiai, jų tyrimai sudaro maždaug 75 % visų tiriamų CCE (Brett ir kt., 2025).
2. Išankstinių sąlygų nulemti įvykiai (angl. *preconditioned events*). Pavyzdys – vėlyvos pavasario šalnos, fiksuojamos jau prasidėjus vegetacijos sezonui.
3. Kompleksiniai įvykiai laiko požiūriu (angl. *temporally compounding*). Neigiamą poveikį sukelia keli vienas paskui kitą vykstantys reiškiniai (pavojai), fiksuojami toje pačioje teritorijoje. Pavyzdys – kelis kartus per trumpą laiką toje pačioje teritorijoje praūžusios audros poveikis stipresnis.
4. Kompleksiniai įvykiai erdviniu požiūriu (angl. *spatially compounding*). Išskiriami, kai keli veiksniai, veikdami skirtingose, tačiau tame pačiame regione esančiose teritorijose, padidina bendrą pavojų ir riziką.

Pavyzdžiui, mažas drėgmės kiekis ir didelis vėjo greitis sukuria palankias miškų gaisrų susidarymo sąlygas skirtingose vietovėse, o bendras poveikis juntamas didesnėje teritorijoje.

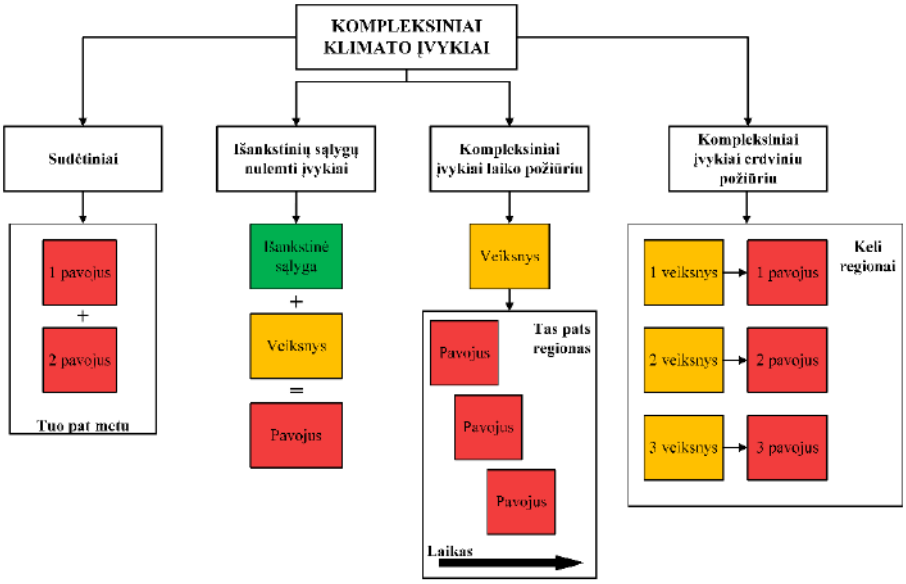

1 pav. Skirtingų tipų kompleksinių klimato įvykių susidarymo schema (parengta pagal Zscheischler ir kt., 2020).

Vis dėlto tas pats įvykis gali būti priskiriamas prie kelių tipų, ribos tarp jų nėra labai griežtai apibrėžtos. To priežastis – CCE neretai sukelia keletas kartu veikiančių, o kartais iš pirmo žvilgsnio net ir nesusijusių procesų (Zscheischler ir kt., 2020).

Rengiant šią disertaciją tirti trys CCE: kompleksiniai sausros ir karščio bangos įvykiai (angl. *Compound Drought and Heatwave Events – CDHE*), vėlyvos pavasario šalnos (angl. *False Spring – FS*) ir kompleksiniai kritulių kiekio bei vėjo greičio ekstremumai (angl. *Compound Precipitation and Wind Extremes – CPWE*). Darbe analizuojami tie CCE, kurie susiformuoja dėl meteorologinių reiškinių sąveikos bei kuriuos sudaro vieni dažniausių ekstremalių reiškinių tiriamame regione (sausros, karščio bangos, stiprūs vėjo gūsiai, gausus kritulių kiekis, vėlyvos pavasario šalnos). Visi trys darbe analizuojami CCE yra aktualūs kylančios oro temperatūros bei kintančio klimato kontekste ir sukelia stiprų neigiamą poveikį skirtinguose Europos regionuose bei Baltijos šalyse (European Environment…, 2025; Guglielmo ir kt., 2026).

CDHE identifikuojami, kai ir sausra, ir karščio banga susidaro toje pačioje teritorijoje tuo pat metu. Įprastai palankios CDHE susidarymo sąlygos formuojasi užsitęsus sausrai. Dėl sumažėjusios dirvožemio drėgmės sumažėja ir šiluminės energijos drėgmei garinti sąnaudos (Benson & Dirmeyer, 2021), o tai lemia spartesnį skirtingų paviršių įšilimą. Regioną pasiekus šiltai oro masei šis procesas padidina karščio bangos intensyvumą. Karščio banga savo ruožtu sustiprina sausrą – išaugus oro temperatūrai padidėja garavimo intensyvumas, todėl dirvožemis dar labiau išdžiūsta (Wang ir kt., 2024). CDHE laikomi vienu daugiausiai žalos padarančių meteorologinių / klimatologinių reiškinių (Yin & Slater, 2023). Jie siejami su išaugusiu mirtingumu (Ducros ir kt., 2025) bei neigiamai veikia žmonių emocinę sveikatą (Sewell ir kt., 2024). 1981–2020 m. laikotarpiu CDHE bent kartą paveikė net 92 % planetos teritorijų, kuriose auginami javai (He ir kt., 2022), tokie įvykiai lemia ir išaugusią miškų gaisrų riziką (Gazol & Camarero, 2022; Markonis ir kt., 2021). Be to, dėl neigiamo CDHE poveikio augalijai, padidėja į atmosferą patenkančio CO_2 kiekis (Ciais ir kt., 2005). Pastaraisiais dešimtmečiais dažniau pasikartojantys CDHE fiksuoti įvairiuose regionuose, taip pat ir Europoje (Bezak & Mikoš, 2020; Geirinhas ir kt., 2021; Sedlmeier ir kt., 2018; Shi ir kt., 2021).

FS sąvoka gali būti interpretuojama įvairiai (Chamberlain ir kt., 2019), tačiau šiame darbe vėlyva pavasario šalna laikomi atvejai, kai dėl anomaliai aukštos vėlyvos žiemos–ankstyvo pavasario oro temperatūros vegetacijos sezonas prasideda anksti, tačiau po to įsiveržia šaltas oras ir minimali paros oro temperatūra nukrinta žemiau 0 °C (Zscheischler ir kt., 2020). Dėl sparčiai kylančios žiemos bei pavasario mėnesių oro temperatūros Šiaurės pusrutulyje ypač ankstyva vegetacijos sezono pradžia fiksuojama vis dažniau (Allstadt ir kt., 2015; Zhu ir kt., 2019). Tai lemia ilgesnį vegetacijos sezoną ir gali atnešti naudos žemės ūkio sektoriui (Peterson & Abatzoglou, 2014). Tačiau dar devintajame praėjusio amžiaus dešimtmetyje nustatyta, kad ankstyvesnė vegetacijos sezono pradžia susijusi su palankesnėmis FS formavimosi sąlygomis (Cannell & Smith 1986), o FS rizikos didėjimas pastaraisiais dešimtmečiais fiksuotas ir skirtinguose regioniniuose tyrimuose (Allstadt ir kt., 2015; Bosdijk ir kt., 2024; Zahradníček ir kt., 2024). FS ypač neigiamai veikia žemės ūkio sektorių (Lamichhane, 2021), dėl jų poveikio gali būti prarandama didelė dalis ar net visas vaismedžių derlius – skaičiuojama, kad FS pasauliniu mastu sukelia nuostolių, galinčių siekti keletą milijardų eurų (Faust & Herbold, 2018; Ma ir kt., 2019). FS ne tik mažina įvairių ekosistemų produktyvumą (Hufkens ir kt., 2012; Zscheischler ir kt., 2020), bet turi ir antrinį neigiamą poveikį: kelia grėsmę įvairių gyvūnų buveinėms, žmonių

aprūpinimui maistu, sutrikdo CO_2 pasisavinimą bei paukščių migracijos kelius (Bateman, 2024; Chamberlain ir kt., 2019; Lamichhane, 2021).

CPWE identifikuojami, kai toje pačioje vietovėje tuo pat metu fiksuojamas ir vėjo greičio, ir kritulių kiekio ekstremumas. Tokių reiškinių formavimasis vidutinėse platumose Europoje dažniausiai siejamas su giliais Atlanto ciklonais bei orografiniu oro kilimu (Martius ir kt., 2016). Kaip ir CDHE, CPWE laikomi vienais daugiausia žalos padarančių ekstremalių klimato reiškinių, galinčių sukelti žmonių mirčių, daryti neigiamą poveikį ekosistemoms ir sutrikdyti kritinės infrastruktūros veikimą (Li ir kt., 2022). Dėl išaugusio kritulių kiekio ir stiprių vėjo gūsių taip pat padidėja nuošliaužų bei virstančių medžių pavojus (Martius ir kt., 2016; Xoplaki ir kt., 2023). Pastaraisiais dešimtmečiais reikšmingų CPWE pasikartojimo pokyčių Europoje nenustatyta (Johansson, 2021), tačiau prognozuojama, kad kintant klimatui jie taps dažnesni ir rytinėje, ir šiaurinėje žemyno dalyje (Ridder ir kt., 2022).

Nustačius dažniau pasikartojančių CCE tendenciją bei stiprų neigiamą socioekonominį poveikį, vis daugiau dėmesio skiriama prisitaikymo prie CCE bei jų padaromo neigiamo poveikio švelninimo strategijoms kurti (Chen ir kt., 2025; Muccione ir kt., 2024; Simpson ir kt., 2023). Tačiau nepaisant to, kad Baltijos jūros regione vidutinės oro temperatūros kilimas pastaraisiais dešimtmečiais buvo spartesnis nei pasauliniu mastu (Helsinki Commission, 2024), įvairūs ekstremalūs orų ir klimato reiškiniai regione iki šiol tirti atskirai. Taigi disertacijos rengimo metu atliktų tyrimų poreikį ir aktualumą pagrindžia nepakankamai išsamus CCE charakteristikų vertinimas rytinėje Baltijos jūros regiono dalyje.

Objektas, tikslas ir uždaviniai

Tyrimo teritorija – rytinė Baltijos jūros regiono dalis. Tyrimo objektas – regione būdingi kompleksiniai klimato įvykiai.

Darbo tikslas – įvertinti kompleksinių klimato įvykių susidarymo ir pasikartojimo ypatumus rytinėje Baltijos jūros regiono dalyje bei nustatyti galimus šių įvykių charakteristikų pokyčius iki XXI a. pabaigos.

Darbo uždaviniai:

1. Įvertinti kompleksinių klimato įvykių pasikartojimo bei intensyvumo pokyčius rytinėje Baltijos jūros regiono dalyje 1950–2022 m.
2. Išanalizuoti kompleksinių sausros ir karščio bangos įvykių, vėlyvų pavasario šalnų bei kompleksinių kritulių kiekio ir vėjo greičio ekstremumų susidarymą lemiančius veiksnius.

3. Prognozuoti kompleksinių klimato įvykių pasikartojimo, trukmės ir intensyvumo pokyčius iki XXI a. pabaigos.
4. Išanalizuoti kompleksinių klimato įvykių pasikartojimo erdvinius skirtumus tyrimo teritorijoje.

Naujumas ir aktualumas

CCE įvairiuose regionuose vis dažniau tiriami nustačius, kad jų neigiamas poveikis neretai viršija atskirų ekstremumų padaromą žalą (Brett ir kt., 2025; Zscheischler ir kt., 2020). Daugumos CCE pasikartojimo bei intensyvumo pokyčiai tiesiogiai ar netiesiogiai susiję su klimato kaita. Pavyzdžiui, pasaulinei temperatūrai pakilus 1 °C, prognozuojama, CDHE trukmė nuo 2020 iki 2100 m. pailgėtų dešimčia dienų (Zhang ir kt., 2022), o vis anksčiau prasidedant vegetacijos sezonui dienų su šalnomis skaičius išaugo 43 % Šiaurės pusrutulio teritorijos (Liu ir kt., 2018).

Įvairių CCE dažnėjimas numatomas ir ateityje. Prognozuojama, kad CDHE skaičius ir intensyvumas išaugs JAV (Rastogi ir kt., 2024) bei Kinijoje (Feng ir kt., 2023; Liu ir kt., 2024; Zhang ir kt., 2024). Tokia tendencija numatoma ir Australijoje (Chapman ir kt., 2025). Europoje XXI a. pabaigoje, palyginti su 1981–2010 m. laikotarpiu, CDHE paveikta teritorija, manoma, padidės 60 % (Dosio ir kt., 2023). CPWE skaičius turėtų išaugti pakrančių regionuose JAV rytuose, Rytų ir Pietų Azijoje (Yaddanapudi ir kt., 2022) bei Europoje, ypač šiaurinėje ir rytinėje žemyno dalyse (Ridder ir kt., 2022). Pasauliniu mastu prognozuojama tendencija, kad ateityje CPWE abejuose pusrutuliuose taps dažnesni regionuose, esančiuose aukščiau 50° platumos (Li ir kt., 2024). Šiltėjant klimatui kai kuriose vietovėse numatomas ir dažnesnis FS pasikartojimas (Allstadt ir kt., 2015; Hufkens ir kt., 2012; Lhotka & Brönnimann, 2020).

Tačiau kol kas dauguma CCE tyrimų yra sukoncentruoti Europoje, Azijoje ir Šiaurės Amerikoje (Brett ir kt., 2025). Tad išsami CCE analizė bei ateities projekcijų sudarymas skirtinguose regionuose sparčiai kintančio klimato kontekste tampa ypač svarbūs. Tokie tyrimai gali padėti geriau suprasti skirtingų CCE susidarymą bei sušvelninti jų padaromą žalą ateityje (Brett ir kt., 2025).

CCE rytinėje Baltijos jūros regiono dalyje iki šiol tirti menkai – daugiau tyrimų atlikta tik Lenkijoje. Čia buvo vertinti CDHE pasikartojimo ir intensyvumo pokyčiai 1966–2023 m. bei šių reiškinių susidarymą lemiantys veiksniai (Wibig & Jędruszkiewicz, 2024). Taip pat tirti FS įvykiai – analizuotas jų pasikartojimas ir intensyvumas bei atmosferos sąlygos, lemiančios šio CCE susiformavimą (Graczyk & Szwed, 2020; Koźmiński ir kt., 2023; Nidzgorska-Lencewicz ir kt., 2024; Piotrowski & Bartoszek, 2025).

Kitais atvejais šioje disertacijoje nagrinėjamų CCE dedamosios įvertintos tik atskirai. Įvairių CCE prognozės iki XXI a. pabaigos rytinėje Baltijos jūros regiono dalyje iki šiol taip pat nebuvo sudarytos. Nors ateities projekcijos buvo įvertintos atliekant pasaulinio ar Europos masto tyrimus (Dosio ir kt., 2023; Ford ir kt., 2025; Lhotka & Brönnimann 2020; Li ir kt., 2024; Ma ir kt., 2019; Zhu ir kt., 2024), jų rezultatai neatskleidžia specifinių CCE charakteristikų pokyčių šiame regione.

Šiame darbe pirmą kartą išsamiai įvertinti CDHE, FS ir CPWE pasikartojimo, trukmės bei erdvinio pasiskirstymo pokyčiai rytinėje Baltijos jūros regiono dalyje nuo praėjusio amžiaus vidurio (**I–III publikacijos**). Taip pat sudaryta tiriamų CCE identifikavimo metodika bei išanalizuoti procesai, lemiantys CCE susiformavimą tyrimo teritorijoje. Rengiant disertaciją pirmą kartą tyrimo teritorijoje įvertinti galimi FS (**IV publikacija**) bei CDHE ir CPWE charakteristikų pokyčiai iki XXI a. pabaigos. Darbe taip pat pasiūlyta FS intensyvumo vertinimo metodika (**II publikacija**), kuri gali būti pritaikoma ir kituose regionuose. Informacija apie CCE susidarymą bei pasikartojimą regione ateityje gali būti panaudota įvairios trukmės CCE prognozėms sudaryti ir gali prisidėti kuriant perspėjimo apie šiuos pavojingus reiškinius sistemas. Tyrimo metu gauti rezultatai leidžia pagerinti CCE sukeliamų rizikų supratimą pasauliniu mastu (Brett ir kt., 2025) bei padėti rengiant neigiamo poveikio mažinimo strategijas.

1. DUOMENYS IR METODIKA

1.1. Tyrimo teritorija

Kompleksiniai klimato įvykiai darbe tirti rytinėje Baltijos jūros regiono dalyje. Tyrimo teritoriją sudarė 0,25° × 0,25° dydžio gardelės, kurių centro taškai apima teritoriją nuo 53,5° iki 59,5° š. pl. ir nuo 20° iki 28,5° r. ilg (2 pav.). Kadangi darbe tiriamų CCE poveikis labiausiai pasireiškia sausumoje, CCE gardelėse, kurių daugiau nei 50 % ploto sudarė Baltijos jūra, nevertinti. Dėl minėtos priežasties pašalintos ir kelios gardelės ties Peipaus ežeru šiaurės rytinėje tyrimo teritorijos dalyje. Sausumos gardelės išskirtos naudojant specialų filtrą (Royal Netherlands..., n.d.). Tokiu būdu iš viso tyrimo teritoriją sudarė 668 gardelės (**I publikacija**). Vis dėlto, analizuojant FS ir CPWE, nustatyta, kad vienos pakrantės gardelės šiaurės vakarinėje Estijos dalyje reikšmės labai skyrėsi nuo aplinkinių gardelių duomenų, todėl, siekiant išvengti galimo rezultatų iškraipymo, ši gardelė iš analizės buvo pašalinta (**II–IV publikacijos**).

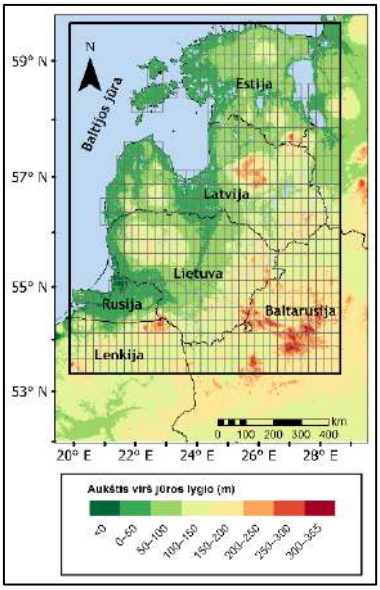

2 pav. Tyrimo teritorija ir jos reljefas. Pilki stačiakampiai žymi gardeles, kurių duomenys naudoti tyrime.

Tyrimo teritorijoje vyrauja žemumos ir lygumos, o aukščiausias taškas, virš jūros lygio iškilęs 355 m, yra pietrytinėje tiriamo arealo dalyje (2 pav.). Pagal atnaujintą Köppen'o–Geiger'io klimato klasifikaciją tyrimo teritorija priklauso *Dfb* klimato tipui: nėra išskiriamas sausasis sezonas, bent keturis

mėnesius vidutinė oro temperatūra yra aukštesnė nei 10 °C, tačiau nesiekia 22 °C, o šalčiausio mėnesio vidutinė temperatūra yra lygi 0 °C arba žemesnė (Beck ir kt., 2018).

Apskaičiuota, kad vidutinė metinė oro temperatūra 1991–2020 m. laikotarpiu regione siekė 7,0 °C ir nuo 1950 m. augo 0,23 °C per dešimtmetį. Šilčiausias mėnuo yra liepa (18,2 °C), o vėsiausias mėnuo – sausis (–3,4 °C). Vidutinės metinės oro temperatūros pasiskirstymą regione lemia platuma bei atstumas nuo jūros – didžiausios šio kintamojo reikšmės (8,0–8,6 °C) būdingos pietvakarinei tyrimo teritorijos daliai, o mažiausios (5,5–6,0 °C) – šiaurės rytinei.

Rytinė Baltijos jūros regiono dalis yra drėgmės pertekliaus zonoje – kritulių kiekis viršija garavimą (Kilkus & Stonevičius, 2011). Metinis kritulių kiekis 1991–2020 m. siekė 610–890 mm, o didžiausios reikšmės būdingos vakarinėje tyrimo teritorijos dalyje bei centrinėje Latvijoje. Didžiausias kritulių kiekis beveik visoje tyrimo teritorijoje fiksuojamas liepą ir rugpjūtį (vidutiniškai 82–86 mm per mėnesį). Vidutinis metinis vėjo greitis kinta nuo 3 m/s rytinėje tyrimo teritorijos dalyje iki 5,5–6 m/s šiaurės vakarinėje, o didžiausias vėjo greitis būdingas žiemai (gruodį–sausį).

1.2. Darbe panaudoti duomenys

CCE vertinti 1950–2022 m. laikotarpiu. Darbe tiriamiems CCE išskirti panaudoti Europos vidutinės trukmės orų prognozių centro (angl. *European Centre for Medium-Range Weather Forecasts – ECMWF*) ERA5 reanalizės paros vidutinės (t_{avg}), minimalios (t_{min}) ir maksimalios (t_{max}) oro temperatūros, paros kritulių kiekio (P) bei valandiniai maksimalaus vėjo greičio (w_{max}) duomenys. Duomenų gardelės dydis – 0,25° × 0,25° (**I–III publikacija**).

ERA5 reanalizė pasirinkta naudoti dėl ilgos duomenų sekos ir gana didelės erdvinės ir laiko skiriamosios gebos (Hersbach ir kt., 2020). Kuriant šios reanalizės duomenis naudojami palydovinių ir antžeminių stebėjimų bei orų radarų duomenys, todėl Europoje ERA5 duomenys kokybiškai atkartoja *in situ* matavimų rezultatus (Bell ir kt., 2021; Hersbach ir kt., 2020; Velikou ir kt., 2022). ERA5 reanalizės duomenų tikslumas sumažėja kalnuotose vietovėse (pvz., Skandinavijos kalnuose) ir tropikuose (Laurila, 2022; Lavers ir kt., 2022). Vis dėlto, tyrimo teritorija nepasižymi didele aukščio virš jūros lygio amplitude (aukščiausias taškas virš jūros lygio 355 m; 2 pav.), todėl ši problema nėra svarbi šio tyrimo kontekste.

Tyrimo metu skirtingų kintamųjų ERA5 duomenys buvo palyginti su Lietuvos hidrometeorologijos tarnybos duomenimis iš trijų meteorologijos stočių (Biržų, Ukmergės ir Varėnos). Šios stotys pasirinktos, nes jų

koordinatės geriausiai atitiko ERA5 gardelių centrų koordinates. Vertinant temperatūros rodiklius (vidutinę metinę oro temperatūrą, minimalią vasario–birželio temperatūrą, vasaros mėnesių minimalią paros oro temperatūrą) 1951–2022 m. laikotarpiu nustatytas glaudus ryšys – Pirsono koreliacijos koeficiento (r) reikšmės tyrimo teritorijoje vidutiniškai siekė 0,94–0,99 ($p <$ 0,001). Vidutinė absoliutinė paklaida (angl. *Mean Absolute Error – MAE*) t_{avg} atveju siekė 0,67–0,82 °C. *MAE* t_{min} ir t_{max} vertės kiek didesnės – atitinkamai 1,46–2,43 °C ir 1,17–1,91 °C. ERA5 reanalizės vėjo gūsių reikšmės taip pat gerai atitiko *in situ* matavimus (r = 0,77–0,83; *MAE* = 1,64–2,32 m/s; $p <$ 0,001). Ne toks glaudus ryšys nustatytas tik vertinant paros kritulių kiekį (r = 0,65–0,66; $p < 0,001$), o *MAE* reikšmės siekė 1,45–1,51 mm. Vis dėlto kritulių kiekis pasižymi dideliu lokalumu, o jo pasiskirstymui didelę įtaką turi įvairūs vietiniai veiksniai. Tai galėjo lemti didesnį ERA5 reanalizės ir meteorologijos stočių šio kintamojo duomenų neatitikimą.

Siekiant įvertinti darbe tiriamų CCE charakteristikų pokyčius iki XXI a. pabaigos panaudoti šeštosios susietųjų modelių palyginimo projekto fazės (angl. *Coupled Model Intercomparison Project Phase 6 – CMIP6*) globalių klimato modelių duomenys, gauti iš *NASA Earth Exchange Global Daily Downscaled Projections* (NEX-GDDP-CMIP6) duomenų bazės (Thrasher ir kt., 2022). Duomenų gardelės dydis – 0,25° × 0,25°, o laiko žingsnis – para. Vis dėlto, nepaisant vienodo gardelės dydžio, šios duomenų bazės taškų koordinatės nesutapo su ERA5 gardelės taškų koordinatėmis. Gardelės suvienodintos naudojant *R* programavimo kalbos paketo *akima* funkcijas (Akima ir kt., 2025), tad CCE charakteristikų ateities projekcijos sudarytos orientuojantis į tuos pačius 667 taškus, kuriuose jos buvo įvertintos ir 1950–2022 m. laikotarpiu.

NASA NEX-GDDP-CMIP6 duomenų bazėje iš viso pateikiami 35 CMIP6 modelių duomenys (Thrasher ir kt., 2022), tačiau tyrimo metu naudoti penki iš jų: CanESM5, ACCESS-CM2, GFDL-CM4, MPI-ESM1-2-LR ir NorESM2-MM. Jie pasirinkti siekiant atspindėti skirtingas modelių jautrumo spektro dalis (**IV publikacija**, **162 p.**).

Rengiant disertaciją naudotos dviejų bendrųjų socialinių ir ekonominių kelių (angl. *Shared Socioecnomic Pathways – SSP*) SSP2–4.5 ir SSP5–8.5 projekcijos (**IV publikacija, 163 p.**). SSP2–4.5 scenarijus nurodo „vidutinį“ kelią, pagal kurį XXI a. pabaigoje vidutinė globali paviršiaus oro temperatūra būtų 2,1–3,5 °C aukštesnė, palyginti su 1850–1900 m. laikotarpiu (Chen ir kt., 2021; Intergovernmental Panel..., 2021). Šiuo metu numatoma, kad iki 2100 metų temperatūra išaugs 1,9–3,7 °C, tad SSP2–4.5 scenarijus atrodo ypač tikėtinas (Hausfather, 2025). SSP5–8.5 numato pokyčius, kurie galėtų įvykti jei nebus imtasi jokių klimato kaitos švelninimo priemonių (Chen ir kt., 2021).

Šio scenarijaus atveju XXI a. pabaigoje globali vidutinė paviršiaus oro temperatūra išaugtų 3,3–5,7 °C, palyginti su priešindustriniu laikotarpiu (Intergovernmental Panel..., 2021). Tai pesimistinis scenarijus.

Svarbu pažymėti, kad NASA NEX-GDDP-CMIP6 duomenų bazėje nepateikiami w_{max} duomenys. Todėl siekiant įvertinti CPWE pokyčius ateityje, w_{max} reikšmės apskaičiuotos vidutinio paros vėjo greičio duomenims pritaikius vėjo gūsių faktorių (angl. *Wind Gust Factor – WGF*). Koeficientas nustatytas naudojant kasdienius w_{max} ir vidutinio vėjo greičio 1950–2022 m. laikotarpio ERA5 reanalizės duomenis. WGF apskaičiuotas w_{max} reikšmę dalijant iš vidutinio vėjo greičio vertės. Panaši WGF nustatymo metodika pasiūlyta dar praėjusiame šimtmetyje (Weggel, 1999) bei taikyta padidintos erdvinės skiriamosios gebos globalių bei regioninių klimato modelių w_{max} vertėms apskaičiuoti (Cheng ir kt., 2012). Atskirai nustatytas kiekvienos tyrimo teritorijos gardelės ir kiekvieno metų laiko koeficientas. Kiekvieno darbe naudoto modelio vidutinio vėjo greičio reikšmės buvo padaugintos iš WGF vertės; taip gautos w_{max} reikšmės iki XXI a. pabaigos.

FS projekcijos sudarytos iki XXI a. vidurio (2041–2060 m.) ir pabaigos (2081–2100 m.) (**IV publikacija**), o CDHE ir CPWE – tik iki paskutinio XXI a. dvidešimtmečio. Siekiant įvertinti darbe tiriamų CCE pasikartojimo, intensyvumo ir trukmės pokyčius ateityje pasirinktas 1995–2014 m. bazinis laikotarpis. 20 metų trukmės laikotarpiai naudoti rengiant pastarąją Tarpvyriausybinės klimato kaitos komisijos (angl. *Intergovernmental Panel on Climate Change – IPCC*) ataskaitą (Chen ir kt., 2021) bei plačiai taikyti kituose tyrimuose, kuriuose vertinami įvairių CCE charakteristikų pasikeitimai XXI a. (Chapman ir kt. 2025; Feng ir kt., 2023; Wang ir kt., 2023). Be to, tokios trukmės laikotarpis yra gana ilgas siekiant parodyti galimus įvairių kintamųjų ateities pokyčius sparčiai kintančio klimato sąlygomis ir gana trumpas, norint įvertinti tų kintamųjų skirtumus per XXI a. (Chen ir kt., 2021).

Globalių CMIP6 klimato modelių duomenys pasižymi žema ir nevienoda erdvine skiriamąją geba, įprastai siekiančia 80–250 km (European Centre..., 2021). Toks gardelės dydis nėra tinkamas regioniniams tyrimams. Būtent todėl šiame tyrime nuspręsta naudoti NASA NEX-GDDP-CMIP6 duomenų bazę. Sudarant šią duomenų bazę, CMIP6 modelių duomenims pritaikytas paklaidų korekcijos ir erdvinis išskaidymo metodas *(angl. Bias Correction Spatial Disaggregation – BCSD*), kuris leido sumažinti ir suvienodinti visų modelių gardelės dydį (Thrasher ir kt., 2022). Ši duomenų bazė plačiai pasitelkta tiriant ekstremalius hidrometeorologinius reiškinius įvairiuose regionuose, ji taip pat naudota sudarant skirtingų CCE projekcijas XXI a. (Ford ir kt., 2025; Xu ir kt., 2024; Zhang ir kt., 2024).

1.3. Kompleksinių klimato įvykių identifikavimas ir vertinimas

1.3.1. Kompleksinių sausros ir karščio bangos įvykių nustatymas

Siekiant išskirti CDHE, pirmiausia identifikuotos sausros ir karščio bangos. Sausroms nustatyti pasitelktas standartizuotas kritulių indeksas (angl. *Standardized Precipitation Index – SPI*) (McKee ir kt., 1993). Tyrimo metu, naudojant praėjusių 30 dienų kritulių kiekio sumą, apskaičiuotas kiekvienos tyrimo laikotarpio dienos SPI. Skaičiuojant SPI vertinamos įvairios trukmės kritulių kiekio sumos – nuo 1 iki 24 mėnesių (World Meteorological..., 2012). Vis dėlto, siekiant identifikuoti meteorologines sausras šiltuoju metų laiku, tiksliau nustatyti šių reiškinių pradžią ir pabaigą bei detaliau apibrėžti kompleksinius sausros ir karščio bangos įvykius, buvo pasirinktas 30 dienų skaičiavimo laikotarpis. SPI apskaičiuoti panaudotas R programavimo kalbos *SPEI* paketas (Beguería & Vicente-Serrano, 2023). Sausra atitinkamoje gardelėje identifikuota, kai SPI reikšmė buvo mažesnė už –1 (World Meteorological..., 2012) bent penkias dienas iš eilės (**I publikacija, 28 p**.).

Karščio bangos identifikuotos naudojant t_{max} 90-to percentilio reikšmes. Percentilių reikšmės atskirai skaičiuotos kiekvienoje tyrimo teritorijos gardelėje, o karščio banga nustatyta, kai percentilio vertė atitinkamoje gardelėje buvo viršyta ne mažiau kaip penkias dienas iš eilės. Penkių dienų kriterijus pasirinktas norint išvengti „statistinio triukšmo“ – naudojant trumpesnį laikotarpį, pavyzdžiui, tris dienas, atitinkamame tyrimo teritorijos taške 1950–2022 m. laikotarpiu gauta vidutiniškai 12 karščio bangos dienų per dešimtmetį – beveik trigubai daugiau nei taikant penkių iš eilės einančių dienų kriterijų. Be to, ilgesnis karščio bangos laikotarpio pasirinkimas grįstas ir galimu stipresniu poveikiu žmogaus sveikatai (Anderson & Bell, 2011; Kent ir kt., 2014). 1950–2022 m. laikotarpio 90-to percentilio reikšmės apskaičiuotos naudojant kiekvienos gardelės penkių dienų slankųjį vidurkį (**I publikacija, 28 p.**). Sudarant karščio bangų ir CDHE charakteristikų ateities projekcijas, minėta ribinė reikšmė kiekviename tyrimo teritorijos taške apskaičiuota orientuojantis į visą šiltąjį laikotarpį – balandžio–rugsėjo mėnesius.

Karščio bangoms identifikuoti pasirinkta 90-to t_{max} percentilio riba, atlikus jautrumo analizę taikant įvairias slenkstines vertes. Taikant 90-to percentilio ribą apskaičiuota, kad CDHE atitinkamoje gardelėje susidaro vidutiniškai 2,7 dienas per metus (1 lentelė). Todėl reiškinius galima laikyti gana ekstremaliais, tačiau kartu užtikrinamas ir pakankamas duomenų kiekis statistinei analizei atlikti. O naudojant aukštesnę slenkstinę reikšmę, pavyzdžiui, 95-ąjį percentilį, CDHE tyrimo teritorijoje tampa daug retesni –

vidutiniškai pasikartoja 1,4 dienas per vasarą (1 lentelė), o to jau nepakanka išsamiai statistinei kompleksinių reiškinių analizei. Analogiška 90-to t_{max} percentilio riba taip pat plačiai taikyta identifikuojant karščio bangas ir kituose Europos regionuose (Kim ir kt., 2018; Prodhomme ir kt., 2022; Rousi ir kt., 2022) bei globaliu mastu (Mukherjee ir kt., 2020; Ridder ir kt., 2020).

1 lentelė. Vidutinė maksimalios paros oro temperatūros reikšmė bei vidutinis kompleksinių sausros ir karščio bangos įvykių (CDHE) skaičius gardelėje vasaros metu, apskaičiuotas taikant skirtingas maksimalias paros oro temperatūros percentilių vertes.

Percentilis	**Vidutinė maksimalios paros oro temperatūros reikšmė** (°C)	**Vidutinis CDHE skaičius per vasarą**
85	24,4	3,8
90	25,4	2,7
95	26,6	1,4
98	27,9	0,6

CDHE identifikuoti kai tiek sausra, tiek karščio banga buvo fiksuota tuo pat metu. 1950–2022 m. laikotarpiu CDHE vertinti vasaros mėnesiais (**I publikacija, 29 p.**), o ateities projekcijos orientuotos į balandį–rugsėjį. Toks pasirinkimas grįstas klimato kaitos poveikiu. Ateityje dėl, numatoma, augsiančios $t_{max,}$ CDHE formuosis ne tik vasarą, bet, tikėtina, ir viso šiltojo sezono metu. 1950–2022 m. laikotarpiu tokių dienų pasikartojimo pokyčių statistinis reikšmingumas įvertintas naudojant Mann‘o–Kendall‘o kriterijų ($p < 0,05$), o sudarant prognozes iki XXI a. pabaigos – Mann‘o–Whitney–Wilcoxon‘o kriterijų ($p < 0,05$) (**I publikacija**).

Taip pat nustatyti ir CDHE laikotarpiai. Jie identifikuoti, kai CDHE maksimalaus išplitimo metu apėmė daugiau nei trečdalį tyrimo teritorijos (**I publikacija**). Nustatant CDHE laikotarpius siekta identifikuoti išskirtines dienas, kai toks kompleksinis klimato įvykis apėmė reikšmingą tyrimo teritorijos dalį. Atlikus jautrumo analizę apskaičiuota, kad taikant trečdalio tyrimo teritorijos kriterijų CDHE laikotarpiai sudarė 1,4 % visų tiriamojo laikotarpio dienų. Pritaikius 50 % gardelių ribą, ši dalis sumažėjo iki 0,9 %, o naudojant 20 % ir 25 % gardelių kriterijus, CDHE laikotarpiai sudarė atitinkamai 1,7–2,0 % visų tiriamojo laikotarpio dienų. Atsižvelgiant į šiuos rezultatus, trečdalio tyrimo teritorijos kriterijus pasirinktas kaip optimalus tolesnei analizei.

CDHE laikotarpio pradžia laikoma diena, kai kompleksinis klimato įvykis buvo fiksuotas daugiau nei 10 % gardelių, o pabaiga – kai sąlyga nebebuvo tenkinama bent tris dienas paeiliui (**I publikacija**). Šios sąlygos buvo įvestos siekiant išvengti atvejų, kai tik keliose gardelėse susiformavę CDHE reiškiniai dirbtinai pailgina CDHE laikotarpio trukmę bei situacijų, kai vos vieną dieną nefiksuoti CDHE sutapimai lemia naujo laikotarpio pradžią.

CDHE laikotarpių intensyvumas 1950–2022 m. įvertintas SPI vertėms bei t_{max} nuokrypių nuo 90-to percentilio reikšmėms pritaikius *Min–Max* normalizacijos metodą (**I publikacija, 28–29 p.**). Prieš taikant šį metodą, apskaičiuotos kiekvienos CDHE laikotarpiui priklausančios dienos SPI ir t_{max} anomalijų medianos. Skaičiavimai atlikti naudojant tik tas gardeles, kuriose buvo užfiksuotas CDHE. Siekiant įvertinti, ar duomenyse nėra reikšmingų išskirčių, buvo taikytas kvartilių skirtumo metodas. Analizė parodė, kad tiek t_{max} anomalijų, tiek SPI duomenų rinkiniuose nustatyta tik po vieną išskirtį. Tad *Min–Max* normalizacijos metodas laikytas tinkamu tolesnei analizei. Siekiant nustatyti CDHE intensyvumo pokyčius iki XXI a. pabaigos, atitinkamai apskaičiuotas 3 dienų SPI medianų vidurkis ir 3 dienų t_{max} nuokrypių nuo 90-ojo percentilio reikšmių vidurkis. Šiuo atveju *Min–Max* normalizacijos nuspręsta netaikyti dėl pernelyg didelio SPI ir t_{max} nuokrypių išskirčių skaičiaus.

1.3.2. Vėlyvų pavasario šalnų nustatymas

Siekiant nustatyti FS, pirmiausia kiekviename tyrimo teritorijos taške identifikuotos vegetacijos sezono pradžios (angl. *Start of the Growing Season – SGS*) ir paskutinės pavasario šalnos (angl. *Last Spring Frost – LSF*) datos. SGS data – pirma šešių iš eilės einančių dienų laikotarpio diena, kai visas šešias dienas $t_{avg} \geq 5$ °C (Swedish Meteorological..., 2024). LSF data – paskutinė diena kovą–birželį, kai $t_{min} < 0$ °C (**II publikacija**). 0 °C riba nustatant LSF datą bei vertinant jos poveikį įvairiems augalams, taip pat plačiai naudota kituose tyrimuose Europoje bei Baltijos jūros regione (Ceglar ir kt., 2019; Koźmiński ir kt., 2023; Wypych ir kt., 2017). Sudarant ateities projekcijas LSF datos nustatymo laikotarpis dėl, tikėtina, augsiančių žiemos bei pavasario mėnesių t_{min} reikšmių, pratęstas iki sausio–birželio (**IV publikacija**).

FS atitinkamoje gardelėje identifikuota, jei LSF fiksuota vėliau nei SGS (Allstadt ir kt., 2015; Chamberlain ir kt., 2019) (**II ir IV publikacijos**). Šie CCE tirti vasario–birželio mėnesiais. FS pasikartojimo pokyčių statistinis reikšmingumas nustatytas naudojant Stjudento kriterijų (**II ir IV publikacijos**).

Siekiant įvertinti FS intensyvumą 1950–2022 m. laikotarpiu panaudoti du kintamieji – iki įvykio sukaupta aktyviųjų temperatūrų (angl. *Growing Degree Days – GDD*) suma ir įvykio metu fiksuota t_{min}. Skaičiuojant aktyviųjų temperatūrų sumas naudota bazinė temperatūra, lygi 5 °C (McMaster & Wilhelm, 1997). Ši bazinė reikšmė GDD skaičiavimui naudota ir kituose tyrimuose (Koźmiński ir kt., 2023; Vitasse ir kt., 2019; Wypych ir kt., 2017).

Norint nustatyti FS intensyvumą GDD bei t_{min} reikšmės suskirstytos į tris kategorijas, iš kurių sudarytos devynios FS intensyvumo klasės (**II publikacija, 9355 p.,** 2 lentelė). Sudarant FS charakteristikų prognozes iki XXI a. pabaigos, intensyvumas įvertintas tik pagal GDD (**IV publikacija, 163 p.**). Dėl CMIP6 modelių minimalių oro temperatūrų (t_{min}) reikšmėms būdingo didelio neapibrėžtumo ir riboto patikimumo, vertinant būsimų FS reiškinių intensyvumą, nebuvo naudojamos konkrečios t_{min} vertės, fiksuotos jų susidarymo metu.

2 lentelė. Kategorijos, pagal kurias visos FS suskirstytos į devynias intensyvumo klases. t_{min} ir GDD – atitinkamai minimali paros oro temperatūra ir aktyviųjų temperatūrų suma.

Kintamasis	Kategorija	Ribinės vertės	Intensyvumo klasė
t_{min}, fiksuota FS metu	F1	$0\ °C > t_{min} \geq -2\ °C$	F1_GDD1, F1_GDD2, F1_GDD3, F2_GDD1, F2_GDD2, F2_GDD3, F3_GDD1, F3_GDD2, F3_GDD3.
	F2	$-2\ °C > t_{min} \geq -5\ °C$	
	F3	$t_{min} < -5\ °C$	
GDD, sukaupta iki FS	GDD1	$0\ °C < GDD \leq 100\ °C$	
	GDD2	$100\ °C < GDD \leq 200\ °C$	
	GDD3	$GDD > 200\ °C$	

1.3.3. Kompleksinių kritulių kiekio ir vėjo greičio ekstremumų nustatymas

Paros kritulių kiekio P ir maksimalaus vėjo greičio w_{max} ekstremumai išskirti, kai atitinkamo kintamojo reikšmė viršijo 98-ojo percentilio vertę. Atskirai apskaičiuotos kiekvienos gardelės percentilių reikšmės tyrimo teritorijoje. 98-ojo percentilio vertė pasirinkta atlikus jautrumo analizę. Taikant šią ribą, identifikuoti vidutiniai ir stiprūs ekstremumai bei gautas pakankamas duomenų kiekis statistinei analizei (3 lentelė). 98-ojo percentilio reikšmės, norint išskirti CPWE, taip pat naudotos ir kituose tyrimuose (Martius ir kt., 2016; Messmer & Simmonds, 2021). CPWE išskirtas, kai toje

pačioje gardelėje tuo pat metu fiksuotas ir kritulių kiekio, ir vėjo greičio ekstremumas. Šių CCE pasikartojimas atskirai įvertintas skirtingais metų laikais. Pokyčių statistinis reikšmingumas nustatytas naudojant Stjudento kriterijų ($p < 0,05$) (**III publikacija**).

Siekiant tyrimo teritorijoje išskirti pačius stipriausius CPWE, apskaičiuotos viso tyrimo laikotarpio P ir w_{max} 99,9-ojo percentilio reikšmės. Tada įvertinta, kiek per tyrimo laikotarpį buvo atvejų, kai abu kintamieji toje pačioje gardelėje viršijo šių percentilių vertes, nustatytas tokių atvejų pasikartojimas skirtingais sezonais bei erdvinis pasiskirstymas (**III publikacija**).

3 lentelė. Paros vidutinis kritulių kiekis, maksimalus vėjo greitis ir vidutinis kompleksinių kritulių bei vėjo greičio ekstremumų (CPWE) skaičius per dešimtmetį, apskaičiuotas taikant skirtingas paros kritulių kiekio ir maksimalaus vėjo greičio percentilių vertes.

Percentilis	Vidutinė kritulių kiekio reikšmė (mm/parą)	Vidutinė maksimalaus vėjo greičio reikšmė (m/s)	Vidutinis CPWE skaičius per dešimtmetį vienoje gardelėje
90	6,0	14,9	83,9
95	8,8	16,5	25,7
98	12,7	18,6	5,5
99	16,0	20,2	1,6

1.4. Kompleksinių klimato įvykių susiformavimą lemiančių atmosferos sąlygų vertinimas

Atmosferos cirkuliacijos sąlygos, vyravusios susiformuojant skirtingiems CCE, nustatytos taikant Heso–Brezovskio atmosferos cirkuliacijos tipų klasifikaciją (Muriset, n.d.; Werner & Gerstengarbe, 2010). Vertinant CPWE atvejus, nustatyta, kokie tipai vyravo, kai reiškinys tą pačią dieną fiksuotas daugiau nei penktadalyje gardelių. Susidarymą lėmę veiksniai nustatyti pasitelkiant papildomus duomenų šaltinius (Jungtinės Karalystės, Vokietijos ir Nyderlandų orų tarnybų sinoptines schemas, ERA5 reanalizės duomenis ir kt.) (**III publikacija, 5 p.**) Atmosferos sąlygos vertinant CPWE atskirai aptartos šiltuoju (balandžio–rugsėjo mėn.) bei šaltuoju (spalio–kovo mėn.) sezonais. Tiriant FS, įvertinta, kaip 1950–2022 m. laikotarpiu keitėsi skirtingų Heso–Brezovskio atmosferos cirkuliacijos tipų pasikartojimas. CDHE atveju

nustatyta, kokios sąlygos vyravo dienomis, kai CCE maksimalaus išplitimo metu apėmė daugiau nei trečdalį tyrimo teritorijos.

2. TYRIMŲ REZULTATAI

2.1. Kompleksiniai sausros ir karščio bangos įvykiai

1950–2022 m. daugiausia 33–36 CDHE įvykiai per dešimtmetį nustatyti rytinėje bei pietrytinėje tyrimo teritorijos dalyse (3a pav.). Toks erdvinis pasiskirstymas glaudžiai siejasi su sausros dienų pasikartojimo tendencijomis – didžiausias skaičius dienų, kai buvo fiksuotas CDHE, taip pat apskaičiuotas rytinėje tiriamo rajono dalyje (**I publikacija, 30 p.**). Per 73 metų laikotarpį CDHE skaičiaus didėjimo tendencija užfiksuota 73 % tyrimo teritorijos gardelių (3b pav.). Toks padidėjimas sietinas su visoje tyrimo teritorijoje išaugusiu karščio bangos dienų skaičiumi (**I publikacija, 31 p**.). Tačiau nustatyti CDHE pasikartojimo pokyčiai beveik visais atvejais nedideli ir pagal Mann‘o–Kendall‘o kriterijų statistiškai reikšmingi (p < 0,05) vos 1,9 % gardelių. Labiausiai CDHE skaičius (5 įvykiais per tyrimo laikotarpį) padidėjo Rytų Lietuvoje (3b pav.).

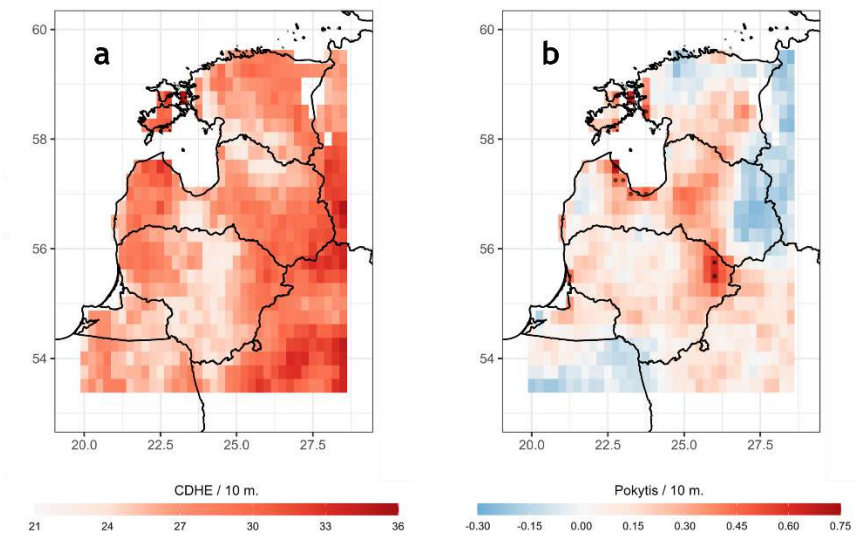

3 pav. Kompleksinių sausros ir karščio bangos įvykių (CDHE) skaičius per dešimtmetį rytinėje Baltijos jūros regiono dalyje (a) ir šių įvykių skaičiaus pokytis per dešimtmetį 1950–2022 m. laikotarpiu (b). Taškais pažymėtose gardelėse nustatyti pokyčiai yra statistiškai reikšmingi taikant Mann‘o–Kendall‘o kriterijų (p < 0,05).

Vasarą (nuo XX a. vidurio iki 2022 m.) rytinėje Baltijos jūros regiono dalyje nustatyta dešimt laikotarpių, kai CDHE maksimalaus išplitimo metu apėmė bent trečdalį tyrimo teritorijos (**I publikacija, 31 p.**). Beveik visi jie

identifikuoti antrojoje vasaros pusėje. Pusė CDHE laikotarpių išskirta paskutiniame XX a. dešimtmetyje. Ypač išsiskyrė 1994 metai, kai buvo nustatyti du tokie laikotarpiai, o CDHE besitęsęs nuo 1994 m. liepos 24 d. iki rugpjūčio 7 d., buvo ne tik pats ilgiausias (truko 15 dienų), bet ir maksimalaus išplitimo metu apėmė didžiausią tyrimo teritorijos dalį (94,2 %) bei buvo pats intensyviausias (**I publikacija, 31 p.**).

CDHE susidarymas regione siejamas su šiltų oro masių pernaša iš pietų ir pietryčių bei anticiklonine veikla. Nustatyta, kad pagal Heso–Brezovskio atmosferos cirkuliacijos tipų klasifikaciją darbe išskirtų CDHE laikotarpių metu dažniausiai vyravo pietinė cirkuliacija (SEA, SEZ, SA, SZ, TB, TRW tipai; 36 % dienų) bei anticiklono gūbrys (BM tipas; 30 % dienų).

Prognozuojama, kad XXI a. pabaigoje, palyginti su baziniu 1995–2014 m. laikotarpiu ir priklausomai nuo taikyto modelio ir scenarijaus, CDHE skaičius balandžio–rugsėjo mėnesiais išaugs daugiau nei 86 % gardelių (4 pav.).

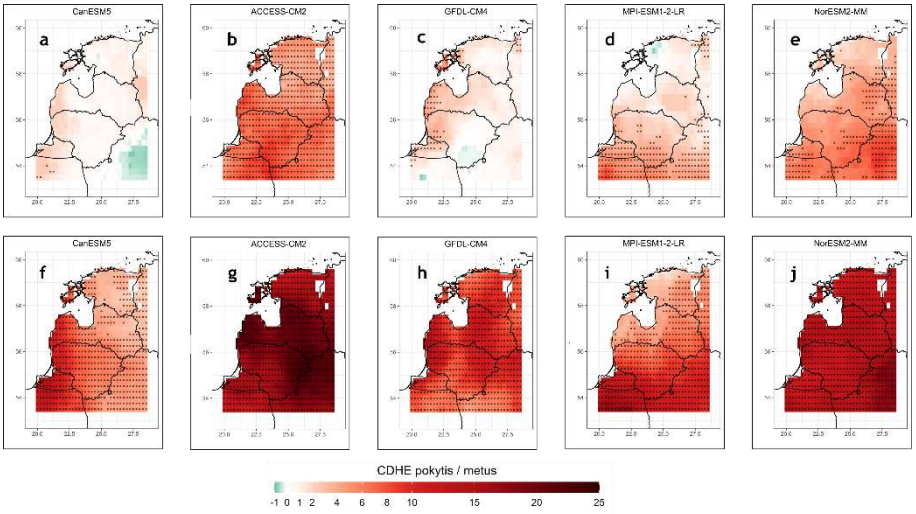

4 pav. Prognozuojamas kompleksinių sausros ir karščio bangos įvykių (CDHE) skaičiaus pokytis per metus tyrimo teritorijos gardelėse pagal penkių skirtingų CMIP6 modelių SSP2–4.5 (a–e) ir SSP5–8.5 (f–j) scenarijų duomenis, nustatytas lyginant 2081–2100 m. laikotarpį su baziniu 1995–2014 m. laikotarpiu. Taškais pažymėtos gardelės, kuriose pokyčiai yra statistiškai reikšmingi taikant Mann‘o–Whitney–Wilcoxon‘o kriterijų ($p < 0,05$).

Pagal SSP2–4.5 scenarijų pokytis sieks vidutiniškai 1–5 įvykius per metus, o pagal SSP5–8.5 – vidutiniškai 6–18 įvykių per metus (4 pav.). Tokį CDHE skaičiaus augimą nulems didėsianti maksimali paros oro temperatūra ir, prognozuojama, išaugsiantis karščio bangų dienų skaičius. Vis dėlto, pokyčių

mastą dažniausiai lems kritulių kiekio erdvinis pasiskirstymas. Būtent todėl didžiausias CDHE skaičiaus augimas XXI a. pabaigoje, palyginti su baziniu laikotarpiu, numatomas pagal ACCESS-CM2 modelio, prognozuojančio sparčiausią karščio bangos dienų skaičius augimą, ir NorESM2-MM modelio, numatančio ženklų sausros dienų skaičiaus pokytį, duomenis (4 pav.).

1995–2014 m. fiksuoti vos keturi CDHE laikotarpiai, kai šis reiškinys maksimalaus išplitimo metu apėmė bent trečdalį tyrimo teritorijos. Ateityje tokių laikotarpių skaičius reikšmingai išaugs. Numatoma, kad amžiaus pabaigoje per dvidešimtmetį susiformuos 11–19 (SSP2–4.5) ir 13–29 (SSP5–8.5) CDHE laikotarpiai, apimantys trečdalį teritorijos. Kita vertus, pagal CanESM5 ir GFDL-CM4 modelių SSP2–4.5 scenarijaus projekcijas numatomi daug mažesni pokyčiai. Išaugs ir CDHE trukmė. Baziniu laikotarpiu trukę vidutiniškai 9 dienas, XXI a. pabaigoje šie reiškiniai, prognozuojama, užsitęs vidutiniškai 10–20 dienų pagal SSP2–4.5 ir 15–33 dienas pagal SSP5–8.5. Išsiplės ir maksimalaus išplitimo metu apimta tyrimo teritorijos dalis. Kaip ir 1950–2022 m. laikotarpiu, prognozuojama, kad ateityje CDHE (33,3–79,4 % visų įvykių) dažniausiai susidarys šiltojo sezono pabaigoje.

2.2. Vėlyvos pavasario šalnos

1950–2022 m. laikotarpiu SGS data rytinėje Baltijos jūros regiono dalyje paankstėjo visoje tyrimo teritorijoje (vidutiniškai 10,6 dienomis), o statistiškai reikšmingi pokyčiai pagal Mann‘o–Kendall‘o kriterijų ($p < 0,05$) gauti 73,9 % gardelių (**II publikacija, 9355 p.**). LSF datos ankstėjimas taip pat užfiksuotas beveik visoje tyrimo teritorijoje (99,4 % gardelių), tačiau pokyčiai šiuo atveju mažesni. Vidutiniškai per 73 metų laikotarpį LSF data paankstėjo beveik savaite (6,3 dienomis), o pokyčiai statistiškai reikšmingi 21,3 % gardelių ($p < 0,05$) (**II publikacija, 9355–9356 p.**). Tokie datų poslinkiai lėmė palankesnių FS susidarymo sąlygų atsiradimą, o tai patvirtina ir LSF ir SGS datų skirtumo pokyčiai 1950–2022 m. Apskaičiuota, kad šis skirtumas išaugo 85,9 % gardelių, vis dėlto, statistiškai reikšmingi pokyčiai ($p < 0,05$) identifikuoti tik 4,8 % tyrimo teritorijos ploto (5a pav.).

Lyginant pasikartojimą laikotarpio pradžioje (1950–1969 m.) ir pabaigoje (2003–2022 m.) apskaičiuota, kad FS skaičius padidėjo beveik visame tiriamame regione (85,9 % gardelių). Didžiausias augimas nustatytas rytinėje tyrimo arealo dalyje bei Pietvakarių Lietuvoje, o statistiškai reikšmingi pokyčiai nustatyti 30 % gardelių (5b pav.). Apskaičiuota, kad per visą tyrimo laikotarpį dažniausiai FS pasikartojo centrinėje Estijoje bei pietvakarinėje regiono dalyje (**II publikacija, 9357 p.**).

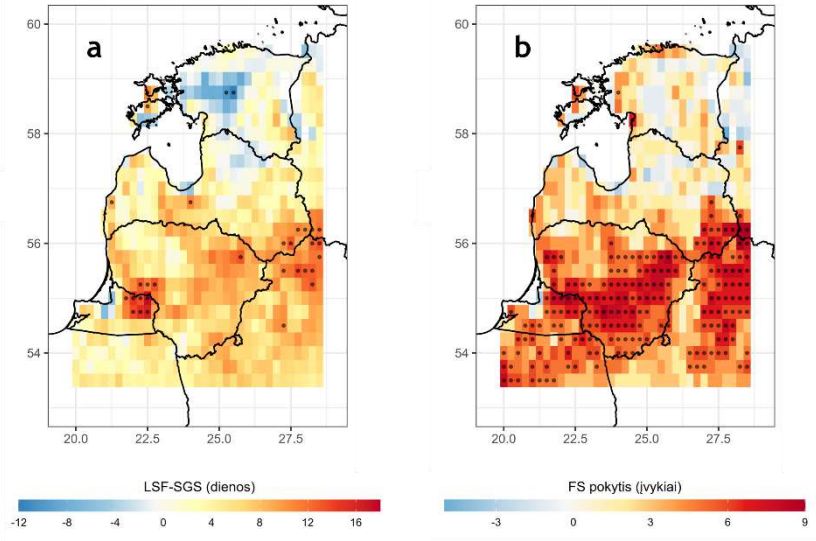

5 pav. Paskutinės pavasario šalnos (LSF) ir vegetacijos sezono pradžios (SGS) datų skirtumo pokytis (dienomis) tyrimo rajono gardelėse 1950–2022 m. (a) ir vėlyvų pavasario šalnų (FS) skaičiaus pokytis, gautas lyginant 2003–2022 m. ir 1950–1969 m. laikotarpius (b). Taškais pažymėtos gardelės, kuriose pokyčiai yra statistiškai reikšmingi ($p < 0,05$) taikant Mann'o–Kendall'o kriterijų (a) ir Stjudento kriterijų (b).

Apskaičiuota, kad 1950–2022 m. laikotarpiu vidutiniškai iki FS buvo sukaupta 67,3 °C GDD. Didžiausia sukauptų GDD mediana (69–72 °C) nustatyta pietvakarinėje tyrimo teritorijos dalyje, Vakarų Latvijoje ir Centrinėje Estijoje. Lyginant 1950–1969 ir 2003–2022 m. laikotarpius, GDD mediana išaugo 56,1 % gardelių, o didžiausias šio rodiklio reikšmių augimas nustatytas pietinėje tyrimo teritorijos dalyje (**II publikacija, 9358–9359 p.**).

Įvertinus FS intensyvumą pagal iki šio reiškinio sukauptas GDD sumas ir įvykio metu fiksuotą t_{min} reikšmę (1 lentelė), reikšmingų pokyčių nenustatyta. Žemiausiai intensyvumo kategorijai priklausė 65,5 % FS atvejų. Pats stipriausias reiškinys, kurio metu buvo sukaupta daugiau nei 200 °C GDD, o t_{min} reikšmė nukrito žemiau –2 °C, užfiksuotas 1975 m. šiaurinėje tiriamo regiono dalyje (**II publikacija, 9359 p.**).

FS susidarymas dažniausiai siejamas su šaltų arktinių oro masių advekcija iš šiaurės vakarų, šiaurės ir šiaurės rytų (Bielec-Bąkowska & Twardosz, 2023; Tomczyk ir kt., 2019). Tačiau 1950–2022 m. laikotarpiu, taikant Heso–Brezovskio klasifikaciją, reikšmingų šiaurės–šiaurės rytų atmosferos cirkuliacijos tipų (NEA, NEZ, HFA, HFZ, HNFA, HNFZ) pasikartojimo pokyčių neužfiksuota.

XXI a. pabaigoje, palyginti su baziniu 1995–2014 m. laikotarpiu, numatomas tolesnis SGS datos ankstėjimas. 2041–2060 m. toks pokytis sieks vidutiniškai 5–14,5 dienos (SSP2–4.5) ir 3–17,5 dienos (SSP5–8.5), o amžiaus pabaigoje – atitinkamai 9,5–27 (SSP2–4.5) ir 21–43 dienas (SSP5–8.5) (**IV publikacija, 164–165 p.**). Prognozuojama, kad LSF data ateityje paankstės. Palyginti su baziniu laikotarpiu, XXI a. viduryje pokyčiai sieks vidutiniškai 8–22 dienas (SSP2–4.5) ir 5,5–26,5 dienos (SSP5–8.5), o 2081–2100 m. laikotarpiu – 7–38 (SSP2–4.5) ir 14–53,5 dienos (SSP5–8.5) (**IV publikacija, 164–165 p.**).

Priešingai nei SGS ir LSF, prognozuojami FS pokyčiai ateityje yra labiau neapibrėžti. Pagal SSP2–4.5 scenarijų dauguma modelių XXI a. viduryje numato šių įvykių pasikartojimo mažėjimą. Panašios tendencijos nustatytos ir pagal SSP5–8.5 projekcijas (**IV publikacija, 165–166 p.**). FS pokyčių prognozės XXI a. pabaigoje nepasižymi vieninga tendencija. Remiantis dviejų darbe taikomų modelių duomenis, didesnėje tyrimo teritorijos dalyje prognozuojamas FS skaičiaus augimas, o pagal likusius – mažėjimas (6 pav.).

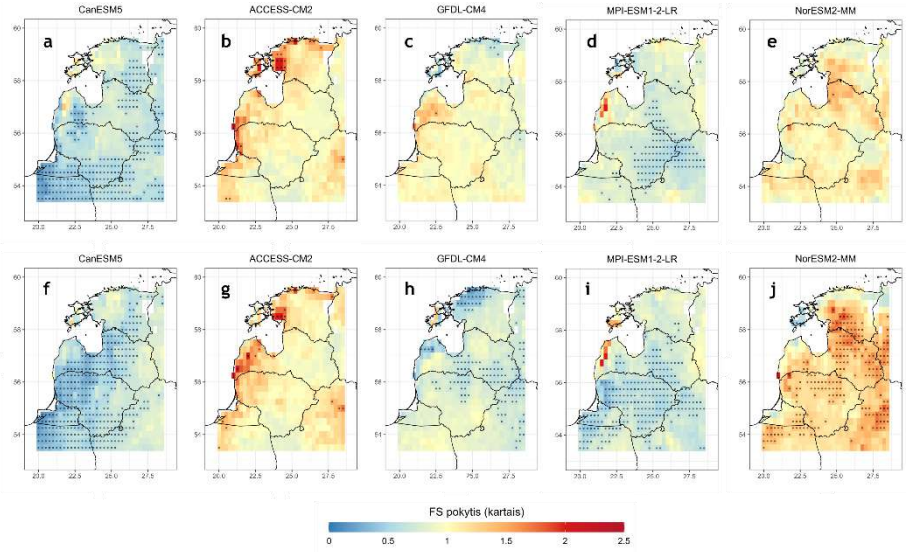

6 pav. Prognozuojamas vėlyvų pavasario šalnų (FS) skaičiaus pokytis kiekvienoje tyrimo teritorijos gardelėje, remiantis penkių skirtingų CMIP6 modelių SSP2–4.5 (a–e) ir SSP5–8.5 (f–j) scenarijų duomenimis, gautais lyginant 2081–2100 m. laikotarpį su baziniu 1995–2014 m. laikotarpiu. Taškais pažymėtos gardelės, kuriose pokyčiai yra statistiškai reikšmingi taikant Stjudento kriterijų ($p < 0,05$).

FS intensyvumo pokyčiai ateityje įvertinti apskaičiavus iki atitinkamo įvykio sukauptą GDD sumą. Pagal SSP2–4.5 scenarijų 2041–2060 m. ir 2081–2100 m. laikotarpiais dauguma modelių prognozuoja šio rodiklio reikšmių mažėjimą. Pagal SSP5–8.5 scenarijų tokia tendencija prognozuojama remiantis trijų modelių (CanESM5, GFDL-CM4 ir MPI-ESM1-2-LR) duomenimis (**IV publikacija, 166–167 p.**). Tačiau pagal ACCESS-CM2 ir NorESM2-MM modelius numatomas iki įvykio sukaupiamos GDD augimas bei didėsiantis atvejų, kai iki FS buvo sukaupta daugiau nei 200 °C GDD (aukščiausia GDD intensyvumo kategorija; 2 lentelė), skaičius (**IV publikacija, 167 p.**).

2.3. Kompleksiniai kritulių kiekio ir vėjo greičio ekstremumai

1950–2022 m. dažniausiai (17,9 % atvejų) CPWE pasikartojo spalį, o rečiausiai šie reiškiniai užfiksuoti pavasarį (**III publikacija, 7 p.**). Daugiausia tokių ekstremumų per 73 metų laikotarpį išskirta Vakarų Lietuvoje (10–11 įvykių per dešimtmetį). Būtent nurodytoje tyrimo teritorijos dalyje CPWE dažniausiai kartojosi ir šaltuoju metų sezonu, t. y. spalio–kovo mėnesiais (7a pav.). Šiltuoju laikotarpiu (balandžio–rugsėjo mėnesiais) CPWE pasiskirstymas buvo tolygesnis (7b pav.).

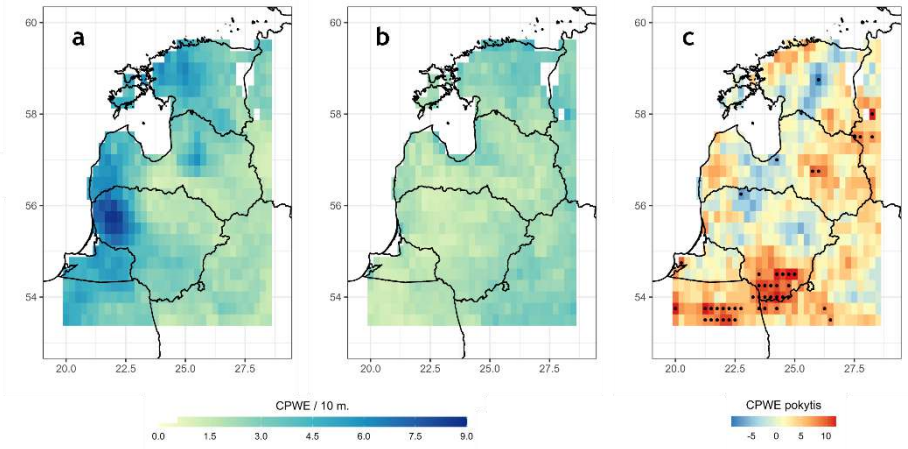

7 pav. Kompleksinių kritulių kiekio ir vėjo greičio ekstremumų (CPWE) atvejų skaičius per dešimtmetį šaltuoju (spalio–kovo mėn.) (a) ir šiltuoju (balandžio–rugsėjo mėn.) (b) laikotarpiais. CPWE skaičiaus pokytis, nustatytas lyginant 2003–2022 m. ir 1950–1969 m. laikotarpius (c). Taškais pažymėtos gardelės, kuriose pokyčiai yra statistiškai reikšmingi taikant Stjudento kriterijų ($p < 0,05$).

Taip pat nustatyta, kad per 1950–2022 m. laikotarpį CPWE atvejų skaičius rytinėje Baltijos jūros regiono dalyje nežymiai išaugo, tačiau šis pokytis statistiškai nereikšmingas ($p < 0,05$) (**III publikacija, 7 p.**). Vis dėlto, įvertinus pasikartojimą tyrimo teritorijos gardelėse 1950–1969 m. ir 2003–2022 m. laikotarpiais, apskaičiuota, kad CPWE skaičius padidėjo 70,2 % gardelių. Statistiškai reikšmingi ($p < 0,05$) didžiausi (10–12 atvejų) pokyčiai nustatyti pietinėje ir pietvakarinėje tyrimo teritorijos dalyse (7c pav.), o labiausiai (65,5 % gardelių) CPWE skaičius išaugo vasarą (**III publikacija, 8–9 p.**).

Identifikuotos vos keturios dienos, kai ir maksimalaus vėjo greičio w_{max}, ir paros kritulių kiekio P reikšmės viršijo 99,9-ojo percentilio vertes daugiau nei 1 % tyrimo teritorijos. Šiomis dienomis fiksuoti ypač ekstremalūs CPWE. Visi šie atvejai užfiksuoti liepos pabaigoje ir rugpjūčio pirmąjį dešimtadienį (**III publikacija, 9–10 p.**).

Dažniausiai tą pačią dieną CPWE fiksuoti tik vienoje ar keliose gardelėse. Iš viso išskirtos 44 dienos, kai CCE apėmė daugiau nei penktadalį tyrimo teritorijos (**III publikacija, 10 p.**). Būtent šie CPWE analizuoti siekiant nustatyti jų susidarymą lemiančias atmosferos sąlygas. Nustatyta, kad šaltuoju laikotarpiu CPWE susiformavimas sietinas su stipria zonine pernaša iš vakarų (WZ tipas) ir gilių Atlanto ciklonų pietinėje periferijoje greitai besivystančia frontine sistema. Šiltuoju laikotarpiu tokius reiškinius rytinėje Baltijos jūros regiono dalyje įprastai nulemia tyrimo teritoriją pasiekiantys pietiniai ciklonai, kurie lėmė ir pačių intensyviausių CPWE susidarymą (**III publikacija, 10–12 p.**).

Prognozuojama, kad ateityje CPWE skaičius rytinėje Baltijos jūros regiono dalyje išaugs. Palyginus 2081–2100 m. su baziniu 1995–2014 m. laikotarpiu, remiantis visų modelių prognozėmis tokia tendencija numatoma daugiau nei pusėje tyrimo teritorijos (8 pav.). Vis dėlto, numatomi pokyčiai nėra dideli, o visais atvejais CPWE skaičiaus statistiškai reikšmingas ($p < 0,05$) pokytis prognozuojamas mažiau nei ketvirtyje tyrimo teritorijos (8 pav.). Šioms prognozėms būdingi neapibrėžtumai pirmiausia sietini su vėjo gūsių faktoriaus naudojimu w_{max} reikšmėms nustatyti.

Tikėtina, kad dažnesnį CPWE pasikartojimą ateityje nulems didėsiantis kritulių kiekio ekstremumų skaičius, numatomas, remiantis visų darbe naudotų modelių projekcijų duomenimis. Maksimalaus vėjo greičio ekstremumų skaičiaus pokyčiai ateityje yra labiau neapibrėžti. Dalis modelių (GFDL-CM4, MPI-ESM1-2-LR) prognozuoja, kad tokie ekstremumai ateityje pasitaikys dažniau, o likę numato mažėjimą.

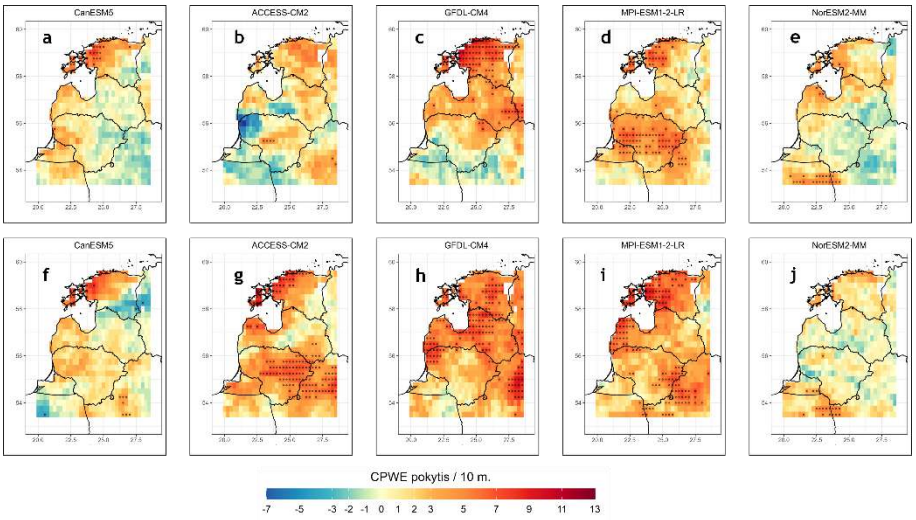

8 pav. Kompleksinių kritulių kiekio ir vėjo greičio ekstremumų (CPWE) skaičiaus pokytis per dešimtmetį lyginant 2081–2100 m. ir 1995–2014 m. laikotarpius, remiantis skirtingų CMIP6 klimato modelių SSP2–4.5 ir SSP5–8.5 scenarijų duomenimis. Taškais pažymėtos gardelės, kuriose pokyčiai statistiškai reikšmingi taikant Mann‘o–Whitney–Wilcoxon‘o kriterijų ($p < 0,05$).

Tikėtina, jog ateityje išliks tendencija, kad daugiau CPWE susidarys šaltuoju metų laiku, ypač rudenį. XXI a. pabaigoje padidės ir dienų skaičius, kai CPWE apims daugiau nei trečdalį tyrimo teritorijos. Pagal SSP2–4.5 scenarijų tokių dienų 2081–2100 m. prognozuojama 6–12, pagal SSP5–8.5 scenarijų – 6–11 per dvidešimtmetį. 1995–2014 m. laikotarpiu, remiantis ERA5 reanalizės duomenis, išskirtos penkios tokios dienos.

Prognozuojama, kad XXI a. pabaigoje pagal daugumos darbe taikytų modelių duomenis dienų skaičius, kai bent 1 % tyrimo teritorijos susidarys ypač intensyvūs CPWE (kurių metu tiek w_{max}, tiek P reikšmės viršys 99,9-to percentilio vertes), nepakis. Baziniu laikotarpiu nustatytos trys tokios dienos, o XXI a pabaigoje numatomos 1–3 (SSP2–4.5) ir 2–4 dienos (SSP5–8.5). Tik pagal GFDL-CM4 modelio abiejų SSP scenarijų projekcijas gauta 10 dienų su ypač stipriais CPWE. Vis dėlto, kadangi ypač intensyvūs CPWE ateityje pasikartos labai retai, šie rezultatai pasižymi gana dideliu neapibrėžtumu.

REZULTATŲ APTARIMAS

1950–2022 m. laikotarpiu CDHE skaičius padidėjo beveik 75 % gardelių. Dažnesnis šių įvykių pasikartojimas pirmiausia sietinas su dėl klimato kaitos išaugusia t_{max} bei tyrimo teritorijoje reikšmingai ($p < 0,05$) padidėjusiu karščio bangų dienų skaičiumi. Vis dėlto, apskaičiuoti CDHE pasikartojimo pokyčiai beveik visose gardelėse buvo nedideli. Tokią situaciją lėmė daugumoje gardelių (89 %) per tyrimo laikotarpį sumažėjęs sausros dienų skaičius (**I publikacija**).

Dauguma tyrimo laikotarpiu nustatytų CDHE buvo išskirti antroje vasaros pusėje, o tokia tendencija sietina su dažnesniu karščio bangų susidarymu liepos pabaigoje ir rugpjūčio mėnesio pradžioje. CDHE skaičiaus augimo tendencija pastaraisiais dešimtmečiais būdinga daugeliui Šiaurės pusrutulio vidutinių platumų regionų (Ridder ir kt., 2020), o pokyčiai dėl spartesnio oro temperatūros augimo didesni nei Pietų pusrutulyje (Mukherjee & Mishra, 2021). CDHE vis dažniau pasikartoja ir šiaurinėje bei centrinėje Europoje (Bezak & Mikoš, 2020; Wibig & Jędruszkiewicz 2024).

XXI a. pabaigoje, palyginti su 1995–2014 m. laikotarpiu, rytinėje Baltijos jūros regiono dalyje numatomas CDHE trukmės ir intensyvumo didėjimas. Remiantis SSP5–8.5 scenarijumi ši tendencija ypač ryški, o pokyčiai didžiojoje tyrimo teritorijos dalyje statistiškai reikšmingi ($p < 0,05$). Pagrindinis CDHE skaičiaus didėjimą lemsiantis veiksnys bus išaugsiantis karščio bangų dienų skaičius. Numatoma, kad palyginti su baziniu laikotarpiu, XXI a. pabaigoje jų skaičius išaugs vidutiniškai 23–44 dienomis (SSP2–4.5 scenarijus) ir 28–84 dienomis (SSP5–8.5 scenarijus) per metus. Tačiau toks nemažas karščio bangų dienų pasikartojimo pokytis lems, kad beveik visos sausros, susidarysiančios XXI a. pabaigoje, sutaps su šiuo reiškiniu (Bevacqua ir kt., 2022). Todėl CDHE pasikartojimo pokyčių mastas priklausys nuo kritulių kiekio ir sausrų erdvinio pasikartojimo tendencijų. Ypatingai svarbu pažymėti, kad t_{max} 90-ojo percentilio reikšmės, kurios naudotos ateities karščio bangoms identifikuoti, XXI a. pabaigoje kintant klimatui taps įprastos. Ribinė vertė, taikyta karščio bangoms identifikuoti, priklausomai nuo modelio vidutiniškai padidės 1,9–5,3 °C (SSP2–4.5 scenarijus) ir 4,3–9,6 °C (SSP5–8.5 scenarijus). Taigi, tikėtina, kad visuomenė bei ekosistemos gebės prisitaikyti prie pasikeitusių klimato sąlygų. Todėl nepaisant gana didelio karščio bangos dienų skaičiaus bei CDHE pasikartojimo augimo, šių reiškinių sukeliamo neigiamo poveikio pokyčiai ateityje gali būti ne tokie dideli.

1950–2022 m. laikotarpiu išaugusi vasario–balandžio mėnesių oro temperatūra lėmė SGS datos ankstėjimą visoje tyrimo teritorijoje (**II publikacija, 9355 p.**). Dėl klimato kaitos nulemtos padidėjusios oro

temperatūros antroje žiemos pusėje bei ankstyvo pavasario LSF data per 73 metų laikotarpį taip pat paankstėjo. Tačiau nustatytas pokytis mažesnis nei SGS atveju, o 1950–2022 m. laikotarpiu beveik visoje tyrimo teritorijoje išaugusi laikotarpio tarp LSF ir SGS datų trukmė nulėmė palankesnes FS formavimosi sąlygas (**II publikacija, 9356 p.**). Didžiausi ir statistiškai reikšmingi pokyčiai apskaičiuoti tose vietovėse, kuriose pavasario oro temperatūra didėjo sparčiausiai. Visgi didžiojoje tyrimo teritorijos dalyje reikšmingų FS pasikartojimo pokyčių nenustatyta. Reikšmingų vėlyvų pavasario šalnų rizikos pokyčių pastaraisiais dešimtmečiais taip pat nenustatyta ir Lenkijoje atliktuose tyrimuose (Graczyk & Szwed, 2020; Koźmiński ir kt., 2023).

Dėl šildančio Baltijos jūros poveikio pakrantės žemumose LSF data vidutiniškai buvo fiksuota keliomis savaitėmis ar net mėnesiu anksčiau nei likusioje tyrimo teritorijos dalyje. Todėl Baltijos jūros pakrantėje FS pasitaikė retai – iki dviejų kartų per dešimtmetį, o tolstant į žemyno gilumą jų skaičius sparčiai išaugo iki 7–8 įvykių per dešimtmetį. Tokia tendencija būdinga ne tik šiame darbe analizuojamai teritorijai, bet ir kitiems regionams (Zohner ir kt., 2020).

Ateityje rytinėje Baltijos jūros regiono dalyje numatomas SGS datos ankstėjimas. Priklausomai nuo taikyto modelio ir scenarijaus vegetacijos sezonas XXI a. pradžioje turėtų prasidėti 3–6 savaitėmis anksčiau nei 1995–2014 m. (**IV publikacija, 164 p.**). Prognozuojama, kad vis anksčiau susidarys ir LSF. Numatoma, kad pokytis 2081–2100 m., palyginti su baziniu laikotarpiu, sieks vidutiniškai 1–6 savaites (**IV publikacija, 165 p.**). Tačiau, nepaisant to, kad pagal visų darbe taikytų modelių duomenis rytinėje Baltijos jūros regiono dalyje numatomas tiek SGS, tiek LSF datų ankstėjimas, FS pasikartojimo prognozės ateityje nėra vienareikšmės. Dalis modelių numato FS skaičiaus didėjimą, kiti – mažėjimą (**IV publikacija, 165–166 p.**). Tai susiję su tuo, kad skirtingi modeliai prognozuoja nevienodą LSF ir SGS datų kaitos greitėjimą. Todėl, jei spartesnis oro temperatūros augimas numatomas žiemos pabaigoje ar ankstyvą pavasarį, FS skaičius padidėtų. Tačiau jei oro temperatūros reikšmės labiau didės antroje pavasario pusėje, šių reiškinių pasikartojimas, tikėtina, sumažės. Panašios, dideliu neapibrėžtumu pasižyminčios FS charakteristikų ateities prognozės gautos ir kituose regionuose (Allstadt ir kt., 2015; Lhotka & Brönnimann, 2020; Mallard ir kt., 2023; Martinuzzi ir kt., 2019).

CPWE pasikartojimo pokyčiai 1950–2022 m. laikotarpiu sietini su klimato kaita. Nustatyta, kad kritulių kiekio ekstremumų skaičius padidėjo visoje tyrimo teritorijoje. Daugelyje gardelių w_{max} ekstremumų skaičius taip pat padidėjo. Vis dėlto, pokyčiai daugeliu atvejų buvo nedideli, todėl statistiškai

reikšmingo CPWE skaičiaus augimo per 73 metų laikotarpį nenustatyta. Reikšmingo CPWE skaičiaus augimo nenustatyta ir Skandinavijoje, Kinijoje bei Iberijos pusiasalyje (He ir kt., 2025; Hénin ir kt., 2021; Johansson, 2021). Palyginus 1950–1969 m. ir 2003–2022 m. laikotarpių duomenis, nustatyta, kad CPWE skaičius labiausiai padidėjo vasarą (**III publikacija**), tai sietina su kylančia vasaros mėnesių oro temperatūra bei didėjančiu vandens garų kiekiu ore, stiprinančiais atmosferos konvekciją, kurios pasekmė – lokalūs P ir w_{max} ekstremumai. CPWE erdviniam pasiskirstymui tyrimo teritorijoje, ypač šaltuoju metų laiku, didžiausią poveikį turi atstumas nuo Baltijos jūros bei reljefas. Todėl dažniausiai CPWE buvo fiksuojami Vakarų Lietuvoje, priešvėjiniuose Žemaičių aukštumos šlaituose. Didesnis CPWE skaičius nei aplinkinėse vietovėse nustatytas ir Vidurio Latvijos aukštumose (**III publikacija, 7 p.**).

XXI a. pabaigoje pagal taikytų modelių prognozes numatoma, kad CPWE skaičius, palyginti su baziniu 1995–2014 m. laikotarpiu, padidės daugiau nei pusėje tyrimo teritorijos. CPWE, tikėtina, ir toliau dažniau bus fiksuojamas šaltuoju metų laiku. Dažnesnis CPWE pasikartojimas ateityje, tikėtina, bus nulemtas didėjančio garavimo, dažnesnių kritulių kiekio ekstremumų ir tropinių bei vidutinių platumų ciklonų trajektorijų pokyčių (Li ir kt., 2024; Seneviratne ir kt., 2021).

Skirtingų CCE susidarymas priklauso nuo atmosferoje vykstančių procesų ir jų dinamikos. CDHE Europoje įprastai siejami su anticiklonine cirkuliacija ir blokuojančių darinių susiformavimu (Ionita ir kt., 2021; Spensberger ir kt., 2020), kurie susilpnina zoninę pernašą bei keičia ciklonų trajektorijas ir nukreipia juos piečiau. Taip pat aukšto slėgio dariniai slopina aukštyneigius oro srautus, sumažina vandens garų kiekį ir silpnina kritulių formavimąsi (Ionita ir kt., 2021). Tokiu būdu sudaromos ypač palankios sausrų ir karščio bangų vystymosi sąlygos. Tokia tendencija nustatyta ir šiame darbe – daugumą dienų, kai buvo fiksuoti tokie CCE, tyrimo teritorijoje vyravo anticiklono gūbrys arba oro masių pernaša iš pietų–pietryčių, kuri sietina su šilto oro patekimu į Baltijos šalis. CDHE formavimasis glaudžiai siejasi ne tik su lokaliais procesais atmosferoje, bet ir su didesnio masto atmosferos cirkuliacija. Nustatyta, kad Lenkijoje karščio bangų susidarymas sutampa su giliu Azorų anticiklonu ir stipria blokuojančia sistema virš Šiaurės Atlanto (Wibig, 2017).

FS įvykių susidarymas taip pat siejamas su blokuojančiais anticiklonais ir teigiamomis atmosferos slėgio jūros lygyje anomalijomis. Pavasarį tokie dariniai neretai lemia šaltų arktinių oro masių advekciją iš šiaurės vakarų, šiaurės ir šiaurės rytų. Vėlyvą pavasarį FS taip pat siejami su neigiama Šiaurės

Atlanto osciliacijos faze (Tomczyk, 2015). Vis dėlto, Baltijos šalyse pavasarį būdinga įvairių oro masių advekcija, o skirtingų tipų oro masių pasikartojimui būdingi dideli tarpmetiniai svyravimai (Krauklis & Draveniece, 2004). Būtent didelis atmosferos sąlygų kintamumas yra viena iš galimų priežasčių, lėmusių tai, kad per visą tyrimo laikotarpį reikšmingų FS pasikartojimo pokyčių didžiojoje tiriamos teritorijos dalyje nenustatyta (**II publikacija**).

Kitaip nei CDHE ir FS atveju, CPWE susidarymas šaltuoju ir šiltuoju metų laiku yra susijęs su skirtingais atmosferoje vykstančiais procesais. Šaltuoju metų laiku CPWE formuojasi įsivyravus intensyviai zoninei pernašai iš vakarų, o šiltuoju sezonu – tiriamą teritoriją pasiekus pietiniams ciklonams bei intensyviai vykstant atmosferos konvekcijai (**III publikacija**). Tokia tendencija Vakarų bei Centrinėje Europoje nėra būdinga. Dažniausiai ekstremalaus kritulių kiekio ir vėjo greičio epizodus čia sukelia Atlanto ciklonai, todėl intensyviausi CPWE susidaro žiemą (de Luca ir kt., 2020; Ridder ir kt., 2020). Ateityje, kylant oro temperatūrai, augs ir vandens garų kiekis ore, todėl, tikėtina, kad didės ir konvekcijos procesų intensyvumas (Kendon ir kt., 2014; Taszarek ir kt., 2021), lemsiantis lokalių CPWE susiformavimą.

Sudarant CCE pokyčių prognozes iki XXI a. pabaigos buvo pasirinkti CMIP6 modeliai, apimantys skirtingas ECS spektro dalis. Modelių jautrumas atsispindi ir kai kuriuose gautuose rezultatuose. Didžiausiu jautrumu pasižymėję CanESM5 ir ACCES-CM2 modeliai prognozuoja didesnius $t_{avg,}$ t_{min} *ir* t_{max} pokyčius, todėl taikant jų duomenis nustatytas didesnis karščio bangų dienų skaičiaus augimas bei SGS ir LSF datų ankstėjimas (**IV publikacija**). Visgi vertinant kitų darbe analizuotų kintamųjų (P, w_{max}) kaitą modelio jautrumo vertė atlieka mažesnį vaidmenį. Didžiausias kritulių kiekio mažėjimas, sudarantis palankesnės sausrų susidarymo sąlygas, nustatytas naudojant NorESM2-MM modelio duomenis, o didžiausias kritulių kiekio didėjimas, palankus kritulių kiekio ekstremumams susidaryti – remiantis CanESM5 modelio duomenimis. Didžiausias w_{max} reikšmių didėjimas būdingas GFDL-CM4 ir MPI-ESM1-2-LR modeliams. Didesni CCE charakteristikų pokyčiai numatomi naudojant SSP5–8.5 scenarijaus projekcijų duomenis.

Vertinant tyrimo metu gautus rezultatus derėtų atsižvelgti į keletą aspektų ir neapibrėžtumų. Pirmiausia, nepaisant glaudaus ryšio su matavimais meteorologijos stotyse, ERA5 duomenims būdingos paklaidos. Be to, duomenų kokybė bėgant laikui kinta. Dėl didėjančio skaičiaus antžeminių bei palydovinių stebėjimų, asimiliuojamų sudarant reanalizę, pastarųjų dešimtmečių ERA5 duomenų tikslumas yra didesnis nei XX a. vidurio (Bell ir kt., 2021). Tiriant CPWE svarbu pažymėti, kad ERA5 duomenys geriau

parodo kritulių kiekio ir vėjo greičio ekstremumus, susijusius su vidutinių platumų ciklonų veikla. Mezomasto konvekcijos procesų sukelti ekstremumai reprezentuojami prasčiau. Įtakos tam turi ir duomenų gardelės dydis. Tiek ERA5 reanalizės, tiek NASA NEX-GDDP-CMIP6 duomenų bazės atveju jis siekia 0,25° × 0,25°. Toks gardelės dydis neleidžia išsamiai įvertinti smulkesnio masto vietinių veiksnių įtakos FS susidarymui. Be to, dėl šios priežasties galėjo likti nenustatyta dalis lokalių ir konvekcinių kritulių epizodų (Chen ir kt., 2024; Gaska, 2023).

Nustatant CDHE labai svarbus sausroms identifikuoti taikomo indekso parinkimas. Rengiant disertaciją nuspręsta naudoti SPI. Skaičiuojant šį indeksą naudojamos tik kritulių kiekio reikšmės ir neatsižvelgiama į oro temperatūrą, dirvos drėgmę bei kitus rodiklius. SPI skirtas meteorologinėms sausroms nustatyti ir yra labiau tinkamas taikyti regionuose, kuriuose pagrindinis sausrų susidarymą lemiantis veiksnys yra kritulių kiekio trūkumas (Wang ir kt., 2025). Lietuvoje vasarą drėgmės kiekis dirvoje labiau priklauso ne nuo temperatūros ar kitų rodiklių, bet nuo kritulių kiekio (Rimkus ir kt., 2020), todėl SPI gali būti sėkmingai taikomas sausroms tiriamame regione identifikuoti. Tačiau taikant SPI galėjo būti nustatytas mažesnis sausros dienų skaičius, palyginti su indeksais, kurių skaičiavimas tiesiogiai ar netiesiogiai grindžiamas oro temperatūros duomenimis. Šis aspektas tampa ypač reikšmingas analizuojant ateities projekcijas, sudarytas kintančio klimato ir kylančios oro temperatūros sąlygomis. Tad siekiant detalesnio ir tikslesnio CDHE charakteristikų ir galimo poveikio įvertinimo, tolesniuose tyrimuose atliekant sausrų identifikavimą vertėtų pasitelkti ir oro temperatūrą ar evapotranspiraciją įtraukiančius indeksus.

Klimatologiniais rodikliais remtasi ir nustatant SGS datą (analizuojant FS įvykius). SGS data identifikuota remiantis tik t_{avg}, tačiau ji taip pat priklauso ir nuo kritulių kiekio, dirvožemio drėgmės, maistinių medžiagų kiekio, evapotranspiracijos ir kitų parametrų (Chen ir kt., 2023; Qu ir kt., 2015). Vis dėlto, būtent oro temperatūra yra pagrindinis veiksnys, lemiantis vegetacijos sezono pradžią (Juknys ir kt., 2017). Vertinant FS bei jų intensyvumą taip pat laikyta, kad šie įvykiai visoms augalų rūšims kelią vienodą pavojų. Iš tiesų taip nėra – FS daroma žala labai priklauso nuo augalo rūšies, fenologinės fazės, augavietės mikroklimato ir geografinės padėties (Chamberlain ir kt., 2019). Įtakos turi ir vietiniai veiksniai – žemėnaudos tipas, dirvožemio charakteristikos, vėjo parametrai (De Melo-Abreu ir kt., 2016; Leslie ir kt., 2014). Todėl, siekiant tikslesnio FS charakteristikų interpretavimo bei išsamaus galimo tokių reiškinių poveikio įvertinimo ateityje, į šiuos veiksnius vertėtų atsižvelgti. Visgi FS pasikartojimo ir intensyvumo ateities projekcijų

sudarymas, įtraukiant platesnį kintamųjų spektrą, gali būti dar labiau metodologiškai sudėtingas ir pasižymėti didesniu neapibrėžtumu.

CPWE pokyčių prognozės pasižymi gana dideliu neapibrėžtumu. Tai susiję ne tik su klimato scenarijų bei modelių skirtumais, bet ir su tuo, kad CMIP6 modelių w_{max} reikšmės gautos taikant vėjo gūsių faktorių. Kadangi šis koeficientas apskaičiuotas naudojant santykį tarp vidutinio ir maksimalaus paros vėjo greičio 1950–2022 m. laikotarpiu, laikoma, kad toks pat ryšys tarp šių dviejų kintamųjų išliks ir ateityje. Tačiau ateityje, kintant klimatui ir atmosferos cirkuliacijos bruožams, WGF reikšmės gali keistis. Globalių klimato modelių vidutinio vėjo greičio prognozių reikšmės taip pat nėra labai patikimos (Deng ir kt., 2021; Wu ir kt., 2020). Tai lemia nepakankamai didelė modelių erdvinė skiriamoji geba, dėl kurios paviršiaus ir jo šiurkštumo charakteristikos modeliavimo metu yra supaprastinamos (Andres-Martin ir kt., 2023). Kita priežastis – duomenyse pateikiami gardelių vidurkiai, tačiau vėjo laukui būdingas didelis nevienalytiškumas, o jo reikšmių pasiskirstymas stipriai priklauso nuo vietovės mikroklimatinių sąlygų, todėl pateikiamuose duomenyse ekstremumai gali būti nugludinti (Shen ir kt., 2022).

Gauti rezultatai taip pat priklauso nuo pasirinktų slenkstinių verčių, kurios naudojamos CCE identifikuoti. Atitinkamai padidinus ar sumažinus percentilių vertes nustatant karščio bangas, kritulių kiekio bei vėjo greičio ekstremumus galėtų pasikeisti ir gautos CCE charakteristikų vertės. Taip pat dėl šios priežasties ir skirtingų metodų, taikomų CCE identifikuoti, gali būti sudėtinga kiekybiškai palyginti tyrimo metu gautus CCE charakteristikų pokyčius su kitų tyrimų rezultatais. Kita vertus, keičiant slenkstines vertes nustatytų pokyčių pobūdis nesikeistų.

Ribotumų turi ir disertacijoje analizuota NASA NEX-GDDP-CMIP6 duomenų bazė. Sudarant šią duomenų bazę, atliekant pasaulinių klimato modelių paklaidų korekciją ir didinant skiriamąją gebą, remiamasi prielaida, kad erdviniai klimato pokyčių dėsningumai, nustatyti 1960–2014 m. laikotarpiu, išliks nepakitę ir ateityje, todėl išliks toks pat ekstremalių įvykių pasikartojimas kaip ir pirminiuose CMIP6 duomenyse. Be to, minėto proceso metu laikoma, kad XXI a. temperatūros rodiklių ir kitų kintamųjų pokyčiai bus tiesiniai – t. y. jei modelis baziniu laikotarpiu, palyginti su antžeminiais matavimais, sistemingai prognozavo 1 °C aukštesnę temperatūrą, toks pats nuokrypis taikomas ir ateities projekcijoms. Tačiau klimato sistemai būdingas didelis kintamumas ir netiesinė dinamika, todėl šis metodas gali nepakankamai tiksliai parodyti būsimus pokyčius (Thrasher ir kt., 2022).

Nepaisant minėtų neapibrėžtumų, tikėtina, kad ateityje CDHE ir CPWE pasikartojimas rytinėje Baltijos jūros regiono dalyje išaugs, dalis modelių

prognozuoja ir galimą FS skaičiaus didėjimą. Todėl, siekiant sumažinti šių reiškinių neigiamą poveikį, vystant prisitaikymo prie klimato kaitos ir jos švelninimo strategijas rekomenduotina atsižvelgti ne tik į pavienius ekstremumus, bet ir kompleksinius klimato įvykius ir numatomos jų charakteristikų pokyčius.

IŠVADOS

1. Klimato kaita lemia dažnesnius kompleksinius klimato įvykius rytinėje Baltijos jūros regiono dalyje. Kylančios oro temperatūros poveikis ypač ryškus vertinant kompleksinių sausros ir karščio bangos įvykių skaičiaus pokyčius matavimų laikotarpiu. Šių reiškinių pasikartojimo didėjimą, nustatytą 73 % gardelių, labiausiai lėmė dėl klimato kaitos visoje tyrimo teritorijoje reikšmingai išaugęs karščio bangų dienų skaičius. Dėl šylančio klimato didėsiantis karščio bangų dienų skaičius taip pat, tikėtina, lems kompleksinių sausros ir karščio bangos įvykių pasikartojimo augimą iki XXI a. pabaigos. Vis dėlto prognozuojamų pokyčių mastą ribos su sausrų pasikartojimo kaita susijęs neapibrėžtumas.
2. Dėl stipriai išaugusios oro temperatūros antroje žiemos pusėje ir ankstyvą pavasarį, vegetacijos sezono pradžios data ankstėjo vidutiniškai 10,6 dienomis, o paskutinės pavasario šalnos data – 6,3 dienomis per tyrimo laikotarpį. Todėl nežymiai padidėjo ir vėlyvų pavasario šalnų (FS) skaičius (vidutiniškai 1,3 karto). Tačiau pokyčiai buvo statistiškai reikšmingi mažiau nei trečdalyje tyrimo teritorijos. Ateityje rytinėje Baltijos jūros regiono dalyje numatomas tolesnis vegetacijos sezono pradžios ir paskutinės pavasario šalnos datų ankstėjimas. Šių datų pokyčių tempas naudotų modelių projekcijose labai skiriasi. Todėl vėlyvų pavasario šalnų pasikartojimo XXI a. pabaigoje prognozėms būdingas gana didelis neapibrėžtumas.
3. Kompleksinių kritulių kiekio ir vėjo greičio ekstremumų skaičius nuo XX a. vidurio išaugo 70,2 % tyrimo teritorijos, o didžiausias didėjimas nustatytas vasarą. Prognozuojama, kad XXI a. pabaigoje pagal taikytų CMIP6 modelių projekcijas kompleksinių kritulių kiekio ir vėjo greičio ekstremumų skaičius padidės daugiau nei pusėje tyrimo teritorijos. Tokią tendenciją, tikėtina, lems didėsiantis kritulių kiekis, o pokyčių mastas priklausys nuo maksimalaus vėjo greičio ekstremumų pasikartojimo tendencijų. Vis dėlto maksimalaus vėjo greičio prognozės pasižymi neapibrėžtumu, pirmiausia susijusiu su vėjo gūsių faktoriaus koeficiento taikymu ir dideliu vėjo lauko nevienalytiškumu, todėl kompleksinių kritulių kiekio ir vėjo greičio ekstremumų prognozes derėtų vertinti atsargiai.
4. Kompleksinių klimato įvykių formavimąsi rytinėje Baltijos jūros regiono dalyje lemia įvairūs lokalūs ir didelio masto atmosferos procesai. Kompleksiniai sausros ir karščio bangos įvykiai bei vėlyvos pavasario šalnos dažniausiai siejami su regione įsivyravusia anticiklonine cirkuliacija, o kompleksinių kritulių kiekio ir vėjo greičio ekstremumų

susidarymą lemia skirtingi sezoniniai atmosferos cirkuliacijos veiksniai. Šaltuoju metų laiku (spalio–kovo mėn.) šie ekstremumai dažniausiai formavosi esant stipriai zoninei pernašai iš vakarų ir sparčiai vystantis frontinėms bangoms pietinėje gilių Atlanto ciklonų periferijoje, o šiltuoju metų laiku buvo daugiausiai susiję su pietinių ciklonų poveikiu.

SUMMARY

INTRODUCTION

Due to human-induced climate change, the global land and ocean surface temperatures have increased by 0.06 °C per decade since 1850 and by 0.2 °C per decade since 1975 (Lindsey & Dahlman, 2025). These changes lead to increasingly frequent occurrences of various extreme weather and climate phenomena (droughts, extreme precipitation, heatwaves, floods, severe spring frosts, etc.) in different regions (AghaKouchak et al., 2020; Di Capua & Rahmstorf, 2023; Seneviratne et al., 2021). Until the past decade, such extremes were typically studied separately. However, it has been observed that greater negative socioeconomic impact occurs when several, not necessarily extreme, phenomena happen simultaneously or interact with one another (Seneviratne et al., 2012; Zscheischler et al., 2020). This phenomenon is referred to as a compound climate event (CCE) (Seneviratne et al., 2012; Zscheischler et al., 2018). Currently, various CCEs are being studied, and they are typically classified into four types (Zscheischler et al., 2020):

1. Multivariate events, when several processes acting together cause an impact.
2. Preconditioned events, determined by processes that occurred beforehand.
3. Temporally compounding events, where negative impacts arise from several consecutive hazards recorded in the same area.
4. Spatially compounding events, identified when several drivers acting in different locations within the same region jointly create a single overall hazard and risk.

In this dissertation, three CCEs were analysed: compound drought and heatwave events (CDHE), false spring (FS), and compound precipitation and wind extremes (CPWE). The selected CCEs result from interactions between meteorological phenomena and encompass some of the most common weather- and climate-related extremes in the study area (droughts, heatwaves, heavy precipitation, etc.). All three analysed CCEs are also relevant in the context of rising temperatures and a changing climate causing significant negative impacts across different regions, including the Baltic States (European Environment…, 2025; Guglielmo et al., 2026).

CDHEs are identified when both a drought and a heatwave occur simultaneously within the same area. Favourable condition for the formation of CDHEs typically develop during extended drought periods. During them, reduced soil moisture decreases the amount of thermal energy required for

moisture evaporation (Benson & Dirmeyer, 2021), which, in turn, leads to more rapid warming of different surfaces. When a warm air mass reaches the region, this process increases the intensity of the heatwave. The heatwave, conversely, intensifies the drought: as air temperatures rise, evaporation rates increase, further drying the soil (Wang et al., 2024). CDHEs are associated with increased mortality (Ducros et al., 2025), affect people's emotional health (Sewell et al., 2024), cause a negative impact on crop yield (He et al., 2022), and increase the risk of forest fires (Gazol & Camarero, 2022; Markonis et al., 2021). In recent decades, increases in CDHE occurrences have been reported across various regions, including Europe (Bezak & Mikoš, 2020; Geirinhas et al., 2021; Sedlmeier et al., 2018; Shi et al., 2021).

FS term can be interpreted in various ways (Chamberlain et al., 2019). In this study, FS is defined as an event in which the growing season begins early due to anomalously high air temperatures in late winter and early spring, but is subsequently followed by an intrusion of cold air during which the daily minimum air temperature falls below 0 °C (Zscheischler et al., 2020). Due to rapidly rising air temperature during winter and spring months in the Northern Hemisphere, an increasingly earlier start of the growing season (SGS) has been observed (Allstadt et al., 2015; Zhu et al., 2019). However, already in the 1980s, it was found that an earlier start of the growing season creates favourable conditions for the formation of false spring events (Cannell & Smith, 1986). FS particularly negatively affects the agricultural sector (Lamichhane, 2021); these events may result in the loss of a large share or even the entire fruit harvest (Faust & Herbold, 2018; Ma et al., 2019).

CPWEs are identified when extremes of both wind speed and precipitation occur simultaneously in the same location. The formation of CPWEs in the mid-latitudes of Europe is typically associated with deep Atlantic cyclones and orographic uplift (Martius et al., 2016). These CCEs are considered among the most damaging extreme climate phenomena, capable of causing fatalities, posing risks to the natural environment, and disrupting critical infrastructure (Li et al., 2022). Although over recent decades the frequency of CPWEs in Europe has remained relatively unchanged (Johansson, 2021), projections suggest that with continued climate warming, these extremes will become more frequent, particularly in the northern and eastern parts of the continent (Ridder et al., 2022).

Even though the increase in mean air temperature in the Baltic Sea region has been faster than the global average in recent decades (Helsinki Commission, 2024), various extreme weather and climate phenomena in the region have so far been studied separately. Therefore, the motivation for the research stems from the lack of CCE studies in the Baltic States.

Research object, aim, and objectives

The study area is the eastern part of the Baltic Sea region. The object of this study is compound climate events typical for the region.

The aim of the thesis is to assess the formation and occurrence of different compound climate events in the eastern part of the Baltic Sea region and to determine changes in the characteristics of these events by the end of the 21st century.

Objectives:

1. To assess changes in the recurrence and intensity of different compound climate events in the eastern part of the Baltic Sea region during 1950–2022.
2. To analyse the factors determining the formation of compound drought and heatwave events, false spring events, and compound wind and precipitation extremes.
3. To evaluate projected changes in the recurrence, duration, and intensity of compound climate events by the end of the 21st century.
4. To analyse the difference in the spatial distribution of the recurrence of compound climate events in the study area.

Novelty and relevance

CCEs are increasingly being studied across different regions, following the observation that their negative impacts often exceed the damage caused by individual extremes (Brett et al., 2025; Zscheischler et al., 2020). Changes in the occurrence and intensity of most of these events are directly or indirectly related to climate change. For example, with a global temperature increase of 1 °C, the duration of CDHEs between 2020 and 2100 is projected to increase by ten days (Zhang et al., 2022). Meanwhile, despite the earlier onset of the growing season, the number of frost days increased across 43% of the Northern Hemisphere (Liu et al., 2018).

In the future, the frequency and intensity of CDHEs are projected to increase in the United States (Rastogi et al., 2024), Australia (Chapman et al., 2025), and China (Feng et al., 2023; Liu et al., 2024; Zhang et al., 2024). It is also estimated that by the end of the 21st century, compared with the 1981–2010 period, the area affected by CDHEs in Europe will increase by 60% (Dosio et al., 2023). The frequency of CPWEs is expected to rise in coastal regions of the eastern United States, East and South Asia (Yaddanapudi et al., 2022), and Europe, particularly in the northern and eastern parts of the continent (Ridder et al., 2022). As the climate continues to warm, a higher

recurrence of FS events is also expected in some areas as well (Allstadt et al., 2015; Hufkens et al., 2012; Lhotka & Brönnimann, 2020). Thus, understanding and forecasting the characteristics of the CCEs analysed in this research will remain vital in the future. However, most CCE studies currently focus on southern and western Europe, Asia, and North America (Brett et al., 2025). Therefore, detailed analysis of these events and the development of future projections across different regions, within the context of a rapidly changing climate, are particularly important.

CCEs in the eastern part of the Baltic Sea region have so far been poorly studied, with more research conducted only in Poland (Graczyk & Szwed, 2020; Koźmiński et al., 2023; Nidzgorska-Lencewicz et al., 2024; Piotrowski & Bartoszek, 2025; Wibig & Jędruszkiewicz, 2024). In other cases, the components of the CCEs analysed in this dissertation have only been assessed separately. Projections of various CCEs for the eastern part of the Baltic Sea region up to the end of the 21st century have also not yet been developed.

In this work, for the first time, changes in the occurrence, duration, and spatial distribution of CDHEs, FS, and CPWEs in the eastern part of the Baltic Sea region since the mid-20th century were assessed in detail (**Papers I–III**), Methodology for identifying these events was developed and changes in the characteristics of the aforementioned CCEs by the end of the 21st century were evaluated. The study also proposes a methodology for assessing FS intensity (**Paper II**), which can be applied in other regions. Information on the formation and occurrence of CCEs in the region in the future may be used to develop warning systems for these hazardous phenomena, while the results obtained improve understanding of CCE formation mechanisms.

1. MATERIALS AND METHODS

1.1. Study area

CCEs were analysed in the eastern part of the Baltic Sea region, covering the area from 53.5° to 59.5° N and from 20° to 28.5° E. The study area is dominated by lowlands and plains, with the highest point rising to 355 m above sea level. According to the updated Köppen–Geiger climate classification, the study area belongs to the *Dfb* climate type: no dry season is distinguished; at least four months have a mean air temperature above 10 °C but below 22 °C, and the mean air temperature of the coldest month is below or equal to 0 °C (Beck et al., 2018). The mean annual air temperature in the region during 1991–2020 was 7.0 °C and from 1950 increased by 0.23 °C per decade. July had the highest mean air temperature (18.2 °C), while January

was the coldest month (–3.4 °C). The study area lies within a moisture surplus zone, where precipitation exceeds evaporation (Kilkus & Stonevičius, 2011). Annual precipitation ranges from 610 to 890 mm, with the highest values occurring in the western part of the study area. July and August are the wettest months in most of the region (averaging 82–86 mm of precipitation per month). The mean annual wind speed varies from 3 m/s in the eastern part of the study area to 5.5–6 m/s in the north-western part, with the strongest winds occurring in winter (December–January).

1.2. Data

CCEs were assessed for the period 1950–2022. ERA5 reanalysis data from the European Centre for Medium-Range Weather Forecasts (ECMWF) were used to identify these events, including daily mean (t_{avg}), minimum (t_{min}), and maximum (t_{max}) air temperature, daily precipitation (P), and hourly maximum wind speed (w_{max}). The grid resolution was 0.25° × 0.25°. As the impacts of the analysed CCEs are most pronounced over land, grid cells in which more than 50% of the area was covered by the Baltic Sea were excluded from the analysis (**Papers I–III**). For the same reason, several grid cells located at Lake Peipus in the north-eastern part of the study area were also removed. Land grid cells were identified using a land mask from the KNMI *Climate Explorer* application (Royal Netherlands..., n.d.).

The ERA5 reanalysis was selected for its long time series and sufficiently high spatial and temporal resolution (Hersbach et al., 2020). The reanalysis incorporates satellite and ground-based observations, as well as weather radar data; therefore, ERA5 closely reproduces *in situ* measurements in Europe (Bell et al., 2021; Hersbach et al., 2020; Velikou et al., 2022). The accuracy of ERA5 reanalysis data decreases in mountainous regions (e.g., the Scandinavian Mountains) and in the tropics (Laurila, 2022; Lavers et al., 2022). Nevertheless, as the highest point in the study area reaches only 355 m above sea level, this limitation is not considered significant in the context of this study.

ERA5 data for different variables were compared with observations from three meteorological stations operated by the Lithuanian Hydrometeorological Service (Biržai, Ukmergė, and Varėna). These stations were selected because their coordinates most closely matched the coordinates of the ERA5 grid-cell centres. Evaluation of temperature indicators (average air temperature, minimum February–June temperature, and the minimum daily air temperature during the summer months) for the 1951–2022 period revealed a strong relationship, with values of the Pearson correlation coefficient (r) across the

study area ranging on average from 0.94 to 0.99 ($p < 0.001$). The Mean Absolute Error (MAE) for t_{avg} ranged from 0.67 to 0.82 °C. MAE values for t_{min} and t_{max} were higher, reaching 1.46–2.43 °C and 1.17–1.91 °C, respectively. Values of w_{max} also showed good agreement with *in situ* measurements ($r = 0.77–0.83$; MAE = 1.64–2.32 m/s; $p < 0.001$). A weaker relationship was found only for daily precipitation totals ($r = 0.65–0.66$; $p < 0.001$), with MAE values ranging from 1.45 to 1.51 mm. However, precipitation exhibits considerable spatial variability and is strongly influenced by local factors. This may have contributed to the greater discrepancies between ERA5 reanalysis data and *in situ* observations.

To evaluate changes in the characteristics of the analysed CCEs by the end of the 21st century, data from global climate models participating in Phase 6 of the Coupled Model Intercomparison Project (CMIP6) were used. Daily model data were obtained from the NASA Earth Exchange Global Daily Downscaled Projections (NEX-GDDP-CMIP6) database (Thrasher et al., 2022) with the spatial resolution of 0.25° × 0.25°. This database has been widely used in the study of extreme hydrometeorological events across different regions and has also been applied to develop projections of various CCEs for the 21st century (Ford et al., 2025; Xu et al., 2024; Zhang et al., 2024). Future projections of CCE characteristics were generated for the same 667 grid points used to assess these extremes in 1950–2022.

The NASA NEX-GDDP-CMIP6 database contains data from 35 CMIP6 models (Thrasher et al., 2022), five of which were used in this study: CanESM5, ACCESS-CM2, GFDL-CM4, MPI-ESM1-2-LR, and NorESM2-MM. These models were selected to represent different parts of the model equilibrium climate sensitivity (ECS) spectrum (**Paper IV, p. 162**). Two Shared Socioeconomic Pathway (SSP) scenarios were used: SSP2–4.5 and SSP5–8.5 (**Paper IV, p. 163**).

It is important to note that the w_{max} data is not provided in the NASA NEX-GDDP-CMIP6 database. Therefore, to assess future CPWE changes, w_{max} values were calculated by applying a wind gust factor (WGF) to daily mean wind speed data. This coefficient was determined using daily w_{max} and mean wind speed ERA5 data for 1950–2022. WGF was calculated by dividing w_{max} by the mean wind speed. The coefficient was determined separately for each grid cell and each season. A similar method for determining WGF was proposed in the last century (Weggel, 1999) and has been applied in other studies (Cheng et al., 2012).

FS projections were produced for mid-century (2041–2060) and end-century (2081–2100) (**Paper IV**), whereas CDHE and CPWE were assessed only for the final two decades of the 21st century. The period 1995–2014 was

used as the reference period for assessing future CCE changes. These 20-year periods were used in the latest Intergovernmental Panel on Climate Change (IPCC) report (Chen et al., 2021) and are widely applied in other studies to evaluate future changes in various CCEs (Chapman et al., 2025; Feng et al., 2023; Wang et al., 2023).

1.3. Assessment of compound climate events

1.3.1. Identification of compound drought and heatwave events

To identify CDHEs, droughts and heatwaves were first determined. Droughts were distinguished using the Standardized Precipitation Index (SPI) (McKee et al., 1993). In this study, SPI was calculated for each day of the study period using the accumulated precipitation over the previous 30 days. When calculating SPI, precipitation totals over various time scales (1–24 months) are used (World Meteorological…, 2012). However, to identify meteorological droughts during the warm season, more precisely determine their onset and end, and more clearly define CDHEs, a 30-day calculation period was selected in this study. The R programming language SPEI package was used to calculate SPI (Beguería & Vicente-Serrano, 2023). A drought was identified in a grid cell if SPI values were below −1 (World Meteorological…, 2012) for at least five consecutive days (**Paper I, p. 28**).

Heatwaves were defined as t_{max} values above the 90th percentile. Percentile values were calculated for each grid cell in the study area, and a heatwave was identified when the percentile threshold in a given cell was exceeded for at least 5 consecutive days. The 90th percentile values for 1950–2022 were calculated using a five-day moving window (**Paper I, p. 28**). To produce future projections of heatwaves, this threshold value was calculated at each grid point for the entire warm season (April–September).

The 90th percentile threshold for t_{max} in heatwave identification was selected based on a sensitivity analysis of different threshold values. It was estimated that CDHEs occur, on average, 2.7 times per summer within a given grid cell using the 90th percentile threshold. This indicates that the events are sufficiently extreme while still providing enough data for statistical analysis. In contrast, using a higher threshold, such as the 95th percentile, makes CDHEs in the study region rare (occurring, on average, 1.4 times per summer), which is insufficient for a detailed statistical analysis of compound events. The 90th percentile approach to distinguish heatwaves was also used in other studies (Kim et al., 2018; Mukherjee et al., 2020; Prodhomme et al., 2022; Ridder et al., 2020; Rousi et al., 2022).

The intensity of CDHE periods during 1950–2022 was assessed by applying the *Min–Max* normalisation method (**Paper I, p. 28–29**) to SPI values and to t_{max} deviations from the 90th percentile. Before applying this method, the medians of SPI and t_{max} anomalies were calculated for each day belonging to a CDHE period. The analysis was carried out using values obtained from grid cells containing CDHEs. To determine changes in intensity by the end of the 21st century, median SPI values and deviations of t_{max} from the 90th percentile were used. In this case, the *Min–Max* normalisation method was not applied due to an excessively large number of outliers in both the SPI and t_{max} deviation datasets.

A CDHE was identified as a day when drought and heatwave conditions occurred simultaneously. For 1950–2022, CDHE were assessed during summer months (**Paper I, p. 29**), while future projections were produced for the warm season (April–September). This choice is based on the assumption that, in the future, due to the expected increase in t_{max}, CDHEs are likely to form not only in summer but also throughout the entire warm season.

CDHE periods were also identified (**Paper I**). These were defined as those cases in which, at maximum extent, the phenomenon covered more than one-third of the study area. Following a sensitivity analysis, it was calculated that, when applying the criterion of one-third of the study area, CDHE periods accounted for 1.4% of all days in the study period. When a 50% grid-cell threshold was applied, this share decreased to 0.9%. Meanwhile, using 20% and 25% grid-cell criteria, CDHE periods accounted for approximately 1.7–2.0% of all days in the study period. Based on these results, the one-third study area criterion was selected as optimal for further analysis. The start of an event was determined as the date when CDHEs were recorded in more than 10% of grid cells, and the end when this condition was no longer met for at least 3 consecutive days (**Paper I**). These conditions were applied to avoid cases in which CDHEs forming in only a few grid cells artificially extend the duration of a CDHE period, as well as situations where the absence of a CDHE for just a single day leads to the initiation of a new period.

1.3.2. Identification of false spring events

To identify FS events, SGS and LSF dates were first determined for each grid point. The SGS date was defined as the first day of a six-day period during which $t_{avg} \geq 5$ °C for all six consecutive days (Swedish Meteorological…, 2024). The LSF date was defined as the last day in January-June with $t_{min} < 0$ °C (**Paper II, IV**). The 0 °C threshold used to determine the timing of LSF has also been applied in other studies in Europe and the Baltic Sea region

(Ceglar et al., 2019; Koźmiński et al., 2023; Wypych et al., 2017). FS was identified in each grid cell if LSF occurred later than SGS (Allstadt et al., 2015; Chamberlain et al., 2019). These CCEs were analysed for February–June (**Papers II, IV**).

To assess FS intensity during 1950–2022, two variables were used: the sum of growing degree days (GDD) (t_{base} = 5 °C) (McMaster & Wilhelm, 1997), accumulated until the event, and t_{min} recorded during FS. To determine FS intensity, GDD and t_{min} values were classified into three categories, forming nine FS intensity classes (**Paper II, p. 9355**). For future projections of FS characteristics, intensity was evaluated only using GDD (**Paper IV, p. 163**). Due to the high uncertainty and limited reliability of CMIP6 global climate models' minimum air temperature (t_{min}) values, specific t_{min} values recorded at the time of FS occurrence were not used when assessing the intensity of future false spring events.

1.3.3. Identification of compound precipitation and wind extremes

Extremes of P and w_{max} were identified when their values exceeded the 98th percentile. Using this threshold, moderate and severe extremes were identified, and sufficient data were obtained for statistical analysis. Following a sensitivity analysis, it was found that using the 98th percentile results in an average of 5.5 CPWEs per decade per grid cell. When the threshold was reduced to the 95th percentile, the number of CPWEs increased by almost a factor of five, meaning that such events could no longer be considered extreme. In contrast, using the 99th percentile, CPWEs were identified very rarely, on average, only 1.6 per decade. The 98th percentile threshold for CPWE identification has also been used in other studies (Martius et al., 2016; Messmer & Simmonds, 2021). Percentiles were calculated separately for each grid cell. CPWEs were identified when both extremes occurred simultaneously within the same grid cell. CPWE occurrence was evaluated separately by season. The statistical significance of changes was determined using Student's t-test ($p < 0.05$) (**Paper III**).

To identify the most intense CPWE, 99.9th percentile values of P and w_{max} were calculated for each grid cell. The number of cases where both variables exceeded these thresholds simultaneously was then assessed, along with their seasonal occurrence and spatial distribution (**Paper III**).

1.4. Assessment of atmospheric conditions determining the formation of compound climate events

Atmospheric circulation conditions during the formation of different CCEs were determined using the Hess–Brezowsky classification of atmospheric circulation types (Muriset, n.d.; Werner & Gerstengarbe, 2010). For CPWEs, circulation types were evaluated when the event occurred in more than one-fifth of grid cells on the same day. Additional data sources were also used to identify factors influencing CPWE formation (synoptic charts from the meteorological services of the United Kingdom, Germany, and the Netherlands, ERA5 reanalysis data, etc.) (**Paper III, p. 5**). Atmospheric conditions associated with these CCEs were analysed separately for the warm (April–September) and cold (October–March) seasons.

For FS, changes in the occurrence of different Hess–Brezowsky circulation types in the study area during 1950–2022 were evaluated. For CDHE, atmospheric conditions were assessed on days when, at maximum extent, these events covered more than one-third of the study area.

2. RESULTS AND DISCUSSION

2.1. Compound drought and heatwave events

During 1950–2022, the highest number of CDHEs was recorded in the eastern and south-eastern parts of the study area (33–36 days per decade). This distribution is closely related to drought occurrence patterns (**Paper I, p. 30**). Over the 73 years, the number of CDHEs increased across 73% of the study area. The more frequent occurrence of these events is primarily associated with climate change–driven increases in t_{max} and a statistically significant, according to the Mann–Kendall test ($p < 0.05$), rise in the number of heatwave days across the study region (**Paper I, p. 31**). However, changes in CDHE occurrence were small in almost all grid cells. This is due to the decrease in drought days across 89% of the study area (**Paper I**). The increasing recurrence of CDHEs in recent decades has been observed across many mid-latitude regions of the Northern Hemisphere (Ridder et al., 2020), whereas changes are more pronounced in the Southern Hemisphere due to a faster rise in air temperature (Mukherjee & Mishra, 2021). CDHEs are also occurring more frequently in Northern and Central Europe (Bezak & Mikoš, 2020; Wibig & Jędruszkiewicz, 2024).

From the mid-20th century to 2022 during the summer, 10 periods were identified during which, at maximum extent, CDHEs covered at least one-

third of the study area (**Paper I, p. 31**). Half of the periods were recorded in the final decade of the 20th century. The year 1994 was particularly notable, with two such periods identified; the CDHE, lasting from 24 July to 7 August 1994, was the longest (15 days), covered the largest part of the study (94.2% of grid cells), and was the most intense (**Paper I, p. 31**).

By the end of the 21st century, compared with the baseline period 1995–2014, the number of CDHEs during April–September is projected to increase in more than 86% of grid cells, depending on the model and scenario. Under SSP2–4.5, the increase is projected to be on average 1–5 days per year, and under SSP5–8.5, 6–18 days per year. The main driver of this increase will be the rising number of heatwave days. However, the magnitude of the changes in CDHE occurrence will depend on the spatial distribution of precipitation. Finally, it is important to note that the 90th percentile values of t_{max} used to identify future heatwaves are likely to represent typical conditions in the future and may no longer be considered extreme. Thus, it is likely that humans and various ecosystems will adapt to changing climatic conditions. Therefore, despite a significant increase in the number of heatwave days and CDHEs, future changes in the negative impacts associated with these events may be less pronounced.

Also, the number of CDHEs largely depends on the index used to identify droughts. In this study, the SPI was selected. This index is calculated using only precipitation values and does not account for air temperature, soil moisture, or other variables. Thus, the SPI is designed to identify meteorological droughts and is more suitable for regions where precipitation deficit is the primary driver of drought formation (Wang et al., 2025). In Lithuania, during the summer, soil moisture is influenced more by precipitation than by temperature or other variables (Rimkus et al., 2020), suggesting that the SPI can be successfully applied to identify droughts in the study region. Nonetheless, the use of SPI may result in fewer drought days than indices that directly or indirectly incorporate air temperature data. This aspect becomes particularly important when analysing future projections under changing climate conditions and rising air temperatures.

2.2. False spring events

During 1950–2022, rising air temperatures in February–April led to an earlier SGS date across the entire study area, advancing on average by 10.6 days (**Paper II, p. 9355**). Owing to climate change and higher air temperature in the second half of winter and early spring, the LSF date also occurred earlier over the 73 years. However, the change was smaller than for SGS, averaging

6.3 days (**Paper II, p. 9356**). Thus, conditions became more favourable for FS formation. This was also confirmed by analysing changes in the difference between LSF and SGS dates during 1950–2022, which increased in 85.9% of grid cells, but statistically significant changes using the Mann–Kendall test ($p < 0.05$) were identified in only 4.8% of the study area (**Paper II, p. 9357**).

Comparing the beginning (1950–1969) and end (2003–2022) of the study period showed that FS recurrence rose across nearly the entire region (85.9% of grid cells). The largest and statistically significant changes were found in locations that experienced the most rapid increases in spring air temperature. However, based on GDD and t_{min} values, no significant changes in FS intensity were identified (**Paper II, p. 9357**). Similar trends in the risk of FS have also been observed in studies conducted in Poland (Graczyk & Szwed, 2020; Koźmiński et al., 2023).

Due to the warming influence of the Baltic Sea, the LSF date in coastal lowlands occurred on average several weeks, or even up to a month, earlier than in the rest of the study area. As a result, FS events were rare along the Baltic coast, occurring no more than 2 times per decade. Moving further inland, the number of these events increased rapidly (up to 7–8 events per decade) **(Paper II, p. 9357).** This tendency is not only characteristic of the study area but also found in the other regions (Zohner et al., 2020).

In the future, the SGS date is projected to advance further in the eastern part of the Baltic Sea region. Depending on the model and scenario used, the growing season at the beginning of the 21st century is expected to start 3–6 weeks earlier than in 1995–2014 (**Paper IV, p. 164**). The LSF date is also projected to occur progressively earlier. By 2081–2100, the change relative to the baseline period is expected to range on average from 1 to 6 weeks (**Paper IV, p. 165**).

Although all models used in this study project earlier SGS and LSF dates in the eastern part of the Baltic Sea region, future projections of FS occurrence do not show a consistent trend. Some models indicate an increase in the number of these events, while others suggest a decrease (**Paper IV, p. 165–166**). The main reason is that different models project different rates of change in LSF and SGS dates. If more rapid warming is projected in late winter or early spring, FS recurrence may increase. Conversely, if air temperatures rise more strongly in the second half of spring, the occurrence of these events is likely to decline. Similar projections of FS characteristics, characterised by high uncertainty, have also been obtained in other regions (Allstadt et al., 2015; Lhotka & Brönnimann, 2020; Mallard et al., 2023; Martinuzzi et al., 2019).

The SGS date (and FS events) were identified from a climatological perspective using only mean air temperature. However, it also depends on precipitation, soil moisture, nutrient availability, evapotranspiration, and other parameters (Chen et al., 2023; Qu et al., 2015). Nevertheless, air temperature is the primary factor determining the onset of the growing season (Juknys et al., 2017). When assessing FS events and their intensity, it was also assumed that these events pose an equal risk to all plant species. In reality, this is not the case as FS damage depends strongly on plant species, phenological stage, microclimatic conditions of the habitat, and geographical location (Chamberlain et al., 2019). Local factors also play an important role, including land-use type, soil characteristics, and wind parameters (De Melo-Abreu et al., 2016; Leslie et al., 2014). Therefore, to achieve a more accurate assessment of FS characteristics and their potential future impacts, these factors should be considered.

2.3. Compound precipitation and wind extremes

During 1950–2022, CPWEs occurred most frequently in October (17.9% of cases) and were least common in spring months (**Paper III, p. 7**). Over the 73 years, the highest number of events was recorded in western Lithuania (10–11 events per decade). The main reasons for such spatial distribution, particularly during the cold season, are the distance from the Baltic Sea and altitude, with CPWEs occurring most frequently on the windward slopes of highlands in Western Lithuania. A higher number of CPWE than in surrounding areas was also recorded in central Latvia, where elevated terrain is likewise present (**Paper III, p. 7**).

The number of CPWEs in the eastern part of the Baltic Sea region increased slightly during 1950–2022, but the change was not statistically significant ($p < 0.05$) according to the Mann–Kendall test (**Paper III, p. 7**). However, comparing 1950–1969 and 2003–2022 showed an increase in 70.2% grid cells. The largest (10–12 events) and statistically significant changes ($p < 0.05$) using Student's t-test were observed in the southern and south-western parts of the study area. Seasonal analysis showed that the greatest increase occurred in summer (65.5% of grid cells) (**Paper III, p. 8–9**). This is associated with rising summer air temperatures and rising atmospheric moisture content, which enhance convection and lead to local precipitation and w_{max} extremes.

Only 4 days were identified in which both P and w_{max} exceeded the 99.9^{th} percentile over more than 1% of the study area in 1950-2022, representing extremely severe CPWE. All such days occurred from late July to early August (**Paper III, p. 9–10**).

By the end of the 21st century, projections from all models used in this dissertation indicate that CPWE frequency might increase across more than half of the study area compared with the 1995–2014 baseline period. These events are expected to continue occurring more often during the cold season. The projected increase in CPWE recurrence is likely to be driven by enhanced evaporation, more frequent precipitation extremes, and changes in the trajectories of tropical and mid-latitude cyclones (Li et al., 2024; Seneviratne et al., 2021), meaning that it will remain closely linked to climate change and rising air temperatures. Finally, the number of days with extremely intense CPWEs affecting at least 1% of the study area (both P and w_{max} exceeding the 99.9th percentile) is projected to remain nearly unchanged. Three such days were identified in the baseline period, while 1–3 (SSP2–4.5) and 2–4 (SSP5–8.5) days are projected by the end of the 21st century. Only the GFDL-CM4 model forecasts 10 days with extremely strong CPWE under both SSP scenarios.

It should be noted that projections of changes in CPWE characteristics are subject to considerable uncertainty. This is related not only to differences between climate scenarios and models, but also to the fact that CMIP6 model w_{max} values were derived using a wind gust factor. Since this coefficient is calculated based on the ratio between mean and maximum daily wind speed over the 1950–2022 period, it is assumed that the same relationship between these two variables will persist in the future. Global climate model projections of mean wind speed are likewise not highly reliable (Deng et al., 2021; Wu et al., 2020). This is due to insufficient spatial resolution in the models, which leads to simplified surface characteristics and roughness parameters (Andres-Martin et al., 2023). Another reason is that the data are provided as grid-cell averages, whereas wind fields are highly heterogeneous and their distribution strongly depends on local microclimatic conditions (Shen et al., 2022).

2.4. Atmospheric conditions leading to the formation of compound climate events

CDHEs in Europe are typically associated with anticyclonic circulation and the development of blocking patterns (Ionita et al., 2021; Spensberger et al., 2020). These weaken the zonal flow and divert cyclone trajectories southwards. Such high-pressure systems also suppress upward motion, reduce water vapour concentration, and limit precipitation formation (Ionita et al., 2021). A similar tendency was observed in this research. On most days when these CCEs were recorded, the study area was dominated by an anticyclonic

ridge or air mass advection from the south and southeast, associated with the influx of warm air into the Baltic States.

The formation of FS events is also associated with blocking anticyclones and positive sea level pressure anomalies. In spring, such patterns often lead to the advection of cold Arctic air masses from the northwest, north, and northeast. These CCEs are also associated with the negative phase of the North Atlantic Oscillation (Tomczyk, 2015). However, in spring, the Baltic States are characterised by the advection of various air masses, and the recurrence of different types exhibits large interannual variability (Krauklis & Draveniece, 2004). This high variability in atmospheric conditions is one of the possible reasons why no significant changes in FS recurrence were identified during the 1950–2022 period (**Paper II**).

CPWE formation is associated with distinct atmospheric processes in the cold and warm seasons. During the cold season, these CCEs form under a strong zonal westerly flow. In the warm season, CPWEs develop in the study area when southern-type cyclones reach the region. These cyclones were also responsible for the most intense CPWEs (**Paper III, p. 10–12**). In the future, as air temperature rises, the amount of water vapour in the atmosphere will increase; consequently, the intensity of convective processes is also likely to rise (Kendon et al., 2014; Taszarek et al., 2021), leading to the formation of local CPWEs. But it is important to note that such extremes are often recorded over areas smaller than the grid size used in this study. Therefore, their recurrence may not be reflected in either the ERA5 data or the CMIP6 model projections.

2.5. Limitations of the study

In addition to the aforementioned uncertainties when discussing CDHEs, FS, and CPWEs, several further aspects and potential limitations should be considered when interpreting the results. Despite the close agreement with measurements from meteorological stations, ERA5 data are subject to inherent errors. Moreover, data quality varies over time. Due to the increasing number of ground-based and satellite observations assimilated into the reanalysis, the accuracy of ERA5 data in recent decades is higher than in the mid-20th century (Bell et al., 2021). Also, ERA5 better captures precipitation and wind speed extremes associated with mid-latitude cyclone activity, whereas those driven by mesoscale convective processes are represented more poorly. This is also influenced by grid resolution. In both the ERA5 reanalysis and the NASA NEX-GDDP-CMIP6 dataset, the spatial resolution is 0.25° × 0.25°. Such a grid size does not allow for a detailed assessment of the influence of finer-

scale local factors on FS formation. In addition, part of the local and convective precipitation events may therefore remain undetected (Chen et al., 2024; Gaska, 2023).

The results also depend on the chosen threshold values for identifying CCEs. Increasing or decreasing percentile thresholds for defining heatwaves, precipitation, and wind speed extremes could alter the resulting CCE characteristics. For the same reason, and because different methods are used to identify CCEs, it may be difficult to quantitatively compare the changes in CCE characteristics reported in this study with those reported in other studies. Nevertheless, the overall nature of the identified trends would not change when the threshold values are modified.

The NASA NEX-GDDP-CMIP6 dataset used in this study also has limitations. In producing this dataset, bias correction and downscaling are based on the assumption that spatial patterns of climate change identified over the 1960–2014 period will remain unchanged in the future, and that the frequency of extreme events will therefore remain the same as in the original CMIP6 outputs. In addition, the procedure assumes that changes in temperature and other variables during the 21st century will be linear. For example, if a model systematically overestimated temperature by 1 °C during the baseline period relative to ground observations, the same bias is applied to future projections. However, the climate system is characterised by strong variability and nonlinear dynamics; therefore, this approach may not fully capture future changes (Thrasher et al., 2022).

Despite these uncertainties, it is likely that the frequency of CDHEs and CPWEs will increase in the eastern Baltic Sea region in the future, and some models also project a potential increase in the number of FS events. Therefore, to reduce the negative impacts of these phenomena, climate change adaptation and mitigation strategies should consider not only individual extremes but also compound climate events and the projected changes in their characteristics.

CONCLUSIONS

1. Climate change is leading to a more frequent occurrence of compound climate events in the eastern part of the Baltic Sea region. The impact of rising air temperatures is particularly evident in changes in the recurrence of compound drought and heatwave events during the study period. The increase in these events, identified in 73% of grid cells, was primarily driven by the significant rise in the number of heatwave days across the entire study area due to climate change. The growing number of heatwave days under a warming climate is also expected to increase the frequency

of compound drought and heatwave events by the end of the 21st century. However, the extent of the projected changes will be constrained by uncertainties in drought dynamics.

2. Due to the substantial increase in air temperatures during the second half of winter and early spring, the date of the start of the growing season during the study period advanced by, on average, 10.6 days, while the date of the last spring frost has shifted earlier by 6.3 days. As a result, the number of false spring events slightly increased (by an average factor of 1.3). However, these changes were statistically significant in less than one-third of the study area. In the future, further advancement of both the start of the growing season and the last spring frost dates is projected in the eastern Baltic Sea region. The rates of change in these dates differ considerably across the model projections. Consequently, projections of the occurrence of false spring events by the end of the 21st century are associated with relatively high uncertainty.
3. Since the mid-20th century, the number of compound precipitation and wind extremes has increased across 70.2% of the study area, with the greatest increase identified during summer. By the end of the 21st century, all CMIP6 model projections used in this study indicate a rise in the number of compound precipitation and wind extremes across more than half of the study area. This trend will likely be driven by increasing precipitation, while the magnitude of the changes will depend on trends in the recurrence of maximum wind speed extremes. Nevertheless, projections of maximum wind speed remain uncertain, primarily because of the application of the wind gust factor and the strong heterogeneity of wind fields. Therefore, projections of compound precipitation and wind events should be interpreted with caution.
4. The formation of compound climate events in the eastern part of the Baltic Sea region is driven by a variety of local and large-scale atmospheric processes. Compound drought and heatwave events, as well as false spring events, are most commonly associated with anticyclonic circulation prevailing over the region, whereas the formation of compound precipitation and wind extremes is linked to different seasonal atmospheric circulation mechanisms. During the cold season (October–March), compound precipitation and wind extremes most frequently developed under strong zonal westerly flow and rapidly intensifying frontal waves on the southern periphery of deep Atlantic cyclones, while during the warm season (April–September), they were primarily associated with the influence of southern cyclones.

LITERATŪROS SĄRAŠAS

AghaKouchak, A., Chiang, F., Huning, L. S., Love, C. A., Mallakpour, I., Mazdiyasni, O., Moftakhari, H., Papalexiou, S. M., Ragno, E., & Sadegh, M. (2020). Climate extremes and compound hazards in a warming world. *Annual Review of Earth and Planetary Sciences*, *48*, 519–567. https://doi.org/10.1146/annurev-earth-071719-055228

Akima, H., Gebhardt, A., Petzold, T., & Maechler, M. (2025). *akima: Interpolation of irregularly and regularly spaced data* (R package version 0.6-3.6). CRAN. https://cran.r-project.org/web/packages/akima/akima.pdf

Anderson, G. B., & Bell, M. L. (2011). Heat waves in the United States: Mortality risk during heat waves and effect modification by heat wave characteristics in 43 U.S. communities. *Environmental Health Perspectives*, *119*(2), 210–218. https://doi.org/10.1289/ehp.1002313

Andres-Martin, M., Azorin-Molina, C., Shen, C., Fernández-Alvarez, J. C., Gimeno, L., Vicente-Serrano, S. M., & Zha, J. (2023). Uncertainty in surface wind speed projections over the Iberian Peninsula: CMIP6 GCMs versus a WRF-RCM. *Annals of the New York Academy of Sciences*, *1529*(1), 101–108. https://doi.org/10.1111/nyas.15063

Allstadt, A. J., Vavrus, S. J., Heglund, P. J., Pidgeon, A. M., Thogmartin, W. E., & Radeloff, V. C. (2015). Spring plant phenology and false springs in the conterminous US during the 21st century. *Environmental Research Letters*, *10*(10), 104008. https://doi.org/10.1088/1748-9326/10/10/104008

Bateman, B. (2024, March 29). False springs: How earlier spring with climate change wreaks havoc on birds. *Audubon*. https://www.audubon.org/news/false-springs-how-earlier-spring-climate-change-wreaks-havoc-birds

Beck, H. E., Zimmermann, N. E., McVicar, T. R., Vergopolan, N., Berg, A., & Wood, E. F. (2018). Present and future Köppen-Geiger climate classification maps at 1-km resolution. *Scientific Data*, *5*, 180214. https://doi.org/10.1038/sdata.2018.214

Beguería, S., & Vicente-Serrano, S. M. (2023). *SPEI: Calculation of the standardized precipitation-evapotranspiration index*. https://spei.csic.es

Bell, B., Hersbach, H., Simmons, A., Berrisford, P., Dahlgren, P., Horányi, A., Muñoz-Sabater, J., Nicolas, J., Radu, R., Schepers, D., Soci, C., Villaume, S., Bidlot, J. R., Haimberger, L., Woollen, J., Buontempo, C., & Thépaut, J. N. (2021). The ERA5 global reanalysis: Preliminary extension to 1950. *Quarterly Journal of the Royal Meteorological Society*, *147*(741), 4186–4227. https://doi.org/10.1002/qj.4174

Benson, D. O., & Dirmeyer, P. A. (2021). Characterizing the relationship between temperature and soil moisture extremes and their role in the exacerbation of heat waves over the contiguous United States. *Journal of Climate*, *34*(6), 2175–2187. https://doi.org/10.1175/JCLI-D-20-0440.1

Bevacqua, E., Zappa, G., Lehner, F., & Zscheischler, J. (2022). Precipitation trends determine future occurrences of compound hot–dry events. *Nature Climate Change, 12*(4), 350–355. https://doi.org/10.1038/s41558-022-01309-5

Bezak, N., & Mikoš, M. (2020). Changes in the compound drought and extreme heat occurrence in the 1961–2018 period at the European scale. *Water*, *12*(12), 3543. https://doi.org/10.3390/w12123543

Bielec-Bąkowska, Z., & Twardosz, R. (2023). Exceptionally cold and warm spring months in Kraków against the background of atmospheric circulation (1874–2022). *Pure and Applied Geophysics*, *180*(9), 3351–3370. https://doi.org/10.1007/s00024-023-03324-9

Bosdijk, J., de Feiter, V. S., Gaiser, A., Smink, T., Thorkelsdottir, G., van Vliet, A. J. H., & Luedeling, E. (2024). False springs in the Netherlands: Climate change impact assessment with the false spring damage indicator model. *Regional Environmental Change*, *24*(2), 1–11. https://doi.org/10.1007/s10113-024-02235-2

Brett, L., White, C. J., Domeisen, D. I. V., van den Hurk, B., Ward, P., & Zscheischler, J. (2025). Review article: The growth in compound weather and climate event research in the decade since SREX. *Natural Hazards and Earth System Sciences*, *25*(8), 2591–2611. https://doi.org/10.5194/nhess-25-2591-2025

Cannell, M. G. R., & Smith, R. I. (1986). Climatic warming, spring budburst and forest damage on trees. *Journal of Applied Ecology*, *23*(1), 177–191. https://doi.org/10.2307/2403090

Ceglar, A., Zampieri, M., Toreti, A., & Dentener, F. (2019). Observed northward migration of agro-climate zones in Europe will further accelerate under climate change. *Earth's Future*, *7*(9), 1088–1101. https://doi.org/10.1029/2019EF001178

Chamberlain, C. J., Cook, B. I., García de Cortázar-Atauri, I., & Wolkovich, E. M. (2019). Rethinking false spring risk. *Global Change Biology*, *25*(7), 2209–2220. https://doi.org/10.1111/gcb.14642

Chapman, S., Trancoso, R., Syktus, J., Eccles, R., & Toombs, N. (2025). Impacts on compound drought heatwave events in Australia per global warming level. *Environmental Research Letters*, *20*(5), 054009. https://doi.org/10.1088/1748-9326/adc8bd

Chen, D., Rojas, M., Samset, B. H., Cobb, K., Diongue Niang, A., Edwards, P., Emori, S., Faria, S. H., Hawkins, E., Hope, P., Huybrechts, P., Meinshausen, M., Mustafa, S. K., Plattner, G. K., & Tréguier, A.-M. (2021). Framing, context, and methods. In V. Masson-Delmotte, P. Zhai, A. Pirani, S. L. Connors, C. Péan, S. Berger, N. Caud, Y. Chen, L. Goldfarb, M. I. Gomis, M. Huang, K. Leitzell, E. Lonnoy, J. B. R. Matthews, T. K. Maycock, T. Waterfield, O. Yelekçi, R. Yu, & B. Zhou (Eds.), *Climate change 2021: The physical science basis. Contribution of Working Group I to the Sixth Assessment Report of the Intergovernmental Panel on Climate Change* (pp. 147–286). Cambridge University Press. https://doi.org/10.1017/9781009157896.003

Chen, H., Zhao, J., Zhang, H., Zhang, Z., Guo, X., & Wang, M. (2023). Detection and attribution of the start of the growing season changes in the Northern Hemisphere. *Science of the Total Environment*, *903*, 166607. https://doi.org/10.1016/j.scitotenv.2023.166607

Chen, J., An, A., Gao, G., & Liu, F. (2025). From compound climate risks to adaptive governance: Sectoral economic exposure to heat-drought compound events in coastal China. *Ocean and Coastal Management*, *267*, 107755. https://doi.org/10.1016/j.ocecoaman.2025.107755

Chen, T. C., Collet, F., & Di Luca, A. (2024). Evaluation of ERA5 precipitation and 10-m wind speed associated with extratropical cyclones using station data over North America. *International Journal of Climatology*, *44*(3), 729–747. https://doi.org/10.1002/joc.8339

Cheng, C. S., Li, G., Li, Q., Auld, H., & Fu, C. (2012). Possible impacts of climate change on wind gusts under downscaled future climate conditions over Ontario, Canada. *Journal of Climate*, *25*(9), 3390–3408. https://doi.org/10.1175/JCLI-D-11-00198.1

Ciais, P., Reichstein, M., Viovy, N., Granier, A., Ogée, J., Allard, V., Aubinet, M., Buchmann, N., Bernhofer, C., Carrara, A., Chevallier, F., De Noblet, N., Friend, A. D., Friedlingstein, P., Grünwald, T., Heinesch, B., Keronen, P., Knohl, A., Krinner, G., … Valentini, R. (2005). Europe-wide reduction in primary productivity caused by the heat and drought in 2003. *Nature*, *437*(7058), 529–533. https://doi.org/10.1038/nature03972

Clarke, B., Otto, F., Stuart-Smith, R., & Harrington, L. (2022). Extreme weather impacts of climate change: An attribution perspective. *Environmental Research: Climate*, *1*(1), 012001. https://doi.org/10.1088/2752-5295/ac6e7d

de Luca, P., Messori, G., Pons, F. M. E., & Faranda, D. (2020). Dynamical systems theory sheds new light on compound climate extremes in Europe and Eastern North America. *Quarterly Journal of the*

Royal Meteorological Society, *146*, 1636–1650. https://doi.org/10.1002/qj.3757

De Melo-Abreu, J. P., Villalobos, F. J., & Mateos, L. (2016). Frost protection. In F. Villalobos & E. Fereres (Eds.), *Principles of agronomy for sustainable agriculture* (pp. 443–457). Springer. https://doi.org/10.1007/978-3-319-46116-8_29

Deng, K., Azorin-Molina, C., Minola, L., Zhang, G., & Chen, D. (2021). American Meteorological Society Global Near-Surface Wind Speed Changes over the Last Decades Revealed by Reanalyses and CMIP6 Model Simulations. *Source: Journal of Climate*, *34*(6), 2219–2234. https://doi.org/10.1175/JCLI-D-20-0310.1

Di Capua, G., & Rahmstorf, S. (2023). Extreme weather in a changing climate. *Environmental Research Letters*, *18*(10), 102001. https://doi.org/10.1088/1748-9326/acfb23

Dosio, A., Spinoni, J., & Migliavacca, M. (2023). Record-breaking and unprecedented compound hot and dry summers in Europe under different emission scenarios. *Environmental Research: Climate*, *2*(4), 045004. https://doi.org/10.1088/2752-5295/acfa1b

Ducros, G., Tiggeloven, T., Ma, L., Daloz, A. S., Schuhen, N., Claassen, J., & de Ruiter, M. C. (2025). Multi-hazards in Scandinavia: Impacts and risks from compound heatwaves, droughts and wildfires. *Natural Hazards and Earth System Sciences*, *25*(11), 4693–4712. https://doi.org/10.5194/nhess-25-4693-2025

European Centre for Medium-Range Weather Forecasts. (2021). *CMIP6 climate projections*. Copernicus Climate Change Service. https://doi.org/10.24381/cds.c866074c

European Environment Agency. (2025, October 27). *Economic losses from weather- and climate-related extremes in Europe*. https://www.eea.europa.eu/en/analysis/indicators/economic-losses-from-climate-related

Faust, E., & Herbold, J. (2018). Spring frost losses and climate change – Not a contradiction in terms. *Topics Geo*, 1–11.

Feng, S., Hao, Z., Zhang, Y., Zhang, X., & Hao, F. (2023). Amplified future risk of compound droughts and hot events from a hydrological perspective. *Journal of Hydrology*, *617*, 129143. https://doi.org/10.1016/j.jhydrol.2023.129143

Ford, T. W., Chen, L., Fernandez, E., Wahle, E., Luedeling, E., Todey, D., Nowatzkie, L., De Agronomía, E., & Cat, P. U. (2025). Historical and projected changes in chill accumulation and spring freeze risk in the

Midwest United States. *Agricultural and Forest Meteorology*, *368*, 110532. https://doi.org/10.1016/j.agrformet.2025.110532

Gaska, J. (2023). Climate change and windstorm losses in Poland in the twenty-first century. *Environmental Hazards*, *22*(2), 99–115. https://doi.org/10.1080/17477891.2022.2076646

Gazol, A., & Camarero, J. J. (2022). Compound climate events increase tree drought mortality across European forests. *Science of the Total Environment*, *816*. https://doi.org/10.1016/j.scitotenv.2021.151604

Geirinhas, J. L., Russo, A., Libonati, R., Sousa, P. M., Miralles, D. G., & Trigo, R. M. (2021). Recent increasing frequency of compound summer drought and heatwaves in Southeast Brazil. *Environmental Research Letters*, *16*(3), 034036. https://doi.org/10.1088/1748-9326/abe0eb

Graczyk, D., & Szwed, M. (2020). Changes in the occurrence of late spring frost in Poland. *Agronomy*, *10*(11), 1835. https://doi.org/10.3390/agronomy10111835

Guglielmo, F., Nicolas, J., Vamborg, F., Emerton, R., Simmons, A., & Burgess, S. (2026). *Global climate highlights 2025*. Copernicus Climate Change Service, European Centre for Medium-Range Weather Forecasts. https://doi.org/10.24381/b3nm-p354

Hausfather, Z. (2025). An assessment of current policy scenarios over the 21st century and the reduced plausibility of high-emissions pathways. *Dialogues on Climate Change*, *2*(1), 26–32. https://doi.org/10.1177/29768659241304854

He, Y., Fang, J., Xu, W., & Shi, P. (2022). Substantial increase of compound droughts and heatwaves in wheat growing seasons worldwide. *International Journal of Climatology*, *42*(10), 5038–5054. https://doi.org/10.1002/joc.7518

He, W., Chen, X., Zhang, Y., Duan, W., & Deng, H. (2025). Spatio-temporal variations of compound precipitation and wind-speed extreme events in Fujian and Jiangxi Provinces, Southeast China. *Meteorological and Atmospheric Physics*, *137*, 7. https://doi.org/10.1007/s00703-024-01059-3

Helsinki Commission. (2024). *Climate change in the Baltic Sea 2024 fact sheet*. https://helcom.fi/wp-content/uploads/2024/10/Baltic-Sea-Climate-Change-Fact-Sheet_2024.pdf

Hénin, R., Ramos, A. M., Pinto, J. G., & Liberato, M. L. R. (2021). A ranking of concurrent precipitation and wind events for the Iberian Peninsula. *International Journal of Climatology*, *41*, 1421–1437. https://doi.org/10.1002/joc.6829

Hersbach, H., Bell, B., Berrisford, P., Hirahara, S., Horányi, A., Muñoz-Sabater, J., Nicolas, J., Peubey, C., Radu, R., Schepers, D., Simmons, A.,

Soci, C., Abdalla, S., Abellan, X., Balsamo, G., Bechtold, P., Biavati, G., Bidlot, J., Bonavita, M., … Thépaut, J. N. (2020). The ERA5 global reanalysis. *Quarterly Journal of the Royal Meteorological Society*, *146*(730), 1999–2049. https://doi.org/10.1002/qj.3803

Hufkens, K., Friedl, M. A., Keenan, T. F., Sonnentag, O., Bailey, A., O'Keefe, J., & Richardson, A. D. (2012). Ecological impacts of a widespread frost event following early spring leaf-out. *Global Change Biology*, *18*(7), 2365–2377. https://doi.org/10.1111/j.1365-2486.2012.02712.x

Intergovernmental Panel on Climate Change. (2021). *Summary for policymakers*. In V. Masson-Delmotte et al. (Eds.), *Climate change 2021: The physical science basis. Contribution of Working Group I to the Sixth Assessment Report of the Intergovernmental Panel on Climate Change* (pp. 3–32). Cambridge University Press. https://doi.org/10.1017/9781009157896.001

Ionita, M., Caldarescu, D. E., & Nagavciuc, V. (2021). Compound hot and dry events in Europe: Variability and large-scale drivers. *Frontiers in Climate*, *3*, 688991. https://doi.org/10.3389/fclim.2021.688991

Johansson, E. (2021). Compound extreme wind and precipitation events in Europe [Degree Project C in Meteorology, Uppsala University]. DiVA. https://uu.diva-portal.org/smash/record.jsf?pid=diva2%3A1567650

Juknys, R., Velička, R., Kanapickas, A., Kriaučiūnienė, Z., Masilionytė, L., Vagusevičienė, I., ... & Sujetovienė, G. (2017). Projecting the impact of climate change on phenology of winter wheat in northern Lithuania. *International journal of biometeorology*, *61*(10), 1765–1775. https://doi.org/10.1007/s00484-017-1360-y

Kendon, E., Roberts, N., Fowler, H., Roberts, M., Chan, S., & Senior, C. (2014). Heavier summer downpours with climate change revealed by weather forecast resolution model. *Nature Climate Change*, *4*, 570–576. https://doi.org/10.1038/nclimate2258

Kent, S. T., McClure, L. A., Zaitchik, B. F., Smith, T. T., & Gohlke, J. M. (2014). Heat waves and health outcomes in Alabama (USA): The importance of heat wave definition. *Environmental Health Perspectives*, *122*(2), 151–158. https://doi.org/10.1289/ehp.1307262

Kilkus, K., & Stonevičius, E. (2011). *Lietuvos vandenų geografija*. Vilniaus universitetas.

Kim, S., Sinclair, V. A., Räisänen, J., & Ruuhela, R. (2018). Heat waves in Finland: Present and projected summertime extreme temperatures and their associated circulation patterns. *International Journal of Climatology*, *38*(3), 1393–1408. https://doi.org/10.1002/joc.5253

Koźmiński, C., Mąkosza, A., Nidzgorska-Lencewicz, J., & Michalska, B. (2023). Air frosts in Poland in the thermal growing season (AT > 5 °C). *Agriculture*, *13*(6), 1228. https://doi.org/10.3390/agriculture13061228

Krauklis, A., & Draveniece, A. (2004). Landscape seasons and air mass dynamics in Latvia. *Folia Geographica*, *12*, 16–47.

Lamichhane, J. R. (2021). Rising risks of late-spring frosts in a changing climate. *Nature Climate Change*, *11*(7), 554–555. https://doi.org/10.1038/s41558-021-01090-x

Laurila, T. K. (2022). *Winds and windstorms in northern Europe and Finland* [Doctoral dissertation, University of Helsinki]. https://doi.org/10.35614/isbn.9789523361546

Lavers, D. A., Simmons, A., Vamborg, F., & Rodwell, M. J. (2022). An evaluation of ERA5 precipitation for climate monitoring. *Quarterly Journal of the Royal Meteorological Society*, *148*(748), 3152–3165. https://doi.org/10.1002/qj.4351

Leslie, A. D., Mencuccini, M., & Perks, M. (2014). Frost damage to eucalypts in a short-rotation forestry trial in Cumbria (England). *iForest*, *7*(3), 156–161. https://doi.org/10.3832/ifor1161-007

Lhotka, O., & Brönnimann, S. (2020). Possible increase of vegetation exposure to spring frost under climate change in Switzerland. *Atmosphere*, *11*(4), 391. https://doi.org/10.3390/ATMOS11040391

Li, D., Chen, Y., Messmer, M., Zhu, Y., Feng, J., Yin, B., & Bevacqua, E. (2022). Compound wind and precipitation extremes across the Indo-Pacific: Climatology, variability, and drivers. *Geophysical Research Letters*, *49*(14), e2022GL098594. https://doi.org/10.1029/2022GL098594

Li, D., Zscheischler, J., Chen, Y., Yin, B., Feng, J., Freund, M., Qi, J., Zhu, Y., & Bevacqua, E. (2024). Intensification and poleward shift of compound wind and precipitation extremes in a warmer climate. *Geophysical Research Letters*, *51*(11), 1–11. https://doi.org/10.1029/2024GL110135

Lindsey, R., & Dahlman, L. (2025, gegužės 29). *Climate change: Global temperature*. NOAA Climate.gov. https://www.climate.gov/news-features/understanding-climate/climate-change-global-temperature

Liu, Q., Piao, S., Janssens, I. A., Fu, Y., Peng, S., Lian, X., Ciais, P., Myneni, R. B., Peñuelas, J., & Wang, T. (2018). Extension of the growing season increases vegetation exposure to frost. *Nature Communications*, *9*(1), 426. https://doi.org/10.1038/s41467-017-02690-y

Liu, T., Zhang, Y., Guo, B., Yin, Y., & Ge, J. (2024). Projected changes of compound droughts and heatwaves in China under 1.5 °C, 2 °C, and 3 °C

of global warming. *Climate Dynamics*, *62*(7), 6417–6431. https://doi.org/10.1007/s00382-024-07215-0

Ma, Q., Huang, J. G., Hänninen, H., Berninger, F. (2019). Divergent trends in the risk of spring frost damage to trees in Europe with recent warming. *Global Change Biology 25*(1), 351–360. https://doi.org/10.1111/gcb.14479

Mallard, M. S., Talgo, K. D., Spero, T. L., Bowden, J. H., & Nolte, C. G. (2023). Dynamically downscaled projections of phenological changes across the contiguous United States. *Journal of Applied Meteorology and Climatology*, *62*(12), 1875–1889. https://doi.org/10.1175/JAMC-D-23-0071.1

Markonis, Y., Kumar, R., Hanel, M., Rakovec, O., Máca, P., & AghaKouchak, A. (2021). The rise of compound warm-season droughts in Europe. *Science Advances*, *7*(6), 1–8. https://doi.org/10.1126/sciadv.abb9668

Martinuzzi, S., Allstadt, A. J., Pidgeon, A. M., Flather, C. H., Jolly, W. M., & Radeloff, V. C. (2019). Future changes in fire weather, spring droughts, and false springs across U.S. National Forests and Grasslands. *Ecological Applications*, *29*(5), 1–14. https://doi.org/10.1002/eap.1904

Martius, O., Pfahl, S., & Chevalier, C. (2016). A global quantification of compound precipitation and wind extremes. *Geophysical Research Letters*, *43*(14), 7709–7717. https://doi.org/10.1002/2016GL070017

McKee, T. B., Doesken, N. J., & Kleist, J. (1993, January). The relationship of drought frequency and duration to time scales. *In Proceedings of the 8th Conference on Applied Climatology*, *17*(22), 179–183.

McMaster, G. S., & Wilhelm, W. W. (1997). Growing degree-days: One equation, two interpretations. *Agricultural and Forest Meteorology*, *87*(4), 291–300. https://doi.org/10.1016/S0168-1923(97)00027-0

Messmer, M., & Simmonds, I. (2021). Global analysis of cyclone-induced compound precipitation and wind extreme events. *Weather and Climate Extremes*, *32*, 100324. https://doi.org/10.1016/j.wace.2021.100324

Muccione, V., Haasnoot, M., Alexander, P., Bednar-Friedl, B., Biesbroek, R., Georgopoulou, E., le Cozannet, G., & Schmidt, D. N. (2024). Adaptation pathways for effective responses to climate change risks. *Wiley Reviews: Climate Change*, *15*(4). https://doi.org/10.1002/wcc.883

Mukherjee, S., Ashfaq, M., & Mishra, A. K. (2020). Compound drought and heatwaves at a global scale: The role of natural climate variability-associated synoptic patterns and land-surface energy budget anomalies. *Journal of Geophysical Research: Atmospheres*, *125*(11), 1–19. https://doi.org/10.1029/2019JD031943

Mukherjee, S., & Mishra, A. K. (2021). Increase in compound drought and heatwaves in a warming world. *Geophysical Research Letters*, *48*(1), e2020GL090617. https://doi.org/10.1029/2020GL090617

Muriset, F. (n.d.). *Wetterlagenkalender [Weather situation calendar]*. orniwetter.info. Gauta 2026 m. kovo 10 d., https://www.orniwetter.info/wetterlagenkalender/

Nidzgorska-Lencewicz, J., Mąkosza, A., Koźmiński, C., & Michalska, B. (2024). Potential risk of frost in the growing season in Poland. *Agriculture*, *14*(3), 501. https://doi.org/10.3390/agriculture14030501

Peterson, A. G., & Abatzoglou, J. T. (2014). Observed changes in false springs over the contiguous United States. *Geophysical Research Letters*, *41*(6), 2156–2162. https://doi.org/10.1002/2014GL059266

Piotrowski, P., & Bartoszek, K. (2025). Atmospheric circulation conditions during spring frosts in Southeastern Poland (1981–2023). *Atmosphere*, *16*(4), 409. https://doi.org/10.3390/atmos16040409

Prodhomme, C., Materia, S., Ardilouze, C., White, R. H., Batté, L., Guemas, V., Fragkoulidis, G., & García-Serrano, J. (2022). Seasonal prediction of European summer heatwaves. *Climate Dynamics*, *58*(7–8), 2149–2166. https://doi.org/10.1007/s00382-021-05828-3

Qu, B., Zhu, W., Jia, S., & Lv, A. (2015). Spatio-temporal changes in vegetation activity and its driving factors during the growing season in China from 1982 to 2011. *Remote Sensing*, *7*(10), 13729–13752. https://doi.org/10.3390/rs71013729

Rastogi, D., Trok, J., Depsky, N., Monier, E., & Jones, A. (2024). Historical evaluation and future projections of compound heatwave and drought extremes over the conterminous United States in CMIP6. *Environmental Research Letters*, *19*(1), 014038. https://doi.org/10.1088/1748-9326/ad0efe

Ridder, N. N., Pitman, A. J., Westra, S., Ukkola, A., Do, H. X., Bador, M., Hirsch, A. L., Evans, J. P., Di Luca, A., & Zscheischler, J. (2020). Global hotspots for the occurrence of compound events. *Nature Communications*, *11*, 15. https://doi.org/10.1038/s41467-020-19639-3

Ridder, N. N., Ukkola, A. M., Pitman, A. J., & Perkins-Kirkpatrick, S. E. (2022). Increased occurrence of high impact compound events under climate change. *npj Climate and Atmospheric Science*, *5*(1), 3. https://doi.org/10.1038/s41612-021-00224-4

Rimkus, E., Maciulyte, V., Stonevicius, E., & Valiukas, D. (2020). A revised agricultural drought index in Lithuania. *Agricultural and Food Science*, *29*(4), 359–371. https://doi.org/10.23986/afsci.92150

Rousi, E., Kornhuber, K., Beobide-Arsuaga, G., Luo, F., & Coumou, D. (2022). Accelerated western European heatwave trends linked to more-persistent double jets over Eurasia. *Nature Communications*, *13*(1), 1–11. https://doi.org/10.1038/s41467-022-31432-y

Royal Netherlands Meteorological Institute (KNMI). (n.d.). *Land/sea mask*. KNMI Climate Explorer. Gauta 2026 m. birželio 15 d., https://climexp.knmi.nl/help/landseamask.shtml

Sedlmeier, K., Feldmann, H., & Schädler, G. (2018). Compound summer temperature and precipitation extremes over central Europe. *Theoretical and Applied Climatology*, *131*(3–4), 1493–1501. https://doi.org/10.1007/s00704-017-2061-5

Seneviratne, S. I., Nicholls, N., Easterling, D., Goodess, C. M., Kanae, S., Kossin, J., Luo, Y., Marengo, J., McInnes, K., Rahimi, M., Reichstein, M., Sorteberg, A., Vera, C., & Zhang, X. (2012). Changes in climate extremes and their impacts on the natural physical environment. In C. B. Field, V. Barros, T. F. Stocker, D. Qin, D. J. Dokken, K. L. Ebi, M. D. Mastrandrea, K. J. Mach, G. K. Plattner, S. K. Allen, M. Tignor, & P. M. Midgley (Eds.), *Managing the risks of extreme events and disasters to advance climate change adaptation: A special report of Working Groups I and II of the Intergovernmental Panel on Climate Change* (pp. 109–230). Cambridge University Press.

Seneviratne, S. I., Zhang, X., Adnan, M., Badi, W., Dereczynski, C., Di Luca, A., Ghosh, S., Iskandar, I., Kossin, J., Lewis, S., Otto, F., Pinto, I., Satoh, M., Vicente-Serrano, S. M., Wehner, M., & Zhou, B. (2021). Weather and climate extreme events in a changing climate. In V. Masson-Delmotte, P. Zhai, A. Pirani, S. L. Connors, C. Péan, S. Berger, N. Caud, Y. Chen, L. Goldfarb, M. I. Gomis, M. Huang, K. Leitzell, E. Lonnoy, J. B. R. Matthews, T. K. Maycock, T. Waterfield, O. Yelekçi, R. Yu, & B. Zhou (Eds.), *Climate change 2021: The physical science basis. Contribution of Working Group I to the Sixth Assessment Report of the Intergovernmental Panel on Climate Change* (pp. 1513–1766). Cambridge University Press.

Sewell, K., Paul, S., de Polt, K., Sugg, M. M., Leeper, R. D., Rao, D., & Runkle, J. D. (2024). Impacts of compounding drought and heatwave events on child mental health: Insights from a spatial clustering analysis. *Discover Mental Health*, *4*(1), 3. https://doi.org/10.1007/s44192-023-00055-0

Shen, C., Zha, J., Li, Z., Azorin-Molina, C., Deng, K., Minola, L., & Chen, D. (2022). Evaluation of global terrestrial near-surface wind speed simulated by CMIP6 models and their future projections. *Annals of the*

New York Academy of Sciences, *1518*(1), 249–263. https://doi.org/10.1111/nyas.14910

Shi, Z., Jia, G., Zhou, Y., Xu, X., & Jiang, Y. (2021). Amplified intensity and duration of heatwaves by concurrent droughts in China. *Atmospheric Research*, *261*, 105743. https://doi.org/10.1016/j.atmosres.2021.105743

Simpson, N. P., Williams, P. A., Mach, K. J., Berrang-Ford, L., Biesbroek, R., Haasnoot, M., ... & Trisos, C. H. (2023). Adaptation to compound climate risks: A systematic global stocktake. *Iscience*, *26*(2), 105926. https://doi.org/10.1016/j.isci.2023.105926

Spensberger, C., Madonna, E., Boettcher, M., Grams, C. M., Papritz, L., Quinting, J. F., Röthlisberger, M., Sprenger, M., & Zschenderlein, P. (2020). Dynamics of concurrent and sequential Central European and Scandinavian heatwaves. *Quarterly Journal of the Royal Meteorological Society*, *146*(732), 2998–3013. https://doi.org/10.1002/qj.3822

Swedish Meteorological and Hydrological Institute. (2024, September 13). *Length of the vegetation period*. SMHI. https://www.smhi.se/en/climate/tools-and-inspiration/climate-indicators/length-of-the-vegetation-period

Taszarek, M., Allen, J. T., Brooks, H. E., Pilguj, N., & Czernecki, B. (2021). Differing trends in United States and European severe thunderstorm environments in a warming climate. *Bulletin of the American Meteorological Society*, *102*, 296–322. https://doi.org/10.1175/BAMS-D-20-0004.1

Thrasher, B., Wang, W., Michaelis, A., Melton, F., Lee, T., & Nemani, R. (2022). NASA global daily downscaled projections, CMIP6. *Scientific Data*, *9*(1), 262. https://doi.org/10.1038/s41597-022-01393-4

Tomczyk, A. M. (2015). Impact of macro-scale circulation types on the occurrence of frosty days in Poland. Bulletin of Geography. *Physical Geography Series*, *9*(9), 55–65. https://doi.org/10.1515/bgeo-2015-0016

Tomczyk, A. M., Bednorz, E., Półrolniczak, M., & Kolendowicz, L. (2019). Strong heat and cold waves in Poland in relation with the large-scale atmospheric circulation. *Theoretical and Applied Climatology*, *137*, 1909–1923. https://doi.org/10.1007/s00704-018-2715-y

Twardosz, R., Walanus, A., & Guzik, I. (2021). Warming in Europe: Recent trends in annual and seasonal temperatures. *Pure and Applied Geophysics*, *178*(10), 4021–4032. https://doi.org/10.1007/s00024-021-02860-6

Velikou, K., Lazoglou, G., Tolika, K., & Anagnostopoulou, C. (2022). Reliability of the ERA5 in replicating mean and extreme temperatures across Europe. *Water*, *14*(4), 543. https://doi.org/10.3390/w14040543

Vitasse, Y., Bottero, A., Cailleret, M., Bigler, C., Fonti, P., Gessler, A., Lévesque, M., Rohner, B., Weber, P., Rigling, A., & Wohlgemuth, T. (2019). Contrasting resistance and resilience to extreme drought and late spring frost in five major European tree species. *Global Change Biology*, *25*(11), 3781–3792. https://doi.org/10.1111/gcb.14803

Wang, A., Tao, H., Ding, G., Zhang, B., Huang, J., & Wu, Q. (2023). Global cropland exposure to extreme compound drought heatwave events under future climate change. *Weather and Climate Extremes*, *40*, 100559. https://doi.org/10.1016/j.wace.2023.100559

Wang, C., Li, Z., Chen, Y., Ouyang, L., Zhao, H., Zhu, J., ... & Zhao, Y. (2024). Characteristic changes in compound drought and heatwave events under climate change. *Atmospheric Research*, *305*, 107440. https://doi.org/10.1016/j.atmosres.2024.107440

Wang, T., She, D., Bao, Z., Zhang, Q., Wang, L., Wei, Y., & Niu, Q. (2025). Elucidating diverse population exposure to compound drought and heatwave events from two meteorological drought indices (SPI and SPEI). *Environmental Research Letters*, *20*(3), 034034. https://doi.org/10.1088/1748-9326/adad01

Weggel, J. R. (1999). Maximum daily wind gusts related to mean daily wind speed. *Journal of Structural Engineering*, *125*(4), 465–468. https://doi.org/10.1061/(ASCE)0733-9445(1999)125:4(465)

Werner, P. C., & Gerstengarbe, F.-W. (2010). *Katalog der Grosswetterlagen Europas (1881–2009) nach Paul Hess und Helmut Brezowsky: 7., verbesserte und ergänzte Auflage* [Catalogue of large-scale weather patterns of Europe (1881–2009) according to Paul Hess and Helmut Brezowsky: 7th, revised and expanded edition] (PIK Report No. 119). Potsdam-Institut für Klimafolgenforschung. https://www.pik-potsdam.de/en/output/publications/pikreports/.files/pr119.pdf

Wibig, J. (2017). Heat waves in Poland in the period 1951–2015: Trends, patterns and driving factors. *Meteorology Hydrology and Water Management*, *6*(1), 1–10. https://doi.org/10.26491/mhwm/78420

Wibig, J., & Jędruszkiewicz, J. (2024). Warm and dry compound events in Poland. *Atmosphere*, *15*(9), 1019. https://doi.org/10.3390/atmos15091019

World Meteorological Organization. (2012). *Standardized Precipitation Index user guide* (WMO-No. 1090). https://digitalcommons.unl.edu/droughtfacpub

Wu, J., Shi, Y., & Xu, Y. (2020). Evaluation and Projection of Surface Wind Speed Over China Based on CMIP6 GCMs. *Journal of Geophysical Research: Atmospheres*, *125*(22). https://doi.org/10.1029/2020JD033611

Wypych, A., Sulikowska, A., Ustrnul, Z., & Czekierda, D. (2017). Variability of growing degree days in Poland in response to ongoing climate changes in Europe. *International Journal of Biometeorology*, *61*(1), 49–59. https://doi.org/10.1007/s00484-016-1190-3

Xoplaki, E., Ellsäßer, F., Grieger, J., Nissen, K. M., Pinto, J. G., Chen, T.-C., Feldmann, H., Friederichs, P., Gliksman, D., Haustein, K., Heinke, J., Jach, L., Knutzen, F., Kollet, S., Luther, N., Mohr, S., Mudersbach, C., Müller, C., Simon, F., … Wolf, F. (2023). Compound events in Germany in 2018: Drivers and case studies. *EGUsphere*, 1–43. https://doi.org/10.5194/egusphere-2023-1460

Xu, L., Yu, W., Yang, S., & Zhang, T. (2024). Concurrent drought and heatwave events over the Asian monsoon region: Insights from a statistically downscaling CMIP6 dataset. *Environmental Research Letters*, *19*(3), 034011. https://doi.org/10.1088/1748-9326/ad2cad

Yaddanapudi, R., Mishra, A., Huang, W., & Chowdhary, H. (2022). Compound wind and precipitation extremes in global coastal regions under climate change. *Geophysical Research Letters*, *49*(15), e2022GL098974. https://doi.org/10.1029/2022GL098974

Yin, J., & Slater, L. (2023). Understanding heatwave-drought compound hazards and impacts on socio-ecosystems. *The Innovation Geoscience*, *1*(3), 100042. https://doi.org/10.59717/j.xinn-geo.2023.100042

Zahradníček, P., Brázdil, R., Řehoř, J., Trnka, M., Bartošová, L., & Rožnovský, J. (2024). Past and present risk of spring frosts for fruit trees in the Czech Republic. *Theoretical and Applied Climatology*, *155*(2), 965–984. https://doi.org/10.1007/s00704-023-04671-2

Zhang, J., Zhang, X., Lyu, J., Qu, Y., & Leng, G. (2024). Increasing socioeconomic exposure to compound dry and hot events under a warming climate in the Yangtze River Basin. *Sustainability*, *16*(24), 11264. https://doi.org/10.3390/su162411264

Zhang, Q., She, D., Zhang, L., Wang, G., Chen, J., & Hao, Z. (2022). High sensitivity of compound drought and heatwave events to global warming in the future. *Earth's Future*, *10*(11), e2022EF002833. https://doi.org/10.1029/2022EF002833

Zhu, L., Meng, J., Li, F., & You, N. (2019). Predicting the patterns of change in spring onset and false springs in China during the twenty-first century. *International Journal of Biometeorology*, *63*(5), 591–606. https://doi.org/10.1007/s00484-017-1456-4

Zhu, X., Tang, J., & Yang, Y. (2024). Assessment and projection of compound wind and precipitation extremes in EC-Earth3 of CMIP6 simulations.

Asia-Pacific Journal of Atmospheric Sciences, *60*, 81–93. https://doi.org/10.1007/s13143-023-00337-1

Zohner, C. M., Mo, L., Renner, S. S., Svenning, J. C., Vitasse, Y., Benito, B. M., ... & Crowther, T. W. (2020). Late-spring frost risk between 1959 and 2017 decreased in North America but increased in Europe and Asia. *Proceedings of the National Academy of Sciences*, *117*(22), 12192–12200. https://doi.org/10.1073/pnas.1920816117

Zscheischler, J., Westra, S., van den Hurk, B. J. J. M., Seneviratne, S. I., Ward, P. J., Pitman, A., AghaKouchak, A., Bresch, D. N., Leonard, M., Wahl, T., & Zhang, X. (2018). Future climate risk from compound events. *Nature Climate Change*, *8*(6), 469–477. https://doi.org/10.1038/s41558-018-0156-3

Zscheischler, J., Martius, O., Westra, S., Bevacqua, E., Raymond, C., Horton, R. M., van den Hurk, B., AghaKouchak, A., Jézéquel, A., Mahecha, M. D., Maraun, D., Ramos, A. M., Ridder, N. N., Thiery, W., & Vignotto, E. (2020). A typology of compound weather and climate events. *Nature Reviews Earth & Environment*, *1*(7), 333–347. https://doi.org/10.1038/s43017-020-0060-z

PADĖKA

Pirmiausia norėčiau nuoširdžiai padėkoti savo darbo vadovui prof. dr. Egidijui Rimkui. Ačiū už įtraukias „Meteorologijos pagrindų“ paskaitas, kurios paskatino rinktis meteorologinę (klimatologinę) tiriamojo darbo temą pirmųjų bakalauro studijų metų pabaigoje. Kaip paaiškėjo, pasirinkimas buvo teisingas ir leido pradėti mokslininko kelią, galop atvedusį iki doktorantūros studijų pabaigos. Taip pat dėkoju profesoriui už nuolatinį skatinimą judėti pirmyn, kartu ir už priminimus, kad kartais laikas sustoti ir pailsėti. Ačiū už išsamias mokslines žinias, diskusijas bei milžinišką pagalbą rengiant mokslinius darbus, o ypač šią disertaciją.

Esu labai dėkingas ir savo žmonai Agnei, kuri supratingai leido vykdyti mokslinę veiklą nesuskaičiuojamą (turbūt per didelį) kiekį valandų, visuomet palaikė, duodavo vertingų patarimų bei maksimaliai palengvino ketverius doktorantūros studijų metus. Taip pat ačiū dukrai Saulei, kuri neįtikėtinai praskaidrino paskutiniuosius studijų metus, sunkesnėmis akimirkomis gražindavo šypseną veide ir išmokė geriau planuoti laiką.

Dėkoju ir visam Vilniaus universiteto Chemijos ir Geomokslų fakulteto Hidrologijos ir klimatologijos katedros darbuotojų kolektyvui. Ačiū, kad taip šiltai ir maloniai priėmėte į savo gretas! Ačiū ir už įvairias (ne)mokslines diskusijas, kurios neabejotinai ne tik padėjo atliekant mokslinius tyrimus, bet ir reikšmingai pagerino disertacinio darbo kokybę.

Taip pat ačiū šio darbo recenzentams prof. dr. Donatui Pupieniui ir doc. dr. Laurai Šukienei, kurių pastabos ir komentarai leido reikšmingai patobulinti disertaciją.

Galiausiai norėčiau padėkoti savo artimiesiems, kurie neprieštaravo dėl galbūt kiek neįprastos studijų programos pasirinkimo. Priešingai – nuolat džiaugėsi pasiektais rezultatais ir padėdavo iškilus problemoms.

Ir ačiū visiems, besidomintiems ekstremaliais orų reiškiniais, kompleksiniais klimato įvykiais bei skaitantiems disertaciją. Tikiuosi, kad ši disertacija suteiks naujų žinių ir, galbūt, pagelbės atliekant tolesnius mokslinius tyrimus.

CURRICULUM VITAE

Disertacijos autorius Laurynas Klimavičius gimė Panevėžyje, 2016 m. baigęs Panevėžio Juozo Balčikonio gimnaziją įstojo į Vilniaus universiteto Gamtos mokslų fakulteto „Meteorologijos ir hidrologijos“ studijų programą. 2020 m. baigė studijas diplomu *cum laude*. Baigiamasis darbas tema „Vegetacijos periodo rodiklių skirtinguose žemėnaudos tipuose vertinimas naudojant palydovinius duomenis“. Mokslus tęsė Vilniaus universiteto Chemijos ir geomokslų fakulteto Geomokslų institute, ten 2022 m., parengęs baigiamąjį darbą „Sausrų išplitimo ir intensyvumo vertinimas naudojant palydovinius duomenis“, diplomu *cum laude* baigė „Hidrometeorologijos“ magistro studijas. 2022 m. įstojo į fizinės geografijos mokslo krypties doktorantūrą Vilniaus universitete.

Nuo 2022 m. iki 2025 m. Vilniaus universiteto Chemijos ir geomokslų fakulteto Hidrologijos ir klimatologijos katedroje dirbo lektoriumi, nuo 2025 m. eina jaunesniojo asistento pareigas. Dėstomi dalykai: „Meteorologijos pagrindai“, „Lietuvos vandenų geografija“, „Hidrologijos / meteorologijos tiriamasis darbas“, „Bakalauro baigiamasis darbas“. Veda „Hidrologijos pagrindų“ seminarus bei „Taikomosios meteorologijos“ pratybas. Taip pat vadovauja bakalauro studentų tiriamiesiems bei baigiamiesiems darbams.

PUBLIKACIJŲ KOPIJOS

I PUBLIKACIJA

Compound drought and heatwave events in the eastern part of the Baltic Sea region

Klimavičius, L., & Rimkus, E. (2024). Compound drought and heatwave events in the eastern part of the Baltic Sea region. *Oceanologia*, 66(1), 26–36. https://doi.org/10.1016/j.oceano.2023.06.010

Oceanologia 66 (2024) 26—36

Available online at www.sciencedirect.com

ScienceDirect

journal homepage: www.journals.elsevier.com/oceanologia



ORIGINAL RESEARCH ARTICLE

Compound drought and heatwave events in the eastern part of the Baltic Sea region

Laurynas Klimavičius*, **Egidijus Rimkus**

Institute of Geosciences, Vilnius University, Vilnius, Lithuania

Received 28 February 2023; accepted 30 June 2023
Available online 11 July 2023

KEYWORDS
Compound climate events;
Drought;
Heatwave

Abstract Droughts and heatwaves are natural phenomena that can cause severe damage to the economy, infrastructure, human health, and agriculture, among others. However, in recent years, it has been noted that their combined effect, known as compound drought and heatwave events (CDHE), often results in even greater harm. The main aim of this study was to identify CDHEs in this region during summers from 1950 to 2022 and assess the frequency and intensity of these events. To this end, the periods of droughts and heatwaves that occurred between 1950 and 2022 were determined, and the recurrence, extent, and intensity of these phenomena were evaluated. In this study, 1-month Standard Precipitation Index (SPI) values calculated for each summer day were used to identify droughts, while heatwaves were defined as a period of five or more consecutive days when the daily maximum air temperature (T_{max}) was higher than the 90th percentile of T_{max}. Precipitation and T_{max} data (with a spatial resolution 0.25° x 0.25°) were obtained from the European Centre of Medium-Range Weather Forecast ERA-5 reanalysis dataset. The study showed that in most of the eastern part of the Baltic Sea region, the number of drought days had decreased from 1950 to 2022, while the number of heatwave days had increased significantly. In total, ten CDHEs were identified during the summers of 1950—2022. Eight of these events were recorded in 1994 or later. However, a statistically significant increase of CDHEs was found only in a small part of the study area.
© 2023 Institute of Oceanology of the Polish Academy of Sciences. Production and hosting by Elsevier B.V. This is an open access article under the CC BY license (http://creativecommons.org/licenses/by/4.0/).

* Corresponding author at: Institute of Geosciences, Vilnius University, Vilnius, Lithuania.
E-mail address: laurynas.klimavicius@chgf.vu.lt (L. Klimavičius).
Peer review under the responsibility of the Institute of Oceanology of the Polish Academy of Sciences.

Production and hosting by Elsevier

https://doi.org/10.1016/j.oceano.2023.06.010
0078-3234/© 2023 Institute of Oceanology of the Polish Academy of Sciences. Production and hosting by Elsevier B.V. This is an open access article under the CC BY license (http://creativecommons.org/licenses/by/4.0/).

1. Introduction

Various extreme weather phenomena have become more frequent over the last decades due to climate change. They cause damage to different areas, including residents and their living environment, infrastructure, wildlife, the economy, etc. Therefore, acquiring a better understanding of the genesis of such phenomena and their possible impacts is particularly important, as it can help not only reduce economic losses but also save lives (Rutgersson et al., 2022; Zscheischler et al., 2020a). Until the middle of the last decade, most research focused only on the impacts of individual elements of the climate system and their potential alterations in a changing climate. However, in recent years, the most significant threats and damage have occurred when several physical processes interacted simultaneously, resulting in a compound climate event (CCE) (Leonard et al., 2014; Ridder et al., 2020; Seneviratne et al., 2012; Zscheischler et al., 2020a). According to Zscheischler et al. (2018), CCEs are defined as a combination of several processes or hazards that pose social or environmental risks. Currently, CCEs are classified into four different groups: 1) preconditioned; 2) multivariate; 3) spatially compounding events; and 4) temporally compounding events (Zscheischler et al., 2020b). Recently, a lot of attention has been paid to the events that belong to the second group, namely multivariate events. These are CCEs where several different recurring processes or phenomena, acting in the same geographical location, cause an impact (Messori et al., 2021; Zscheischler et al., 2020b). Droughts and heatwaves, which are the focus of this study, are examples of such multivariate CCEs as well.

Although droughts and heatwaves cause significant damage when acting individually, during the first decades of this century, it was noted that their combined effect, defined as a compound drought and heatwave event (CDHE), often resulted in even greater harm. Furthermore, these compound events can have a negative impact even when the individual components, droughts and heatwaves, are not extreme and do not pose a significant threat (Mazdiyasni and AghaKouchak, 2015). Indeed, CDHEs cause harm to various natural systems, water resources, and the economy, and can cause natural disasters, have a negative socio-economic impact, and pose a threat to human lives (Bezak and Mikoš, 2020; Feng et al., 2020; Mukherjee and Mishra, 2020; Shi et al., 2021; Wang et al., 2022; Wu et al., 2019; Zhang et al., 2022). One of the main consequences of CDHEs is an increased risk of forest fires and tree mortality (Gazol and Camarero, 2022; Markonis et al., 2021; Rutgersson et al., 2022; Zscheischler et al., 2020a). According to a study by Gazol and Camarero in 2022, 63% of tree mortality events in Europe between 1901 and 2018 were associated with these compound events. Another area affected by CDHEs is crop production and their yield (He et al., 2022; Ribeiro et al., 2020). It has been found that globally, during the period from 1981 to 2020, more than 92% of the areas where crops were grown were affected by at least one CDHE through the vegetation season. During this period, the areas affected by extreme CDHEs increased (from 62% to 75%) along with the likelihood of recurrence of such events (from 20% to 33%) (He et al., 2022). Compound droughts and heatwaves also have a negative impact on the carbon cycle. During the 2003 drought and heatwave in Europe, gross primary productivity in Europe decreased by 30%, leading to an anomalously strong flux of carbon dioxide into the atmosphere (Ciais et al., 2005).

The damage and negative impact caused by CDHEs have become an increasingly relevant topic in recent years, as it has been observed that such events are becoming more frequent in various regions of the world. From 2000 to 2016, the number of CDHEs in various parts of the planet had increased by 1—5 events per year (Mukherjee et al., 2022). Another study found that from 1983 to 2016, the frequency (by 1—3 events per year), duration (by 2—10 days per year), and intensity of these compound events had increased in different areas of the planet. The most significant changes were recorded in the United States, the Amazon basin, Central and Northern Europe, Eastern and Central Asia, and Australia (Mukherjee and Mishra, 2020; Ridder et al., 2020). In various regions of Europe, the frequency and intensity of CDHEs have also increased since the mid-20th century (Ionita and Nagavciuc, 2021b). Such changes have been observed in Eastern Europe as well (Vyshkvarkova and Sukhonos, 2022), with the greatest increases occurring in Central Europe and the Mediterranean region, where one-third of the most intense CDHEs were recorded between 2000 and 2015 (Ionita and Nagavciuc, 2021b; Markonis et al., 2021). In another study, the main hotspots of CDHEs on the continent were found to be in Northern and Eastern Europe, Western European regions, Italy, and the Balkan Peninsula (Bezak and Mikoš, 2020). The main causes of these changes, according to the latest IPCC report, are human influence and anthropogenic climate change (Seneviratne et al., 2021).

However, despite the changing climate and an increasing interest in compound climate events at the global and European level, droughts and heatwaves in the eastern part of the Baltic Sea region have only been studied separately. The formation and recurrence of CDHEs in this area have not been analysed, making this study the first of its kind in the region. Therefore, the main goal of this study was to identify CDHEs in the eastern part of the Baltic Sea region during summers from 1950 to 2022 and assess the frequency and intensity of these events. To achieve this objective, the periods of droughts and heatwaves between 1950 and 2022 were also determined, and the recurrence, extent, and intensity of these phenomena in the eastern part of the Baltic Sea region were evaluated.

2. Data and methods

2.1. Study area and data

The eastern part of the Baltic Sea region was investigated in this study, encompassing the region from 53.5° to 60° N and from 20° to 28.5° E. This area covers the entire territory of Lithuania, Latvia, Estonia, the Kaliningrad region of Russia, the northern-eastern part of Poland, the western part of Russia, and the north-western part of Belarus (Figure 1).

According to the W. Köppen climate classification, whole study area belongs to the warm-summer humid continental climate (*Dfb*) type as the average air temperature during the coldest months of the year (December—February) falls

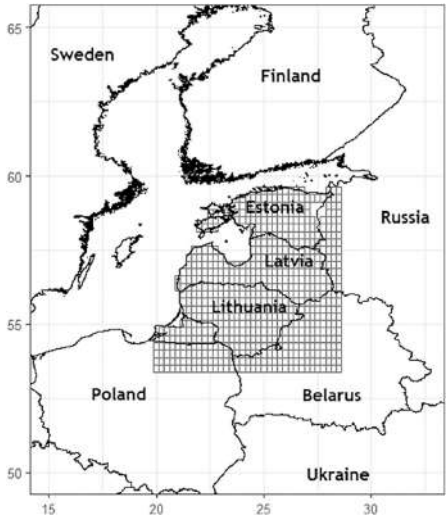

Figure 1 Map of the study area. Grey grid cells mark the territory analysed in this study.

below 0°C (Peel et al., 2007). The highest average monthly temperature in the region is recorded in July and reaches 17–18°C. The annual precipitation in the eastern part of the Baltic Sea region is 550–900 mm, with the highest amount recorded in the western part of Lithuania. The most rainfall in the study area occurs in July and August, with an average of 70–90 mm per month.

Daily data of maximum daily air temperature (T_{max}) and precipitation from 1950 to 2022 were used to identify and evaluate droughts, heatwaves, and CDHEs in the summer months in the eastern part of the Baltic Sea region. The data was obtained from the European Centre of Medium-range Weather Forecast ERA-5 reanalysis database. The grid size of the data was 0.25 × 0.25°. In total, 668 land grid cells covered the study area.

2.2. Evaluation of droughts

The SPI (Standardized Precipitation Index) was used to identify droughts during the study period (McKee et al., 1993). Daily precipitation data were used to calculate this index. The main advantage of the SPI is that it is universal and can be successfully applied to any location in the world, due to the normalisation of the precipitation data sequence during its calculation (Tsakiris and Vangelis, 2004; WMO, 2012). Finally, because of its simple calculation mechanism and applicability to various locations, the World Meteorological Organisation (WMO) recommends using this index for drought identification and evaluation (WMO, 2012). Another distinctive feature of the SPI is that it can be calculated at different time scales, from one to 48 months (WMO, 2012). However, in order to evaluate short-term changes, a 1-month time scale is typically used, as in other studies of droughts and CDHEs (He et al., 2022; Kong et al., 2020; Sharma and Mujumdar, 2017; Shi et al., 2021). SPI values range from +3 to −3. If SPI > +1, conditions are wet; when +1 > SPI > −1, average moisture conditions are identified; SPI < −1 represents dry conditions; and if SPI < −2, conditions are extremely dry (McKee et al., 1993).

In this study, 1-month SPI values were calculated for each day of the study period. Because 30 days of precipitation data are required to calculate the SPI values for June days, values of this meteorological variable for the months of May were also used. Droughts were distinguished if the SPI values were lower than −1 for at least five or more consecutive days and this condition was met in at least one third of the study area during the maximum extent of the drought. The beginning of a drought was considered when SPI values were lower than −1 in more than 10% of the points of the study area, and the end of a drought was determined when this criterion was no longer met. Drought recurrence and duration changes during the summer months were evaluated from 1950 to 2022. The statistical significance of changes was evaluated by performing a Mann-Kendall test. These changes were considered statistically significant if $p < 0.05$. The intensity of each drought was determined by calculating the median of the SPI values in the area affected by a drought. Then, during the maximum spread of each drought, the 5-day average of SPI medians was calculated and the Min-Max normalisation method was applied.

2.3. Evaluation of heatwaves

Summer daily maximum temperature data (T_{max}) were used to identify heatwaves For each summer day and each grid cell of interest, the 90th percentile of the daily maximum air temperature (T_{90}) was calculated on a 5-day moving window. A heatwave was identified if it was found that $T_{max} > T_{90}$ for at least five consecutive days and this condition was met for at least one-third of the study area. This criterion has been used in other studies (Mazdiyasni and AghaKouchak, 2015; Sharma and Mujumdar, 2017) and the method of using the 90th percentile of daily maximum temperature is widely applied in identifying heatwaves in Europe (García-León et al., 2021; Kim et al., 2018; Prodhomme et al., 2022; Rousi et al., 2022) and globally (Mukherjee et al., 2020; Perkins-Kirkpatrick and Gibson, 2017; Ridder et al., 2020). Its main advantage is that the method is relative rather than absolute, so it can be successfully applied to any location at any time of the year (Basarin et al., 2020; Ridder et al., 2020). Calculations are usually performed using various moving averages (ranging from 3 to 31 days), but the most commonly used criterion is 15 days (Geirinhas et al., 2021; Perkins-Kirkpatrick and Gibson, 2017; Sharma and Mujumdar, 2017; Wang et al., 2022). However, there is no consensus on the number of days to be considered, which also depends on the duration of the period under investigation. Since only summer months (92 days) were analysed in this study, a 5-day moving average period, which has been used in other studies (He et al., 2022), was chosen.

In this study, the start date of a heatwave was defined as a day when a heatwave was recorded in at least 10% of the grid cells based on the 90th percentile criterion. The end date of a heatwave was defined as the last day when T_{max} still satisfied this criterion. Changes in the frequency and duration of heatwaves during the study period were

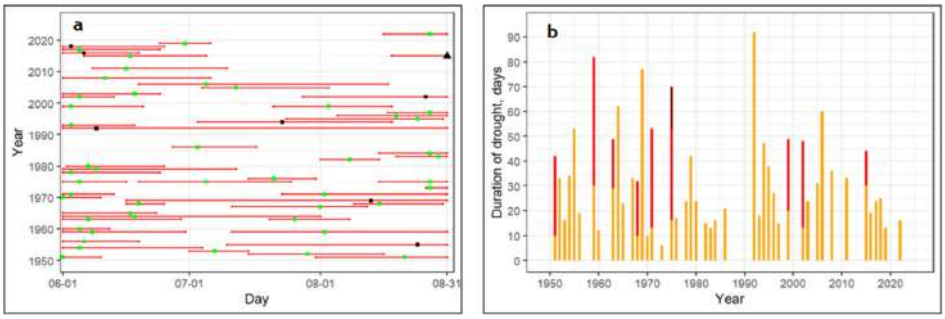

Figure 2 a) Droughts and their duration in the eastern part of the Baltic Sea region from 1950 to 2022. Squares indicate the days when each drought affected the largest part of the study area. Black squares indicate droughts whose intensity, according to the normalised 5-day SPI median average values, was greater than 0.5, while green squares indicate droughts whose intensity was less than 0.5. The black triangle indicates the date when the most intense drought reached its maximum extent. b) The duration of droughts (in days) from 1950 to 2022. The orange colour indicates the first drought in the corresponding year, red indicates the second, and dark red indicates the third.

assessed by evaluating the statistical significance of the observed changes. Heatwaves were also examined separately and assessed in each grid cell by evaluating the frequency of heatwave days and changes in the recurrence of this phenomenon over the period from 1950 to 2022. The intensity of the heatwaves was assessed by calculating the 5-day median average during the maximum spread of each heatwave and normalising the obtained values using the Min-Max method — the same principle was used in drought analysis.

2.4. Definition of CDHE

In this study, CDHEs were identified when both droughts and heatwaves reached their maximum extent in at least one-third of the studied area at the same time. The beginning of such events was considered as the day when the coincidence of these phenomena was detected in at least one-tenth of the study area points. Each CDHE lasted until the number of such grid cells no longer exceeded one-tenth of all points. The duration of each identified CDHE, the date of its maximum extent, and the percentage of the study area affected during that time were evaluated. The recurrence and duration of such events in the study area were also determined. The intensity of a CDHE was determined using the Min-Max normalization method, and the statistical significance of the changes in CDHE cases at each study grid cell was assessed by performing the Mann-Kendall test ($p < 0.05$).

3. Results

3.1. Droughts

Fifty-five droughts were identified in the eastern part of the Baltic Sea region during the period of 1950—2022 according to selected criteria (Figure 2a). The highest number of droughts (10) was identified during the period of 1970—1979 while three separate drought events were detected in the summer of 1975 (Figure 2b). Later on, there was a decrease in the number of droughts in the region — only five of them were recorded in the 1990s, and no droughts were identified in the study area between 1987 and 1991. Another period of increased drought reoccurrence was observed from 1992 to 1999, during which eight droughts were identified. In particular, in 1992, the longest drought lasting throughout the entire summer (92 days) was recorded according to selected criteria (Figure 2a). Despite this, it was noted that the number and duration of droughts decreased over the entire study period of 1950—2022 (Figure 2b). However, these changes were not statistically significant (when $p < 0.05$).

Two droughts that affected the majority of the study area were distinguished in 1955 (lasting from July 10th to August 31st) and 1994 (lasting from July 3rd to August 18th). Both of these droughts covered the entire study area at their maximum spatial extent. According to the normalised values of the 5-day median average, the most severe (intense) drought was the one that occurred at the end of the summer of 2015 (Figure 2a).

The largest number of drought days (>140 per decade) was identified in the eastern part of the study region, while the lowest number of such days (around 100) was found in the southwestern part of the study area (Figure 3a). It was calculated that the number of drought days from 1950 to 2022 had decreased in 89% of the study area's grid cells. However, statistically significant changes (when $p < 0.05$) were only found at three points in Estonia. In the majority of the study area, although the changes were negative, they were close to zero. The number of days with droughts had slightly increased only in the central part of Latvia and the southeastern edge of the study area over the 73-year period (Figure 3b).

3.2. Heatwaves

Thirty-seven heatwave events were identified in the eastern part of the Baltic Sea region from 1950 to 2022. Remarkably, heatwaves have become increasingly frequent in

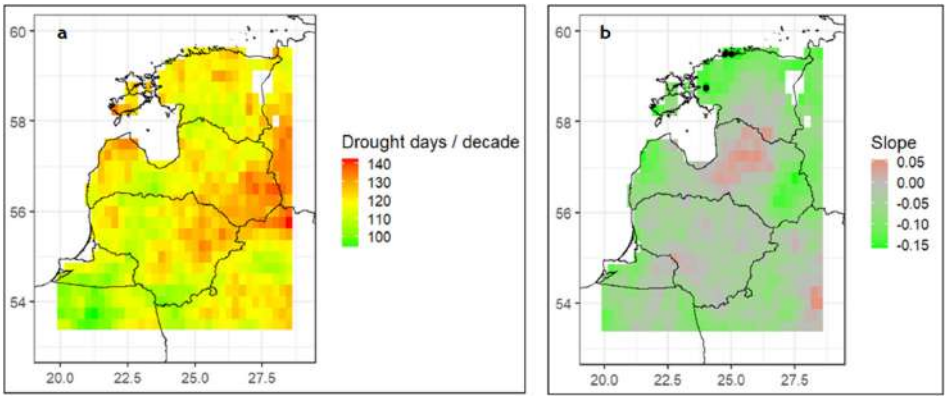

Figure 3 The number of drought days per decade in the study area (a) and the change in the number of drought days from 1950 to 2022 in each grid cell (b). Black dots indicate grid cells where the changes were statistically significant ($p < 0.05$).

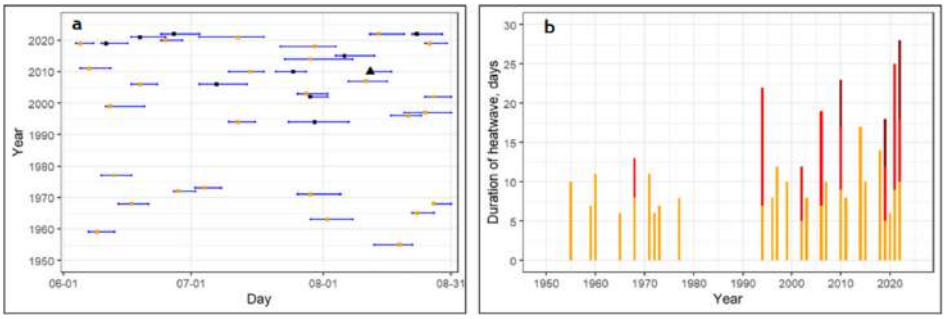

Figure 4 a) Heatwaves and their duration in the eastern part of the Baltic Sea region from 1950 to 2022. Squares indicate the days when each heatwave affected the largest part of the study area. Black squares indicate heatwaves whose intensity, according to the normalised 5-day SPI median average values, was greater than 0.5, while green squares indicate heatwaves whose intensity was less than 0.5. The black triangle indicates the date when the most intense heatwave reached its maximum extent. b) The duration of heatwaves (in days) from 1950 to 2022. The orange colour indicates the first heatwave in the corresponding year, red indicates the second, and dark red indicates the third.

recent decades. These phenomena were not identified between 1978 and 1993, whereas in the past 13 years (from 2010 to 2022), as many as 16 heatwaves have been distinguished (Figure 4a). The longest heatwave was identified in the summer of 2014. It lasted for 17 days (from July 23rd to August 8th). More heatwaves were observed in the second half of the summer (Figure 4a). It was also found that during the summers of 2010, 2019, and 2022, three heatwaves were recorded in the eastern part of the Baltic Sea region, whereas no such cases were identified prior to 2010. When assessing the changes in the frequency and duration of heatwaves from 1950 to 2022, our analyses showed that the number of days when a heatwave was identified in the entire study area during the summer season exhibited statistically significant increase (Figure 4b).

The heatwave which covered the highest number of grid cells during its maximum extent date occurred in 2021. On its peak day, June 19th, it covered the entire study area. The 2014 and 2006 heatwaves also covered almost the entire study area at their peak, with the 2014 heatwave reaching 99.85% of the study area on July 29th and the 2006 heatwave reaching 99.55% of the area on July 7th. The most severe heatwave was also identified in the 21st century, in 2010 (Figure 4a). Finally, it should be noted that of the ten most intense heatwaves, nine were recorded during the period from 2002 to 2022 (Figure 4a).

The highest number of heatwave days, when considering their occurrence in separate grid cells in the study area, was found in the northern part of the study area in Estonia. Here, the number of such cases in some places exceeded 40 per decade. The lowest number of heatwave days occurred in the southern and southwestern parts of the analysed area, where the number of such days per decade was just over 20 (Figure 5a). It was also found that the number

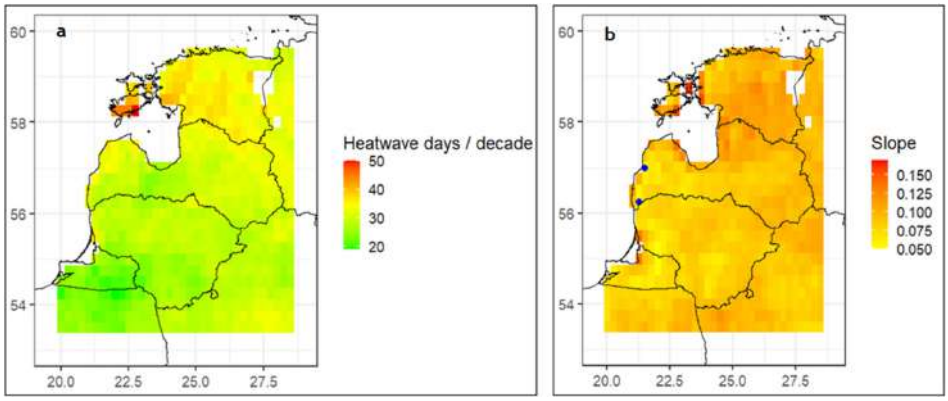

Figure 5 Heatwave days per decade in different points of the eastern part of the Baltic Sea region (a) and the change in the number of heatwave days from 1950 to 2022 in each point of the study area (b). Blue dots indicate those points where the changes were statistically insignificant (when $p > 0.05$).

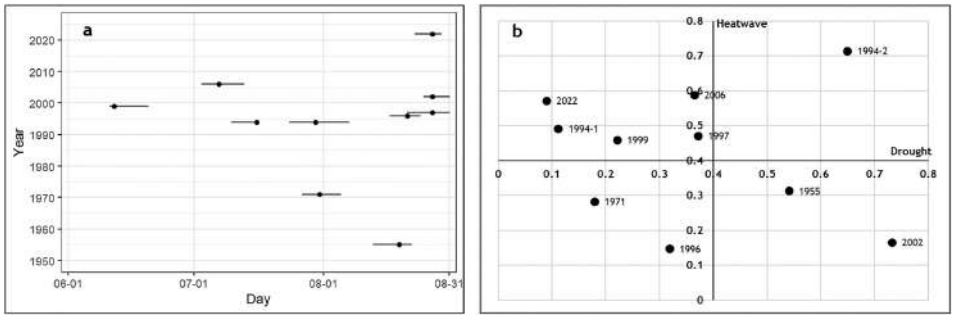

Figure 6 a) Compound drought and heatwave events (CDHE) over 1950—2022 and their duration in the eastern part of the Baltic Sea region. Black dots mark the days when the corresponding CDHE covered the largest part of the studied area. b) The intensity of each CDHE obtained by calculating the normalised SPI and $T_{max} - T_{90}$ values. 1994-1 indicates the first CDHE of that year, and 1994-2 indicates the second one.

of heatwave days from 1950 to 2022 increased throughout the whole eastern part of the Baltic Sea region, and this change was not statistically significant (when $p < 0.05$) in only two grid cells located in western Latvia. The greatest increase in the number of heatwave days over 73 years was found in coastal regions (Figure 5b).

3.3. Compound drought and heatwave events

A total of ten CDHEs (periods when a compound event was recorded in more than a third of the study area during its largest extent) were identified in the eastern part of the Baltic Sea region during the summer months of 1950—2022 (Figure 6a). The majority of these were recorded in the second half of summer, with only one CDHE identified in June (in 1999, from June 11th to 20th). Most of CDHEs (half of all cases) were recorded in the 1990s, specifically from 1994 to 1999. The year 1994 was the only year when two CDHEs were identified during the summer. The second complex event in that year was the longest of all CDHEs identified in this study, lasting for 15 days (from July 24th to August 7th) (Figure 6a). This event also covered the largest part of the study area (94.2%) and was the most intense (Figure 6b). When considering the intensity of the CDHEs, the one recorded in 2002 also stood out among all compound events. In fact, it was accompanied by the most intense drought (among those that coincided with heatwaves in at least a third of the study area points). However, the heatwave was weak, which resulted in a lower intensity of this CDHE compared to the second CDHE in 1994 (Figure 6b).

During the analysis of individual grid cells within the study area, the largest number of CDHEs (when droughts and heatwaves coincided only in individual points) during the summer months of 1950—2022 was identified in the eastern and southeastern parts of the study area, which were characterised by a high number of droughts. In these areas, the

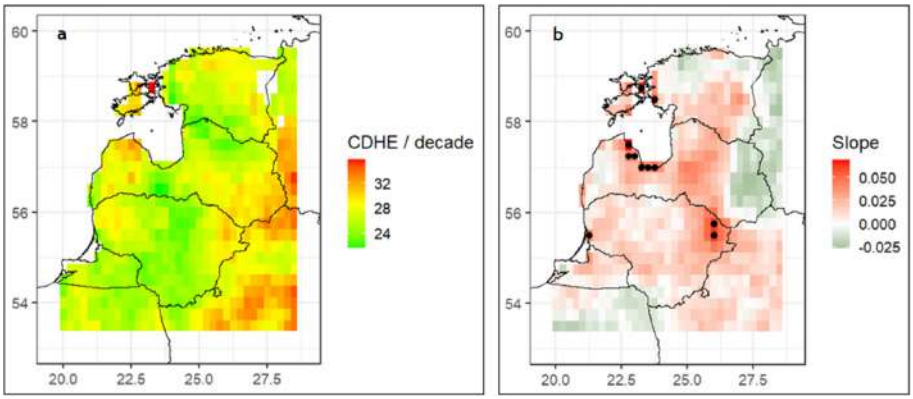

Figure 7 Number of compound drought and heatwave events (CDHE) per decade in different points of the eastern part of the Baltic Sea region (a) and changes in the number of CDHE cases from 1950 to 2022 in each point of the study area (b). Black dots indicate those grid points where the changes were statistically significant (when $p < 0.05$).

number of CDHE days in individual grid cells over the entire study period exceeded 240 (more than 33 per decade). However, the largest number of CDHEs was recorded on Muhu Island, which belongs to Estonia, where 261 CDHE days were identified from 1950 to 2022 (Figure 7a).

An analysis of the variability of CDHEs in individual points over the entire study period showed that such events were occurring more frequently in a large part of the study area. However, this change was statistically significant ($p < 0.05$) in only 1.6% of the entire study area (11 grid cells), and most of the points showing such changes are located along the coast of the Gulf of Riga (Figure 7b). Meanwhile, decreasing tendencies in the occurrence of CDHEs were observed in the northeast-eastern and southwestern parts of the study area. This was primarily due to less frequent droughts occurring in these regions (Figure 4b). However, the changes in this case were small and statistically insignificant.

4. Discussion

The main factor determining the decrease in the number of droughts since the mid-20th century in this and other studies (Jaagus and Aasa, 2018; Jaagus et al., 2022; Rimkus et al., 2013; Valiukas, 2015) was an increased amount of rainfall. However, in most cases, the changes are small and statistically insignificant. The greatest (and statistically significant) decrease in the number of drought days was observed in the northern part of the study area (Estonia), where a statistically significant increase in rainfall has been recorded since the mid-20th century (Jaagus and Aasa, 2018). Although the number of droughts has not changed significantly in various parts of the Baltic Sea region over the past few decades, their intensity has been increasing, and they have been becoming more extreme (Somorowska, 2016; Valiukas, 2015). This study confirmed these trends, with eight out of the ten of the most intense droughts identified in 1994 or later, and the most intense drought occurring in August 2015. It is predicted that in the future, due to a rapidly changing climate, the unevenness of rainfall distribution will further increase and temperatures will rise, leading to more intense droughts in the eastern Baltic Sea region as well as various regions of the world (Keršytė et al., 2015; Rimkus et al., 2020; Seneviratne et al., 2021).

In contrast to droughts, the number and duration of heatwaves increased in the eastern Baltic Sea region during the period from 1950 to 2022. Changes were statistically significant in almost the entire study area. Such trends have been observed in various parts of the world, including the eastern part of the Baltic Sea region (Awasthi et al., 2022; BACC II, 2015; Basarin et al., 2020; Seneviratne et al., 2021; Suursaar, 2022; Yoon et al., 2020). The main explanation for this is an increasing maximum daily temperature caused by climate change.

The highest number of heatwave days was identified in the northern part of the study area, which may be related to the 90th percentile method used to determine them. In the northern part of the study area (Estonia), the T_{90} values on a corresponding summer day during the study period were generally lower than in the areas further south. Therefore, when a heatwave formed and the temperature was similar throughout the study area, the T_{90} was often exceeded on more days at higher latitudes than in the southern part of the study area. The largest increase in the number of heatwave days since the mid-20th century was observed in coastal territories and the Muhu and Sarema islands.

It has been noted that the number and extremeness (the maximum area covered and intensity) of heatwave days had both increased during the study period. This was also a consequence of a warming climate. Similar trends have been observed in Poland when studying heatwaves — 11 heatwaves have been recorded since 1980, covering more than a quarter of the country's territory and lasting for at least a week. However, only one such event had been recorded prior to 1990, and more than half have occurred in the last decade (Wibig, 2021). The longest heatwaves in Poland were recorded in 1994 and 2015 (Tomczyk et al., 2020; Wibig, 2017).

All the characteristics defining the aforementioned heatwaves (number of heatwave days, intensity, covered area) are expected to increase in the future (Basarin et al., 2020; Rutgersson et al., 2022; Seneviratne et al., 2021). It has been determined that the number of heatwave days will increase by 4—34 days per season for each degree Celsius of global warming, depending on the region. The duration of heatwaves is expected to increase by 2—10 days/°C, with the greatest changes predicted to occur at lower latitudes (Perkins-Kirkpatrick and Gibson, 2017). These changes will also increase the damage caused by heatwaves. If adaptation and mitigation measures are not taken, it is likely that their impact in Europe could increase by a factor of five by 2060, compared to the historical period of 1981—2010 (García-León et al., 2021); in some areas of the Baltic Sea region, the risk of heatwaves may double by the end of this century (Rutgersson et al., 2022).

When evaluating the recurrence of CDHEs in the eastern part of the Baltic Sea region, it was observed that the vast majority of these (8 out of 10 events) were recorded from 1994 onwards. When assessing changes of CDHEs in individual grid cells, it was also found that the CDHE frequency increased in 73% of these cells during the 1950—2022 period. Similar results, indicating an increasingly frequent recurrence of CDHEs, have been obtained through studies of such events in various regions of the world and Europe (Bezak and Mikoš, 2020; Geirinhas et al., 2021; Kong et al., 2020; Mazdiyasni and AghaKouchak, 2015; Sedlmeier et al., 2018; Shi et al., 2021). However, during this study, a statistically significant increase in the occurrence of CDHEs was found in a very small area due to the decreasing frequency of droughts.

The majority of CDHEs occurred during the second half of the summers, which was closely related to the occurrences of heatwaves during the summers. The distribution of CDHEs in different points of the studied territory largely coincided with the distribution of dry days — in both cases, the most frequent occurrences of droughts and CDHEs were identified in the eastern and southeastern parts of the study area, as well as in the northwestern part of Latvia and on the islands of Muhu and Saaremaa. The most exceptional CDHE occurred between July 24 and August 7, 1994. This was the longest-lasting and the most intense event, covering the largest part of the studied territory at its maximum extent. This was also the only case when a CDHE was identified twice during the same summer (1994), which could have contributed to the extremeness of this complex event.

It is predicted that in the future, with ongoing climate change and increasing global mean temperatures, CDHEs will occur more frequently and an increase in intensity and duration will also be expected (Seneviratne et al., 2021). It has been calculated that with every degree Celsius of global warming, the duration of these complex events will increase by an average of ten days (Zhang et al., 2022). The frequency and occurrence of CDHEs in Europe will also increase in the future (Mukherjee et al., 2022; Sedlmeier et al., 2018), leading to a growing probability of negative impacts and damages. The forestry sector will be most affected, with an increased risk of forest fires and tree mortality (Feng et al., 2020; Gazol and Camarero, 2022; Seneviratne et al., 2021).

Atmospheric processes and their dynamics play a significant role in the formation of both droughts, heatwaves, and CDHE. One notable process is the prevalence of anticyclonic circulation and atmospheric blocking (Ionita et al., 2021a; Liu et al., 2020; Sousa et al., 2018; Spensberger et al., 2020). It has been observed that drought formation in the Baltic countries is almost always influenced by strong anticyclonic circulation (Rimkus et al., 2014). Similar tendencies were identified when studying the drought that affected Poland during the summer of 2019 (Ziernicka-Wojtaszek, 2021). Furthermore, it was determined that 60% of heatwaves in Central Europe during the period of 2001—2011 coincided with the formation of blocking systems (Porebska and Zdunek, 2013). However, statistically significant changes in the recurrence of such systems in the Northern Hemisphere from 1901 to 2010 have not been detected. Nevertheless, it has been observed that the duration of blocking systems is becoming longer (Wazneh et al., 2021).

The formation of droughts and/or heatwaves is also influenced by large-scale atmospheric circulation, not just local atmospheric processes. When studying the recurrence of heatwaves in Poland, it has been observed that several synoptic features play a role in their formation. These include a strong Azores high-pressure system, higher-than-usual atmospheric pressure over Central Europe, resulting in calm and sunny weather, and a strong blocking system over the North Atlantic (Wibig, 2017).

Finally, several aspects must be considered in further research. First, an important aspect that can influence the accuracy and reliability of obtained results and trends is the uncertainties and biases of the data obtained from the ERA5 database. ERA5 uses a 10-member ensemble that provides uncertainty information. However, in this case, one of the problems encountered is the lack of small-scale variability in ensemble members, and the model itself tends to have overconfidence in the uncertainty characterization (Bandhauer et al., 2022). This is because the perturbations are oriented towards large-scale dynamic variables (Hersbach et al., 2020).

However, the inaccuracies of ERA5 reanalysis data are mostly encountered in mountainous regions (e.g., in the Alps) or continents other than Europe (Bell et al., 2021; Hersbach et al., 2020; Lavers et al., 2022; Velikou et al., 2022). Only a few issues were found while analysing the performance of ERA5 in mid-latitudes. During the evaluation of extremely high temperature (above 95th percentile), it was observed that ERA5 tends to overestimate values of this variable, but the differences compared to observations are not statistically significant (Velikou et al., 2022). It was also found that random errors of precipitation data increase during the summer in mid-latitudes (Lavers et al., 2022). However, in more than 90% of cases, the variability of monthly precipitation values in Europe coincides with observations (Bell et al., 2021). Therefore, despite the shortcomings, ERA5 precipitation and temperature data are sufficiently accurate to use in mid-latitudes in Europe (Bandhauer et al., 2022; Lavers et al., 2022; Nogueira, 2020; Velikou et al., 2022).

Also, when evaluating long-term trends, it is important to emphasize that the accuracy of ERA5, like any other reanalysis data, decreases and errors increase going further

back in time. The reason for this is simple – a significantly smaller number of observations were available at the beginning of the period (1950's) compared to the past decades (Bell et al., 2021). Additionally, the number of satellite observations and their quality increased rapidly, which also plays a significant role in the accuracy of the obtained data (ECMWF, 2023).

The choice of the index used to identify droughts is also crucial. Although the SPI which was used in this study was suitable for assessing droughts in the study region, it has several limitations. The main one is that it only considers precipitation and does not take into account the effect of temperature on drought formation. As the climate changes and mean temperature rapidly increase, the latter factor will become crucial in accurately identifying droughts (Vicente-Serrano et al., 2010; WMO, 2012). It is also important to investigate the processes that lead to the formation of CDHEs in the eastern part of the Baltic Sea region and to evaluate the possible changes in CDHE characteristics in the future. This would help develop more effective adaptation and mitigation strategies and thus minimise the risks posed by CDHEs (Bezak and Mikoš, 2020; Mazdiyasni and AghaKouchak, 2015; Sedlmeier et al., 2018).

5. Conclusions

A decrease in the number of drought days was observed from 1950 to 2022 in most of the eastern part of the Baltic Sea region (89%). However, almost all these changes were statistically insignificant. Only a slight increase in the number of drought days was identified in the central part of Latvia and the southeastern outskirts of the study area. In contrast to droughts, the number and duration of heatwaves, have increased in the entire research area. The obtained changes were statistically significant in 99.7% of the study area. The extremeness of heatwaves (intensity and the area covered during their maximum extent) has also increased in the region due to rising temperatures caused by changing climate. The largest number of heatwave days was identified in the northern part of the study region and on the coast of the Baltic Sea. Ten CDHEs were identified in the eastern part of the Baltic Sea region, with eight of them recorded in 1994 or later. Moreover, an increase in the number of CDHEs was observed in 73% of the study area, but statistically significant changes were only found in 1.9% of the region. The largest positive changes were found in coastal regions, as well as in the northeastern part of Lithuania.

Declaration of competeing interest

The authors declare that they have no known competing financial interests or personal relationships that could have appeared to influence the work reported in this paper.

References

Awasthi, A., Vishwakarma, K., Pattnayak, K.C., 2022. Retrospection of heatwave and heat index. Theor. Appl. Climatol. 147 (1–2), 589–604. https://doi.org/10.1007/s00704-021-03854-z

BACC II Author Team, 2015. Second Assessment of Climate Change for the Baltic Sea Basin. Helmholtz-Zentrum Geesthacht GmbH, Germany, 501 pp.

Bandhauer, M., Isotta, F., Lakatos, M., Lussana, C., Båserud, L., Izsák, B., Szentes, O., Tveito, O.E., Frei, C., 2022. Evaluation of daily precipitation analyses in E-OBS (v19.0e) and ERA5 by comparison to regional high-resolution datasets in European regions. Int. J. Climatol. 42 (2), 727–747. https://doi.org/10.1002/joc.7269

Basarin, B., Lukić, T., Matzarakis, A., 2020. Review of biometeorology of heatwaves and warm extremes in Europe. Atmosphere 11 (12), 1–21. https://doi.org/10.3390/atmos11121276

Bell, B., Hersbach, H., Simmons, A., Berrisford, P., Dahlgren, P., Horányi, A., Muñoz-Sabater, J., Nicolas, J., Radu, R., Schepers, D., Soci, C., Villaume, S., Bidlot, J.R., Haimberger, L., Woollen, J., Buontempo, C., Thépaut, J.N., 2021. The ERA5 global reanalysis: Preliminary extension to 1950. Q. J. R. Meteorol. 147 (741), 4186–4227. https://doi.org/10.1002/qj.4174

Bezak, N., Mikoš, M., 2020. Changes in the compound drought and extreme heat occurrence in the 1961–2018 period at the european scale. Water (Switz.) 12 (12). https://doi.org/10.3390/w12123543

Ciais, P., Reichstein, M., Viovy, N., Granier, A., Ogée, J., Allard, V., Aubinet, M., Buchmann, N., Bernhofer, C., Carrara, A., Chevallier, F., De Noblet, N., Friend, A.D., Friedlingstein, P., Grünwald, T., Heinesch, B., Keronen, P., Knohl, A., Krinner, G., Loustau, D., Manca, G., Matteucci, G., Miglietta, F., Ourcival, J.M., Papale, D., Pilegaard, K., Ramball, S., Seufert, G., Soussana, J.F., Sanz, M.J., Schulze, E.D., Vesala, T., Valentini, R., 2005. Europe-wide reduction in primary productivity caused by the heat and drought in 2003. Nature 437 (7058), 529–533. https://doi.org/10.1038/nature03972

ECMWF, 2023. ERA5: uncertainty estimation Accessed on May 30th, 2023. https://confluence.ecmwf.int/display/CKB/ERA5%3A+uncertainty+estimation

Feng, Y., Liu, W., Sun, F., Wang, H., 2020. Changes of compound hot and dry extremes on different land surface conditions in China during 1957–2018. Int. J. Climatol. 41 (S1), E1085–E1099. https://doi.org/10.1002/joc.6755

García-León, D., Casanueva, A., Standardi, G., Burgstall, A., Flouris, A.D., Nybo, L., 2021. Current and projected regional economic impacts of heatwaves in Europe. Nat. Commun. 12 (1), 1–10. https://doi.org/10.1038/s41467-021-26050-z

Gazol, A., Camarero, J.J., 2022. Compound climate events increase tree drought mortality across European forests. Sci. Total Environ. 816, 151604. https://doi.org/10.1016/j.scitotenv.2021.151604

Geirinhas, J.L., Russo, A., Libonati, R., Sousa, P.M., Miralles, D.G., Trigo, R.M., 2021. Recent increasing frequency of compound summer drought and heatwaves in Southeast Brazil. Environ. Res. Lett. 16 (3). https://doi.org/10.1088/1748-9326/abe0eb

He, Y., Fang, J., Xu, W., Shi, P., 2022. Substantial increase of compound droughts and heatwaves in wheat growing seasons worldwide. Int. J. Climatol. 42 (10), 5038–5054. https://doi.org/10.1002/joc.7518

Hersbach, H., Bell, B., Berrisford, P., Hirahara, S., Horányi, A., Muñoz-Sabater, J., Nicolas, J., Peubey, C., Radu, R., Schepers, D., Simmons, A., Soci, C., Abdalla, S., Abellan, X., Balsamo, G., Bechtold, P., Biavati, G., Bidlot, J., Bonavita, M., De Chiara, G., Dahlgren, P., Dee, D., Diamantakis, M., Dragani, R., Flemming, J., Forbes, R., Fuentes, M., Geer, A., Haimberger, L., Healy, S., Hogan, R.J., Hólm, E., Janisková, M., Keeley, S., Laloyaux, P., Lopez, P., Lupu, C., Radnoti, G., de Rosnay, P., Rozum, I., Vamborg, F., Villaume, S., Thépaut, J.N., 2020. The ERA5 global reanalysis. Q. J. R. Meteorol. 146 (730), 1999–2049. https://doi.org/10.1002/qj.3803

Ionita, M., Caldarescu, D.E., Nagavciuc, V., 2021a. Compound Hot and Dry Events in Europe: Variability and Large-Scale Drivers.

Front. Clim. 3 (June), 1—19. https://doi.org/10.3389/fclim.2021.688991

Ionita, M., Nagavciuc, V., 2021b. Changes in drought features at the European level over the last 120 years. Nat. Hazards Earth Syst. Sci. 21 (5), 1685—1701. https://doi.org/10.5194/nhess-21-1685-2021

Jaagus, J., Aasa, A., 2018. Changes in drought indices in Estonia during the period of the contemporary climate warming. In: Proceedings of the 2nd Baltic Earth Conference, 11—15 June 2018. Helsingør, Denmark.

Jaagus, J., Aasa, A., Aniskevich, S., Boincean, B., Bojariu, R., Briede, A., Danilovich, I., Castro, F.D., Dumitrescu, A., Labuda, M., Labudová, L., Lõhmus, K., Melnik, V., Mõisja, K., Pongracz, R., Potopová, V., Řezníčková, L., Rimkus, E., Semenova, I., Stonevičius, E., Štepánek, P., Trnka, M., Vicente-Serrano, S.M., Wibig, J., Zahradníček, P., 2022. Long-term changes in drought indices in eastern and central Europe. Int. J. Climatol. 42 (1), 225—249. https://doi.org/10.1002/joc.7241

Keršytė, D., Rimkus, E., Kažys, J., 2015. Klimato rodiklių scenarijai Lietuvos teritorijoje XXI a. Geologija. Geografija 1 (1), 22—35. https://doi.org/10.6001/geol-geogr.v1i1.3069

Kim, S., Sinclair, V.A., Räisänena, J., Ruuhelac, R., 2018. Heat waves in Finland: Present and projected summertime extreme temperatures and their associated circulation patterns. Int. J. Climatol. 38 (3), 1393—1408. https://doi.org/10.1002/joc.5253

Kong, Q., Guerreiro, S.B., Blenkinsop, S., Li, X.F., Fowler, H.J., 2020. Increases in summertime concurrent drought and heatwave in Eastern China. Weather Clim. Extremes 28, 100242. https://doi.org/10.1016/j.wace.2019.100242

Lavers, D.A., Simmons, A., Vamborg, F., Rodwell, M.J., 2022. An evaluation of ERA5 precipitation for climate monitoring. Q. J. R. Meteorol. 148 (748), 3152—3165. https://doi.org/10.1002/qj.4351

Leonard, M., Westra, S., Phatak, A., Lambert, M., van den Hurk, B., Mcinnes, K., Risbey, J., Schuster, S., Jakob, D., Stafford-Smith, M., 2014. A compound event framework for understanding extreme impacts. WIREs Clim. Change 5 (1), 113—128. https://doi.org/10.1002/wcc.252

Liu, X., He, B., Guo, L., Huang, L., Chen, D., 2020. Similarities and Differences in the Mechanisms Causing the European Summer Heatwaves in 2003, 2010, and 2018. Earth's Future 8 (4), 1—11. https://doi.org/10.1029/2019EF001386

Markonis, Y., Kumar, R., Hanel, M., Rakovec, O., Máca, P., Kouchak, A.A., 2021. The rise of compound warm-season droughts in Europe. Sci. Adv. 7 (6), 1—8. https://doi.org/10.1126/sciadv.abb9668

Mazdiyasni, O., AghaKouchak, A., 2015. Substantial increase in concurrent droughts and heatwaves in the United States. PNAS 112 (37), 11484—11489. https://doi.org/10.1073/pnas.1422945112

McKee, T.B., Doesken, N.J., Kleist, J., 1993. The Relationship of Drought Frequency and Duration to Time Scales. In: Proceedings of the 8th Conference on Applied Climatology, 17—22 January 1993, Anaheim, CA.

Messori, G., Bevacqua, E., Caballero, R., Coumou, D., De Luca, P., Faranda, D., Kornhuber, K., Martius, O., Pons, F., Raymond, C., Ye, K., Yiou, P., Zscheischler, J., 2021. Compound climate events and extremes in the midlatitudes: Dynamics, simulation, and statistical characterization. Bull. Am. Meteorol. Soc. 102 (4), 774—781. https://doi.org/10.1175/BAMS-D-20-0289.1

Mukherjee, S., Ashfaq, M., Mishra, A.K., 2020. Compound Drought and Heatwaves at a Global Scale: The Role of Natural Climate Variability-Associated Synoptic Patterns and Land-Surface Energy Budget Anomalies. J. Geophys. Res.: Atmos. 125 (11), 0—19. https://doi.org/10.1029/2019JD031943

Mukherjee, S., Mishra, A.K., 2020. Increase in Compound Drought and Heatwaves in a Warming World. Geophys. Res. Lett. 48 (1), 1—13. https://doi.org/10.1029/2020GL090617

Mukherjee, S., Mishra, A.K., Ashfaq, M., Kao, S.C., 2022. Relative effect of anthropogenic warming and natural climate variability to changes in Compound drought and heatwaves. J. Hydrol. 605 (September 2021), 127396. https://doi.org/10.1016/j.jhydrol.2021.127396

Nogueira, M., 2020. Inter-comparison of ERA-5, ERA-interim and GPCP rainfall over the last 40 years: Process-based analysis of systematic and random differences. J. Hydrol. 583 (January), 124632. https://doi.org/10.1016/j.jhydrol.2020.124632

Peel, M.C., Finlayson, B.L., McMahon, T.A., 2007. Updated world map of the Köppen-Geiger climate classification. Hydrol. Earth Syst. Sc. 11, 1633—1644. https://doi.org/10.5194/hess-11-1633-2007

Perkins-Kirkpatrick, S.E., Gibson, P.B., 2017. Changes in regional heatwave characteristics as a function of increasing global temperature. Sci. Rep. 7 (1), 1—12. https://doi.org/10.1038/s41598-017-12520-2

Porebska, M., Zdunek, M., 2013. Analysis of extreme temperature events in central Europe related to high pressure blocking situations in 2001-2011. Meteorol. Z. 22 (5), 533—540. https://doi.org/10.1127/0941-2948/2013/0455

Prodhomme, C., Materia, S., Ardilouze, C., White, R.H., Batté, L., Guemas, V., Fragkoulidis, G., García-Serrano, J., 2022. Seasonal prediction of European summer heatwaves. Clim. Dynam. 58 (7—8), 2149—2166. https://doi.org/10.1007/s00382-021-05828-3

Ribeiro, A.F.S, Russo, A., Gouveia, C.M., Páscoa, P., Zscheischler, J., 2020. Risk of crop failure due to compound dry and hot extremes estimated with nested copulas. Biogeosciences 17 (19), 4815—4830. https://doi.org/10.5194/bg-17-4815-2020

Ridder, N.N., Pitman, A.J., Westra, S., Ukkola, A., Hong, X.Do, Bador, M., Hirsch, A.L., Evans, J.P., Di Luca, A., Zscheischler, J., 2020. Global hotspots for the occurrence of compound events. Nat. Commun. 11 (1), 1—10. https://doi.org/10.1038/s41467-020-19639-3

Rimkus, E., Kažys, J., Valiukas, D., Stankūnavičius, G., 2014. The atmospheric circulation patterns during dry periods in Lithuania. Oceanologia 56 (2), 223—239. https://doi.org/10.5697/oc.56-2.223

Rimkus, E., Maciulyte, V., Stonevicius, E., Valiukas, D., 2020. A revised agricultural drought index in Lithuania. Agric. Food Sci. 29 (4), 359—371. https://doi.org/10.23986/afsci.92150

Rimkus, E., Stonevičius, E., Korneev, V., Kažys, J., Valiuškevičius, G., Pakhomau, A., 2013. Dynamics of meteorological and hydrological droughts in the Neman River basin. Environ. Res. Lett. 8 (4). https://doi.org/10.1088/1748-9326/8/4/045014

Rousi, E., Kornhuber, K., Beobide-Arsuaga, G., Luo, F., Coumou, D., 2022. Accelerated western European heatwave trends linked to more-persistent double jets over Eurasia. Nat. Commun. 13 (1), 1—11. https://doi.org/10.1038/s41467-022-31432-y

Rutgersson, A., Kjellström, E., Haapala, J., Stendel, M., Danilovich, I., Drews, M., Jylhä, K., Kujala, P., Larsén, X.G., Halsnæs, K., Lehtonen, I., Luomaranta, A., Nilsson, E., Olsson, T., Särkkä, J., Tuomi, L., Wasmund, N., 2022. Natural hazards and extreme events in the Baltic Sea region. Earth Syst. Dynam. 13 (1), 251—301. https://doi.org/10.5194/esd-13-251-2022

Sedlmeier, K., Feldmann, H., Schädler, G., 2018. Compound summer temperature and precipitation extremes over central. Europe. Theor. Appl. Climatol. 131 (3—4), 1493—1501. https://doi.org/10.1007/s00704-017-2061-5

Seneviratne, S.I., Nicholls, N., Easterling, D., Goodess, C.M., Kanae, S., Kossin, J., Luo, Y., Marengo, J., Mc Innes, K., Rahimi, M., Reichstein, M., Sorteberg, A., Vera, C., Zhang, X., 2012. Changes in climate extremes and their impacts on the natural physical environment. In: Field, C.B., Barros, V., Stocker, T.F, Qin, D., Dokken, D.J., Ebi, K.L., Mastrandrea, M.D., Mach, K.J., Plattner, G.K., Allen, S.K., Tignor, M., Midgley, P.M. (Eds.), A Special Report of Working Groups I and II of the

Intergovernmental Panel on Climate Change (IPCC). Managing the Risks of Extreme Events and Disasters to Advance Climate Change Adaptation. Cambridge University Press, Cambridge, UK, and New York, NY, USA, 109–230.

Seneviratne, S.I., Zhang, X., Adnan, M., Badi, W., Dereczynski, C., Di Luca, A., Ghosh, S., Iskandar, I., Kossin, J., Lewis, S., Otto, F., Pinto, I., Satoh, M., Vicente-Serrano, S.M., Wehner, M., Zhou, B., 2021. Weather and Climate Extreme Events in a Changing Climate. In: Masson-Delmotte, V., Zhai, P., Pirani, A., Connors, S.L., Péan, C., Berger, S., Caud, N., Chen, Y., Goldfarb, L., Gomis, M.I., Huang, M., Leitzell, K., Lonnoy, E., Matthews, J.B.R., Maycock, T.K., Waterfield, T., Yelekçi, O., Yu, R., Zhou, B. (Eds.), Climate Change 2021: The Physical Science Basis. Contribution of Working Group I to the Sixth Assessment Report of the Intergovernmental Panel on Climate Change. Cambridge University Press, Cambridge, United Kingdom and New York, NY, USA, 1513–1766.

Sharma, S., Mujumdar, P., 2017. Increasing frequency and spatial extent of concurrent meteorological droughts and heatwaves in India. Sci. Rep. 7 (1), 1–9. https://doi.org/10.1038/s41598-017-15896-3

Shi, Z., Jia, G., Zhou, Y., Xu, X., Jiang, Y., 2021. Amplified intensity and duration of heatwaves by concurrent droughts in China. Atmos. Res. 261 (April), 105743. https://doi.org/10.1016/j.atmosres.2021.105743

Somorowska, U., 2016. Changes in drought conditions in Poland over the past 60 years evaluated by the standardized precipitation-evapotranspiration index. Acta Geophys. 64 (6), 2530–2549. https://doi.org/10.1515/acgeo-2016-0110

Sousa, P.M., Trigo, R.M., Barriopedro, D., Soares, P.M.M., Santos, J.A., 2018. European temperature responses to blocking and ridge regional patterns. Clim. Dynam. 50 (1–2), 457–477. https://doi.org/10.1007/s00382-017-3620-2

Spensberger, C., Madonna, E., Boettcher, M., Grams, C.M., Papritz, L., Quinting, J.F., Röthlisberger, M., Sprenger, M., Zschenderlein, P., 2020. Dynamics of concurrent and sequential Central European and Scandinavian heatwaves. Q. J. R. Meteorol. 146 (732), 2998–3013. https://doi.org/10.1002/qj.3822

Suursaar, Ü., 2022. Summer 2021 marine heat wave in the Gulf of Finland from the perspective of climate warming. Est. J. Earth Sci. 71 (1), 1–16. https://doi.org/10.3176/earth.2022.01

Tomczyk, A.M., Bednorz, E., Matzarakis, A., 2020. Human-biometeorological conditions during heat waves in Poland. Int. J. Climatol. 40 (12), 5043–5055. https://doi.org/10.1002/joc.6503

Tsakiris, G., Vangelis, H., 2004. Towards a Drought Watch System based on spatial SPI. Water Resour. Manage. 18 (1), 1–12. https://doi.org/10.1023/B:WARM.0000015410.47014.a4

Valiukas, D., 2015. Analysis of droughts and dry periods in Lithuania. Summary of doctoral thesis. Vilnius University.

Velikou, K., Lazoglou, G., Tolika, K., Anagnostopoulou, C., 2022. Reliability of the ERA5 in Replicating Mean and Extreme Temperatures across Europe. Water (Switz.). 14 (4). https://doi.org/10.3390/w14040543

Vicente-Serrano, S.M., Beguería, S., López-Moreno, J.I., 2010. A multiscalar drought index sensitive to global warming: The standardized precipitation evapotranspiration index. J. Clim. 23 (7), 1696–1718. https://doi.org/10.1175/2009JCLI2909.1

Vyshkvarkova, E., Sukhonos, O., 2022. Compound Extremes of Air Temperature and Precipitation in Eastern Europe. Climate 10, 133. https://doi.org/10.3390/cli10090133

Wang, C., Li, Z., Chen, Y., Li, Y., Liu, X., Hou, Y., Wang, X., Kulaixi, Z., Sun, F., 2022. Increased Compound Droughts and Heatwaves in a Double Pack in Central Asia. Remote Sens. 14 (13), 1–19. https://doi.org/10.3390/rs14132959

Wazneh, H., Gachon, P., Laprise, R., de Vernal, A., Tremblay, B., 2021. Atmospheric blocking events in the North Atlantic: trends and links to climate anomalies and teleconnections. Clim. Dynam. 56 (7–8), 2199–2221. https://doi.org/10.1007/s00382-020-05583-x

Wibig, J., 2017. Heat waves in Poland in the period 1951-2015: trends, patterns and driving factors. Meteorology Hydrology and Water Management 6 (1), 1–10. https://doi.org/10.26491/mhwm/78420

Wibig, J., 2021. Hot days and heat waves in Poland in the period 1951-2019 and the circulation factors favoring the most extreme of them. Atmosphere 12 (3). https://doi.org/10.3390/atmos12030340

WMO, 2012. Standardized Precipitation Index User Guide. WMO-No. 1090, Geneva. Accessed on February 12th, 2023. https://digitalcommons.unl.edu/cgi/viewcontent.cgi?article=1208&context=droughtfacpub

Wu, X., Hao, Z., Hao, F., Singh, V.P., Zhang, X., 2019. Dry-hot magnitude index: A joint indicator for compound event analysis. Environ. Res. Lett. 14 (6). https://doi.org/10.1088/1748-9326/ab1ec7

Yoon, D., Cha, D.H., Lee, M.I., Min, K.H., Kim, J., Jun, S.Y., Choi, Y., 2020. Recent changes in heatwave characteristics over Korea. Clim. Dynam. 55 (7–8), 1685–1696. https://doi.org/10.1007/s00382-020-05420-1

Zhang, Q., She, D., Zhang, L., Wang, G., Chen, J., Hao, Z., 2022. High Sensitivity of Compound Drought and Heatwave Events to Global Warming in the Future. Earth's Future 10 (11). https://doi.org/10.1029/2022EF002833

Ziernicka-Wojtaszek, A., 2021. Summer drought in 2019 on Polish territory – a case study. Atmosphere 12 (11). https://doi.org/10.3390/atmos12111475

Zscheischler, J., Martius, O., Westra, S., Bevacqua, E., Raymond, C., Horton, R.M., van den Hurk, B., AghaKouchak, A., Jézéquel, A., Mahecha, M.D., Maraun, D., Ramos, A.M., Ridder, N.N., Thiery, W., Vignotto, E., 2020a. A typology of compound weather and climate events. Nat. Rev. Earth Environ. 1 (7), 333–347. https://doi.org/10.1038/s43017-020-0060-z

Zscheischler, J., Van Den Hurk, B., Ward, P.J., Westra, S., 2020b. Multivariate extremes and compound events. In Climate Extremes and Their Implications for Impact and Risk Assessment. Elsevier. https://doi.org/10.1016/B978-0-12-814895-2.00004-5

Zscheischler, J., Westra, S., Van Den Hurk, B.J.J.M., Seneviratne, S.I., Ward, P.J., Pitman, A., Aghakouchak, A., Bresch, D.N., Leonard, M., Wahl, T., Zhang, X., 2018. Future climate risk from compound events. Nat. Clim. Change. 8 (6), 469–477. https://doi.org/10.1038/s41558-018-0156-3

II PUBLIKACIJA

False spring events in the eastern part of the Baltic Sea region

Klimavičius, L., & Rimkus, E. (2024). False spring events in the eastern part of the Baltic Sea region. *Theoretical and Applied Climatology*, 155(10), 9351–9365. https://doi.org/10.1007/s00704-024-05194-0 (*Reproduced with permission from Springer Nature*)

Theoretical and Applied Climatology (2024) 155:9351–9365
https://doi.org/10.1007/s00704-024-05194-0

RESEARCH

False spring events in the eastern part of the Baltic Sea region

Laurynas Klimavičius[1] · Egidijus Rimkus[1]

Received: 28 June 2024 / Accepted: 16 September 2024 / Published online: 24 September 2024
© The Author(s), under exclusive licence to Springer-Verlag GmbH Austria, part of Springer Nature 2024

Abstract
Spring frosts can cause substantial economic and ecological damage, especially when occurring after the growing season has begun and leading to compound climate events, known as false spring (FS) events. This study examines the recurrence, spatial distribution and intensity of FS events in the eastern part of the Baltic Sea region from 1950 to 2022. These events were identified by determining the dates of the last spring frost (LSF) and the start of the growing season (SGS) for each grid cell annually. FS events were distinguished when the LSF date occurred later than the date of the SGS. The sum of growing degree days (t_{base} = 5 °C), accumulated until the event, and the minimum air temperature (t_{min}) during the day of the FS event were used to assess the intensity of FS events. Throughout the study period, LSF and SGS dates shifted earlier by an average of 6.3 and 10.6 days, respectively. In 85.9% of the grid cells, the SGS date changed more rapidly than the LSF date. Although the number of FS events increased over the 73 years in most of the study area, no significant changes were observed according to the Mann–Kendall test. However, comparing 1950–1969 and 2003–2022, 85.9% of grid cells saw more FS events, with the largest increase in the eastern part of the study area and southwestern Lithuania. Significant changes were determined in 30% of cells according to the t-test.

1 Introduction

Since 1982, the average global annual air temperature has increased by 0.2 °C per decade, with 2023 being the warmest year on record since the start of instrumental measurements (Lindsey and Dahlman 2024). In Europe, from 1985 to 2020, the fastest rise in air temperature (at a rate of 0.061 °C per year) was recorded in spring, with the most significant changes occurring in the northeastern part of the continent (Twardosz et al. 2021). These changes can have effects on vegetation, such as an earlier start of the growing season, lengthening its duration and in some cases increasing the productivity of plants and harvest efficiency (Ceglar et al. 2019; Liu et al. 2018; Peterson and Abatzoglou 2014; Wypych et al. 2017).

However, the impact of rising temperatures is only partially positive. For example, a warming of 2 °C might increase the risk of frost damage to apple trees in Germany by 10% relative to the present day (Pfleiderer et al. 2019). This risk arises because warmer winters cause the trees to bloom earlier increasing their exposure to frost days after the blossom, which counteracts the effect of a general decline in the number of frost days (Zscheischler et al. 2020). Temperate plants are the ones particularly at risk of being exposed to such late spring freezes and the occurrence of them in spring after the growing season has already started is known as a false spring event (Chamberlain et al. 2019; Ma et al. 2019; Zscheischler et al. 2020). These events occur when unseasonably warm weather at the end of winter or the start of spring in mid-latitudes prompts an unusually early onset of the growing season. This early onset is followed by a cold spell, often due to arctic air moving in from the north, resulting in frost. Since the growing season has already started, the frost causes more significant damage to plants than it would if the warm spell had not occurred, and the spring had remained consistently cold (Gu et al. 2008; Vitasse and Rebetez 2018; Zscheischler et al. 2020).

False spring events can lead to significant economic losses and negative ecological consequences and affect the vital functions of plants and animals, reducing the overall productivity of forest ecosystems and decreasing crop yields (Chamberlain et al. 2019; Liu et al. 2018; Ma et al. 2019; Unterberger et al. 2018; Zohner et al. 2020b). The damage is particularly severe if these events occur after the

✉ Laurynas Klimavičius
laurynas.klimavicius@chgf.vu.lt

[1] Institute of Geosciences, Vilnius University, Vilnius, Lithuania

budburst and during the flowering period of various plants, especially fruit trees (Faust and Herbold 2018; Rodrigo 2000). Even a mild frost, with temperatures dropping just one or two degrees below zero, can cause significant damage to plants (Vitasse and Rebetez 2018). Thus, the negative impact of false spring events can surpass the benefits of a warmer climate and an extended growing season (Ceglar et al. 2019; Liu et al. 2018).

It has been found that late spring frosts in North America and Europe cause more economic damage to agriculture than other climate-related hazards (Lamichhane 2021). For example, a false spring event in early 2010 in the northeastern United States caused significant damage to maples and reduced ecosystem productivity by 7–14% (Hufkens et al. 2012; Zscheischler et al. 2020). In 2021, about 80% of France's grape and fruit tree regions were affected by the false spring event (Lamichhane 2021), while in 2017, such an event in Europe caused damage to fruit trees and vineyards amounting to 3.3 billion EUR (Faust and Herbold 2018; Zscheischler et al. 2020). All these impacts also have secondary adverse effects: threatening the survival of various animals, food security, and disrupting carbon dioxide absorption. Furthermore, numerous methods (burning solid and liquid fuels, lighting fires in vineyards and orchards) are used to reduce the potential risk of such late frosts and false spring events, which can increase air and environmental pollution (Anandhi 2016; Chamberlain et al. 2019; Lamichhane 2021).

False spring events also negatively impact the competitiveness of various plants and affect their distribution ranges (Chamberlain et al. 2019; Lamichhane 2021; Wypych et al. 2017). In spring, different plant species do not unfold their leaves at the same time, and each species has its frost resistance threshold. Thus, the impact of late spring frosts is distinct for each species (Potter and Cate 1999). The extent of damage caused by frost is also influenced by regional climate differences and geographical location (Chamberlain et al. 2019; Peterson and Abatzoglou 2014). In recent decades, the number of late spring frosts has mostly increased in regions where this risk was previously low, such as coastal areas of Europe, the eastern part of Europe, and East Asia. The local tree species in these areas are not highly resistant to negative temperatures, so the negative impact of false spring events in the future may increase (Zohner et al. 2020a).

It is predicted that in the future, fruit trees will bloom earlier due to the warming climate, while the risk of false spring events will persist and may even increase (Hufkens et al. 2012; Unterberger et al. 2018), thus increasing the focus on studying such events. However, most studies conducted in the eastern part of the Baltic Sea region have focused only on the changes in various indicators of the growing season (e.g. start date, duration) (Kalvāne et al. 2009; Mačiulytė and Stankūnavičius 2020) and thermal resources during the growing season (Radzka 2021). The resistance of various fruit trees, bushes, and crops to frost and its damage has also been analysed (Grāvīte 2022; Sepp et al. 2022). Nonetheless, false spring events have been little studied in the Baltic States.

The aim of this study is to evaluate the recurrence, spatial distribution, and intensity of false spring (FS) events in the eastern Baltic Sea region and long-term changes in these indicators from 1950 to 2022. In the first part of the research, the spatial distribution and changes of dates of the start of the growing season (SGS) and the last spring frost (LSF) from 1950 to 2022 were analysed. The second part discusses the trends of FS events over the 73 years. Finally, the last part focuses on assessing the intensity of FS events.

2 Data and methods

2.1 Study area

The study area covers the eastern part of the Baltic Sea region, spanning from 53.5° to 59.5° N and from 20.0° to 28.5° E (Fig. 1). This region includes all three Baltic countries (Lithuania, Latvia, and Estonia), as well as small parts of Poland, Russia, and Belarus. According to the updated Köppen–Geiger climate classification, this area falls under the Dfb climate type (Beck et al. 2018; Peel et al. 2007).

The average annual air temperature in the eastern part of the Baltic Sea region from 1950 to 2022 was 6.4 °C and an increase of 0.23 °C per decade was found over the study period. The average air temperature in the analysed region during spring (March to May) was 5.6 °C. The southern part of the study area was characterised by the highest average spring air temperature while the lowest values of this variable were found in the northern part (Fig. 1). The average spring air temperature has also increased over the study period. This change averaged 0.29 °C per decade and was statistically significant across the entire territory (when $p < 0.05$), with the greatest changes along the Baltic Sea coast in western Lithuania and in the northern part of the study area, reaching 0.33–0.35 °C.

Specific territorial climate differences are influenced by latitude, terrain, and proximity to the Baltic Sea. The influence of the distance from the sea is particularly noticeable at the beginning of spring and end of spring–early summer The average air temperature in early spring (March) over the study period ranges from 1.7 °C at the western edge of the study area to −2.5 °C in the northeast. In April, latitudinal temperature distribution becomes more pronounced (from 3.5 °C in the north to 7.4 °C in the southern part of the

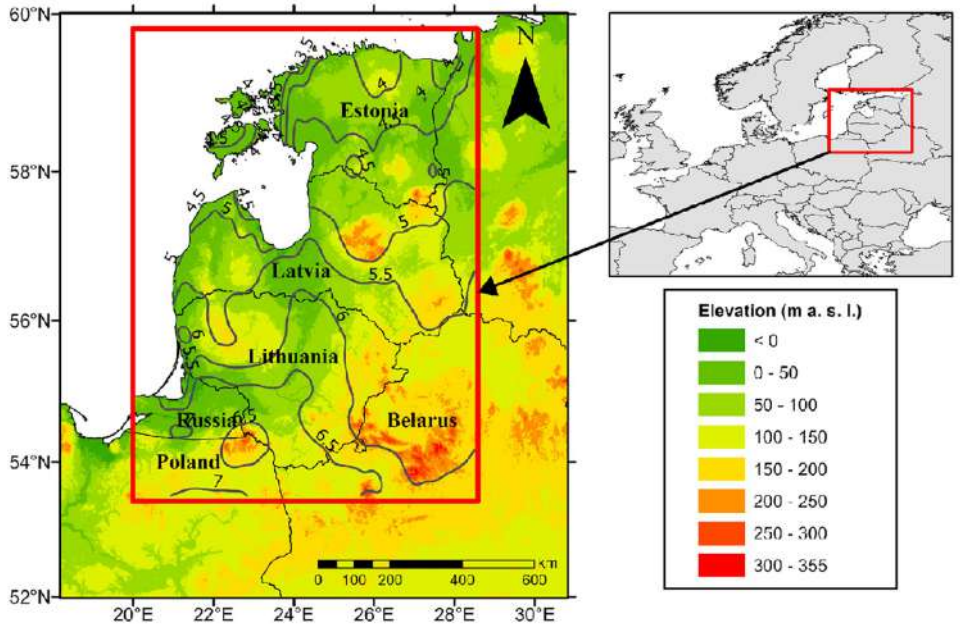

Fig. 1 The study area, its topography and isotherms of the average spring (March–May) air temperature over the study period of 1950–2022

study area). At the end of spring (May) and the beginning of summer, in the first ten days of June, the cooling effect of the Baltic Sea is evident. The average air temperature of May ranges from 8.5 to 9.0 °C in coastal areas of Estonia to 13.0–13.2 °C in the southern part of the region while the average air temperature of the first ten days of June over the study period varies from 11.5 to 13.0 °C in the coastal regions to 16.0–16.2 °C in the southern and southeastern parts of the study area. From March to June, episodes of cold arctic air advection are typical in the eastern part of the Baltic Sea region, creating favourable conditions for late frosts and FS events.

The highest point in the study area is situated in the southeastern part of the research area (355 m a.s.l.) (Fig. 1). The terrain influences the distribution of average March–June air temperature. In higher elevations, air temperature is approximately 0.5–1 °C lower than in the surrounding areas.

2.2 Data

To assess the frequency and severity of FS events, reanalysis data covering February to June from 1950 to 2022 were analysed. Daily minimum (t_{min}) and average air temperature data were downloaded from the ERA-5 database using the KNMI Climate Explorer web application (https://climexp.knmi.nl/start.cgi) with a spatial resolution of 0.25×0.25°. Using the land mask provided by this application only grid cells where over 50% of the area is land were extracted.

The ERA-5 database was chosen for its long data availability period and sufficient temporal and spatial resolution. A comparison of different reanalysis datasets with meteorological station data indicated that ERA-5 is the most accurate in 50% of cases. Additionally, in 75% of cases, it is one of the two most precise reanalysis datasets (Horton 2022). A comparison between ERA-5 and climatological data obtained from meteorological stations shows that the data of this reanalysis are accurate, reliable, and suitable for various scientific studies in Europe (Bell et al. 2021). However, it is essential to note that the accuracy of reanalysis data varies slightly during the study period. Data for some variables, including air temperature, are more accurate in the second half of the research period (since the last decade of the 20th century). This is due to an increase in the number of observational inputs from meteorological stations used in reanalysis, leading to reduced ensemble spread and uncertainties. Additionally, the accuracy of the data was enhanced by incorporating meteorological satellite information (Bell et al. 2021; ECMWF 2024).

2.3 Definition of false spring events

To identify FS events, we first determined the dates of SGS and LSF. The SGS date at a particular point of the research area is defined as the first day within a consecutive six-day period when the average daily air temperature exceeds or equals 5 °C for all six days. This methodology for determining SGS dates is proposed by the Swedish Meteorological and Hydrological Institute (SMHI) and has been applied in other studies in the Baltic Sea region (Graczyk and Szwed 2020; Ruosteenoja et al. 2011; SMHI 2022; Walther and Linderholm 2006). LSF date is defined as the day when the t_{min} falls below the 0 °C threshold for the last time during March–June. This 0 °C threshold has been used in various studies investigating the recurrence of spring–early summer frosts and their potential negative impact on fruit trees and other plants in Europe and the Baltic Sea region (Ceglar et al. 2019; Koźmiński et al. 2021, 2023; Wypych et al. 2017; Zohner et al. 2020a). Although plant leaves and tissues may withstand temperatures slightly below 0 °C, radiative cooling and calm weather during frost events often result in plant tissue temperatures dropping several degrees below the air temperature. Therefore, it is appropriate to use the 0 °C air temperature threshold (Zohner et al. 2020a, b). After establishing the SGS and LSF dates, we assessed the changes in these dates over the 73 years. The non-parametric Mann-Kendall was employed to determine the statistical significance of the observed changes, with changes considered statistically significant when $p < 0.05$. Additionally, the spatial mean of LSF and SGS dates was calculated for each year of the study period using information from all grid points.

FS events were considered to occur at a particular grid point when the LSF date occurred later than the SGS date. We evaluated the recurrence of such events across the entire territory for each study year and the changes in event frequency between the first (1950–1969) and the last (2003–2022) 20-year periods. These two periods were chosen to better highlight the changes in the frequency of FS events under a rapidly changing climate. The significance of changes was evaluated using Student's t-test.

2.4 Intensity of false spring events

Two variables were used to assess the intensity of FS events. First, we calculated the sum of growing degree days (GDD) accumulated until each FS event. The method for calculating GDD, developed as early as 1730, despite occasional criticism for its simplicity, is still widely employed to evaluate various growth stages of plants (Anandhi 2016; Bonhomme 2000; Paparrizos and Matzarakis 2017; Spinoni et al. 2015; Vitasse and Rebetez 2018). Several methods for calculating GDD exist, but in this study, we used the most commonly taken approach (Eq. 1).

$$GDD = t_{avg} - t_{base} \quad (1)$$

where t_{avg} – represents the average daily air temperature at each specific point within the study area, t_{base} – threshold temperature. If on a given day at a particular grid point $t_{avg} < t_{base}$, it is considered that $t_{avg} = t_{base}$ (McMaster and Wilhelm 1997).

In this study, t_{base} = 5 °C was used. Ruosteenoja et al. (2016) found that the colder the climate, the closer the beginning of the growing season is to the temperature transition of 5 °C. Therefore, this threshold temperature should be applied when calculating GDD in colder climate zones. The 5 °C threshold temperature was also considered as the temperature marking the start of the growing season in other studies (Koźmiński et al. 2023; Sujetovienė et al. 2018; Szyga-Pluta 2022; Vitasse et al. 2019; Wypych et al. 2017). Additionally, a t_{base} of 5.5 °C has been used for assessing the development stages and yield of various widely cultivated crops in Europe (Graczyk and Kundzewicz 2016; Spinoni et al. 2015). It is considered that the higher the sum of GDD accumulated until the occurrence of an FS event, the more dangerous and potentially harmful it can be for various plants (Vitasse and Rebetez 2018). Changes in the amount of GDD accumulated before FS events were also evaluated and the significance of these changes was investigated using Student's t-test ($p < 0.05$). Furthermore, the distribution of the sum of GDD, accumulated until the FS event, was evaluated for each decade of the study period. In this case, a time step of a decade was chosen for the purpose to emphasize the large variability of this parameter.

Another variable considered when evaluating the intensity of FS events is the t_{min} reached during the FS event. The lower the t_{min} during the event, the more significant the potential negative impact. The severity of frost, expressed in terms of t_{min}, and the sum of GDD accumulated before the frost were found to be critical factors in determining the potential severity of the negative effects of FS events on plants (Vitasse and Rebetez 2018; Graczyk and Szwed 2020).

To assess the intensity of each FS event, the values of the GDD sum accumulated until the event and t_{min} were divided into three categories. Frosts according to these categories were divided into mild (F1 category), severe (F2 category), and extreme (F3 category) (Table 1). A similar categorisation of frosts occurring after the start of the growing season has been used in other studies (Chmielewski et al. 2018; Koźmiński et al. 2021; Zhu et al. 2019). Finally, nine intensity classes of FS events were formed based on different frost and GDD categories (Table 1).

Table 1 The categories used to classify false spring (FS) events into nine intensity classes. Letters F and GDD indicate the minimum daily air temperature (t_{min}) recorded during the day of the FS event and the sum of growing degree days (GDD) accumulated until the FS event respectively

Variable	Category	Threshold values	Intensity classes
t_{min} during the day of the FS event	F1	0 °C > t_{min} ≥ -2 °C	F1_GDD1, F1_GDD2, F1_GDD3, F2_GDD1, F2_GDD2, F2_GDD3, F3_GDD1, F3_GDD2, F3_GDD3
	F2	-2 °C > t_{min} ≥ -5 °C	
	F3	t_{min} < -5 °C	
GDD, accumulated until the FS event	GDD1	0 °C < GDD ≤ 100 °C	
	GDD2	100 °C < GDD ≤ 200 °C	
	GDD3	GDD > 200 °C	

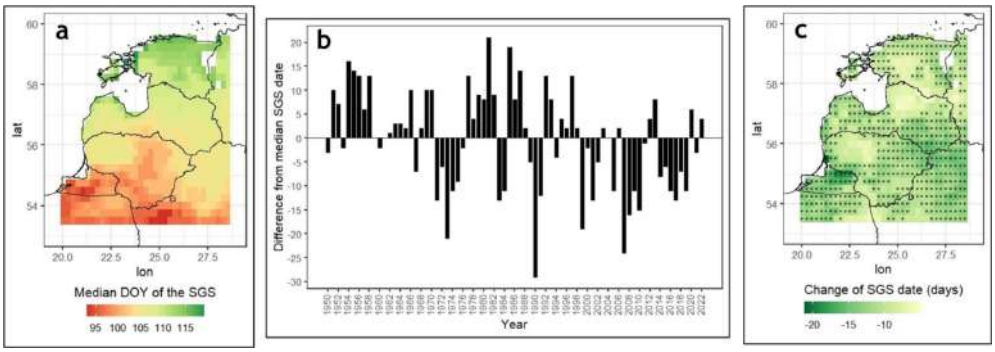

Fig. 2 (**a**) Median date (DOY) of the SGS in 1950–2022; (**b**) Deviation of the SGS date from the median value. The spatial mean for the entire territory was calculated (**c**) Change of the SGS date (in days) over the study period. Dots indicate grid cells where the changes were statistically significant ($p < 0.05$) according to the Mann-Kendall test

3 Results

3.1 Date of the start of the growing season

The average SGS date during the study period (1950–2022) shows a latitudinal distribution. On average, the earliest start of the growing season was recorded in the southern and southwestern parts of the study area on the 93–95th day of the year (DOY) (3–5 April), while the latest SGS date was determined in northern Estonia and the coastal regions of this country averaging on the 117–119th DOY (27–29 April) (Fig. 2a).

Over the 73 analysed years, the median SGS date in the study area was 14 April. Exceptionally early average SGS dates were observed in 1990 and 2007. In those years, the average deviation of the SGS date in the study area from the median SGS date was − 29 and − 24 days, respectively (75th and 80th DOY) (Fig. 2b).

During the 1950–2022 period, the SGS date has become earlier in the study area on average by 10.6 days. The greatest changes were identified in the southwestern part of the study area, where the SGS date during the 73 years shifted earlier by nearly three weeks (19–21 days). In other regions, although the changes were smaller, they were statistically significant ($p < 0.05$) in the majority (73.9%) of grid cells (Fig. 2c).

3.2 Date of the last spring frost

The median date of the LSF in the eastern part of the Baltic Sea region during the period of 1950–2022 was the 118th DOY (28 April), meaning that the LSF date, on average, was recorded two weeks later than the date of SGS. This date ranged from the 99th–100th DOY along the Baltic Sea coast in Lithuania and the Kaliningrad region to the 125th–127th DOY in central Estonia (Fig. 3a). 1968 and 1980 were particularly notable years, with especially late frosts recorded throughout the research area—the median LSF date those years was the 142nd and 143rd DOY (22–23 May) respectively. However, in recent decades such late frosts have become less common. For example, in 2018, the median LSF date in the study area was only the 97th DOY (7 April) (Fig. 3b). There has also been a decrease in very late frosts that occur in the second half of May or in June—from 62% of years in 1950–1999 to 30% in 2000–2022.

Like the SGS date, the LSF has shifted earlier over the study period. This trend has been observed at 99.4% of grid points. Nevertheless, the changes are not so prominent—they are found to be statistically significant ($p < 0.05$) only in 21.3% of the grid cells (Fig. 3c). The most notable shift in the LSF date over the study period occurred in coastal regions and the northern part of the study area where the changes of LSF date has been more than two weeks and, in

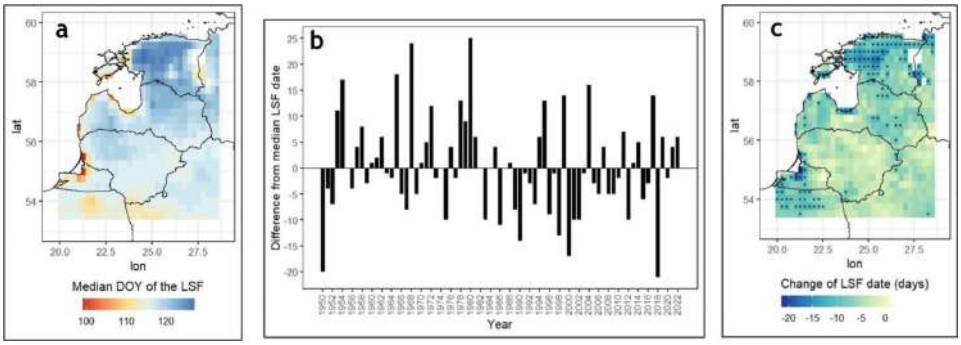

Fig. 3 (**a**) Median date (DOY) of the LSF in 1950–2022; (**b**) Deviation of the LSF date from the median value. The spatial mean for the entire territory was calculated; (**c**) Change of the LSF date (in days) over the study period. Dots indicate grid cells where the changes were statistically significant ($p < 0.05$) according to the Mann-Kendall test

some places, nearly three weeks (19–21 days) (Fig. 3c). On average, over the 73 years, the LSF date has become earlier by almost one week (6.3 days).

3.3 False spring events

Except for 1998, an FS event was recorded every year in at least one grid cell during the investigation period. In 78% of analysed years, FS events were detected in more than half of grid cells, and in this century, such a situation has occurred almost every year (except for 2020). 1962, 1991, 1999, 2005, and 2017 were the years with the highest prevalence of FS events. In all these years, FS events were recorded in more than 98% of the study area (Fig. 4a).

To determine whether the conditions for FS events became more favourable, the changes in the difference between the LSF and SGS dates were calculated. It was found that over 73 years this difference increased at 85.9% of the grid cells. Thus, favourable conditions for more intensive FS events developed in most of the research area. However, statistically significant changes ($p < 0.05$) were determined only in 4.8% of the territory. Across the entire study area, the southwestern and eastern regions showed the biggest increases in the difference between the LSF and SGS dates (up to 13–17 days). In contrast, the most prominent negative and in a few cases statistically significant change, reaching almost 12 days, was observed in central Estonia (Fig. 4b).

Despite the widening gap between the LSF and SGS dates across nearly the entire study area, the number of FS events increased by an average of only 18.6% over the 73 years and no significant changes were observed. Also, the highest number of FS events was observed in central Estonia and the southwestern part of the study region, while these events rarely occurred in the coastal areas (Fig. 4c).

The difference in the number of FS events was also assessed between the beginning (1950–1969) and the end (2003–2022) of the study period. It was found that in 85.9% of the grid cells, more FS events were recorded in the last twenty years compared to the first two decades of the study period. The largest increase, reaching up to nine events, was observed in the eastern part of the study area and the southwestern part of Lithuania. In total, statistically significant changes ($p < 0.05$) were found in 30% of grid cells (Fig. 4d).

3.4 Evaluation of the intensity of false spring events

To assess the intensity of each FS event, we calculated the sum of GDD accumulated until the event and evaluated the t_{min} recorded during the event. On average, the sum of 67.3 °C GDD was accumulated before an FS event. 2004 and 1968 stood out as a year with exceptionally high median GDD values (171.7 °C and 164.6 °C, respectively). In 2004, FS events were recorded at 90.6%, while in 1968 they were recorded at 77.4% of the grid cells. Also, the distribution of GDD sums for different periods from 1950 to 2022 was assessed (Fig. 5a). The periods of 1990–1999 and 1950–1959 had the highest median GDD sums accumulated before FS events, with values of 74.8 °C and 76.7 °C, respectively.

The GDD sums accumulated before FS events were also evaluated at each grid point of the study area. The highest median of GDD sums over the 73 years were found in grid cells located in the southwestern part of the study area, western Latvia, and central Estonia. In these areas, the median GDD value ranged from 69 to 72 °C (Fig. 5b).

The difference in the median values of this indicator between the last 20 years of the study period (2003–2022) and the first 20 years of the study period (1950–1969) was calculated. It was found that the median of GDD at the end

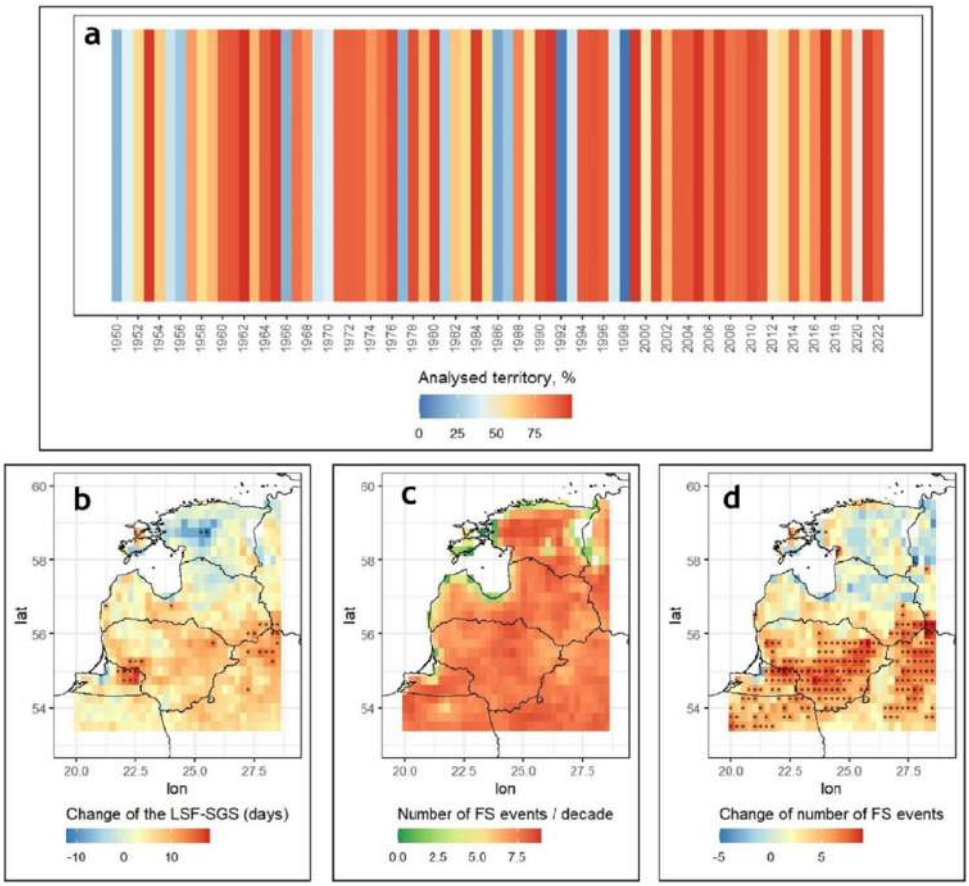

Fig. 4 (**a**) The percentage of the territory (%) in which false spring (FS) events occurred during the period from 1950 to 2022; (**b**) Change in the duration (days) between LSF and SGS dates over the study period; (**c**) Number of FS events per decade at each grid cell in the study area; (**d**) Difference in the number of FS events observed during two periods 2003–2022 and 1950–1969. Dots in figures (**b**) and (**d**) indicate grid cells where the changes were statistically significant (when $p < 0.05$) according to the Mann-Kendall (**b**) and t-test (**d**)

of the study period was higher in 56.1% of the grid cells, with the highest increase observed in the southern part of the study area, where the change ranged from 30 to 38 °C. However, according to the t-test changes were statistically significant in only a few grid cells (Fig. 5c).

FS events of the second intensity category (based on the accumulated GDD sum) occurred in at least one grid cell of the study area in 68.5% of the study period years. However, such events affected more than half of the area in only six years, with the largest extent (81.4% of grid cells) occurring in 1999. Meanwhile, FS events of the third intensity class, characterised by a GDD sum exceeding 200 °C, occurred in just 20.4% of the study period years. These events covered the largest area in 1968 (27.9% of the grid cells) (Fig. 6a).

The t_{min} values recorded during these events were categorised into three intensity categories (Table 1). Severe frosts ($-2\ °C > t_{min} > -5\ °C$) during FS events in more than half of the territory occurred only in 1964 (59.5%). Extreme frosts ($t_{min} < -5\ °C$) in at least one grid cell were recorded in 16.4% of studied years. The largest area affected by such events (7.2%) was in 1959 (Fig. 6b).

All FS events were classified into nine intensity classes (Table 1). At least one event fell into each class except for

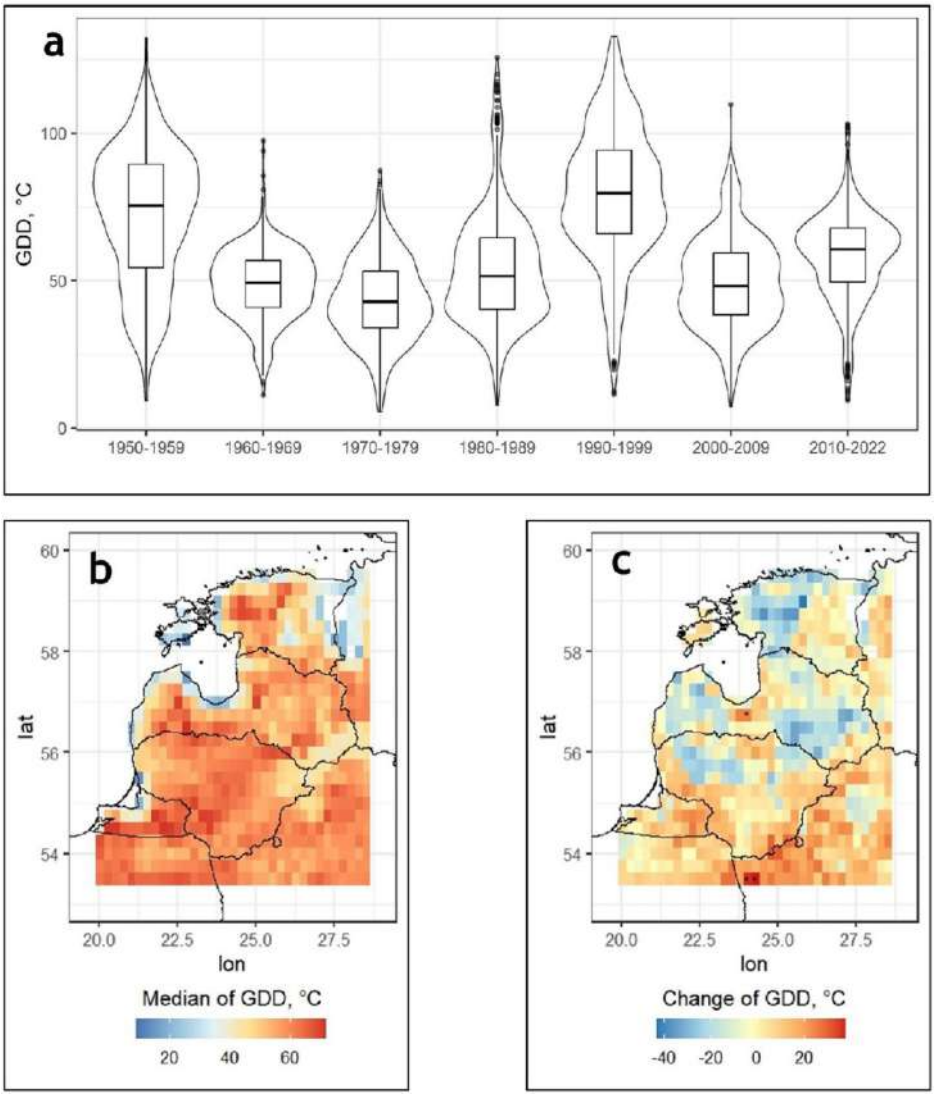

Fig. 5 (**a**) Violin plot of growing degree days (GDD) accumulated until the false spring (FS) event for different periods from 1950 to 2022; (**b**) Median of GDD sums accumulated until FS events; (**c**) Difference in the medians of GDD sums accumulated until FS events during two periods 2003–2022 and 1950–1969. Dots indicate grid cells where the changes were statistically significant (when $p < 0.05$) according to the t-test

the F3_GDD2 class. The majority, 65.1% of all events, belonged to the lowest intensity class (F1_GDD1).

17.7% of FS events fell into the F1_GDD2 intensity class. With the accumulation of 100–200 °C GDD in spring, various fruit trees begin to blossom, buds start to develop, and the leaves of trees (such as oak, beech, birch, etc.) unfold (Fu et al. 2019; Wypych et al. 2017; Zavalloni et al. 2006). At this phenology stage, plant resistance to cold is

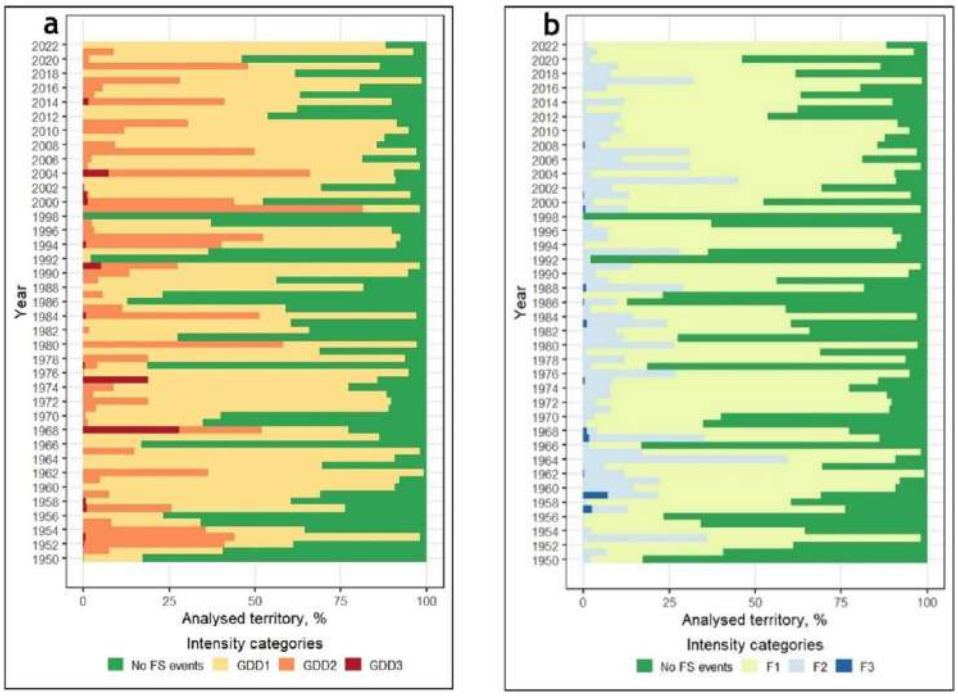

Fig. 6 Percentage of the study area where the sum of GDD (**a**) and the frosts (**b**) of the corresponding intensity categories were recorded from 1950 to 2022 during the false spring (FS) events. Detailed information on the intensity categories is provided in Table 1

minimal, and even slightly negative temperatures (−1 to −3 °C) can damage flower buds, leaves, and other tissues (Chamberlain et al. 2019; Vitasse et al. 2014; Wypych et al. 2017). Events belonging to this intensity class covered the largest area (71.1% of grid cells) in 1999 (Fig. 7) and they were most frequent in central Estonia and the eastern edge of the study area (Fig. 8).

13.8% of all FS events belonged to the F2_GDD1 intensity class (Fig. 7). Events in this class can harm vegetation. However, since the accumulated GDD sum at the time of the event is still low, even severe frost causes relatively minor damage as plants in early growth stages are generally well adapted to temperatures below freezing (Scheifinger et al. 2003).

The remaining five intensity classes accounted for only 3.4% of FS events, while events classified under the highest intensity classes, F2_GDD3 and F3_GDD3, constituted only 0.05% of all FS events. Events in these two classes were characterised by severe or extreme frost, with the sum of GDD exceeding 200 °C. Such events not only cause a negative impact on fruit trees, potentially destroying a significant portion of future harvests, but also harm other plants, disrupting the entire food chain structure (Gu et al. 2008). All FS events belonging to these two intensity classes were observed in 1975 (Fig. 7) in the northern part of the study area (Fig. 8). The year 1975 was notable for an exceptional FS event on 25 May in Estonia, which also saw snowfall up to 10 cm, leading to significant ecological and economic damage (Kohler 2013).

4 Discussion

The rising temperatures from February to April, driven by climate change, have primarily accelerated the onset of the growing season across the analysed territory, shifting on average by nearly two weeks during the investigation period. These changes were statistically significant in three-quarters of the study area's grid cells, except in regions of highlands (western Lithuania, central Latvia).

The obtained SGS date changes agree with the results of other studies in the research area. In Lithuania, the SGS date

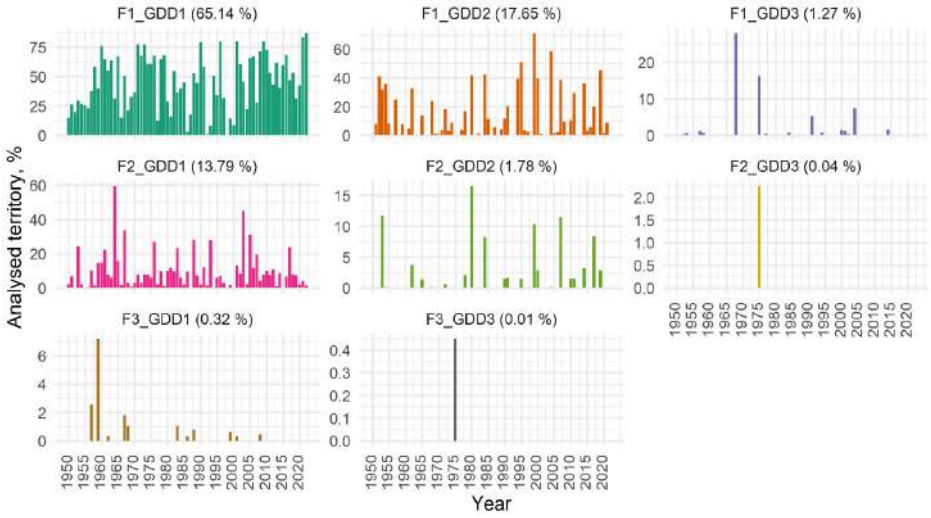

Fig. 7 Percentage of the study area where false spring (FS) events of the corresponding intensity class were recorded during the investigation period (1950–2022). The numbers in parentheses next to the class name indicate what percentage of all FS events identified during the study period belong to the corresponding intensity class. Detailed information on the intensity classes is provided in Table 1

shifted earlier by approximately 13 days over the period from 1961 to 2018 (Mačiulytė and Stankūnavičius 2020). In Latvia, from 1960 to 2008, due to the rising winter temperatures, budburst occurred earlier by 22–25 days, and the temperature rise in April led to an earlier start of flowering by 9–16 days, depending on the plant species (Kampuss et al. 2009). However, such changes in SGS dates and flowering of plants are not solely positive—they not only increase the risk of late frost damage but also may influence the spread of pests and diseases (Meier et al. 2022).

Due to the changing climate and the increasing late winter and early spring temperatures, the last frost date has also become earlier throughout the study area. Nevertheless, the changes in this case were smaller, averaging 6.3 days. Similar changes were observed in other studies, such as in Lithuania from 1961 to 2018 (Mačiulytė and Stankūnavičius 2020) and in the USA from 1900 to 2014 (Kukal and Irmak 2018). The shift of LSF dates from the beginning of the 20th century to the end of the 21st century has also been recorded in Poland and Central Europe (Graczyk and Kundzewicz 2016; Ma et al. 2019; Wypych et al. 2017).

The main factor determining the distribution of LSF dates is the distance from the Baltic Sea, while latitude also influences it. Due to the Baltic Sea's warming effect, in the lower-lying coastal areas, such as western Lithuania and the southwestern part of the study area, the median LSF date is, on average, nearly a month earlier than in central Estonia. The distance from the Baltic Sea also influenced the spatial distribution of FS events. In coastal areas, FS events were rarely recorded during the study period (up to 2 occurrences per decade). Moving away from the Baltic Sea, the number of FS events rapidly increased, with more than half of the study area experiencing 7–8 events per decade. Nonetheless, comparing the first 20 years of the study period with the last two decades (2003–2022), it was found that the greatest increase in FS events occurred in areas characterised by a more rapid rise in spring temperatures.

The topography of the study area is another factor that could influence the spatial distribution of FS events (De Melo-Abreu et al. 2016; Pellerin et al. 2012). However, in this study, it is challenging to identify a clear relationship between terrain and the recurrence or intensity of FS events. This may be largely due to the lack of significant elevation variation within the study area, where the highest point is only 355 m above sea level.

Although the number of FS events increased over the 73-year study period, no significant changes were found. Similar tendencies have been observed in FS events in other countries or regions. It was found that during the period from 1971 to 2020 in Poland the number of frosts occurring after the SGS date did not change significantly, and the spatial distribution of these phenomena is also primarily influenced by the distance from the sea (Koźmiński et al. 2021, 2023; Nidzgorska-Lencewicz et al. 2024). The risk of frosts causing damage to plants has also remained unchanged since 1864 in the lowlands of Switzerland and Germany

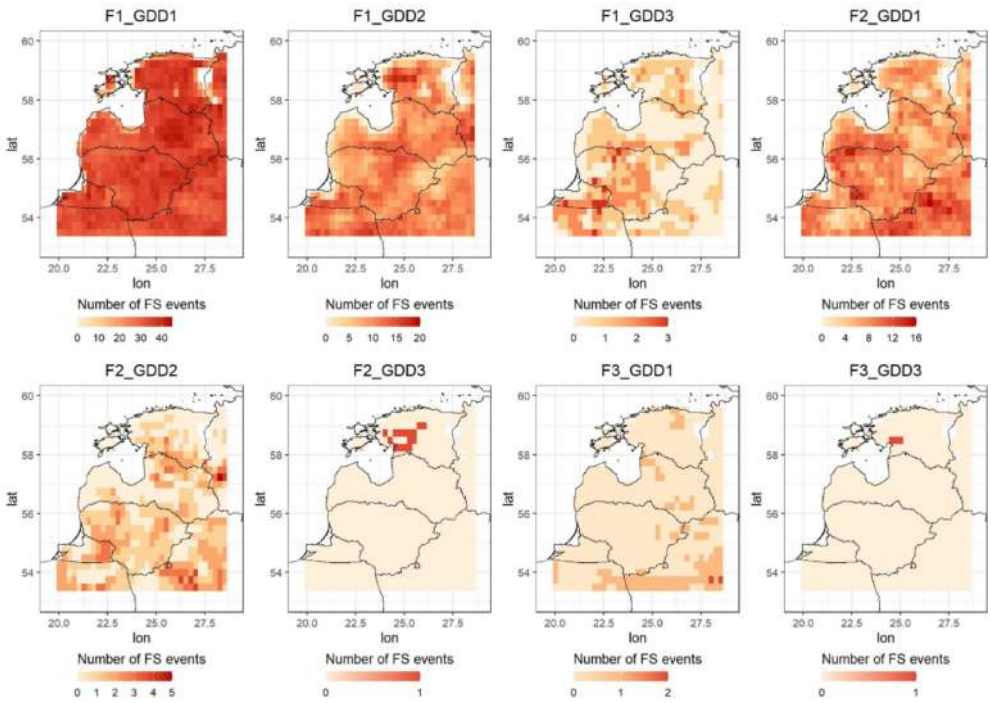

Fig. 8 The sum of false spring (FS) events from 1950 to 2022 belonging to the corresponding intensity class. Detailed information on the intensity classes is provided in Table 1

(Vitasse and Rebetez 2018). Despite that, frosts remain dangerous for crops and other plants (Liu et al. 2018; Nidzgorska-Lencewicz et al. 2024. FS events capable of causing strong ecological and economic losses also occurred in the eastern Baltic Sea region in the 21st century. For example, in the spring of 2007, 11.8% of the study area's grid cells, primarily in the southwestern and northeastern parts, experienced FS events when a GDD sum of 100 to 200 °C was accumulated and the t_{min} ranged from −2 to −5 °C. Such events occurred during budburst and leaf unfolding when plant frost resistance is minimal (Chamberlain et al. 2019). However, significant changes in the intensity of FS events over the study period in this research were not found.

In the future, as temperatures continue to rise, the growing season is expected to start even earlier, and the dates of leaf unfolding and flowering will also change (Juknys et al. 2017; Ruosteenoja et al. 2016; Szyga-Pluta et al. 2022; Zhu et al. 2019). Therefore, the risk of FS events may persist or even increase (Chmielewski et al. 2018; Ma et al. 2019; Unterberger et al. 2018; Vitasse et al. 2019), especially in areas where the shift of SGS dates exceeds that of LSF dates, and frosts are recorded closer to the date of budburst (Jönsson and Bärring 2011). However, when assessing the damage caused by FS events to vegetation both in the past and the foreseeable future, it is essential to consider that plant frost sensitivity depends on the species (Jönsson and Bärring 2011; Liu et al. 2018; Morin and Chuine 2014) and growth stage (Chamberlain et al. 2019).

The occurrence of FS events in the eastern Baltic Sea region is closely related to atmospheric circulation patterns, and future changes in these patterns may influence both the frequency and intensity of FS events, as well as the extent of the resulting damage. Typical conditions leading to the formation of severe or extreme spring frosts are associated with blocking processes and positive sea level pressure anomalies. Such a situation leads to the advection of cold Arctic air masses from the northwest, north, and northeast (Bielec-Bąkowska and Twardosz 2023; Tomczyk et al. 2019). This advection is most often recorded when blocking patterns form in the North Atlantic and northern Europe (Pfahl 2014). FS events can also occur during easterly advection. However, it is less common for late spring

frosts in the study area to form with northerly airflow associated with a cyclonic trough and frontal passage (Ustrnul et al. 2014).

The occurrence of FS events in late spring may also be linked to the North Atlantic Oscillation (NAO). It has been found that during the negative phase of the NAO, the number of frost days in Poland increases (Tomczyk 2015). The study area is also characterised by the advection of various types of air masses in the spring, with their recurrence showing interannual variability (Krauklis and Dravienece 2004). This variability could be one of the reasons for the lack of trend in the recurrence of FS events.

It has been found that in Estonia, the frequency of air movement from the north-northwest increased during the 1966–2015 period, with the most significant and statistically significant changes occurring in spring (Lakson et al. 2019). Such changes in the eastern part of the Baltic Sea region may increase the likelihood of spring frosts and, consequently, FS events.

Several factors must be considered when conducting future research on FS events in the eastern part of the Baltic Sea region. In this study, the SGS date was defined solely based on the mean daily air temperature without accounting for other variables influencing the SGS date, such as precipitation, soil moisture and nutrient content, evapotranspiration, and other relevant parameters (Chen et al. 2023; Linderholm 2006; Qu et al. 2015; Rimkus et al. 2017). However, it has been established that for determining the SGS date in spring, the air temperature is crucial (Juknys et al. 2017; Ladwig et al. 2019; Romanovskaja and Bakšienė 2009). Additionally, this study used only two variables to identify FS events: the dates of SGS and LSF. This approach assumes uniform damage from FS events across different species, their life stages and habitats (Chamberlain et al. 2019). Therefore, future research should focus more on specific species to better understand the negative impact and severity of FS events on plants (Ladwig et al. 2019).

When evaluating FS events, it is important to consider not only the plant species, topography, and distance from the sea, but also local factors such as land use type, soil characteristics (composition and moisture) and wind among others (De Melo-Abreu et al. 2016; Leslie et al. 2014). These factors influence the frequency of FS events and can also affect the severity of their impact on vegetation. A detailed assessment of FS event intensity on a local scale would require consideration of all these factors. However, this would require higher spatial resolution than the one used in this study. The size of the grid cell used in this work ($0.25 \times 0.25°$) diminishes the influence of local factors and even within the same grid cell, local factors may vary and have different effects.

5 Conclusions

This study evaluated the recurrence, spatial distribution, and intensity of FS events in the eastern Baltic Sea region, alongside the spatial distribution and long-term changes in the SGS and LSF dates from 1950 to 2022. Latitude was the main factor influencing SGS distribution, while LSF dates were primarily determined by the distance to the Baltic Sea, with latitude also playing a role. Over the study period, the SGS date moved earlier by an average of 10.6 days, with significant changes in 73.9% of grid cells. The LSF date also shifted earlier by 6.3 days, with significant changes found in 21.3% of cells. No significant changes in the number of FS events over the study period were observed according to the Mann-Kendall test. Significant interannual variability in atmospheric circulation can be an influencing factor that determines such tendencies. However, when comparing the periods of 1950–1969 and 2003–2022, 85.9% of grid cells saw an increase in FS events, with significant changes occurring in 30% of cells. Distance from the Baltic Sea emerged as the main factor determining the distribution of FS events. The intensity of FS events was evaluated based on the sum of GDD accumulated until the FS event and the t_{min} recorded during the event. Each FS event was assigned to one of nine intensity classes, with most (65.1%) falling to the lowest intensity class. The intensity of FS events remained unchanged. The only FS event of the highest intensity class occurred in Estonia in 1975.

This research analysed FS events from a climatological perspective, but a more detailed study of FS spring events in the eastern part of the Baltic Sea region, with emphasis on local factors, would be beneficial. This could improve predictions of future FS events, helping to mitigate the ecological and economic impacts of these events on agriculture and forestry in changing climate conditions.

Author contributions All authors contributed to the study's conception and design. Material preparation, data collection and analysis were performed by L. K. and E. R. The first draft of the manuscript was written by L. K. and all authors commented on previous versions of the manuscript. Both authors read and approved the final manuscript.

Funding The authors declare that no funds, grants, or other support were received during the preparation of this manuscript.

Data availability The datasets generated during and/or analysed during this study are available from the corresponding author upon reasonable request.

Declarations

Ethical approval Not applicable.

Consent to participate Not applicable.

Consent for publication Not applicable.

Competing interests The authors declare no competing interests.

References

Anandhi A (2016) Growing degree days - ecosystem indicator for changing diurnal temperatures and their impact on corn growth stages in Kansas. Ecol Indic 61:149–158. https://doi.org/10.1016/j.ecolind.2015.08.023

Beck HE, Zimmermann NE, McVicar TR, Vergopolan N, Berg A, Wood EF (2018) Present and future Köppen-Geiger climate classification maps at 1-km resolution. Sci Data 5:1–12. https://doi.org/10.1038/sdata.2018.214

Bell B, Hersbach H, Simmons A, Berrisford P, Dahlgren P, Horányi A, Muñoz-Sabater J, Nicolas J, Radu R, Schepers D, Soci C, Villaume S, Bidlot JR, Haimberger L, Woollen J, Buontempo C, Thépaut JN (2021) The ERA5 global reanalysis: preliminary extension to 1950. Q J R Meteorol Soc 147(741):4186–4227. https://doi.org/10.1002/qj.4174

Bielec-Bąkowska Z, Twardosz R (2023) Exceptionally cold and warm spring months in Kraków against the background of Atmospheric circulation (1874–2022). Pure Appl Geophys 180(9):3351–3370. https://doi.org/10.1007/s00024-023-03324-9

Bonhomme R (2000) Bases and limits to using 'degree.day' units. Eur J Agron 13(1):1–10. https://doi.org/10.1016/S1161-0301(00)00058-7

Ceglar A, Zampieri M, Toreti A, Dentener F (2019) Observed northward Migration of Agro-climate zones in Europe will further accelerate under Climate Change. Earths Future 7(9):1088–1101. https://doi.org/10.1029/2019EF001178

Chamberlain CJ, Cook BI, García de Cortázar-Atauri I, Wolkovich EM (2019) Rethinking false spring risk. Glob Chang Biol 25(7):2209–2220. https://doi.org/10.1111/gcb.14642

Chen H, Zhao J, Zhang H, Zhang Z, Guo X, Wang M (2023) Detection and attribution of the start of the growing season changes in the Northern Hemisphere. Sci Total Environ. https://doi.org/10.1016/j.scitotenv.2023.166607

Chmielewski FM, Götz KP, Weber KC, Moryson S (2018) Climate change and spring frost damages for sweet cherries in Germany. Int J Biometeorol 62(2):217–228. https://doi.org/10.1007/s00484-017-1443-9

De Melo-Abreu JP, Villalobos FJ, Mateos L (2016) Frost Protection. In: Villalobos F, Fereres E (eds) Principles of Agronomy for sustainable agriculture. Springer, Cham, pp 443–457. https://doi.org/10.1007/978-3-319-46116-8_29

ECMWF (2024) ERA5: Data documentation. https://confluence.ecmwf.int/display/CKB/ERA5%3A+data+documentation#ERA5:datadocumentation-Knownissues. Accessed 20 March 2024

Faust E, Herbold J (2018) Spring frost losses and climate change – Not a contradiction in terms. Munich Re. Topics Geo 2017

Fu YH, Zhang X, Piao S, Hao F, Geng X, Vitasse Y, Zohner C, Peñuelas J, Janssens IA (2019) Daylength helps temperate deciduous trees to leaf-out at the optimal time. Glob Chang Biol 25(7):2410–2418. https://doi.org/10.1111/gcb.14633

Graczyk D, Kundzewicz ZW (2016) Changes of temperature-related agroclimatic indices in Poland. Theor Appl Climatol 124(1–2):401–410. https://doi.org/10.1007/s00704-015-1429-7

Graczyk D, Szwed M (2020) Changes in the occurrence of late spring frost in Poland. Agronomy 10(11). https://doi.org/10.3390/agronomy10111835

Grāvīte I (2022) Cold Resistance of Flower buds of Latvian Plum cultivars. Proc Latv Acad Sci sect B Nat Exact. Appl Sci 76(4):500–504. https://doi.org/10.2478/prolas-2022-0077

Gu L, Hanson PJ, Post WM, Kaiser DP, Yang B, Nemani R, Pallardy SG, Meyers T (2008) The 2007 eastern US spring freeze: increased cold damage in a warming world? Bioscience 58(3):253–262. https://doi.org/10.1641/B580311

Horton P (2022) Analogue methods and ERA5: benefits and pitfalls. Int J Climatol 42(7):4078–4096. https://doi.org/10.1002/joc.7484

Hufkens K, Friedl MA, Keenan TF, Sonnentag O, Bailey A, O'Keefe J, Richardson AD (2012) Ecological impacts of a widespread frost event following early spring leaf-out. Glob Chang Biol 18(7):2365–2377. https://doi.org/10.1111/j.1365-2486.2012.02712.x

Jönsson AM, Bärring L (2011) Ensemble analysis of frost damage on vegetation caused by spring backlashes in a warmer Europe. Nat Hazards Earth Syst Sci 11(2):401–418. https://doi.org/10.5194/nhess-11-401-2011

Juknys R, Velička R, Kanapickas A, Kriaučiūnienė Z, Masilionytė L, Vagusevičienė I, Pupalienė R, Klepeckas M, Sujetovienė G (2017) Projecting the impact of climate change on phenology of winter wheat in northern Lithuania. Int J Biometeorol 61(10):1765–1775. https://doi.org/10.1007/s00484-017-1360-y

Kalvāne G, Romanovskaja D, Briede A, Bakšiene E (2009) Influence of climate change on phenological phases in Latvia and Lithuania. Clim Res 39(3):209–219. https://doi.org/10.3354/cr00813

Kampuss K, Strautina S, Laugale V (2009) Influence of climate change on berry crop growing in Latvia. Acta Hortic 838:45–51. https://doi.org/10.17660/ActaHortic.2009.838.5

Kohler V (2013) Late winter to reign on for weeks. Estonian news. https://news.postimees.ee/1189832/late-winter-to-reign-on-for-weeks. Accessed 25 March 25 2024

Koźmiński C, Nidzgorska-Lencewicz J, Makosza A, Michalska B (2021) Ground frosts in Poland in the growing season. Agric (Switzerland) 11(7). https://doi.org/10.3390/agriculture11070573

Koźmiński C, Mąkosza A, Nidzgorska-Lencewicz J, Michalska B (2023) Air frosts in Poland in the Thermal growing season (AT > 5°C). Agric (Switzerland) 13(6). https://doi.org/10.3390/agriculture13061228

Krauklis A, Draveniece A (2004) Landscape seasons and air mass dynamics in Latvia. Folia Geogr 12:16–47

Kukal MS, Irmak S (2018) U.S. Agro-climate in 20th Century: growing degree days, First and last Frost, growing season length, and impacts on crop yields. Sci Rep 8(1):1–14. https://doi.org/10.1038/s41598-018-25212-2

Ladwig LM, Chandler JL, Guiden PW, Henn JJ (2019) Extreme winter warm event causes exceptionally early bud break for many woody species. Ecosphere 10(1). https://doi.org/10.1002/ecs2.2542

Lakson M, Post P, Sepp M (2019) The impact of atmospheric circulation on air temperature rise in Estonia. Front Earth Sci 7:1–12. https://doi.org/10.3389/feart.2019.00131

Lamichhane JR (2021) Rising risks of late-spring frosts in a changing climate. Nat Clim Chang 11(7):554–555. https://doi.org/10.1038/s41558-021-01090-x

Leslie AD, Mencuccini M, Perks M (2014) Frost damage to eucalypts in a short-rotation forestry trial in Cumbria (England). IForest 7(3):156–161. https://doi.org/10.3832/ifor1161-007

Linderholm HW (2006) Growing season changes in the last century. Agric Meteorol 137(1–2):1–14. https://doi.org/10.1016/j.agrformet.2006.03.006

Lindsey R, Dahlman L (2024) Climate change: Global temperature. https://www.climate.gov/news-features/understanding-climate/climate-change-global-temperature. Accessed 5 March 2024

Liu Q, Piao S, Janssens IA, Fu Y, Peng S, Lian X, Ciais P, Myneni RB, Peñuelas J, Wang T (2018) Extension of the growing season increases vegetation exposure to frost. Nat Commun. https://doi.org/10.1038/s41467-017-02690-y

Ma Q, Huang JG, Hänninen H, Berninger F (2019) Divergent trends in the risk of spring frost damage to trees in Europe with

recent warming. Glob Chang Biol 25(1):351–360. https://doi.org/10.1111/gcb.14479
Mačiulytė V, Stankūnavičius G (2020) Agrothermal changes in 1961–2018 in Lithuania. Proceedings of the 3rd Baltic Earth Conference. https://archive.baltic.earth/hel2020/material/3rd_BalticEarth_Conference_Proceedings.pdf. Accessed 10 March 2024
McMaster GS, Wilhelm WW (1997) Growing degree-days: one equation, two interpretations. Agric Meteorol 87(4):291–300. https://doi.org/10.1016/S0168-1923(97)00027-0
Meier HEM, Kniebusch M, Dieterich C, Gröger M, Zorita E, Elmgren R, Myrberg K, Ahola MP, Bartosova A, Bonsdorff E, Börgel F, Capell R, Carlén I, Carlund T, Carstensen J, Christensen OB, Dierschke V, Frauen C et al (2022) Climate change in the Baltic Sea region: a summary. Earth Syst Dyn 13(1):457–593. https://doi.org/10.5194/esd-13-457-2022
Morin X, Chuine I (2014) Will tree species experience increased frost damage due to climate change because of changes in leaf phenology? Can J Res 44(12):1555–1565. https://doi.org/10.1139/cjfr-2014-0282
Nidzgorska-Lencewicz J, Mąkosza A, Koźmiński C, Michalska B (2024) Potential risk of Frost in the growing season in Poland. Agriculture 14(3):501. https://doi.org/10.3390/agriculture14030501
Paparrizos S, Matzarakis A (2017) Present and future assessment of growing degree days over selected Greek areas with different climate conditions. Meteorol Atmos Phys 129(5):453–467. https://doi.org/10.1007/s00703-016-0475-8
Peel MC, Finlayson BL, McMahon TA (2007) Updated world map of the Köppen-Geiger climate classification. Hydrol Earth Syst Sc 11(5):1633–1644. https://doi.org/10.5194/hess-11-1633-2007
Pellerin M, Delestrade A, Mathieu G, Rigault O, Yoccoz NG (2012) Spring tree phenology in the alps: effects of air temperature, altitude and local topography. Eur J Res 131(6):1957–1965. https://doi.org/10.1007/s10342-012-0646-1
Peterson AG, Abatzoglou JT (2014) Observed changes in false springs over the contiguous United States. Geophys Res Lett 41(6):2156–2162. https://doi.org/10.1002/2014GL059266
Pfahl S (2014) Characterising the relationship between weather extremes in Europe and synoptic circulation features. Nat Hazards Earth Syst Sci 14(6):1461–1475. https://doi.org/10.5194/nhess-14-1461-2014
Pfleiderer P, Menke I, Schleussner CF (2019) Increasing risks of apple tree frost damage under climate change. Clim Change 157(3–4):515–525. https://doi.org/10.1007/s10584-019-02570-y
Potter BE, Cate TW (1999) A climatology of late-spring freezes in the northeastern United States. US Dept. of Agriculture, Forest Service, North Central Research Station, St. Paul, Minnesota
Qu B, Zhu W, Jia S, Lv A (2015) Spatio-temporal changes in vegetation activity and its driving factors during the growing season in China from 1982 to 2011. Remote Sens 7(10):13729–13752. https://doi.org/10.3390/rs71013729
Radzka E (2021) Variation in growing season Thermal resources in Central-East Poland. J Ecol Eng 22(6):145–150. https://doi.org/10.12911/22998993/137358
Rimkus E, Stonevičius E, Kilpys J, Mačiulytė V, Valiukas D (2017) Drought identification in the eastern baltic region using NDVI. Earth Syst Dyn 8(3):627–637. https://doi.org/10.5194/esd-8-627-2017
Rodrigo J (2000) Spring frosts in deciduous fruit trees. Morphological damage and flower hardiness. Sci Hortic 85(3):155–173. https://doi.org/10.1016/S0304-4238(99)00150-8
Romanovskaja D, Bakšiene E (2009) Influence of climate warming on beginning of flowering of apple tree (Malus domestica Borkh.) In Lithuania. Agron Res 7(1):87–96
Ruosteenoja K, Räisänen J, Pirinen P (2011) Projected changes in thermal seasons and the growing season in Finland. Int J Climatol 31(10):1473–1487. https://doi.org/10.1002/joc.2171
Ruosteenoja K, Räisänen J, Venäläinen A, Kämäräinen M (2016) Projections for the duration and degree days of the thermal growing season in Europe derived from CMIP5 model output. Int J Climatol 36(8):3039–3055. https://doi.org/10.1002/joc.4535
Scheifinger H, Menzel A, Koch E, Peter C (2003) Trends of spring time frost events and phenological dates in Central Europe. Theor Appl Climatol 74(1–2):41–51. https://doi.org/10.1007/s00704-002-0704-6
Sepp T, Rätsep R, Libek AV, Kikas A (2022) Evaluation of Ribes Rubrum Cultivars in Estonia. Proceedings of the Latvian Academy of Sciences, Section B: Natural, Exact, and Applied Sciences 76(4):448–454. https://doi.org/10.2478/prolas-2022-0069
SMHI (2022) Climate indicator – Length of the vegetation period. https://www.smhi.se/en/climate/climate-indicators/climate-indicators-length-of-vegetation-period-1.91482. Accessed 10 September 2023
Spinoni J, Vogt J, Barbosa P (2015) European degree-day climatologies and trends for the period 1951–2011. Int J Climatol 35(1):25–36. https://doi.org/10.1002/joc.3959
Sujetovienė G, Velička R, Kanapickas A, Kriaučiuniene Z, Romanovskaja D, Bakšiene E, Vagusevičiene I, Klepeckas M, Juknys R (2018) Climate-change-related long-term historical and projected changes to spring barley phenological development in Lithuania. J Agric Sci 156(9):1061–1069. https://doi.org/10.1017/S0021859618000904
Szyga-Pluta K (2022) Assessment of changing agroclimatic conditions in Poland based on selected indicators. Atmosphere. https://doi.org/10.3390/atmos13081232
Tomczyk AM (2015) Impact of macro-scale circulation types on the occurrence of frosty days in Poland. Bull Geogr Phys Geogr Ser 9(9):55–65. https://doi.org/10.1515/bgeo-2015-0016
Tomczyk AM, Bednorz E, Półrolniczak M, Kolendowicz L (2019) Strong heat and cold waves in Poland in relation with the large-scale atmospheric circulation. Theor Appl Climatol 137:1909–1923. https://doi.org/10.1007/s00704-018-2715-y
Twardosz R, Walanus A, Guzik I (2021) Warming in Europe: recent trends in Annual and Seasonal temperatures. Pure Appl Geophys 178(10):4021–4032. https://doi.org/10.1007/s00024-021-02860-6
Unterberger C, Brunner L, Nabernegg S, Steininger KW, Steiner AK, Stabentheiner E, Monschein S, Truhetz H (2018) Spring frost risk for regional apple production under a warmer climate. PLoS ONE 13(7):1–18. https://doi.org/10.1371/journal.pone.0200201
Ustrnul Z, Wypych A, Winkler JA, Czekierda D (2014) Late spring freezes in Poland in relation to atmospheric circulation. Quaest Geogr 33(3):165–172. https://doi.org/10.2478/quageo-2014-0039
Vitasse Y, Rebetez M (2018) Unprecedented risk of spring frost damage in Switzerland and Germany in 2017. Clim Change 149(2):233–246. https://doi.org/10.1007/s10584-018-2234-y
Vitasse Y, Lenz A, Körner C (2014) The interaction between freezing tolerance and phenology in temperate deciduous trees. Front Plant Sci 5:1–12. https://doi.org/10.3389/fpls.2014.00541
Vitasse Y, Bottero A, Cailleret M, Bigler C, Fonti P, Gessler A, Lévesque M, Rohner B, Weber P, Rigling A, Wohlgemuth T (2019) Contrasting resistance and resilience to extreme drought and late spring frost in five major European tree species. Glob Chang Biol 25(11):3781–3792. https://doi.org/10.1111/gcb.14803
Walther A, Linderholm HW (2006) A comparison of growing season indices for the Greater Baltic Area. Int J Biometeorol 51(2):107–118. https://doi.org/10.1007/s00484-006-0048-5
Wypych A, Sulikowska A, Ustrnul Z, Czekierda D (2017) Variability of growing degree days in Poland in response to ongoing climate

changes in Europe. Int J Biometeorol 61(1):49–59. https://doi.org/10.1007/s00484-016-1190-3

Zavalloni C, Andresen JA, Flore JA (2006) Phenological models of flower bud stages and fruit growth of Montmorency sour cherry based on growing degree-day accumulation. J Am Soc Hortic Sci 131(5):601–607. https://doi.org/10.21273/jashs.131.5.601

Zhu L, Meng J, Li F, You N (2019) Predicting the patterns of change in spring onset and false springs in China during the twenty-first century. Int J Biometeorol 63(5):591–606. https://doi.org/10.1007/s00484-017-1456-4

Zohner CM, Mo L, Renner SS, Svenning JC, Vitasse Y, Benito BM, Ordonez A, Baumgarten F, Bastin JF, Sebald V, Reich PB, Liang J, Nabuurs GJ, De-Migueln S, Alberti G, Antón-Fernández C, Balazy R, Brändli UB, Chen HYH et al (2020a) Late-spring frost risk between 1959 and 2017 decreased in North America but increased in Europe and Asia. Proc Natl Acad Sci USA. https://doi.org/10.1073/pnas.1920816117

Zohner CM, Mo L, Sebald V, Renner SS (2020b) Leaf-out in northern ecotypes of wide-ranging trees requires less spring warming, enhancing the risk of spring frost damage at cold range limits. Glob Ecol Biogeogr 29(6):1065–1072. https://doi.org/10.1111/geb.13088

Zscheischler J, Martius O, Westra S, Bevacqua E, Raymond C, Horton RM, van den Hurk B, AghaKouchak A, Jézéquel A, Mahecha MD, Maraun D, Ramos AM, Ridder NN, Thiery W, Vignotto E (2020) A typology of compound weather and climate events. Nat Rev Earth Environ 1(7):333–347. https://doi.org/10.1038/s43017-020-0060-z

Publisher's note Springer Nature remains neutral with regard to jurisdictional claims in published maps and institutional affiliations.

Springer Nature or its licensor (e.g. a society or other partner) holds exclusive rights to this article under a publishing agreement with the author(s) or other rightsholder(s); author self-archiving of the accepted manuscript version of this article is solely governed by the terms of such publishing agreement and applicable law.

III PUBLIKACIJA

Compound precipitation and wind extremes in the eastern part of the Baltic Sea region

Klimavičius, L., Rimkus, E., & Stankūnavičius, G. (2025). Compound precipitation and wind extremes in the eastern part of the Baltic Sea region. *Atmosphere*, 16(3), 276. https://doi.org/10.3390/atmos16030276

atmosphere

MDPI

Article

Compound Precipitation and Wind Extremes in the Eastern Part of the Baltic Sea Region

Laurynas Klimavičius, Egidijus Rimkus * and Gintautas Stankūnavičius

Institute of Geosciences, Vilnius University, LT-03225 Vilnius, Lithuania; laurynas.klimavicius@chgf.vu.lt (L.K.); gintas.stankunavicius@gf.vu.lt (G.S.)
* Correspondence: egidijus.rimkus@gf.vu.lt

Abstract: Compound wind and precipitation extremes (CPWEs) pose significant threats to infrastructure, economies, the environment, and human lives. In this study, the recurrence, spatial distribution, intensity, and synoptic conditions leading to the formation of CPWEs were assessed in the eastern part of the Baltic Sea region. Using ERA5 reanalysis data, CPWEs were identified when both daily precipitation and maximum wind speed exceeded the 98th percentile thresholds on the same day at the same grid cell. Due to the proximity of the Baltic Sea and the influence of terrain, CPWEs were most frequent on the windward slopes of highlands in the western part of the investigation area. The most severe CPWEs occurred in the second half of summer and early September. Based on data from the Hess–Brezowsky synoptic classification catalogue and various synoptic datasets, the formation of CPWEs during the cold season (October–March) is associated with intense zonal (westerly) flow, while during the warm season (April–September), it is linked to the activity of southern-type cyclones. The number of CPWEs increased across all seasons, with the largest changes observed during the summer. However, the majority of changes are insignificant according to the Mann–Kendall test.

Keywords: compound climate events; precipitation extremes; wind extremes; ERA5; Hess–Brezowsky classification

check for updates

Academic Editor: Eugene Rozanov

Received: 28 January 2025
Revised: 19 February 2025
Accepted: 24 February 2025
Published: 26 February 2025

Citation: Klimavičius, L.; Rimkus, E.; Stankūnavičius, G. Compound Precipitation and Wind Extremes in the Eastern Part of the Baltic Sea Region. *Atmosphere* **2025**, *16*, 276. https://doi.org/10.3390/atmos16030276

Copyright: © 2025 by the authors. Licensee MDPI, Basel, Switzerland. This article is an open access article distributed under the terms and conditions of the Creative Commons Attribution (CC BY) license (https://creativecommons.org/licenses/by/4.0/).

1. Introduction

In recent decades, human-induced climate change has led to increased frequency and intensity of different weather and climate extremes. Particularly notable is the rise in hot extremes and heavy precipitation events, with these trends observed across various regions of the planet [1]. Such extreme events cause significant negative impacts on infrastructure, economies, and natural environments. Between 2000 and 2020, 773 million people were injured during such events, with losses amounting to USD 1.3 trillion [2]. In the European Union alone, weather and climate events caused over 200,000 deaths between 1980 and 2023 [3].

However, the past decade has shown that more significant damage and negative socio-economic impacts occur when two or more weather or climate extremes interact, resulting in a compound climate event [4,5]. Four different types of such events have been distinguished [6], one of which includes compound precipitation and wind speed extremes (CPWEs). These occur when extreme precipitation and wind speed are simultaneously recorded in the same area [6,7].

CPWEs are among the most damaging extreme climate events. They can negatively affect various economic sectors, pose threats to the natural environment, disrupt critical infrastructure, and result in human fatalities [8]. For instance, in January 2018, the

storm "Friederike" struck Central Europe, causing traffic disruptions, power outages, building damage due to falling trees, and fatalities. In Germany alone, the storm caused EUR 900 million in damage [9]. CPWEs can also trigger landslides and pose risks from falling trees, which become more vulnerable to wind as soil moisture increases [7,9]. A study in the Czech Republic found that during winter CPWEs, mortality rates increase by 3% within 0–2 days after the event. The mortality rate was higher than that associated with individual precipitation or wind speed extremes [10]. Therefore, understanding CPWEs' formation, recurrence trends, and associated risks is increasingly critical [7,11].

CPWEs have been studied at both global [7,12,13] and regional scales [8,14–18]. Globally, CPWEs occur most frequently and pose significant risks, including flash floods and storm surges, in coastal regions [7,19,20] and areas prone to tropical cyclones [12]. In Europe, CPWEs are most commonly observed along Norway's western coastline, the Iberian Peninsula, and Central Europe [14,15]. Over recent decades, their frequency in Europe has remained relatively unchanged [15], but projections suggest that with continued climate warming, CPWEs will become more frequent, particularly in the northern and eastern parts of the continent [13]. Globally, these extremes are expected to shift towards higher latitudes in both hemispheres, with the most significant increases projected for regions above 50° latitude [21].

Investigations of CPWEs have also focused on the factors driving their formation. In mid-latitudes, CPWEs are associated with intense zonal westerly flows [22] and mid-latitude cyclones [7,19,23]. In northwestern and northern Europe, their formation is closely linked to the North Atlantic Oscillation (NAO), with CPWEs being more frequent and intense during a positive NAO phase [24]. Additionally, a strong relationship has been found between CPWEs in Western Europe and cold extremes in eastern North America [24,25]. Finally, the formation of these extremes also depends on local topography. During winter, more CPWEs are observed in the highlands, whereas in summer, they are more common in the lowlands [23].

Despite increasing attention to CPWEs globally and in Europe, no studies have investigated these compound extremes in the eastern part of the Baltic Sea region—this research is the first of its kind. Until now, precipitation and wind speed extremes in the Baltic states have been studied separately, focusing on their historical recurrence and future projections [26–31].

The primary goal of this study is to evaluate the recurrence, spatial distribution, intensity, and synoptic processes driving the formation of CPWEs in the eastern part of the Baltic Sea region from 1950 to 2022. The first part of the study assesses precipitation and wind speed extremes separately, determining their spatial distribution and recurrence over the 1950–2022 period. The second part focuses on the recurrence and trends of CPWEs, while the third part evaluates their intensity. Finally, the study concludes with an analysis of the synoptic conditions and factors leading to the formation of those compound extremes.

2. Materials and Methods

2.1. Study Area

The study focuses on the eastern part of the Baltic Sea region, covering an area between 53.5° and 59.5° N latitude and 20.0° and 28.5° E longitude (Figure 1).

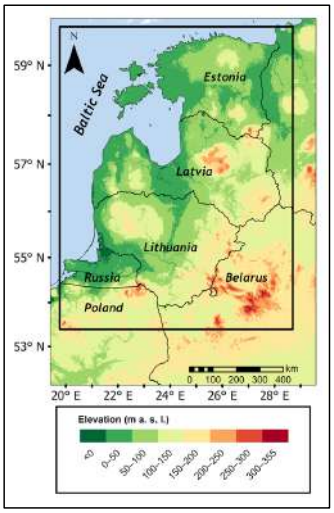

Figure 1. Study area and its topography (elevation above sea level).

The study area is characterised by lowlands and plains, with the highest point reaching 355 m above sea level (Figure 1). According to the updated Köppen–Geiger climate classification, the eastern part of the Baltic Sea region falls under the Dfb climate type [32,33], where the mean temperature of the warmest month (July) does not exceed 22 °C, but at least four months per year have a daily mean temperature above 10 °C [33].

The average temperature during the warmest summer months is around 16–18 °C, while in winter, it drops to −3 to −6 °C. Along the Baltic Sea coast, the air temperature during winter is close to 0 °C. The region experiences an average annual precipitation ranging from 550 to 800 mm, with the highest amounts recorded in the western part of the study area. The maximum precipitation occurs in July and August, averaging 70–90 mm monthly. The mean annual wind speed ranges from 2 m/s in the eastern part of the study area to 6 m/s on islands in the northeast, with the highest average wind speed observed in December and January.

2.2. Data

To identify CPWEs, daily precipitation (P) data and hourly maximum wind speed at 10 m height data from the European Centre for Medium-Range Weather Forecasts (ERA5) reanalysis were used. The daily maximum wind speed (w_{max}) at each grid point within the study area was determined from the hourly values. The spatial resolution of the processed data grids is 0.25 × 0.25°. The period from 1950 to 2022 was analysed.

This study focused on land areas only, analysing grids where more than 50% of the area is classified as land. Such grids were selected using the land filter in the KNMI Climate Explorer application (https://climexp.knmi.nl/start.cgi (accessed on 25 February 2024)), which was also used to obtain precipitation data. Hourly maximum wind speed data were retrieved from the Copernicus Climate Data Store (https://cds.climate.copernicus.eu/ (accessed on 25 February 2024)).

ERA5 reanalysis was chosen for this study due to its detailed temporal and spatial resolution and the long time series of its dataset [34]. It was also found that ERA5 reanalysis data for wind speed and precipitation closely align with ground-based observations in mid-latitudes. The accuracy of ERA5 reanalysis data, particularly when assessing extreme

values, tends to decrease in mountainous regions and tropical areas [35–37]. However, the study area in this research does not exhibit significant variation in altitude (Figure 1), so this issue is avoided. When using ERA5 data for evaluating P and w_{max} extremes, inaccuracies may arise due to the grid cell size ($0.25 \times 0.25^{\circ}$). This resolution in some cases might be insufficient for identifying extremes associated with mesoscale processes, such as thermal convection during the summer storms.

The assimilation of satellite, ground station, and radar data during dataset development is also an important factor for the accuracy of ERA5 reanalysis. In Europe, where such data are abundant, ERA5 data closely align with meteorological observations [38]. Finally, comparing precipitation and wind speed data from various widely used reanalysis datasets with ground-based measurements revealed that ERA5 provides the highest accuracy for both variables in Central Europe [38,39].

2.3. Identification of Compound Precipitation and Wind Extremes (CPWEs)

The 98th percentile values of P and w_{max} were calculated for each grid cell within the study area over the entire analysis period to identify CPWEs. The percentile method is widely used to identify extremes of these variables due to its simplicity and adaptability to various datasets and regions [40]. Different percentiles of P and w_{max} have been used in CPWE studies across various regions and on a global scale [7,8,11,14,41]. In this study, the 98th percentile values were chosen. To determine the appropriate percentile value for identifying P and w_{max} extremes, various threshold values (95th, 97th, 98th, and 99th percentiles) were tested. After evaluating the number of extremes identified in each case, it was established that the 98th percentile is optimal. This threshold captures both moderate and severe extremes while providing sufficient data for statistical analysis. At least one of these conditions was not met when using the other percentile values. Similar reasoning for using the 98th percentile was also provided in other studies [7,40].

In this study, P or w_{max} extremes were identified when the value of a variable at a given grid cell exceeded its 98th percentile value. Changes in such extremes were assessed for each grid cell over the 73-year study period. The statistical significance of these changes was determined using the non-parametric Mann–Kendall test, with results considered significant at $p < 0.05$.

CPWEs were defined as instances where both P and w_{max} extremes occurred on the same day at the same grid cell. The recurrence and changes in such compound extremes were assessed from 1950 to 2022. Additionally, the monthly and seasonal recurrence of CPWEs was analysed for the following seasons: December–February (DJF), March–May (MAM), June–August (JJA), and September–November (SON). Finally, the number of CPWEs in each grid cell was determined for the first (1950–1969) and last (2003–2022) 20 years of the study period, and the changes in these compound extremes were evaluated. These two time periods were selected to highlight the changes in the CPWEs under rapidly changing climate conditions. The statistical significance of these changes ($p < 0.05$) was determined using Student's *t*-test.

Once CPWEs were identified, the total number of days with at least one CPWE in any part of the study area was calculated. The recurrence of such days over the study period was evaluated, the season with the highest number of such days was identified, and the days with the most extensive spatial coverage of CPWEs were determined.

To identify the most intense CPWEs, the 99th and 99.9th percentile values of P and w_{max} were calculated for each grid cell. The frequency of compound extremes where both variables exceeded these percentile thresholds within the same grid cell during the study period was assessed. Similar methodologies have been applied in the analysis of various compound climate events [42,43], including CPWEs [44,45].

2.4. Evaluation of Atmospheric Processes During CPWE Formation

CPWE formation can be explained by the specific atmospheric circulation conditions that have developed in the region or larger area. To accomplish that, several complementary information sources were used to assess atmospheric conditions over Europe:

(a) Manual classification of daily large-scale circulation patterns by Hess–Brezowsky;
(b) Freely available synoptic schemes over Europe from three different weather centres—United Kingdom Met Office (available from 1988), German Meteorological Service (available from 2003), and Royal Netherlands Meteorological Institute (available from 2003);
(c) Global forecast system (GFS) analysis charts (available from 1979) and ERA5 post-processed daily statistics (available from 1940);
(d) The archive of weather maps from the Lithuanian Hydrometeorological Service under the Ministry of Environment (available from 1946).

The Hess–Brezowsky synoptic classification (GWL) represents 29 typical patterns of the daily synoptic circulation over Central Europe. Four types of them depend on zonal or westerly circulations (WA, WZ, WS, and WW), eight on southerly circulations (SWA, SWZ, SA, SZ, TB, TRW, SEA, and SEZ), eight on northwesterly and northerly circulations (NWA, NWZ, NA, NZ, HNA, HNZ, HB, and TRM), six on northeasterly and easterly circulations (NEA, NEZ, HFA, HFZ, HNFA, and HNFZ) and the last three on the main high/low-pressure area over Central Europe pattern (HM, TM, BM) [46]. These types are widely used in research areas such as synoptic meteorology, applied meteorology, climatology, environmental sciences, etc. The GWL data have been available since 1881, while descriptions of circulation types are provided in many similar studies [46–51]. The subjective classification of atmospheric processes by Hess–Brezowsky has a long history. It is widely used in atmospheric, climatic, and interdisciplinary studies, allowing for easier comparison of results across different authors and countries. An objective analysis provides a more precise depiction of atmospheric flow and structure. However, it depends on the selected domain, variables, and classification method, often yielding circulation types that differ from traditional subjective analyses.

Hess and Brezowsky circulation types were useful in determining the general flow pattern over Europe. The synoptic schemes were good for identifying the evolution of frontal systems and surface-pressure gradients within low-pressure fields. GFS analysis charts also allowed the tracking of the progress of surface pressure fields as well as temperature and humidity fields in the lower part of the troposphere. ERA5 daily data were used for similar purposes as GFS analysis, only prior to 1979. Operational (archived) weather maps were very useful in determining the development of the weather systems in Eastern and Central Europe, especially in the period before the 1980s.

The synoptic situation and atmospheric conditions that led to the formation of CPWEs were assessed only on the days within the study period when these compound extremes affected more than one-fifth of the study area. Atmospheric circulation was evaluated on each of these days as a major driving factor, as well as two days before, to determine the conditions for development, and one day after, to observe the decay of the event. The atmospheric conditions that influenced CPWE formation were separately analysed for the cold season (October–March) and the warm season (April–September).

3. Results

3.1. Extremes of Precipitation and Maximum Wind Speed

The highest 98th percentile daily precipitation (P_{98}) value, reaching 16.2 mm/day, was recorded along the Lithuanian Baltic Sea coast, while the lowest values (11–12 mm/day)

were observed in the northern part of the study area and around the Estonian islands (Figure 2a). It is evident that the distribution of these values is influenced by topography. Higher P_{98} values were found in the uplands of western Lithuania and central Latvia.

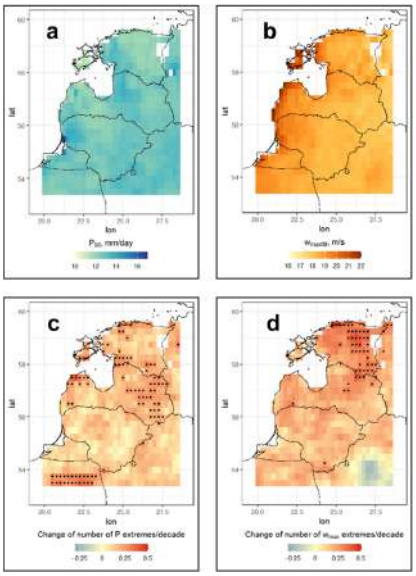

Figure 2. The 98th percentile values of daily precipitation (**a**) and maximum wind speed (**b**) in the study area for the entire 1950–2022 period. Decadal changes in the number of daily precipitation (**c**) and maximum wind speed (**d**) extremes in the study area. Grid cells with statistically significant changes, according to the Mann–Kendall test ($p < 0.05$), are marked with dots.

The distribution of the 98th percentile maximum daily wind speed (w_{max98}) across the study area is predominantly affected by the distance from the Baltic Sea (Figure 2b). The highest w_{max98} values, ranging from 21 to 22 m/s, were observed along the Baltic Sea coast. In contrast, the lowest w_{max98} values (16–17 m/s) were identified in the eastern part of the study area (Figure 2b).

After calculating the P_{98} and w_{max98} values for each grid cell separately, reoccurrence extremes for both P and w_{max} were assessed for cases when the values exceeded the 98th percentile. The analysis of the recurrence of P extremes in the area revealed that their number has increased (on average across the area), but this change was not significant. The highest number of P extremes occurred in 1998, accounting for 2.2% of all P extremes. When examining the changes in the number of these extremes at each point in the study area, it was found that the number increased in 98.9% of the grid cells. However, statistically significant changes were found in only 13.8% of the points (Figure 2c).

The number of w_{max} extremes in the eastern Baltic Sea region also increased over the study period. This change was more pronounced compared with P extremes, but it was not statistically significant either. The most frequent w_{max} extremes occurred in 1990, which accounted for 3.5% of all w_{max} extremes during the investigation period. The number of w_{max} extremes increased across almost the entire study area (94% of the grid cells). The largest growth was observed in the northern and northeastern parts of the study area. However, statistically significant changes were found in only 8.1% of the grid cells (Figure 2d).

3.2. Compound Precipitation and Wind Extremes (CPWEs)

After evaluating the P and w_{max} extremes in each grid cell, CPWEs, cases where both extreme values coincided, were identified. The highest number of CPWEs, 3.7% of all cases, occurred in 1962 (Figure 3a). Over the 73-year study period, the number of such extremes in the eastern part of the Baltic Sea region slightly increased, but this change was not statistically significant. When examining the recurrence of CPWEs in different months, the highest occurrence (17.9%) was observed in October, while the lowest was in the spring months (Figure 3b).

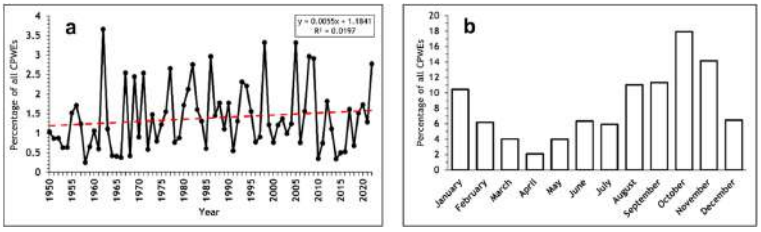

Figure 3. (**a**) The percentage of CPWEs identified annually over the 1950–2022 period, with the red dashed line indicating the trend. (**b**) The percentage of CPWEs identified during each month of the year.

An evaluation of CPWE recurrence within each grid cell of the study area revealed that over the entire study period, the highest frequency, 10–11 occurrences per decade, was recorded in western Lithuania (Figure 4a). A similar distribution was observed in winter, with most CPWEs occurring in the western and northeastern parts of the study area during this season (Figure 4b).

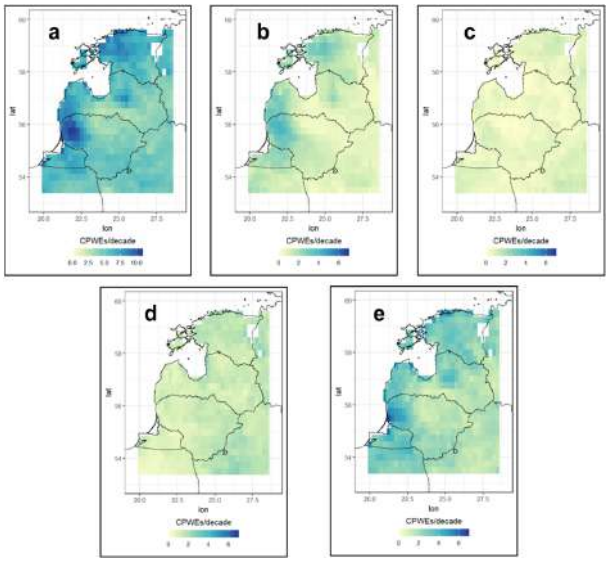

Figure 4. The number of CPWEs per decade: (**a**) annually; (**b**) December–February (DJF); (**c**) March–May (MAM); (**d**) June–August (JJA); (**e**) September–November (SON).

The lowest number of CPWEs (no more than 1.5 extremes per decade) was recorded during the spring months (MAM), with a relatively uniform spatial distribution across the study area (Figure 4c). In summer (JJA), the number of CPWEs increased, with the highest frequency (2–2.6 extremes per decade) observed in the southeastern and eastern parts of the study area, which are the furthest from the Baltic Sea (Figure 4d). In contrast, the spatial distribution of CPWEs during autumn (SON) was opposite to JJA. During this season, as well as over the entire study period, the highest number of CPWEs (5–6.5 extremes per decade) was recorded in western Lithuania (Figure 4e). Furthermore, when assessing all four seasons, 78% of the grid cells showed the highest frequency of CPWEs during SON.

The change in the number of compound precipitation and wind extremes (CPWEs) was also assessed in each grid cell by comparing their occurrence at the end of the study period (2003–2022) to the beginning (1950–1969). It was found that the number of CPWEs increased in 70.2% of the grid cells, while a decrease was observed in only 21.7%. The most significant increase, reaching up to 12 cases in individual grid cells, was identified in the southern and southwestern parts of the study area. However, statistically significant changes were detected in only 6.5% of the grid cells (Figure 5a). Across all four seasons, an increase in the number of CPWEs was observed (Figure 5b–e). However, statistically significant changes ($p < 0.05$) were identified in only a few grid points. The highest percentage of grid cells, with a statistically significant increase in CPWEs (4.8%), occurred during JJA. This season also showed the largest overall increase in CPWEs, with 65.5% of grid cells experiencing growth.

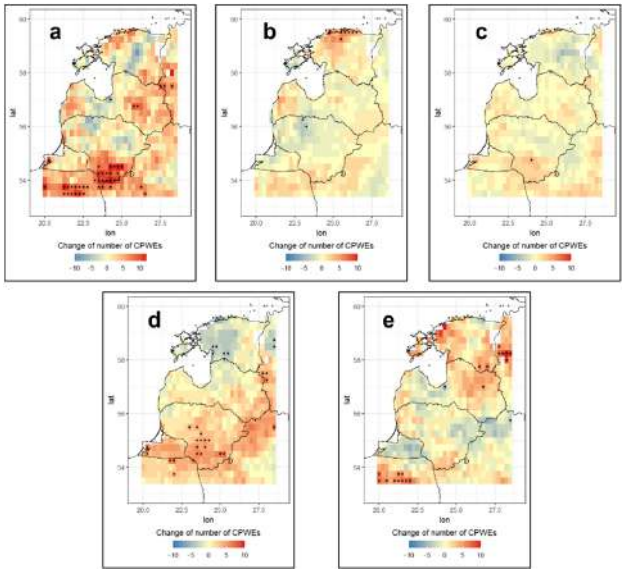

Figure 5. Change in the number of CPWEs between the 2003–2022 and 1950–1969 periods for each grid cell: (**a**) annually; (**b**) December–February (DJF); (**c**) March–May (MAM); (**d**) June–August (JJA); (**e**) September–November (SON). Grid cells with statistically significant changes based on the *t*-test ($p < 0.05$) are marked with dots.

Notably, during DJF and SON, the most pronounced increases in CPWEs were concentrated in the northern part of the study area (Figure 5b,e). In contrast, during JJA, the

largest growth was observed in the eastern and southern regions of the analysed territory (Figure 5c,d).

Days when, at least in one grid cell, a CPWE was recorded were also identified. A total of 797 such days were observed over the 73 years, with their frequency increasing over the investigation period (Figure 6a). The changes are statistically significant based on the Mann–Kendall test ($p < 0.05$). October recorded the highest share (14.8%) of all such days (Figure 6b).

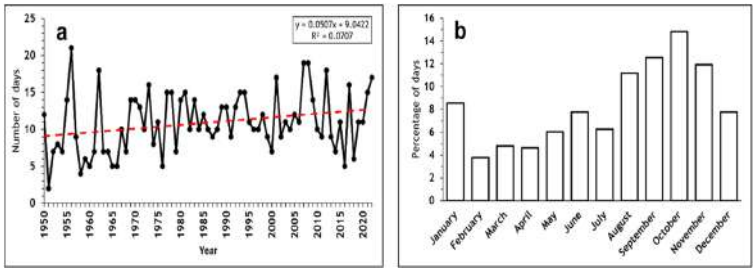

Figure 6. (**a**) Dynamics of the number of days with CPWEs from 1950 to 2022. The red dashed line represents the trend. (**b**) Distribution of the number of days with CPWEs throughout the year.

In most cases, CPWEs were recorded on the same day in only one or a few grid cells. CPWEs were identified in more than one-fifth of the grid cells in the study area on only 44 days (6% of the days with at least one CPWE) and in more than half of the grid cells on just 3 days: 22 October 1971 (CPWEs recorded in 51.1% of the grid cells), 28 October 1998 (75.4% of the grid cells), and 14 October 2009 (57.4% of the grid cells).

3.3. Intensity of CPWEs

By calculating the 99th and 99.9th percentile values of P and w_{max}, the CPWEs with the highest intensity were identified. Over the entire study period, the 99th percentile values of both variables were exceeded in 29.5% of all CPWEs. Meanwhile, CPWEs during which both P and w_{max} exceeded the 99.9th percentile values in the same grid cell accounted for 0.9% of all CPWEs. During these particularly intense CPWEs, the average daily precipitation amount was 46.7 mm, and the w_{max} averaged 26.5 m/s. Such severe CPWEs in at least one grid cell were recorded in only 11 days. All these days occurred in the second half of summer and the first ten days of September, as only during the summer months were precipitation amounts high enough to exceed the 99.9th percentile threshold.

However, during just four days, P and w_{max} both exceeded the 99.9th percentile values and severe CPWEs formed in more than 1% of the grid cells within the study area. These cases occurred on 6–7 August 1967, when intense CPWEs were observed in 5.8% of the grid cells; 7 August 1987 (10.2% of the grid cells); 28 July 1988 (4.3% of the grid cells); and 9–10 August 2005 (12.1% of the grid cells). These events were recorded in different locations within the analysed area (Figure 7).

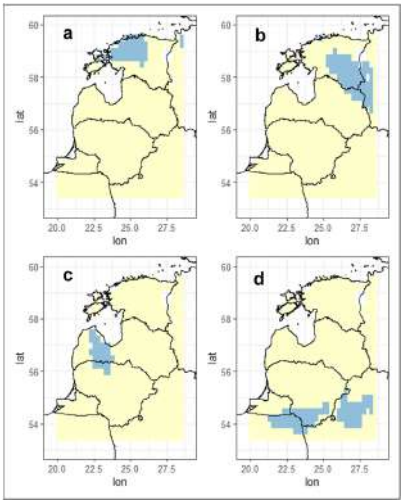

Figure 7. The part of the study area (in blue colour) where the most intense CPWEs (above the 99.9th percentile) were recorded: (**a**) 6–7 August 1967; (**b**) 7 August 1987; (**c**) 28 July 1988; (**d**) 9–10 August 2005.

The most intense CPWEs were observed during the summer (JJA). However, in many cases, they were localised and caused by mesoscale convection processes. In contrast, the CPWEs that covered the largest portion of the area were found during the autumn (SON). It was also determined that CPWEs with w_{max} values exceeding the 99.9th percentile most frequently occurred during the DJF and SON seasons, primarily in the southwestern and northern parts of the study area. In contrast, CPWEs with P values exceeding the 99.9th percentile showed opposite trends. Most of these cases (65.5%) occurred in JJA, mainly in the southeastern part of the study area.

3.4. Atmospheric Conditions Leading to the Formation of CPWEs

A total of 44 days were identified when CPWEs occurred in more than 1/5 of the study area, and 28 days were recorded during the cold season and 16 during the warm season. These specific days were selected for further analysis of the atmospheric conditions.

Different forcing to CPWEs mechanisms were found in the cold and warm half of the year. Most cold-season compound extremes appear to be forced by intensive mid-tropospheric zonal and only a few subzonal circulations over the southern part of Northern Europe. Such patterns of atmospheric circulation over Europe correspond to the WZ type of Hess–Brezowsky circulation, and only a few cases were identified as SWZ, WA, or NZ types (Table 1). During the cold season, CPWEs typically form due to rapidly developing frontal waves along the southern periphery of a deep depression over the Northeast Atlantic or North Sea region. Moreover, such atmospheric circulation patterns show a large persistence. This form is usually established not only on the day of the appearance of the CPWE but at least 3–5 days before it. Most of these developing waves caused deepening of local minima over the Baltic region, which is not typical for classic Atlantic cyclones moving eastward. However, this explains the increased pressure gradients in the rear of such cyclones well. Other important features of this type of atmospheric circulation are: (a) the clear zonal separation of cold and warm air masses over Central and/or Northern Europe and (b) the advection of moist air from the subtropical part of the North Atlantic through the

British Isles, southern Scandinavia, and into the Baltic region (Figure 8a,b). The CPWE location in such cases has been predetermined by the proximity of the centre or, rarely, triple (occlusion) point of the fast-moving cyclone or the wave: the further north the trajectory of the developing cyclone, the more northerly the position of the CPWE and vice versa.

Table 1. The recurrence of different circulation types (% of the days when CPWEs covered > 20% of the study area) derived according to the Hess–Brezowsky classification during CPWE formation in the cold and warm seasons. D0 represents the day of CPWE formation, D − 2 and D − 1 represent two and one day before, respectively, and D + 1 represents one day after the CPWE formation date.

Circulation Pattern	Type	Cold Season (October–March)				Warm Season (April–September)			
		D − 2	D − 1	D0	D + 1	D − 2	D − 1	D0	D + 1
Zonal (westerly)	WA, WZ, WS, WW	57.1	60.7	60.7	67.9	18.8	18.8	18.8	37.5
Southerly	SWA, SWZ, SA, SZ, TB, TRW, SEA, SEZ	17.9	17.9	14.3	7.1	12.5	6.3	6.3	6.3
Northwesterly and northerly	NWA, NWZ, NA, NZ, HNA, HNZ, HB, TRM	14.3	10.7	21.4	17.9	43.8	43.8	31.3	18.8
Northeasterly and easterly	NEA, NEZ, HFA, HFZ, HNFA, HNFZ	0	0	0	0	6.3	12.5	12.5	12.5
High/low-pressure area over Central Europe	HM, TM, BM	10.7	10.7	3.6	7.1	18.8	18.8	31.3	25.0

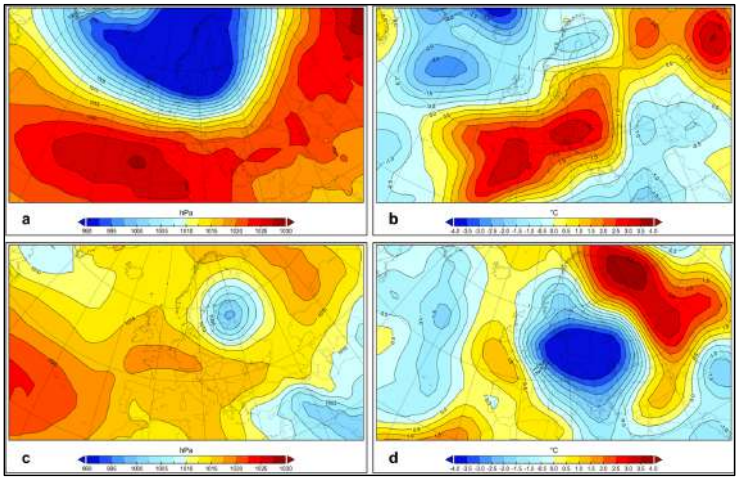

Figure 8. Composite analysis of the CPWEs in the cold (October–March) (**a**,**b**) and the warm (April–September) (**c**,**d**) half of the year: (**a**,**c**) sea level pressure (hPa) and (**b**,**d**) temperature anomaly (cC) at the 850 hPa level. Anomalies were calculated according to 1991–2020 daily smoothed climatology.

In the warm half of the year (April–September), the typical circulation patterns exhibit much greater diversity (Table 1). The common feature in most analysed compound extremes is the lower-than-normal pressure in the upper troposphere over Central or Eastern Europe or both. According to the Hess–Brezowsky classification, the TM, NZ, NWZ, HNZ, HNFZ, TRM, WS, BM, and HB types of circulation are capable of maintaining low pressure over Central Europe and further east while other types (HB, NWA, HFA) are capable of

maintaining low pressure over Eastern Europe. The diversity of listed circulation types is very large; however, these types can be combined depending on the predominant blocking process (HNZ, HNFZ, HFA), cut-off-low (TM, HB, HM), slowly developing Rossby wave ridge (NWZ, NWA), or trough (WS, BM, TRM).

During the warm season's CPWEs, all mentioned circulation types are related to southern-type cyclone development over the analysed region. In almost all warm season cases, the CPWE location appears to agree with the structure of these cyclones: the heaviest precipitation is almost always located on the cyclone's forward (northern) side.

The composite analysis of all southern-type cyclone-related extremes revealed the high-pressure gradient area over the Baltic States, with pressure minima over eastern Latvia and Estonia and northwestern Russia (Figure 8c). At the same time, the temperature anomaly composition confirms typical large-scale temperature distribution in such cases: much colder than normal temperatures over the eastern part of Central Europe and higher than normal over the northern part of Eastern Europe (Figure 8d).

During the most intense warm season's CPWEs, the prevailing circulation pattern in the study area, according to the Hess–Brezowsky classification, was northwesterly, northerly, or a high/low-pressure area over Central Europe. The highest average P value, reaching 35.5 mm, was recorded under northwesterly and northerly circulation. Meanwhile, the highest average w_{max} value (22.2 m/s) was observed during the dominance of a high/low-pressure area over Central Europe.

During the cold season, the formation of CPWEs was dominated by westerly (zonal) flow types. This circulation pattern also resulted in the highest average w_{max} value (22.6 m/s). Nevertheless, the highest average P value in the cold season, reaching 18.9 mm, was recorded in the study region under the dominance of a northwesterly and northerly circulation pattern similar to the warm season.

4. Discussion

From 1950 to 2022, the number of precipitation extremes increased in almost the entire study area. However, the observed changes were statistically significant only in a small part of it. The increase in the recurrence of precipitation extremes in recent decades has also been observed in various regions worldwide (e.g., the USA, China, and Central Europe) [52–55], as well as in the eastern part of the Baltic Sea region [26,28,31]. These changes are closely related to climate change. A study conducted in the Benelux countries found that, during the summer, the intensity of precipitation extremes increased by a factor of 1.2–9 compared with a climate that was 1.2 °C cooler [55]. Future projections suggest that the recurrence and intensity of precipitation extremes will continue to grow [27,55–57]. Similar trends are anticipated for the Baltic Sea region and Northern Europe [30,58].

While the number of wind extremes also increased across most of the study area during the research period, the changes are statistically significant in less than one-tenth of the study area. Similar trends, indicating minor changes in the recurrence of wind extremes, have been reported in other studies [59–61]. It has been found that the direction and magnitude of the changes are highly dependent on the selected study period and region [61]. Most of the extremes in northern Europe occurred during the last two decades of the 20th century, after which their frequency decreased [60,62]. Similar tendencies were observed in the eastern part of the Baltic Sea region during this study, with the highest frequency of extremes occurring in the 1990s. In the future, no significant changes in wind extremes are projected for either Europe or the Baltic Sea region [31,59,61].

The number of CPWEs also slightly increased in the eastern part of the Baltic Sea region. However, the observed changes were not significant (when $p < 0.05$). The low statistical power of the observed changes could be attributed to the high natural variability

of CPWEs. No significant trends in the recurrence of such compound extremes were identified in other regions either [15,63,64]. An analysis of CPWE changes across the study area during 1950–1969 and 2003–2022 showed that the significant increase in the frequency of these compound extremes in the highest number of grid cells occurred during summer. Rising air temperatures lead to larger water vapour amounts in the atmosphere, intensifying convection processes [65–67], which, in turn, result in localised precipitation and wind speed extremes.

The number of CPWEs in the eastern part of the Baltic Sea region exhibited a meridional distribution, with their recurrence decreasing inland from the coast. The highest number of CPWEs was recorded in western Lithuania, which was influenced by two factors: the distance from the Baltic Sea and the terrain. Reduced surface friction and thermal contrasts enhance wind speeds and variability near coasts. Topography accelerates winds, intensifies turbulence, and enhances precipitation through orographic lifting, increasing precipitation amounts on windward slopes. Therefore, the likelihood of observing both extreme events simultaneously is higher in coastal areas and nearby highlands. Similar trends in the spatial distribution of CPWEs were identified in Central Europe [23]. Also, by calculating the Pearson correlation coefficient (r), a positive statistically significant relationship (when $p < 0.05$) was found between the number of CPWEs and altitude above sea level. Higher r values were observed during the cold season. More CPWEs were observed in areas dominated by precipitation extremes, indicating that precipitation, rather than wind, is the limiting factor for the spatial distribution of these compound extremes [12].

Analysis of the circulation conditions during CPWEs revealed that the factors influencing their formation differ between the cold (October–March) and warm (April–September) seasons. During the cold season, these compound extremes typically form under intense zonal flow from the west. This pattern has also been observed in other regions of Europe [7]. A study by Owen et al. (2021) [11] found that in Europe, during 70% of CPWEs, the cyclone centre was located within a radius of no less than 1100 kilometres from the CPWE formation site. In contrast, during the warm season in the eastern part of the Baltic Sea region, CPWEs predominantly formed when southern-type cyclones reached the region. Intense convection processes also drove local CPWE formation during this period. Such cyclones were more frequent, and convection processes were generally more intense in the eastern and southeastern parts of the study area. As a result of these differing factors, CPWEs were more frequently recorded in the western and northern parts of the study area during winter and autumn. In summer, they were more common in the eastern and southeastern parts.

The most intense CPWEs in the study area were recorded in the second part of summer. Such a tendency is uncommon in Western and Central Europe, where the strongest compound extremes typically occur during winter [24,41]. This pattern in the eastern part of the Baltic Sea region is closely linked to the activity of southern-type cyclones. These cyclones, originating from regions such as the southern Alps, the Balkans, the Mediterranean, the Black Sea, or even the Carpathians, and moving northward during the warm season, carry more moisture than their Atlantic counterparts. Their rapid development under the leading edge of an upper-level trough or low creates large surface-pressure gradients. Such cyclones were responsible for all four of the most intense CPWEs recorded during the investigation period. In recent decades, an increase in the intensity of these cyclones reaching Northern Europe and the Baltic States has also been found [68].

In the future, CPWEs are expected to increase. The most significant growth is projected in mid- and high-latitude regions [21,69], along coastal areas in North America, as well as in South and East Asia [20]. Nevertheless, the global increase in CPWEs is expected to be greater over the ocean than over land, where the projected increase in the recurrence of these compound extremes is not statistically significant [69]. A slight increase in CPWEs

was also observed in this study. However, it is noted that during the period 1950–2022, this increase was more pronounced in the southern part of the study area.

The future increase in CPWEs is primarily linked to climate change, rising evaporation, more intense precipitation, and changes in tropical and extratropical cyclone trajectories [1,21]. For instance, it is projected that mid-latitude cyclones in Great Britain and Ireland will cause CPWEs 3.6 times more frequently, primarily driven by increasing precipitation intensity [70]. However, these compound extremes are characterised by high spatial and natural variability, with significant influences from other factors such as the terrain, land cover and its changes, and the ocean–atmosphere interaction [69]. These factors could explain why the changes observed during the study were not significant.

The number of deep, mid-latitude cyclones in the Baltic Sea region is expected to increase slightly. However, the reliability of these projections is low, as the magnitude of changes and shifts in cyclone trajectories will depend on the evolving temperature gradients between low and high latitudes [58]. Another critical factor influencing the recurrence and intensity of CPWEs in the eastern Baltic Sea region, as well as other regions, will be changes in the characteristics of storms generated by convective processes. Convective weather events in Europe are projected to become more frequent [71,72], and the recurrence of conditions favourable for convection is expected to increase by 5–20% for every 1 °C rise in global temperature, with the most significant growth anticipated in higher latitudes of the Northern Hemisphere [73]. These changes could lead to an increase in the number and intensity of summer CPWEs.

Several aspects should be considered when conducting further research on CPWEs in the eastern part of the Baltic Sea region. First, the reliability of ERA5 reanalysis data for precipitation and maximum wind speed varies across the study period and different seasons. As the number of data sources has increased during the 1950–2022 period, with more data being assimilated into reanalysis datasets, their accuracy has improved significantly in recent decades compared with the first part of the study period [61,74]. Additionally, it has been observed that ERA5 data in mid-latitudes for the two variables used in this study are more accurate during the winter months compared with summer. This is because ERA5 better simulates precipitation and wind extremes associated with mid-latitude cyclones than those caused by mesoscale convective systems, which are more typical in summer [36,57,75].

Another aspect to consider when interpreting the results of this study is the spatial resolution of the data grid, which is $0.25 \times 0.25^{\circ}$. Such a spatial resolution is insufficient for accurately capturing localised CPWEs that occur during convective processes in summer [75,76]. Reanalysis data also provide grid cell averages, which may overlook the most extreme values occurring within a grid cell [35,77]. To assess the accuracy of ERA5 data, the number of CPWEs obtained using this reanalysis was compared with the number of compound extremes derived from data from several Lithuanian meteorological stations. It was found that the total number of CPWEs obtained using different data sources differed by no more than 10%. It is also important to note that ground-based observations create a different challenge. The obtained results effectively represent only CPWEs occurring at a specific location, and they are strongly influenced by local factors, thus failing to adequately reflect patterns across larger areas [61].

5. Conclusions

This study evaluated the recurrence, spatial distribution, intensity, and atmospheric conditions driving CPWEs in the eastern part of the Baltic Sea region. Changes in the recurrence of precipitation and wind speed extremes were also assessed. Between 1950 and 2022, their frequency increased, but statistically significant changes were observed in

only 13.8% and 8.1% of the area, respectively. Comparing the beginning (1950–1969) and end (2003–2022) of the study period, CPWEs increased across most of the study area in all seasons. However, the changes were generally small, with statistically significant increases primarily observed in summer.

The main factors determining the spatial distribution of CPWEs are distance from the Baltic Sea and terrain. Due to these factors, the highest frequency of CPWEs (10–11 extremes per decade) was recorded in the western part of the study area. CPWEs also exhibit seasonal spatial patterns: in autumn and winter, they are most frequent in the western and northern parts, while in summer, they are concentrated in the east.

Such distribution results from differing synoptic conditions influencing CPWE formation. In the cold season (October–March), CPWEs are mainly associated with strong zonal flows from the west and rapidly developing frontal waves on the southern periphery of deep Atlantic cyclones. In the warm season (April–September), they are linked to southern-type cyclones entering the study region. Notably, these cyclones were responsible for the most intense CPWEs, typically occurring in late summer and early September.

In this study, using ERA5 reanalysis data, certain CWPEs that formed due to local processes (e.g., thermal convection) may not have been accounted for as a consequence of insufficient spatial resolution of the data ($0.25 \times 0.25^{\circ}$). To avoid this issue in future research, it would be advisable to use higher-spatial-resolution data and ground-based observations.

Author Contributions: Conceptualization, L.K., E.R., and G.S.; methodology, L.K, E.R., and G.S.; software, L.K.; formal analysis, L.K., E.R., and G.S.; investigation, L.K., E.R., and G.S.; resources, L.K., and G.S.; data curation, L.K.; writing—original draft preparation, L.K., E.R., and G.S.; visualization, L.K. All authors have read and agreed to the published version of the manuscript.

Funding: This research received no external funding.

Institutional Review Board Statement: Not applicable.

Informed Consent Statement: Not applicable.

Data Availability Statement: ERA5 data are available at the Copernicus Climate Data Store (https://doi.org/10.24381/cds.adbb2d47 (accessed on 25 February 2024)). Synoptic schemes and surface analysis charts from the German Weather Service and GFS analysis charts can be accessed at https://www.wetter3.de (accessed on 25 February 2024), UK MetOffice (UKMO) charts at https://www.wetterzentrale.de/ (accessed on 25 February 2024), and The Royal Netherlands Meteorological Institute (KNMI) charts at https://www.knmi.nl/ (accessed on 25 February 2024). The datasets generated during this study are available from the corresponding author upon request.

Conflicts of Interest: The authors declare no conflicts of interest.

References

1. Seneviratne, S.I.; Zhang, X.; Adnan, M.; Badi, W.; Dereczynski, C.; Di Luca, A.; Ghosh, S.; Iskandar, I.; Kossin, J.; Lewis, S.; et al. Weather and Climate Extreme Events in a Changing Climate. In *Climate Change 2021: The Physical Science Basis. Contribution of Working Group I to the Sixth Assessment Report of the Intergovernmental Panel on Climate Change*; Cambridge University Press: Cambridge, UK, 2021. [CrossRef]
2. Clarke, B.; Otto, F.; Stuart-Smith, R.; Harrington, L. Extreme weather impacts of climate change: An attribution perspective. *Environ. Res. Clim.* **2022**, *1*, 012001. [CrossRef]
3. European Environment Agency Economic Losses from Weather- and Climate-Related Extremes in Europe. 2024. Available online: https://www.eea.europa.eu/en/analysis/indicators/economic-losses-from-climate-related (accessed on 14 January 2025).
4. Seneviratne, S.I.; Nicholls, N.; Easterling, D.; Goodess, C.M.; Kanae, S.; Kossin, J.; Luo, Y.; Marengo, J.; Mc Innes, K.; Rahimi, M.; et al. Changes in climate extremes and their impacts on the natural physical environment. In *Managing the Risks of Extreme Events and Disasters to Advance Climate Change Adaptation: Special Report of the Intergovernmental Panel on Climate Change*; Cambridge University Press: Cambridge, UK, 2012; Volume 3, pp. 109–230. [CrossRef]

5. Zscheischler, J.; Westra, S.; Van Den Hurk, B.J.J.M.; Seneviratne, S.I.; Ward, P.J.; Pitman, A.; Aghakouchak, A.; Bresch, D.N.; Leonard, M.; Wahl, T.; et al. Future climate risk from compound events. *Nat. Clim. Change* **2018**, *8*, 469–477. [CrossRef]
6. Zscheischler, J.; Raymond, C.; Horton, R.M.; Ramos, A.M. A typology of compound weather. *Nat. Rev. Earth Environ.* **2020**, *1*, 333–347. [CrossRef]
7. Martius, O.; Pfahl, S.; Chevalier, C. A global quantification of compound precipitation and wind extremes. *Geophys. Res. Lett.* **2016**, *43*, 7709–7717. [CrossRef]
8. Li, D.; Chen, Y.; Messmer, M.; Zhu, Y.; Feng, J.; Yin, B.; Bevacqua, E. Compound Wind and Precipitation Extremes Across the Indo-Pacific: Climatology, Variability, and Drivers. *Geophys. Res. Lett.* **2022**, *49*, e2022GL098594. [CrossRef]
9. Xoplaki, E.; Ellsäßer, F.; Grieger, J.; Nissen, K.M.; Pinto, J.G.; Chen, T.-C.; Feldmann, H.; Friederichs, P.; Gliksman, D.; Haustein, K.; et al. Compound events in Germany in 2018: Drivers and case studies. *EGUsphere* **2023**, 1–43. [CrossRef]
10. Plavcová, E.; Urban, A. Intensified impacts on mortality due to compound winter extremes in the Czech Republic. *Sci. Total Environ.* **2020**, *746*, 141033. [CrossRef]
11. Owen, L.E.; Catto, J.L.; Stephenson, D.B.; Dunstone, N.J. Compound precipitation and wind extremes over Europe and their relationship to extratropical cyclones. *Weather Clim. Extrem.* **2021**, *33*, 100342. [CrossRef]
12. Messmer, M.; Simmonds, I. Global analysis of cyclone-induced compound precipitation and wind extreme events. *Weather Clim. Extrem.* **2021**, *32*, 100324. [CrossRef]
13. Ridder, N.N.; Ukkola, A.M.; Pitman, A.J.; Perkins-Kirkpatrick, S.E. Increased occurrence of high impact compound events under climate change. *Npj Clim. Atmos. Sci.* **2022**, *5*, 3. [CrossRef]
14. Alvarez, I.; Pereira, H.; Picado, A.; Sousa, M.C.; Lorenzo, M.N.; Dias, J.M. Projection of Compound Wind and Precipitation Extreme Events in the Iberian Peninsula Based on CMIP6. *Earth Syst. Environ.* **2024**, *8*, 801–814. [CrossRef]
15. Johansson, E. Compound Extreme Wind and Precipitation Events in Europe. Bachelor's Thesis, Uppsala University, Uppsala, Sweden, 2021. Available online: https://urn.kb.se/resolve?urn=urn:nbn:se:uu:diva-446009 (accessed on 25 February 2024).
16. Ridder, N.N.; Pitman, A.J.; Ukkola, A.M. High impact compound events in Australia. *Weather. Clim. Extrem.* **2022**, *36*, 100457. [CrossRef]
17. Tilloy, A.; Malamud, B.D.; Joly-Laugel, A. A methodology for the spatiotemporal identification of compound hazards: Wind and precipitation extremes in Great Britain (1979–2019). *Earth Syst. Dyn.* **2022**, *13*, 993–1020. [CrossRef]
18. Zscheischler, J.; Naveau, P.; Martius, O.; Engelke, S.; C. Raible, C. Evaluating the dependence structure of compound precipitation and wind speed extremes. *Earth Syst. Dyn.* **2021**, *12*, 1–16. [CrossRef]
19. Catto, J.L.; Dowdy, A. Understanding compound hazards from a weather system perspective. *Weather Clim. Extrem.* **2021**, *32*, 100313. [CrossRef]
20. Yaddanapudi, R.; Mishra, A.; Huang, W.; Chowdhary, H. Compound Wind and Precipitation Extremes in Global Coastal Regions Under Climate Change. *Geophys. Res. Lett.* **2022**, *49*, e2022GL098974. [CrossRef]
21. Li, D.; Zscheischler, J.; Chen, Y.; Yin, B.; Feng, J.; Freund, M.; Qi, J.; Zhu, Y.; Bevacqua, E. Intensification and Poleward Shift of Compound Wind and Precipitation Extremes in a Warmer Climate. *Geophys. Res. Lett.* **2024**, *51*, e2024GL110135. [CrossRef]
22. Messori, G.; Caballero, R. On double Rossby wave breaking in the North Atlantic. *J. Geophys. Res. Atmos.* **2015**, *120*, 11,129–11,150. [CrossRef]
23. Müller, M.; Kašpar, M.; Ближňák, V. Central European wind and precipitation compound events are not just due to winter storms. *Nat. Hazards Earth Syst. Sci.* **2022**, 1–19. [CrossRef]
24. De Luca, P.; Messori, G.; Pons FM, E.; Faranda, D. Dynamical systems theory sheds new light on compound climate extremes in Europe and Eastern North America. *Q. J. R. Meteorol. Soc.* **2020**, *146*, 1636–1650. [CrossRef]
25. Leeding, R.; Riboldi, J.; Messori, G. On Pan-Atlantic cold, wet and windy compound extremes. *Weather Clim. Extrem.* **2023**, *39*, 100524. [CrossRef]
26. Avotniece, Z.; Klavins, M.; Rodinovs, V. Changes of extreme climate events in Latvia. *Environ. Clim. Technol.* **2012**, *9*, 4–11. [CrossRef]
27. Cardell, M.F.; Amengual, A.; Romero, R.; Ramis, C. Future extremes of temperature and precipitation in Europe derived from a combination of dynamical and statistical approaches. *Int. J. Climatol.* **2020**, *40*, 4800–4827. [CrossRef]
28. Dyrrdal, A.V.; Olsson, J.; Médus, E.; Arnbjerg-Nielsen, K.; Post, P.; Aņiskeviča, S.; Thorndahl, S.; Førland, E.; Wern, L.; Mačiulytė, V.; et al. Observed changes in heavy daily precipitation over the Nordic-Baltic region. *J. Hydrol. Reg. Stud.* **2021**, *38*, 100965. [CrossRef]
29. Lizuma, L.; Briede, A.; Klavins, M. Long-term changes of precipitation in Latvia. *Hydrol. Res.* **2010**, *41*, 241–252. [CrossRef]
30. Nikulin, G.; Kjellström, E.; Hansson, U.; Strandberg, G.; Ullerstig, A. Evaluation and future projections of temperature, precipitation and wind extremes over Europe in an ensemble of regional climate simulations. *Tellus Ser. A Dyn. Meteorol. Oceanogr.* **2011**, *63*, 41–55. [CrossRef]
31. Ramanauskas, E.; Bukantis, A.; Dringelis, L.; Kaveckis, G.; Jonkutė-Vilkė, G. Climate Change and Cities of Lithuania: Threats, Problems and Prerequisites for Solution. *Urban Sci.* **2024**, *8*, 186. [CrossRef]

32. Kottek, M.; Grieser, J.; Beck, C.; Rudolf, B.; Rubel, F. World map of the Köppen-Geiger climate classification updated. *Meteorol. Z.* **2006**, *15*, 259–263. [CrossRef]
33. Peel, M.C.; Finlayson, B.L.; McMahon, T.A. Updated world map of the Köppen-Geiger climate classification. *Hydrol. Earth Syst. Sci.* **2007**, *11*, 1633–1644. [CrossRef]
34. Hersbach, H.; Bell, B.; Berrisford, P.; Hirahara, S.; Horányi, A.; Muñoz-Sabater, J.; Nicolas, J.; Peubey, C.; Radu, R.; Schepers, D.; et al. The ERA5 global reanalysis. *Q. J. R. Meteorol. Soc.* **2020**, *146*, 1999–2049. [CrossRef]
35. Laurila, T.K. Winds and Windstorms in Northern Europe and Finland. Ph.D. Thesis, University of Helsinki, Helsinki, Finland, 2022. [CrossRef]
36. Lavers, D.A.; Simmons, A.; Vamborg, F.; Rodwell, M.J. An evaluation of ERA5 precipitation for climate monitoring. *Q. J. R. Meteorol. Soc.* **2022**, *148*, 3152–3165. [CrossRef]
37. Minola, L.; Zhang, F.; Azorin-Molina, C.; Pirooz, A.A.S.; Flay, R.G.J.; Hersbach, H.; Chen, D. Near-surface mean and gust wind speeds in ERA5 across Sweden: Towards an improved gust parametrization. *Clim. Dyn.* **2020**, *55*, 887–907. [CrossRef]
38. Hassler, B.; Lauer, A. Comparison of reanalysis and observational precipitation datasets including ERA5 and WFDE5. *Atmosphere* **2021**, *12*, 1462. [CrossRef]
39. Wu, L.; Su, H.; Zeng, X.; Posselt, D.J.; Wong, S.; Chen, S.; Stoffelen, A. Uncertainty of Atmospheric Winds in Three Widely Used Global Reanalysis Datasets. *J. Appl. Meteorol. Climatol.* **2024**, *63*, 165–180. [CrossRef]
40. Zhang, X.; Alexander, L.; Hegerl, G.C.; Jones, P.; Tank, A.K.; Peterson, T.C.; Trewin, B.; Zwiers, F.W. Indices for monitoring changes in extremes based on daily temperature and precipitation data. *Wiley Interdiscip. Rev. Clim. Change* **2011**, *2*, 851–870. [CrossRef]
41. Ridder, N.N.; Pitman, A.J.; Westra, S.; Ukkola, A.; Do, H.X.; Bador, M.; Hirsch, A.L.; Evans, J.P.; Di Luca, A.; Zscheischler, J. Global hotspots for the occurrence of compound events. *Nat. Commun.* **2020**, *11*, 15. [CrossRef]
42. Bevacqua, E.; Vousdoukas, M.I.; Zappa, G.; Hodges, K.; Shepherd, T.G.; Maraun, D.; Mentaschi, L.; Feyen, L. More meteorological events that drive compound coastal flooding are projected under climate change. *Commun. Earth Environ.* **2020**, *1*, 1–11. [CrossRef]
43. Lücke, L.J.; Dent, C.J.; Hegerl, G.C.; Wilson, A.L.; Schurer, A.P. Severe compound events of low wind and cold temperature for the British power system. *Meteorol. Appl.* **2024**, *31*, 1–22. [CrossRef]
44. Ranjan, R.; Karmakar, S. Compound hazard mapping for tropical cyclone-induced concurrent wind and rainfall extremes over India. *Npj Nat. Hazards* **2024**, *1*, 1–12. [CrossRef]
45. Sanuy, M.; Rigo, T.; Jiménez, J.A.; Llasat, M.C. Classifying compound coastal storm and heavy rainfall events in the north-western Spanish Mediterranean. *Hydrol. Earth Syst. Sci.* **2021**, *25*, 3759–3781. [CrossRef]
46. James, P.M. An Objective Classification Method for Hess and Brezowsky Grosswetterlagen over Europe. *Theor. Appl. Climatol.* **2007**, *88*, 17–42. [CrossRef]
47. Gerstengarbe, F.; Werner, P. Katalog der Großwetterlagen Europas (1881–2004). In *Nach Paul Hess und Helmuth Brezowsky—6. Verbesserte und Ergänzte Auflage*; PIK Report 100; Potsdam Institute For Climate Impact Research (PIK): Potsdam, Germany, 2005.
48. Kučerová, M.; Beck, C.; Philipp, A.; Huth, R. Trends in frequency and persistence of atmospheric circulation types over Europe derived from a multitude of classifications. *Int. J. Clim.* **2017**, *37*, 2502–2521. [CrossRef]
49. Rimkus, E.; Kažys, J.; Butkutė, S.; Gečaitė, I. Snow cover variability in Lithuania over the last 50 years and its relationship with large-scale atmospheric circulation. *Boreal Environ. Res.* **2014**, *19*, 337–357.
50. Quénol, H.; Corgne, S.; Planchon, O. Assessing Precipitation and Large-Scale Weather Situations in Brittany: The Usefulness of the Hess-Brezowsky Classification. *Die Erde* **2009**, *140*, 195–217.
51. Werner, P.C. Katalog der Großwetterlagen Europas (1881–2009). In *Nach Paul Hess und Helmut Brezowsky*; Potsdam Institute for Climate Impact Research (PIK): Potsdam, Germany, 2010.
52. Hänsel, S.; Hoy, A.; Brendel, C.; Maugeri, M. Record summers in Europe: Variations in drought and heavy precipitation during 1901–2018. *Int. J. Climatol.* **2022**, *42*, 6235–6257. [CrossRef]
53. Li, X.; Zhang, K.; Gu, P.; Feng, H.; Yin, Y.; Chen, W.; Cheng, B. Changes in precipitation extremes in the Yangtze River Basin during 1960–2019 and the association with global warming, ENSO, and local effects. *Sci. Total Environ.* **2021**, *760*, 144244. [CrossRef]
54. Prein, A.F.; Rasmussen, R.M.; Ikeda, K.; Liu, C.; Clark, M.P.; Holland, G.J. The future intensification of hourly precipitation extremes. *Nat. Clim. Change* **2017**, *7*, 48–52. [CrossRef]
55. Tradowsky, J.S.; Philip, S.Y.; Kreienkamp, F.; Kew, S.F.; Lorenz, P.; Arrighi, J.; Bettmann, T.; Caluwaerts, S.; Chan, S.C.; De Cruz, L.; et al. Attribution of the heavy rainfall events leading to severe flooding in Western Europe during July 2021. *Clim. Change* **2023**, *176*, 90. [CrossRef]
56. Rajczak, J.; Schär, C. Projections of Future Precipitation Extremes Over Europe: A Multimodel Assessment of Climate Simulations. *J. Geophys. Res. Atmos.* **2017**, *122*, 10,773–10,800. [CrossRef]
57. O'Gorman, P.A. Precipitation Extremes Under Climate Change. *Curr. Clim. Change Rep.* **2015**, *1*, 49–59. [CrossRef]
58. Rutgersson, A.; Kjellström, E.; Haapala, J.; Stendel, M.; Danilovich, I.; Drews, M.; Jylhä, K.; Kujala, P.; Larsén, X.G.; Halsnæs, K.; et al. Natural hazards and extreme events in the Baltic Sea region. *Earth Syst. Dyn.* **2022**, *13*, 251–301. [CrossRef]

59. Kumar, D.; Mishra, V.; Ganguly, A.R. Evaluating wind extremes in CMIP5 climate models. *Clim. Dyn.* **2015**, *45*, 441–453. [CrossRef]
60. Laurila, T.K.; Sinclair, V.A.; Gregow, H. Climatology, variability, and trends in near-surface wind speeds over the North Atlantic and Europe during 1979–2018 based on ERA5. *Int. J. Climatol.* **2021**, *41*, 2253–2278. [CrossRef]
61. Meier, H.E.M.; Kniebusch, M.; Dieterich, C.; Gröger, M.; Zorita, E.; Elmgren, R.; Myrberg, K.; Ahola, M.P.; Bartosova, A.; Bonsdorff, E.; et al. Climate change in the Baltic Sea region: A summary. *Earth Syst. Dyn.* **2022**, *13*, 457–593. [CrossRef]
62. Pryor, S.C.; Barthelmie, R.J.; Clausen, N.E.; Drews, M.; MacKellar, N.; Kjellström, E. Analyses of possible changes in intense and extreme wind speeds over northern Europe under climate change scenarios. *Clim. Dyn.* **2012**, *38*, 189–208. [CrossRef]
63. He, W.; Chen, X.; Zhang, Y.; Duan, W.; Deng, H. Spatio-temporal variations of compound precipitation and wind-speed extreme events in Fujian and Jiangxi Provinces, Southeast China. *Meteorol. Atmos. Phys.* **2025**, *137*, 7. [CrossRef]
64. Hénin, R.; Ramos, A.M.; Pinto, J.G.; Liberato, M.L.R. A ranking of concurrent precipitation and wind events for the Iberian Peninsula. *Int. J. Climatol.* **2021**, *41*, 1421–1437. [CrossRef]
65. Kendon, E.; Roberts, N.; Fowler, H.; Roberts, M.; Chan, S.; Senior, C. Heavier summer downpours with climate change revealed by weather forecast resolution model. *Nat. Clim. Change* **2014**, *4*, 570–576. [CrossRef]
66. Taszarek, M.; Allen, J.T.; Brooks, H.E.; Pilguj, N.; Czernecki, B. Differing Trends in United States and European Severe Thunderstorm Environments in a Warming Climate. *Bull. Amer. Meteor. Soc.* **2021**, *102*, E296–E322. [CrossRef]
67. Ye, H.; Fetzer, E.J.; Wong, S.; Lambrigtsen, B.H. Rapid decadal convective precipitation increase over Eurasia during the last three decades of the 20th century. *Sci. Adv.* **2017**, *3*, e1600944. [CrossRef]
68. Mändla, K.; Jaagus, J.; Sepp, M. Climatology of cyclones with southern origin in northern Europe during 1948–2010. *Theor. Appl. Climatol.* **2015**, *120*, 75–86. [CrossRef]
69. Zhu, X.; Tang, J.; Yang, Y. Assessment and Projection of Compound Wind and Precipitation Extremes in EC-Earth3 of CMIP6 Simulations. *Asia-Pac. J. Atmos. Sci.* **2024**, *60*, 81–93. [CrossRef]
70. Manning, C.; Kendon, E.J.; Fowler, H.J.; Catto, J.L.; Chan, S.C.; Sansom, P.G. Compound wind and rainfall extremes: Drivers and future changes over the UK and Ireland. *Weather. Clim. Extrem.* **2024**, *44*, 100673. [CrossRef]
71. Rädler, A.T.; Groenemeijer, P.H.; Faust, E.; Sausen, R.; Púčik, T. Frequency of severe thunderstorms across Europe expected to increase in the 21st century due to rising instability. *Npj Clim. Atmos. Sci.* **2019**, *2*, 3–7. [CrossRef]
72. Tippett, M.K.; Allen, J.T.; Gensini, V.A.; Brooks, H.E. Climate and Hazardous Convective Weather. *Curr. Clim. Change Rep.* **2015**, *1*, 60–73. [CrossRef]
73. Lepore, C.; Abernathey, R.; Henderson, N.; Allen, J.T.; Tippett, M.K. Future Global Convective Environments in CMIP6 Models. *Earth's Future* **2021**, *9*, 1–21. [CrossRef]
74. Soci, C.; Hersbach, H.; Simmons, A.; Poli, P.; Bell, B.; Berrisford, P.; Horányi, A.; Muñoz-Sabater, J.; Nicolas, J.; Radu, R.; et al. The ERA5 global reanalysis from 1940 to 2022. *Q. J. R. Meteorol. Soc.* **2024**, *150*, 4014–4048. [CrossRef]
75. Chen, T.C.; Collet, F.; Di Luca, A. Evaluation of ERA5 precipitation and 10-m wind speed associated with extratropical cyclones using station data over North America. *Int. J. Climatol.* **2024**, *44*, 729–747. [CrossRef]
76. Gaska, J. Climate change and windstorm losses in Poland in the twenty-first century. *Environ. Hazards* **2023**, *22*, 99–115. [CrossRef]
77. Hersbach, H.; Bell, B.; Berrisford, P.; Biavati, G.; Horányi, A.; Muñoz Sabater, J.; Nicolas, J.; Peubey, C.; Radu, R.; Rozum, I.; et al. *ERA5 Hourly Data on Single Levels from 1940 to Present*; Copernicus Climate Change Service (C3S); Climate Data Store (CDS): Brussels, Belgium, 2023. [CrossRef]

Disclaimer/Publisher's Note: The statements, opinions and data contained in all publications are solely those of the individual author(s) and contributor(s) and not of MDPI and/or the editor(s). MDPI and/or the editor(s) disclaim responsibility for any injury to people or property resulting from any ideas, methods, instructions or products referred to in the content.

IV PUBLIKACIJA

Future projections of false spring events in the eastern part of the Baltic Sea region

Klimavičius, L., & Rimkus, E. (2025). Future projections of false spring events in the eastern part of the Baltic Sea region. *Baltica*, 38(2), 160–173. https://doi.org/10.5200/baltica.2025.2.4

since 1961

Baltica

BALTICA Volume 38 Number 2 December 2025: 160–173
https://doi.org/10.5200/baltica.2025.2.4

Future projections of false spring events in the eastern part of the Baltic Sea region

Laurynas Klimavičius*, Egidijus Rimkus

Klimavičius, L., Rimkus, E. 2025. Future projections of false spring events in the eastern part of the Baltic Sea region. *Baltica 38 (2)*, 160–173. Vilnius. ISSN 1648-858X.
Manuscript submitted 12 May 2025 / Accepted 10 November 2025 / Available online 27 November 2025

© Baltica 2025

Abstract. In recent decades, rising winter and spring temperatures have led to an earlier onset of the growing season. However, this shift is often accompanied by false spring (FS) events – situations when the last spring frost (LSF) occurs after the start of the growing season (SGS). This study evaluates future changes in the recurrence and intensity of FS events in the eastern part of the Baltic Sea region. The SGS and LSF dates for each grid cell within the study area for each year were determined to identify FS events. An FS event was recorded when LSF occurred later than the SGS date. The intensity of FS events was assessed using growing degree days (GDD) accumulated until the event. Future projections were generated using five CMIP6 models (CanESM5, ACCESS-CM2, GFDL-CM4, MPI-ESM1-2-LR, and NorESM2-MM), two SSP scenarios (SSP2-4.5 and SSP5-8.5), and data obtained from the NASA NEX-GDDP-CMIP6 dataset. The period from 1995 to 2014 was used as the baseline, and projections were made for the years 2041–2060 and 2081–2100. Analysis showed that SGS and LSF dates are projected to shift significantly earlier under all models and scenarios. However, FS recurrence projections are less consistent. Most models indicate a decline in FS events by mid-century, while forecasts for 2081–2100 are mixed – two models suggest an increase, while the other three suggest a decrease. The mean GDD sum accumulated until the FS event increases only when the frequency of FS events is projected to rise, suggesting that future FS events may be more intense.

Keywords: *spring frost; growing season; compound climate events; Baltic States*

Laurynas Klimavičius (laurynas.klimavicius@chgf.vu.lt), https://orcid.org/0009-0002-0243-1421; Egidijus Rimkus*
Institute of Geosciences, Vilnius University, Vilnius, Lithuania
**Corresponding author*

INTRODUCTION

In recent decades, under warming climate conditions, due to increased air temperatures in winter and spring months, the growing season in various regions of the Northern Hemisphere has been starting increasingly earlier (Jeong *et al*. 2011; Allstadt *et al*. 2015; Xia *et al*. 2015; Zhu *et al*. 2019; Wang *et al*. 2021). This results in a longer growing season and may offer potential benefits for the agricultural sector (Peltonen-Sainio *et al*. 2009; Peterson, Abatzoglou 2014; Grigorieva *et al*. 2023). However, it was already observed in the early 1980s that despite the earlier start of the growing season due to climate change, the risk of spring frosts does not decrease and may even increase (Cannell, Smith 1986), creating favourable conditions for a compound climate event known as a 'false spring' (Zscheischler *et al*. 2020). A false spring occurs when unusually high temperatures in early spring trigger the onset of vegetation growth, followed by a cold period during which the daily minimum air temperature drops below 0 °C (Ault *et al.* 2013; Chamberlain *et al*. 2019).

False spring events primarily affect fruit trees (Jarzyna 2021; Bateman 2022; Bosdijk *et al*. 2024). During the leaf emergence and blooming stages of fruit trees, frosts are especially dangerous (Rodrigo 2000; Crassweller 2024) and can result in the loss of a large part or even the entirety of the harvest, causing economic losses that may reach several billion euros (Faust, Herbold 2017; Ma *et al*. 2019; Bateman 2022). However, these compound climate events

cause harm not only to plants. The indirect negative impacts of false springs are also felt in other areas. They can threaten ecosystem services, making information about these events and their potential effects and damages important for various institutions, such as national parks (Monahan *et al*. 2016; Martinuzzi *et al*. 2019).

False spring events can also indirectly affect various ecosystems – for example, by disrupting bird migration cycles and reducing food availability, especially when accompanied by snowfall or ice formation (Bateman 2022). The development of leaves and flowers stimulates the flow of sap, nectar, and nutrients in plants. It provides shelter and food for various organisms. A false spring event disrupts this entire system, causing harm to various plant and animal species. For example, repeated false spring events over several consecutive years contributed to the extinction of Edith's checkerspot butterfly species in the Sierra Nevada in the late 20th century (Grossman 2014).

Various climatic, geographic, and biological factors determine the recurrence, intensity, and potential adverse effects of false spring events. The primary geographic factors are the distance from large water bodies (seas, oceans) and terrain. Also critical are the average spring air temperature and prevailing atmospheric circulation patterns and anomalies (Ma *et al*. 2019; Cook *et al*. 2020; Chamberlain *et al*. 2021; Hájková *et al*. 2023). Nevertheless, plant species are the most critical factor in determining the strength of a false spring (Ball *et al*. 2011; Chamberlain *et al*. 2019; Baumgarten *et al.* 2023). A plant's cold tolerance depends on its species – some are damaged when temperatures fall below –2.2 °C, while others can withstand temperatures below –8.5 °C (Chamberlain *et al*. 2021). Another critical factor dependent on species is a plant's ability to recover after experiencing a false spring event (Augspurger 2013; Baumgarten *et al*. 2023; Muffler *et al*. 2024). The unequal impact of these events on different species and their differing abilities to recover means some plants may gain a competitive advantage (Hufkens *et al*. 2012). This may lead to negative ecological consequences and contribute to shifts or reductions in species distribution ranges (European Climate Risk Assessment 2024).

Various indicators can be used to assess the intensity of false spring (FS) events and their potential impact on plants. One of the most applied measures is the sum of growing degree days (GDD), accumulated until the FS event (Chamberlain, Wolkovich 2023). The GDD assesses the amount of heat required for a plant to reach a particular developmental stage (Miller *et al.* 2001). The method is based on the principle that plant growth begins once temperatures exceed a certain base threshold, with higher temperatures leading to more rapid plant development (Miller *et al.* 2001; Chun, Changnon 2019). This approach is widely applied to model and predict various phenological stages of plants (McMaster, Wilhelm 1997; Clark, Thompson 2010; Wang *et al.* 2025) and to evaluate the effects of frost on species (Wypych *et al.* 2017; Chun, Changnon 2019; Qiu *et al.* 2024). The use of GDD is appropriate as air temperature is the primary factor directly determining plant development. Another advantage of this method is its practicality – GDD can be applied even in cases where field measurements are not feasible, as it only requires air temperature data (Bhatti *et al.* 2025).

Despite climate warming, the risk of false spring events persists in various regions – the number of frost days during the growing season has increased across 43% of the Northern Hemisphere (Liu *et al*. 2018). The persistence or even rise in the risk of false spring events has also been confirmed in regional studies (Allstadt *et al*. 2015; Jarzyna 2021; Bosdijk *et al*. 2024; Zahradníček *et al*. 2024). Therefore, in recent years, more attention has been paid to assessing changes in the recurrence and intensity of these compound climate events across different parts of the Northern Hemisphere (Ma *et al.* 2019; Martinuzzi *et al*. 2019; Zhu *et al*. 2019; Helali *et al.* 2022; Ford *et al*. 2025). Despite that, no studies have examined future changes in false spring event characteristics in the Baltic States. Only the recurrence and intensity of these compound climate events for the 1950–2022 period have been assessed (Klimavičius, Rimkus 2024). In Poland, more detailed analyses have examined the recurrence and intensity of these events as well as the atmospheric circulation conditions driving their occurrence (Graczyk, Szwed 2020; Koźmiński *et al*. 2023; Nidzgorska-Lencewicz *et al*. 2024; Piotrowski, Bartoszek 2025), but projections for the future have not been made there either.

The primary objective of this study is to evaluate the potential changes in the recurrence and intensity of false spring (FS) events by the middle and end of the 21st century in the eastern Baltic Sea region. In the first part of the study, the median dates of the start of the growing season (SGS) and the last spring frost (LSF), FS event recurrence, and the sums of accumulated growing degree days up to the FS event were evaluated for the baseline period of 1995–2014. The second part assesses projected changes in the SGS and LSF dates. The third part discusses projected changes in the recurrence of FS events by the mid and late 21st century compared to the baseline period. Finally, the last part is devoted to assessing the projected changes in the intensity of these compound climate events.

DATA AND METHODS

Study area

FS events were investigated in the eastern part of the Baltic Sea region (from 53.5° to 59.5° N latitude and from 20° to 28.5° E longitude) (Fig. 1).

The study area is located in the temperate climate zone and, according to the updated Köppen–Geiger climate classification, is classified as the *Dfb* climate type (Beck *et al*. 2018). The eastern part of the Baltic Sea region is situated in an excessive moisture zone – annual precipitation exceeds evaporation (Kilkus, Stonevičius 2011). Therefore, the main factor determining the start of the growing season is air temperature. In the study area, the average spring (March–May) temperature ranges from 3.5 °C in north-western Estonia to 7 °C in the southern part of the study area (Klimavičius, Rimkus 2024).

Data

FS events were first assessed using ERA5 reanalysis data of daily minimum (t_{min}) and average (t_{avg}) air temperatures for the period from 1995 to 2014, covering the months from January to June. The grid size of the data is 0.25° × 0.25°. Only grids with more than half of their area covered by land were analysed. The ERA5 reanalysis of air temperature data in mid-latitude areas with a well-developed meteorological station network and without steep elevation changes (e.g., mountains) shows a strong correlation with ground-based observations (McNicholl *et al*. 2022; Velikou *et al*. 2022; Xu *et al*. 2022; Liu *et al*. 2024). This is due to the assimilation of modelled and meteorological station data in creating reanalysis datasets (Hersbach *et al*. 2020).

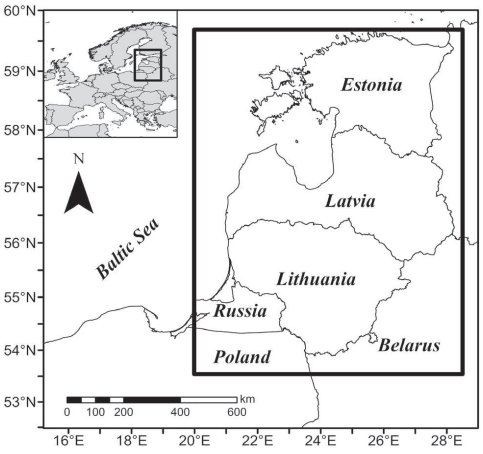

Fig. 1 The map of the study area

To assess future changes in FS event recurrence, t_{min} and t_{avg} data from various Coupled Model Intercomparison Project Phase 6 (CMIP6) general circulation models (GCMs) were used. The data were obtained from the NASA Earth Exchange (NEX) Global Daily Downscaled Projections database (NEX-GDDP-CMIP6), which uses the same 0.25° × 0.25° grid size as ERA5. This database provides historical data for the period 1950–2014 and climatic projections for the years 2015–2100.

Although the NEX-GDDP-CMIP6 database contains data from 35 different CMIP6 models, only five were selected for this study: CanESM5, ACCESS-CM2, GFDL-CM4, MPI-ESM1-2-LR, and NorESM2-MM (Table 1). These models were chosen based on equilibrium climate sensitivity (ECS), which indicates that the global surface temperature increases when atmospheric CO_2 concentration is doubled relative to pre-industrial levels (Hausfather 2018). The ECS values of the models used in this study range from 2.5 °C to 5.6 °C (Table 1), thus representing different parts of the sensitivity spectrum (Hausfather 2019).

The NEX-GDDP-CMIP6 database includes data for four Shared Socioeconomic Pathways (SSP) scenarios. However, only two scenarios were used in this study – SSP2-4.5 and SSP5-8.5 – representing medium (radiative forcing increase of 4.5 W/m² by 2100) and high (radiative forcing increase of 8.5 W/m²) future changes, respectively (Chen *et al*. 2021).

The NEX-GDDP-CMIP6 database was selected for several reasons. First, bias correction was applied during its development to better reflect the conditions at specific locations and align the modelled data more closely with historical climatological data (Thrasher *et al*. 2022). Another issue with using raw CMIP6 GCM data is the low and uneven spatial resolution (typically 80–250 km), which is unsuitable for regional-scale studies (ECMWF 2021). This problem is addressed in the NEX-GDDP-CMIP6 dataset by downscaling all models to a uniform 0.25° × 0.25° (~ 25 km) resolution (Thrasher *et al*. 2022). Lastly, this database has been

Table 1 General circulation models (GCMs) used in the study and their equilibrium climate sensitivity (°C)

Institution and Country of Origin	Model ID	Equilibrium climate sensitivity (°C)
Canadian Centre for Climate Modelling and Analysis, Canada	CanESM5	5.6
CSIRO-BOM, Australia	ACCESS-CM2	4.7
Geophysical Fluid Dynamics Laboratory, USA	GFDL-CM4	3.9
Max Planck Institute for Meteorology, Germany	MPI-ESM1-2-LR	3.0
Norwegian Climate Centre, Norway	NorESM2-MM	2.5

widely used in studies of extreme hydrometeorological events in various regions (Rao *et al*. 2024; Sun *et al*. 2024; Talchabhadel *et al*. 2025), including analyses of spring frosts (Ford *et al.* 2025).

The period from 1995 to 2014 was selected as the baseline period in this study, as it is also used for the same purpose in the IPCC AR6 report (Chen *et al*. 2021). Projections were made for two future periods – mid-century (2041–2060) and end-century (2081–2100).

Definition of the start of the growing season and the last spring frost

The SGS and LSF dates were determined annually for each grid cell in the study area to identify FS events and assess future changes. Multiple definitions of vegetation season can be found, including the "growing", "phenological", "productive", and "meteorological" seasons (Körner *et al*. 2023). This study adopted the "meteorological season" definition. It identifies the window of opportunity during which meteorological conditions are favourable for growth, and the SGS is determined based on a threshold average daily air temperature and, in some cases, soil moisture values (Körner *et al*. 2023). According to the method proposed by SMHI (SMHI 2025), SGS is defined as the first day of six consecutive days with $t_{avg} > 5$ °C. The SGS calculations begin on the day of the year when the 10-day running average of air temperature reaches a minimum value. A 5 °C threshold has also been used in studies in Northern and Central Europe (Carter 1998; Vitasse, Rebetez 2018; Miś, Tomczyk 2025), as it was found that in Northern European countries, this temperature threshold marks the start of noticeable growth in many plant species (trees, natural vegetation, crops) (Carter 1998).

The LSF is defined as the last day from January to June when the minimum temperature (t_{min}) drops below 0 °C. At this temperature, most plant physiological processes are disrupted (Ceglar *et al*. 2019), and damage may occur to fruit trees and agricultural crops (FAO 2024). The changes in SGS and LSF dates were assessed for each grid cell by comparing the base (1995–2014) with the 2041–2060 and 2081–2100 periods. The statistical significance of the observed changes was evaluated using the Student's *t*-test. Changes were considered statistically significant if $p < 0.05$.

Definition of false spring events

The FS event was identified in a given grid cell if the LSF occurred after the SGS. Changes in the future frequency and spatial distribution of these compound events were assessed. FS event intensity was also evaluated using accumulated GDD before the event (Eq. 1):

$$GDD = t_{avg} - t_{base} \quad (1),$$

where t_{avg} is the daily average air temperature, and t_{base} is the threshold temperature. If on a given day $t_{avg} < t_{base}$, then t_{avg} is set equal to t_{base} (McMaster, Wilhelm 1997).

Depending on the plant species, t_{base} may vary (Anandhi 2016; Kukal, Irmak 2018; Giolo *et al.* 2021). However, this study used $t_{base} = 5$ °C as this threshold is most suitable for crops in cooler and mid-latitude climates, especially cereals (Ruosteenoja *et al.* 2016). Moreover, the same 5 °C threshold was used to determine the SGS.

To assess FS event intensity, these compound climatic events were categorised into three intensity categories based on the GDD accumulated before the event:

- **GDD1**: 0 °C < GDD ≤ 100 °C;
- **GDD2**: 100 °C < GDD ≤ 200 °C;
- **GDD3**: GDD > 200 °C.

The higher the intensity category, the more severe the event. The study assessed how the accumulated GDD before FS events and the share of events in each intensity category will change by the mid- and late-21st century.

RESULTS

SGS, LSF dates, and FS events in 1995-2014

Using ERA5 data, the dates of SGS and LSF, as well as FS events and their spatial distribution were assessed during the baseline period of 1995–2014. The 12th of April was the median SGS date over the two decades in the study area. A latitudinal pattern is apparent in the spatial distribution of the median SGS date. The earliest median SGS date was recorded in the south-western and southern parts of the study area (30 March), while the latest occurred in the northern part (24 April) (Fig. 2a).

During 1995–2014, the LSF date occurred nearly two weeks later than the SGS date, with a median of 25April. A spatial pattern is also evident in the median LSF date, with the northern part of the study area showing LSF occurring 10–15 days later than in the south. However, the distance from the Baltic Sea was the primary factor influencing the spatial variation in LSF date. Grid cells located along the coast in western Lithuania had the earliest LSF dates, with a median date of 4 April. In contrast, the latest LSF date was observed in central Estonia (5–6 May) (Fig. 2b).

The distance from the Baltic Sea was also the main factor determining the spatial distribution of FS events during 1995–2014. Due to LSF occurring early in coastal regions, these areas recorded the fewest FS events – only 1–2 per decade, with none recorded in some grid cells. As the distance from the Baltic

Sea increased, so did the frequency of FS events. The highest number of these compound climate events (9.5 per decade) occurred in the eastern and south-eastern parts of the study area (Fig. 2c).

The GDD sum accumulated until the FS event was also assessed (Fig. 2d). The median value of this variable in the study area was approximately 58.5 °C. The highest GDD sums were observed in the southern part of the study area (95–102 °C), whereas coastal areas showed the lowest values for this variable, indicating weaker FS event intensity (Fig. 2d).

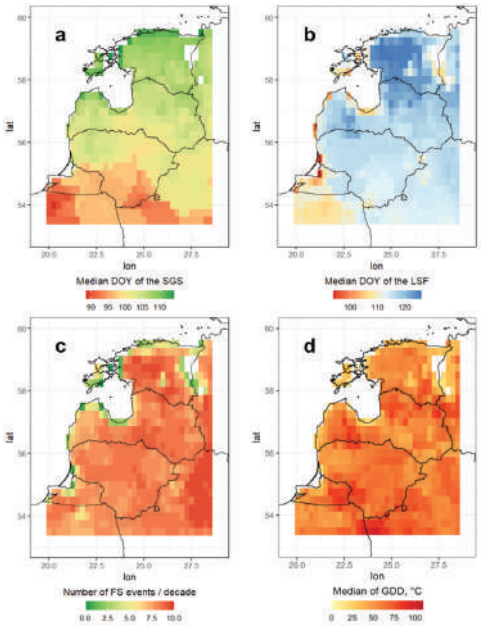

Fig. 2 Median SGS date (DOY) (a), median LSF date (DOY) (b), number of FS events per decade (c), and median GDD sums (°C), accumulated until FS events (d) during 1995–2014

Future projections of SGS and LSF dates

Using data from five different CMIP6 models under the SSP2-4.5 and SSP5-8.5 scenarios, a significant shift of SGS toward earlier dates was identified for the periods 2041–2060 and 2081–2100, compared to the baseline period of 1995–2014.

By 2041–2060, the SGS is projected to advance by 5–14.5 days under SSP2-4.5 and by 3–17.5 days under SSP5-8.5 (Fig. 3a). This advancement is evident across more than 90% of the study area. Except for the NorESM2-MM model, the SSP5-8.5 scenario consistently shows a 2–6 days earlier SGS compared to SSP2-4.5.

By the end of the 21st century, SGS dates are expected to shift even earlier. Under SSP2-4.5, SGS is projected to occur 9.5–27 days earlier, and under SSP5-8.5, 21–43 days earlier than during 1995–2014 (Fig. 3b). All models and both scenarios show statistically significant SGS advances across the entire territory, except for MPI-ESM1-2-LR and NorESM2-MM projections under the SSP2-4.5 scenario. The most prominent changes are projected using the CanESM5 and GFDL-CM4 models, which are characterised by high ECS values.

Similar trends were found for the LSF dates (Fig. 4). In 2041–2060, LSF is expected to occur 8–22 days earlier under SSP2-4.5 and 5.5–26.5 days earlier under SSP5-8.5, depending on the model (Fig. 4a). However, the scenario-driven differences are less consistent: only three models (CanESM5, GFDL-CM4, and MPI-ESM1-2-LR) project greater changes under SSP5-8.5 than under SSP2-4.5.

By 2081–2100, LSF is projected to shift 7–38 days

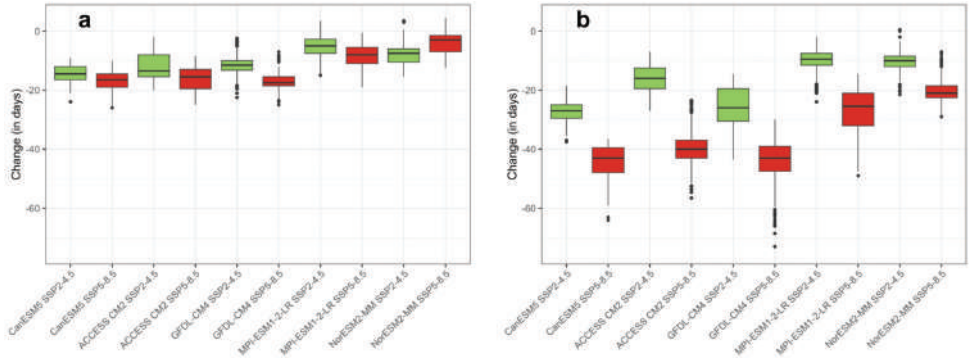

Fig. 3 Box plots of SGS date changes (in days), comparing 2041–2060 (a) *vs* 1995–2014 and 2081–2100 *vs* 1995–2014 (b) based on five different CMIP6 models under two SSP scenarios. Green indicates the SSP2-4.5 scenario, and red represents SSP5-8.5

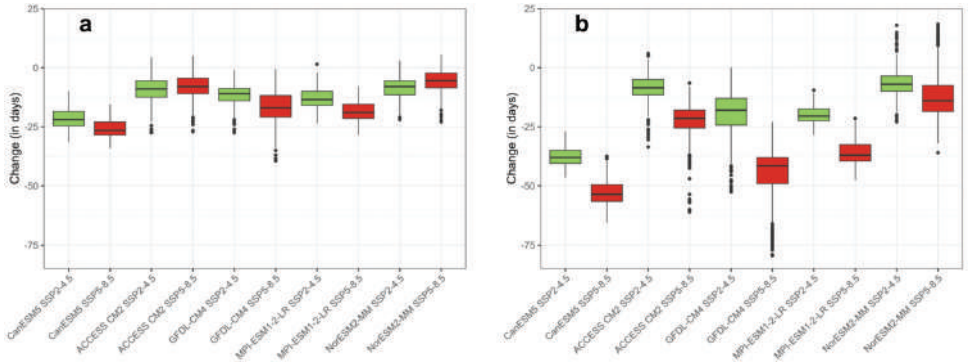

Fig. 4 Box plots of LSF date changes (in days), comparing 2041–2060 (a) *vs* 1995–2014 and 2081–2100 *vs* 1995–2014 (b) based on five different CMIP6 models under two SSP scenarios. Green indicates the SSP2-4.5 scenario, and red represents SSP5-8.5

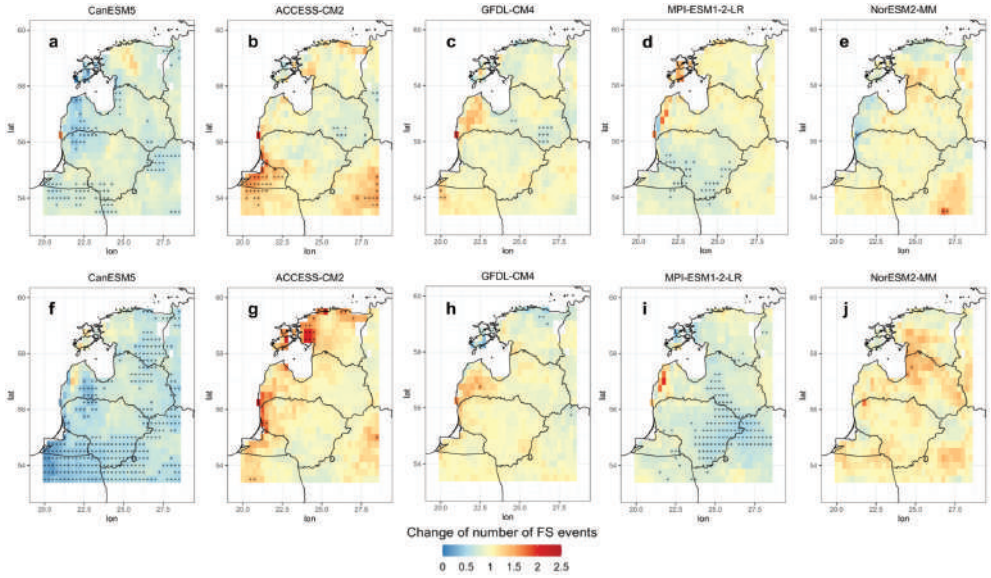

Fig. 5 Changes in FS event frequency (number of occurrences) comparing the periods 2041–2060 *vs* 1995–2014 (a–e) and 2081–2100 *vs* 1995–2014 (f–j), based on SSP2-4.5 scenario data from different CMIP6 models. Dots indicate grid cells with statistically significant changes according to the Student's *t*-test (when $p < 0.05$)

earlier under SSP2-4.5 and 14–53.5 days earlier under SSP5-8.5. Although the trend of earlier LSF persists, for some models (ACCESS-CM2 under SSP2-4.5 and NorESM2-MM under both scenarios), the change affects a smaller portion of the area compared to mid-century (Fig. 4b). Nevertheless, all models show greater average LSF shifts under SSP5-8.5 than under SSP2-4.5. The most significant and widespread shifts – statistically significant ($p < 0.05$) across the entire study area – are projected by CanESM5 under both scenarios and periods.

Future projections of false spring events

Unlike the projections for SGS and LSF dates, future changes in the recurrence of FS events show no consistent pattern and are more uncertain. Under the SSP2-4.5 scenario for 2041–2060, most models project a decrease in FS events across much of the study area, with the most significant decline (96.4%) expected using CanESM5 model data (Fig. 5a).

By 2081–2100, an apparent decrease under SSP2-4.5 is projected only by three models (CanESM5,

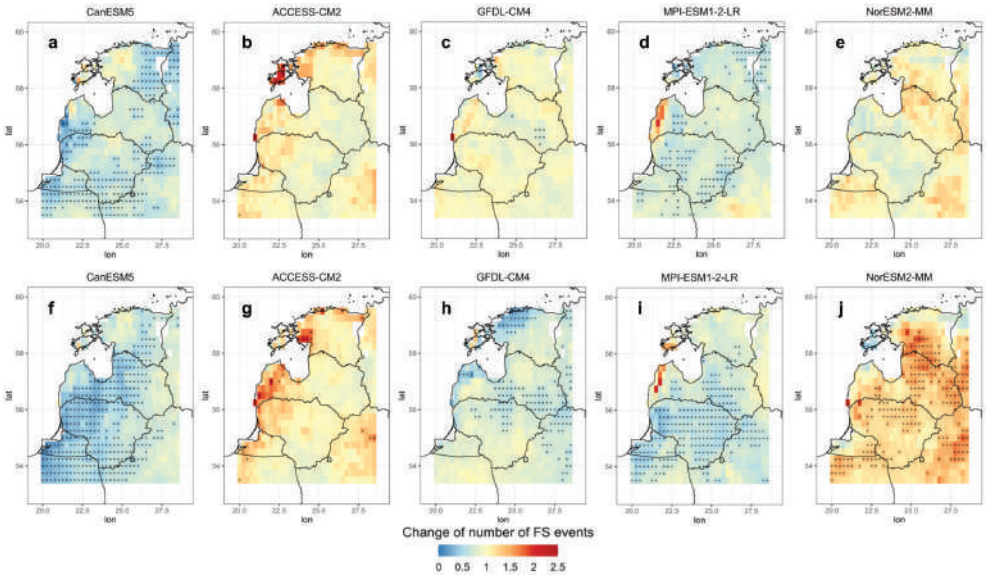

Fig. 6 Same as Figure 5, but for the SSP5-8.5 scenario

GFDL-CM4, and MPI-ESM1-2-LR), while ACCESS-CM2 and NorESM2-MM show an increase of over 55% of the area (Fig. 5f–j). In most cases, changes under SSP2-4.5 are small, with statistically significant results in more than 10% of the study area only for CanESM5 and MPI-ESM1-2-LR.

Under SSP5-8.5, similar patterns emerge. For the period between 2041 and 2060, most models (except NorESM2-MM) project a decline in FS events, although only CanESM5 and MPI-ESM1-2-LR exhibit statistically significant decreases in over 20% of the area (Fig. 6a–e). However, for 2081–2100, three models (CanESM5, GFDL-CM4, and MPI-ESM1-2-LR) show a broad decline (over 94% of the area), while the other two (ACCESS-CM2 and NorESM2-MM) project increases in over half of the territory (Fig. 6f–j). The most significant and widespread changes, including statistically significant ones (up to 52.3% of grid cells), are again projected by CanESM5 (Fig. 6f).

In both periods and scenarios, the most significant increases and decreases are projected along the Baltic Sea coast, while the inland regions in the eastern part of the study area show minor, mostly non-significant changes. Overall, the most pronounced deviations from the 1995–2014 baseline are projected for 2081–2100 under SSP5-8.5 (Fig. 6f–j).

Intensity of false spring events

Changes in the difference between LSF and SGS dates were analysed to assess whether future climate conditions will favour the formation and increase in the intensity of FS events. Under the SSP2-4.5 scenario, projections for 2041–2060 suggest a decreasing difference between these dates in over half of the study area across all five CMIP6 models, with the highest mean reduction (4.2 days) forecasted by the MPI-ESM1-2-LR model (Table 2). However, by 2081–2100, the agreement between models is projected to weakens. CanESM5 and MPI-ESM1-2-LR project a further decrease (up to 12.6 days on average), while ACCESS-CM2 and GFDL-CM4 suggest a growing difference between LSF and SGS dates, indicating more favourable conditions for FS development.

Similar inconsistencies appear under the SSP5-8.5 scenario. By mid-century, four models (except ACCESS-CM2) predict a narrowing LSF–SGS gap, whereas by the century's end, ACCESS-CM2 and NorESM2-MM project an increase in the difference between these dates, with the most significant change expected (by 17.3 days on average) using the ACCESS-CM2 model's data.

Changes in the GDD accumulated before FS events align well with the observed patterns in changes of LSF–SGS: a smaller difference between these two dates corresponds to lower GDD. For 2041–2060, most models project reduced GDD sums, particularly under CanESM5 and MPI-ESM1-2-LR (down by, on average, 25.6–42.5 °C depending on the scenario). By 2081–2100, the reduction in the mean GDD sum accumulated until FS events is even higher in these models, while ACCESS-CM2 and NorESM2-MM predict increases up to 37.1 °C.

Table 2 Percentage of the study area where, based on five different CMIP6 models and two SSP scenarios (SSP2-4.5 and SSP5-8.5), the difference between LSF and SGS dates is projected to decrease, increase, or remain unchanged in the periods 2041–2060 and 2081–2100 compared to the baseline period 1995–2014, along with the mean change in this difference (in days), and the change in mean GDD sums (°C) accumulated before FS events

Model	Period	SSP2-4.5 scenario					SSP5-8.5 scenario				
		Decrease, %	Increase, %	No change, %	Mean change of LSF–SGS, days	Mean change of GDD, °C	Decrease, %	Increase, %	No change, %	Mean change of LSF–SGS, days	Mean change of GDD, °C
CanESM5	2041–2060	78.4	16.2	5.5	−4.9	−25.6	97.6	1.5	1.0	−12.9	−42.5
	2081–2100	93.4	4.9	1.8	−12.6	−30.7	88.8	10.8	0.6	−10.1	−31.4
ACCESS-CM2	2041–2060	57.0	39.0	4.0	−0.9	−14.9	17.1	81.3	1.6	4.3	5.0
	2081–2100	10.5	87.9	1.6	6.5	14.6	2.5	97.5	0.0	17.3	35.3
GFDL-CM4	2041–2060	53.8	43.2	3.0	−0.9	−8.8	56.2	40.9	2.8	−1.8	−31.2
	2081–2100	23.5	75.1	1.3	6.1	1.6	72.4	25.5	2.1	−5.1	−30.5
MPI-ESM1-2-LR	2041–2060	70.0	23.7	6.4	−4.2	−27.9	91.3	6.0	2.8	−8.9	−36.8
	2081–2100	88.5	8.1	3.6	−9.2	−32.1	91.3	7.6	1.2	−10.8	−36.9
NorESM2-MM	2041–2060	56.7	39.4	3.9	−2.0	−21.4	61.8	34.3	3.9	−2.2	0.9
	2081–2100	49.8	47.7	2.5	0.4	3.8	31.9	64.5	3.6	5.1	37.1

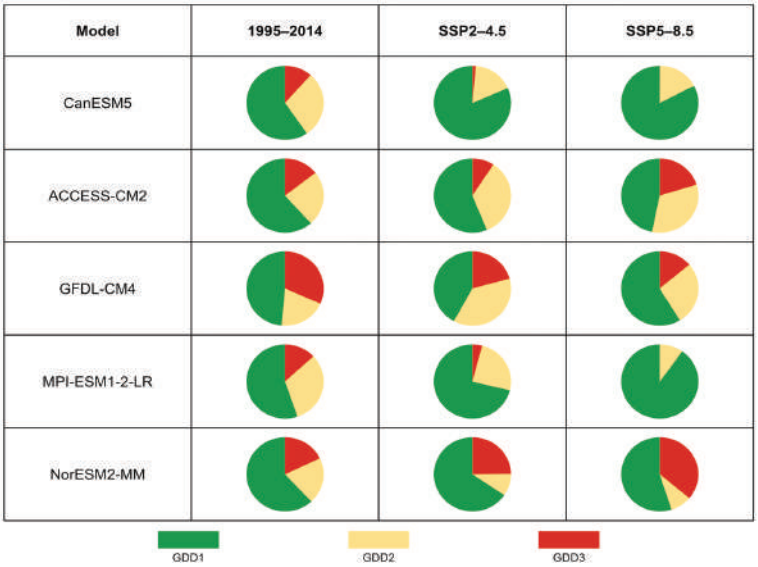

Fig. 7 Percentage of FS events belonging to different intensity categories (%), based on data from five CMIP6 models for 1995–2014 and 2081–2100. Projections for 2081–2100 are based on SSP2-4.5 and SSP5-8.5 scenarios. More details on intensity categories are provided in Section 2.4

Lastly, projections of FS events belonging to different intensity categories for the period 2081–2100 also vary (Fig. 7). According to data from the CanESM5 and MPI-ESM1-2-LR models, fewer FS events are expected to fall into the highest intensity category (GDD3), with none anticipated under SSP5-8.5. In contrast, ACCESS-CM2 and NorESM2-MM foresee an increase in high-intensity events, especially under SSP5-8.5, where over one-third of FS events fall into the GDD3 category. Models projecting more FS events also anticipate greater intensity, while those projecting fewer events indicate a decline in the severity of these events.

DISCUSSION

During this research, a clear trend of SGS date advancement was identified across the entire study area for the mid- and late-21st century. Such a trend was observed in almost all grid cells, regardless of climate model and SSP scenario. It was also found that the changes are statistically significant in most

cases, with the most pronounced advancement of the SGS date projected for 2081–2100 under the SSP5-8.5 scenario. According to data from various climate models, by the end of the 21st century, the SGS date is expected to shift, on average, 3 to 6 weeks earlier than during the base period of 1995–2014. Similar trends of SGS date advancement are also projected in various regions of the Northern Hemisphere (Xia *et al.* 2015; Zhu *et al.* 2019). Ruosteenoja *et al.* (2016) found that under a pessimistic scenario, the SGS date in Europe could become 1 to 1.5 months earlier. An average advancement of 1.5 to 3.5 weeks by the end of the 21st century is also projected in Poland (Marcinkowski *et al.* 2023; Szyga-Pluta *et al.* 2023), while in Estonia, the growing season is expected to begin 1 to 1.5 months earlier by 2100 than in 1990 (Saue *et al.* 2015). Such SGS changes in the future are linked to the projected rise in the average air temperature. Therefore, the derived SGS date and its changes only reflect how the "window of opportunity" for the potential start of the growing season is expected to shift (Körner *et al.* 2023).

Similar to the changes in the SGS date, the LSF date will also shift earlier in the future, and this tendency is expected in the majority of grid cells. Depending on the model and scenario, by the middle of the 21st century these changes are expected to range from five days to nearly four weeks. By the end of the 21st century, the advancement of the LSF date is even greater. Compared to the 1995–2014 period, the LSF date is expected to shift earlier from one to six weeks on average. Similar to changes in the SGS date, the rise in t_{min} values resulting from anthropogenic climate change is the primary reason for the advancement of the LSF date. A shift in the LSF date to earlier has also been projected for other regions of the Northern Hemisphere, both in the near future and by the end of the 21st century (Charalampopoulos, Droulia 2022; Helali *et al.* 2022; Chen *et al.* 2024; Ford *et al.* 2025).

During the assessment of changes in SGS and LSF dates, it was observed that the CanESM5 model projects the most pronounced advancement of these dates. In contrast, the modest changes occurred while using the NorESM2-MM model's data. Depending on the period and SSP scenario, the CanESM5 model projects changes 7–22 days greater than those of the NorESM2-MM model. For LSF dates, this difference is even more pronounced, ranging from 14 to 39.5 days. This variability is primarily attributed to differences in ECS values among the models, with CanESM5 exhibiting the highest ECS values, and NorESM2-MM the lowest of the models assessed in this study (Table 1).

Although an overall shift to earlier dates is expected, individual models show different magnitudes of change in SGS and LSF. Some models project a larger advancement in SGS compared to LSF, while others show a greater shift in LSF. These differences are reflected in the projected changes between the LSF and SGS dates. For the period between 2041 and 2060, all models project a reduction in this difference under the SSP2-4.5 scenario. Under the SSP5-8.5 scenario, a similar trend is projected by four out of five models used in this study. By the end of the century, a decrease in the mean difference between LSF and SGS dates is projected by two models under SSP2-4.5 and by three models under SSP5-8.5. In these cases, the LSF date is expected to advance more than the SGS date, implying less favourable conditions for the formation of FS events. However, the remaining models suggest an increase in the difference between LSF and SGS dates, indicating a more rapid advancement of the SGS date compared to the LSF date.

The different rates of change in LSF and SGS dates have been predicted to result in projected changes in the recurrence of FS events showing no consistent pattern, unlike those in SGS or LSF dates. It has been observed that according to model scenarios that predict a decrease in the difference between LSF and SGS dates, the number of FS events will also be lower in most cases in the future, and *vice versa*. Therefore, in this case, the ECS values of the models, unlike when assessing changes in SGS and LSF dates, are not so essential in determining the magnitude of future changes. If a more rapid temperature increase is projected for the end of winter or early spring, the number of FS events may rise; however, if more significant warming is expected in the second half of spring, the number of FS events may decrease.

For the period between 2041 and 2060, most models indicate a decreasing trend in the number of FS events. Meanwhile, by the end of the 21st century, these compound climate events are projected to increase according to two models and decrease according to the remaining three. However, in most cases, the projected changes are not substantial. Similar FS event projections have also been observed in other regions, which are characterised by high uncertainty and the absence of a unified trend. In some areas, an increase in the number of these events is expected, while in others a decrease is projected (Allstadt *et al.* 2015; Martinuzzi *et al.* 2019; Lhotka, Brönnimann 2020; Masaki 2020; Mallard *et al.* 2023). Therefore, forecasting future changes in FS events remains a complex task (Allstadt *et al.* 2015).

The mean changes in the difference between LSF and SGS dates are consistent with changes in the mean sums of GDD accumulated before FS events. It was found that as the difference between LSF and SGS decreases, the amount of GDD accumulated before an FS event also declines. The intensity of FS events was also assessed by classifying these events

into three intensity categories based on the sum of GDD accumulated until the event. The tendency was observed where models predicting an increase in the number of FS events also forecast an increase in the intensity of these compound climate events. An increasing intensity of FS events is also projected for France (Vautard *et al.* 2023), certain regions of China (Chen *et al*. 2024), and south-eastern Europe (Charalampopoulos, Droulia 2022). However, according to the remaining models used in this study, which project a decrease in FS events, the intensity of these compound climate events is expected to diminish.

In this study, FS events were assessed using a meteorological approach – this approach was employed to determine the SGS date and to evaluate the intensity of FS events. However, the risk and potential damage of FS events also depend on other factors, primarily the plant species, precipitation levels, soil moisture, local topography, and other variables (Chamberlain *et al.* 2019; Ma *et al.* 2019). Therefore, to improve the prediction of these compound climate events, future studies should consider the influence of these variables.

Furthermore, the intensity of FS events was evaluated based on the sum of GDD accumulated prior to an FS event. By doing this, a widely accepted assumption was applied, whereby a higher accumulation of GDD corresponds to greater potential damage caused by an FS event. This assumption is appropriate, as it has been proven that the accumulated GDD sum determines the plant developmental stage, and the later in spring the FS event occurs, the more severe the damage it causes (Miller *et al*. 2001; Chun, Changnon 2018; Qiu *et al.* 2024; Bhatti *et al.* 2025). However, the GDD method has limitations. In this study, t_{base} = 5 °C was applied for the calculation of GDD; however, to assess the impact of FS events on specific plant species more accurately, different t_{base} values should be considered (Chamberlain, Walkovich 2023). Finally, plant development depends not only on temperature and GDD but also on moisture availability. When moisture levels are low, even if the required GDD sum has been reached, the particular phenological stage may not be reached and, as a result, the damage caused by an FS event may vary accordingly (Miller *et al.* 2001).

Another limitation encountered in this study is the spatial resolution of grid cells (~ 25 km), which may be too coarse to evaluate local-scale changes. Finally, the NEX-GDDP-CMIP6 dataset used in this study also has some limitations. The BCSD bias correction method used to produce this dataset is based on the assumption that the spatial climate patterns observed between 1960 and 2014 will persist unchanged in the future. It also retains the original trend slopes of GCM projections, thereby maintaining the rate of change defined by the original scenario. Although the method includes bias correction and offers finer spatial resolution, it only applies linear adjustments to projection offsets, which may not adequately reflect the nonlinear dynamics of climate systems (Thrasher *et al.* 2012). Furthermore, since a constant bias across different distribution quantiles is assumed, future extremes may remain inadequately assessed (Zhang *et al.* 2024).

CONCLUSIONS

During this study, future projections of FS events recurrence and intensity in the eastern part of the Baltic Sea region were developed using the data from five different CMIP6 models and two SSP scenarios (SSP2-4.5 and SSP5-8.5). These projections were generated for 2041–2060 and 2081–2100. Changes in SGS and LSF dates were also evaluated.

According to all five climate models and two SSP scenarios, the SGS date is projected to advance in the future compared to the 1995–2014 reference period. During 2041–2060, the SGS date, depending on the model, is expected to shift earlier by 5–14.5 days under the SSP2-4.5 scenario and by 3–17.5 days under the SSP5-8.5 scenario. By 2081–2100, this change is projected to reach 9.5–27 days and 21–43 days, respectively. A similar trend is also projected for the LSF date across all models used. In the mid-21st century, the LSF date is expected to occur 8–22 days earlier under SSP2-4.5 and 5.5–26.5 days earlier under the SSP5-8.5 scenario. By the end of the 21st century, these changes are projected to increase to 7–38 days and 14–53.5 days, respectively. The most significant changes in SGS and LSF dates are projected using the CanESM5 scenario data, which is characterised by the highest ECS value.

Both LSF and SGS dates are projected to shift earlier; however, the magnitude of these changes will vary depending on the climate model used. This variability results in the absence of a clear tendency in the projections of future FS events. For the period between 2041 and 2060, most models predict a general decline in the frequency of these compound climate events. However, for the period between 2081 and 2100, only three models continue to project a decreasing trend, while the remaining two predict an increase in the number of FS events. During the assessment of FS event intensity, it was observed that models and scenarios projecting a decline in FS event frequency also indicate a decrease in their intensity – and *vice versa*.

This study focused on future FS event projections in the eastern part of the Baltic Sea region for the first time. As such, it may serve as a foundational step toward more detailed and accurate forecasts and

the evaluation of risks posed by these events to fruit trees, crops, and other sectors. These insights could help create adaptation strategies to reduce the potential damage of FS events in a changing climate.

ACKNOWLEDGMENTS

We thank two anonymous reviewers for their insightful advice and constructive comments.

REFERENCES

Allstadt, A.J., Vavrus, S.J., Heglund, P.J., Pidgeon, A.M., Thogmartin, W.E., Radeloff, V.C. 2015. Spring plant phenology and false springs in the conterminous US during the 21st century. *Environmental Research Letters 10(10)*. https://doi.org/10.1088/1748-9326/10/10/104008

Anandhi, A. 2016. Growing degree days – Ecosystem indicator for changing diurnal temperatures and their impact on corn growth stages in Kansas. *Ecological Indicators 61*, 149–158. https://doi.org/10.1016/j.ecolind.2015.08.023

Augspurger, C.K. 2013. Reconstructing patterns of temperature, phenology, and frost damage over 124 years: Spring damage risk is increasing. *Ecology 94(1)*, 41–50. https://doi.org/10.1890/12-0200.1

Ault, T.R., Henebry, G.M., De Beurs, K.M., Schwartz, M.D., Betancourt, J.L., Moore, D. 2013. The false spring of 2012, earliest in North American record. *Eos 94(20)*, 181–182. https://doi.org/10.1002/2013EO200001

Ball, M.C., Harris-Pascal, D., Egerton, J.J.G., Lenné, T. 2011. The paradoxical increase in freezing injury in a warming climate: Frost as a driver of change in cold climate vegetation. *Temperature Adaptation in a Changing Climate: Nature at Risk November 2011*, 179–185. https://doi.org/10.1079/9781845938222.0179

Bateman, B. 2022. *False Springs: How Earlier Spring With Climate Change Wreaks Havoc on Birds*. [online] Audubon. Available at: https://www.audubon.org/news/false-springs-how-earlier-spring-climate-change-wreaks-havoc-birds [Accessed 28 April 2025].

Baumgarten, F., Gessler, A., Vitasse, Y. 2023. No risk – no fun: Penalty and recovery from spring frost damage in deciduous temperate trees. *Functional Ecology 37(3)*, 648–663. https://doi.org/10.1111/1365-2435.14243

Beck, H.E., Zimmermann, N.E., McVicar, T.R., Vergopolan, N., Berg, A., Wood, E.F. 2018. Present and future Köppen-Geiger climate classification maps at 1-km resolution. *Scientific data 5(1)*, 1–12. https://doi.org/10.1038/sdata.2018.214

Bhatti, S., Jeranyama, P., Kennedy, C.D., Buda, A.R., Ghantous, K., Millar, D.J., DeMoranville, C.J. 2025. Changes in cranberry phenology from 1958 to 2022: Implications for spring frost protection in Massachusetts, United States. *International Journal of Biometeorology 69*, 1297–1309. https://doi.org/10.1007/s00484-025-02892-w

Bosdijk, J., de Feiter, V.S., Gaiser, A., Smink, T., Thorkelsdottir, G., van Vliet, A.J.H., Luedeling, E. 2024. False springs in the Netherlands: climate change impact assessment with the false spring damage indicator model. *Regional Environmental Change 24(2)*, 1–11. https://doi.org/10.1007/s10113-024-02235-2

Cannell, M.G.R., Smith, R.I. 1986. Climatic Warming, Spring Budburst and Forest Damage on Trees. *Journal of Applied Ecology 23(1)*, 177–191. https://doi.org/10.2307/2403090

Carter, T.R. 1998. Changes in the thermal growing season in Nordic countries during the past century and prospects for the future. *Agricultural and Food Science in Finland 7(2)*, 161–179. https://doi.org/10.23986/afsci.72857

Ceglar, A., Zampieri, M., Toreti, A., Dentener, F. 2019. Observed northward migration of agro-climate zones in Europe will further accelerate under climate change. *Earth's Future 7(9)*, 1088–1101. https://doi.org/10.1029/2019EF001178

Chamberlain, C.J., Wolkovich, E.M. 2023. Variation across space, species and methods in models of spring phenology. *Climate Change Ecology 5*, 100071. https://doi.org/10.1016/j.ecochg.2023.100071

Chamberlain, C.J., Cook, B.I., García de Cortázar-Atauri, I., Wolkovich, E.M. 2019. Rethinking false spring risk. *Global Change Biology 25(7)*, 2209–2220. https://doi.org/10.1111/gcb.14642

Chamberlain, C.J., Cook, B.I., Morales-Castilla, I., Wolkovich, E.M. 2021. Climate change reshapes the drivers of false spring risk across European trees. *New Phytologist 229(1)*, 323–334. https://doi.org/10.1111/nph.16851

Charalampopoulos, I., Droulia, F. 2022. Frost Conditions Due to Climate Change in South-Eastern Europe via a High-Spatio temporal-Resolution Dataset. *Atmosphere 13(9)*, 1407. https://doi.org/10.3390/atmos13091407

Chen, D., Rojas, M., Samset, B.H., Cobb, K., Diongue Niang, A., Edwards, P., Emori, S., Faria, S.H., Hawkins, E., Hope, P., Huybrechts, P., Meinshausen, M., Mustafa, S.K., Plattner, G.K., Tréguier, A.-M. 2021. *Framing, context, and methods*. In: V. Masson-Delmotte, P. Zhai, A. Pirani, S.L. Connors, C. Péan, S. Berger, N. Caud, Y. Chen, L. Goldfarb, M.I. Gomis, M., Huang, K., Leitzell, E., Lonnoy, J.B.R., Matthews, T.K., Maycock, T., Waterfield, O., Yelekçi, R. Yu, Zhou, B., eds. *Climate Change 2021: The Physical Science Basis. Contribution of Working Group I to the Sixth Assessment Report of the Intergovernmental Panel on Climate Change*. Cambridge: Cambridge University Press, 147–286 pp. https://doi.org/10.1017/9781009157896.003

Chen, R., Wang, J., Li, Y., Bai, R., Huang, M., Zhang, Z., Zhao, L., Qu, Z., Liu, L. 2024. Higher risk of spring frost under future climate change across China's apple planting regions. *European Journal of Agronomy 159* (May), 127288. https://doi.org/10.1016/j.eja.2024.127288

Chun, S.E., Changnon, D. 2019. Predicting major peach yield reductions in the Midwest and Southeast United

States. *Meteorological Applications 26(1)*, 97–107. https://doi.org/10.1002/met.1740
Clark, R.M., Thompson, R. 2010. Predicting the impact of global warming on the timing of spring flowering. *International Journal of Climatology 30(11)*, 1599–1613. https://doi.org/10.1002/joc.2004
Cook, B.I., Chamberlain, C., Wolkovich, E.M., Morales-Castilla, I. 2020. *Climate change reshapes the drivers of false spring risk across European trees. [online] Nasa. gov*. Available at: https://ntrs.nasa.gov/citations/20205006353 [Accessed 30 April 2025].
Crassweller, R. 2024. *Frost, Critical Temperatures, and Frost Protection*. [online] Available at: https://extension.psu.edu/frost-critical-temperatures-and-frost-protection [Accessed 29 April 2025].
ECMWF. 2021. *CMIP6 climate projections*. Copernicus. eu. https://doi.org/10.24381/cds.c866074c
European Climate Risk Assessment. 2024. *European Environment Agency*, Luxembourg: Publications Office of the European Union, 486 pp. https://doi.org/10.2800/8671471
FAO. 2024. *Frost protection: fundamentals, practice, and economics* – Volume 1. [online] Available at: https://www.fao.org/4/y7223e/y7223e0a.htm. [Accessed 30 April 2025].
Faust, E., Herbold, J. 2017. Spring frost losses and climate change – Not a contradiction in terms. *Topics Geo May*, 1–11.
Ford, T.W., Chen, L., Fernandez, E., Wahle, E., Luedeling, E., Todey, D., Nowatzkie, L., Agronomía, E.De, Cat, P.U. 2025. Agricultural and Forest Meteorology Historical and Projected Changes in Chill Accumulation and Spring Freeze Risk in the Midwest United States. *Agricultural and Forest Meteorology 368* (March), 110532. https://doi.org/10.1016/j.agrformet.2025.110532
Giolo, M., Sallenave, R., Pornaro, C., Velasco-Cruz, C., Macolino, S., Leinauer, B. 2021. Base temperatures affect accuracy of growing degree day model to predict emergence of bermuda grasses. *Agronomy Journal 113(3)*, 2960–2966. https://doi.org/10.1002/agj2.20660
Graczyk, D., Szwed, M. 2020. Changes in the occurrence of late spring frost in Poland. *Agronomy 10(11)*. https://doi.org/10.3390/agronomy10111835
Grigorieva, E., Livenets, A., Stelmakh, E. 2023. Adaptation of Agriculture to Climate Change: A Scoping Review. *Climate 11(10)*, 1–37. https://doi.org/10.3390/cli11100202
Grossman, E. 2014. *Why You Shouldn't Hope for An Early Spring*. [online] *Climate Central*. Available at: https://www.climatecentral.org/news/why-you-shouldnt-hope-for-an-early-spring-17105 [Accessed 29 April 2025].
Hájková, L., Možný, M., Oušková, V., Bartošová, L., Dížková, P., Žalud, Z. 2023. Increasing Risk of Spring Frost Occurrence during the Cherry Tree Flowering in Times of Climate Change. *Water (Switzerland) 15(3)*. https://doi.org/10.3390/w15030497
Hausfather, Z. 2018. *Explainer: How scientists estimate climate sensitivity*. [online] *Carbon Brief*. Available at: https://www.carbonbrief.org/explainer-how-scientists-estimate-climate-sensitivity/ [Accessed 30 April 2025].
Hausfather, Z. 2019. *CMIP6: the next generation of climate models explained – Carbon Brief*. [online] *Carbon Brief*. Available at: https://www.carbonbrief.org/cmip6-the-next-generation-of-climate-models-explained/ [Accessed 30 April 2025].
Helali, J., Oskouei, E.A., Hosseini, S.A., Saeidi, V., Modirian, R. 2022. Projection of changes in late spring frost based on CMIP6 models and SSP scenarios over cold regions of Iran. *Theoretical and Applied Climatology 149(3–4)*, 1405–1418. https://doi.org/10.1007/s00704-022-04124-2
Hersbach, H., Bell, B., Berrisford, P., Hirahara, S., Horányi, A., Muñoz-Sabater, J., Nicolas, J., Peubey, C., Radu, R., Schepers, D., Simmons, A., Soci, C., Abdalla, S., Abellan, X., Balsamo, G., Bechtold, P., Biavati, G., Bidlot, J., Bonavita, M., … Thépaut, J.N. 2020. The ERA5 global reanalysis. *Quarterly Journal of the Royal Meteorological Society 146(730)*, 1999–2049. https://doi.org/10.1002/qj.3803
Hufkens, K., Friedl, M.A., Keenan, T.F., Sonnentag, O., Bailey, A., O'Keefe, J., Richardson, A.D. 2012. Ecological impacts of a widespread frost event following early spring leaf-out. *Global Change Biology 18(7)*, 2365–2377. https://doi.org/10.1111/j.1365-2486.2012.02712.x
Jarzyna, K. 2021. Climatic hazards for native tree species in Poland with special regards to silver fir (*Abies alba* Mill.) and European beech (*Fagus sylvatica* L.). *Theoretical and Applied Climatology 144(1–2)*, 581–591. https://doi.org/10.1007/s00704-021-03550-y
Jeong, S.J., Ho, C.H., Gim, H.J., Brown, M.E. 2011. Phenology shifts at start vs. end of growing season in temperate vegetation over the Northern Hemisphere for the period 1982–2008. *Global Change Biology17*(7), 2385–2399. https://doi.org/10.1111/j.1365-2486.2011.02397.x
Kilkus, K., Stonevičius, E. 2011. *Lietuvos vandenų geografija*. Lithuania: Vilniaus universitetas, 188 pp. [In Lithuanian].
Klimavičius, L., Rimkus, E. 2024. False spring events in the eastern part of the Baltic Sea region. *Theoretical and Applied Climatology 155*, 9351–9365. https://doi.org/10.1016/j.oceano.2023.06.010
Körner, C., Möhl, P., Hiltbrunner, E. 2023. Four ways to define the growing season. *Ecology Letters 26(8)*, 1277–1292. https://doi.org/10.1111/ele.14260
Koźmiński, C., Mąkosza, A., Nidzgorska-Lencewicz, J., Michalska, B. 2023. Air Frosts in Poland in the Thermal Growing Season (AT > 5 °C). *Agriculture (Switzerland) 13(6)*. https://doi.org/10.3390/agriculture13061228
Kukal, M.S., Irmak, S. 2018. U.S. Agro-Climate in 20th Century: Growing Degree Days, First and Last Frost, Growing Season Length, and Impacts on Crop Yields. *Scientific Reports 8(1)*, 1–14. https://doi.org/10.1038/s41598-018-25212-2

Lhotka, O., Brönnimann, S. 2020. Possible increase of vegetation exposure to spring frost under climate change in Switzerland. *Atmosphere 11(4)*. https://doi.org/10.3390/ATMOS11040391

Liu, Q., Piao, S., Janssens, I.A., Fu, Y., Peng, S., Lian, X., Ciais, P., Myneni, R.B., Peñuelas, J., Wang, T. 2018. Extension of the growing season increases vegetation exposure to frost. *Nature Communications 9(1)*. https://doi.org/10.1038/s41467-017-02690-y

Liu, R., Zhang, X., Wang, W., Wang, Y., Liu, H., Ma, M., Tang, G. 2024. Global-scale ERA5 product precipitation and temperature evaluation. *Ecological Indicators 166* (January), 112481. https://doi.org/10.1016/j.ecolind.2024.112481

Ma, Q., Huang, J.G., Hänninen, H., Berninger, F. 2019. Divergent trends in the risk of spring frost damage to trees in Europe with recent warming. *Global Change Biology 25(1)*, 351–360. https://doi.org/10.1111/gcb.14479

Mallard, M.S., Talgo, K.D., Spero, T.L., Bowden, J.H., Nolte, C.G. 2023. Dynamically Down scaled Projections of Phenological Changes across the Contiguous United States. *Journal of Applied Meteorology and Climatology 62(12)*, 1875–1889. https://doi.org/10.1175/JAMC-D-23-0071.1

Marcinkowski, P., Piniewski, M., Jefimow, M. 2023. Assessment of projected climate change impact on agro-climatic indicators in Poland. *International Journal of Climatology 43(13)*, 6003–6019. https://doi.org/10.1002/joc.8185

Martinuzzi, S., Allstadt, A.J., Pidgeon, A.M., Flather, C.H., Jolly, W.M., Radeloff, V.C. 2019. Future changes in fire weather, spring droughts, and false springs across U.S. National Forests and Grasslands. *Ecological Applications 29(5)*, 1–14. https://doi.org/10.1002/eap.1904

Masaki, Y. 2020. Future risk of frost on apple trees in Japan. *Climatic Change 159(3)*, 407–422. https://doi.org/10.1007/s10584-019-02610-7

McMaster, G.S., Wilhelm, W.W. 1997. Growing degree-days: One equation, two interpretations. *Agricultural and Forest Meteorology 87(4)*, 291–300. https://doi.org/10.1016/S0168-1923(97)00027-0

McNicholl, B., Lee, Y.H., Campbell, A.G., Dev, S. 2022. Evaluating the Reliability of Air Temperature from ERA5 Reanalysis Data. *IEEE Geoscience and Remote Sensing Letters 19*, 1–5. https://doi.org/10.1109/LGRS.2021.3137643

Miller, P., Lanier, W., Brandt, S. 2001. Using Growing Degree Days to Predict Plant Stages. Ag/Extension Communications Coordinator, Communications Services, Montana State University-Bozeman, Bozeman. *MO 59717(406)*.

Miś, F., Tomczyk, A.M. 2025. Spatial and temporal differentiation of the thermal growing season in central and northern Europe. *Theoretical and Applied Climatology 156(2)*. https://doi.org/10.1007/s00704-025-05382-6

Monahan, W.B., Rosemartin, A., Gerst, K.L., Fisichelli, N.A., Ault, T.R., Schwartz, M.D., Gross, J.E., Weltzin, J.F. 2016. Climate change is advancing spring onset across the U.S. national park system. *Ecosphere 7(10)*, e01465. https://doi.org/10.1002/ecs2.1465

Muffler, L., Weigel, R., Beil, I., Leuschner, C., Schmeddes, J., Kreyling, J. 2024. Winter and spring frost events delay leaf-out, hamper growth and increase mortality in European beech seedlings, with weaker effects of subsequent frosts. *Ecology and Evolution 14(7)*, e70028. https://doi.org/10.1002/ece3.70028

Nidzgorska-Lencewicz, J., Mąkosza, A., Koźmiński, C., Michalska, B. 2024. Potential risk of Frost in the growing season in Poland. *Agriculture 14(3)*, 501. https://doi.org/10.3390/agriculture14030501

Peltonen-Sainio, P., Jauhiainen, L., Hakala, K., Ojanen, H. 2009. Climate change and prolongation of growing season: Changes in regional potential for field crop production in Finland. *Agricultural and Food Science 18(3–4)*, 171–190. https://doi.org/10.2137/145960609790059479

Peterson, A.G., Abatzoglou, J.T. 2014. Observed changes in false springs over the contiguous United States. *Geophysical Research Letters 41(6)*, 2156–2162. https://doi.org/10.1002/2014GL059266

Piotrowski, P., Bartoszek, K. 2025. Atmospheric Circulation Conditions During Spring Frosts in Southeastern Poland (1981–2023). *Atmosphere 16(4)*, 409. https://doi.org/10.3390/atmos16040409

Qiu, H., Yan, Q., Yang, Y., Huang, X., Wang, J., Luo, J., Peng, L., Bai, G., Zhang, L., Zhang, R., Fu, Y.H., Wu, C., Peñuelas, J., Chen, L. 2024. Flowering in the Northern Hemisphere is delayed by frost after leaf-out. *Nature communications 15(1)*, 9123. https://doi.org/10.1038/s41467-024-53382-3

Rao, K.K., Al Mandous, A., Al Ebri, M., Al Hameli, N., Rakib, M., Al Kaabi, S. 2024. Future changes in the precipitation regime over the Arabian Peninsula with special emphasis on UAE: insights from NEX-GDDP CMIP6 model simulations. *Scientific Reports 14(1)*, 1–21. https://doi.org/10.1038/s41598-023-49910-8

Rodrigo, J. 2000. Spring frosts in deciduous fruit trees. Morphological damage and flower hardiness. *Scientia Horticulturae 85(3)*, 155–173. https://doi.org/10.1016/S0304-4238(99)00150-8

Ruosteenoja, K., Räisänen, J., Venäläinen, A., Kämäräinen, M. 2016. Projections for the duration and degree days of the thermal growing season in Europe derived from CMIP5 model output. *International Journal of Climatology 36(8)*, 3039–3055. https://doi.org/10.1002/joc.4535

Saue, T., Käremaa, K., Nejedlík, P., Eliášová, M. 2015. Lengthening of the thermal growing season due climate change in Estonia. In: Šiška et al. (eds) *Towards climatic services, Nitra.*

SMHI. 2025. *Length of the vegetation period*. [online] Available at: https://www.smhi.se/en/climate/tools-and-inspiration/climate-indicators/length-of-the-vegetation-period [Accessed 30 April 2025].

Sun, Y., Zhu, R., Wang, T. 2024. Projection of ex-

treme climate change in the Asian arid region and the Tibetan Plateau in the early and middle 21st century based on NEX-GDDP-CMIP6. *Atmospheric and Oceanic Science Letters 18(3)*, 100534. https://doi.org/10.1016/j.aosl.2024.100534

Szyga-Pluta, K., Tomczyk, A.M., Piniewski, M., Eini, M.R. 2023. Past and future changes in the start, end, and duration of the growing season in Poland. *Acta Geophysica 71(6)*, 3041–3055. https://doi.org/10.1007/s11600-023-01117-1

Talchabhadel, R., Bhattarai, S., Bista, S. 2025. Projected Changes in Precipitation Extremes Across the Mississippi River Basin Using the NASA Global Daily Downscaled Datasets NEX-GDDP-CMIP6. *International Journal of Climatology 45(5)*, e8748. https://doi.org/10.1002/joc.8748

Thrasher, B., Maurer, E.P., McKellar, C., Duffy, P.B. 2012. Technical Note: Bias correcting climate model simulated daily temperature extremes with quantile mapping. *Hydrology and Earth System Sciences 16(9)*, 3309–3314, https://doi.org/10.5194/hess-16-3309-2012

Thrasher, B., Wang, W., Michaelis, A., Melton, F., Lee, T., Nemani, R. 2022. NASA Global Daily Downscaled Projections, CMIP6. *Scientific Data 9(1)*, 1–6. https://doi.org/10.1038/s41597-022-01393-4

Vautard, R., Van Oldenborgh, G.J., Bonnet, R., Li, S., Robin, Y., Kew, S., Philip, S., Soubeyroux, J.M., Dubuisson, B., Viovy, N., Reichstein, M., Otto, F., Garcia De Cortazar-Atauri, I. 2023. Human influence on growing-period frosts like in early April 2021 in central France. *Natural Hazards and Earth System Sciences 23(3)*, 1045–1058. https://doi.org/10.5194/nhess-23-1045-2023

Velikou, K., Lazoglou, G., Tolika, K., Anagnostopoulou, C. 2022. Reliability of the ERA5 in Replicating Mean and Extreme Temperatures across Europe. *Water (Switzerland) 14(4)*. https://doi.org/10.3390/w14040543

Vitasse, Y., Rebetez, M. 2018. Unprecedented risk of spring frost damage in Switzerland and Germany in 2017. *Climatic change 149(2)*, 233–246. https://doi.org/10.1007/s10584-018-2234-y

Wang, J., Guan, Y., Wu, L., Guan, X., Cai, W., Huang, J. 2021. Changing lengths of the four seasons by global warming. *Geophysical Research Letters 48*, e2020GL091753. https://doi.org/10.1029/2020GL091753

Wang, T., Zhong, S., Andresen, J. 2025. Impacts of spring freeze events on a perennial tree fruit crop across the central and eastern USA. *International Journal of Biometeorology 69*, 1237–1252. https://doi.org/10.1007/s00484-025-02887-7

Wypych, A., Sulikowska, A., Ustrnul, Z., Czekierda, D. 2017. Variability of growing degree days in Poland in response to ongoing climate changes in Europe. *International Journal of Biometeorology 61(1)*, 49–59. https://doi.org/10.1007/s00484-016-1190-3

Xia, J., Yan, Z., Jia, G., Zeng, H., Jones, P.D., Zhou, W., Zhang, A. 2015. Projections of the advance in the start of the growing season during the 21st century based on CMIP5 simulations. *Advances in Atmospheric Sciences 32*(6), 831–838. https://doi.org/10.1007/s00376-014-4125-0

Xu, W., Lei, X., Chen, S., Yu, T., Hu, Z., Zhang, M., Jiang, L., Bao, R., Guan, X., Ma, M., Wei, J., Gao, L., Feng, A. 2022. How Well Does the ERA5 Reanalysis Capture the Extreme Climate Events Over China? Part II: Extreme Temperature. *Frontiers in Environmental Science 10*(June), 1–15. https://doi.org/10.3389/fenvs.2022.921659

Zahradníček, P., Brázdil, R., Řehoř, J., Trnka, M., Bartošová, L., Rožnovský, J. 2024. Past and present risk of spring frosts for fruit trees in the Czech Republic. *Theoretical and Applied Climatology 155(2)*, 965–984. https://doi.org/10.1007/s00704-023-04671-2

Zhang, X., Huang, T., Wang, W., Shen, P. 2024. Change of global land extreme temperature in the future. *Global and Planetary Change 242*(September), 104583. https://doi.org/10.1016/j.gloplacha.2024.104583

Zhu, L., Meng, J., Li, F., You, N. 2019. Predicting the patterns of change in spring onset and false springs in China during the twenty-first century. *International Journal of Biometeorology 63(5)*, 591–606. https://doi.org/10.1007/s00484-017-1456-4

Zscheischler, J., Raymond, C., Horton, R.M., Ramos, A.M. 2020. A typology of compound weather. *Nature Reviews Earth & Environment 1*, 333–347. http://dx.doi.org/10.1038/s43017-020-0060-z

Vilniaus universiteto leidykla
Saulėtekio al. 9, III rūmai, LT-10222 Vilnius
El. p. info@leidykla.vu.lt, www.leidykla.vu.lt
bookshop.vu.lt, journals.vu.lt
Tiražas 20 egz.